# POSTLAUNCH MEMORANDUM REPORT

## FOR

## APOLLO PAD ABORT I [ı ı]

N79-76468

(NASA-TM-X-66756) POSTLAUNCH MEMORANDUM
REPORT FOR APOLLO PAD ABORT 1 (NASA) 188 p

Unclas
00/18 11509

FF No. 602 (D)

/ 8 8 (PAGES)

(CODE)

NASA-TMX-66756

(NASA CR OR TMX OR AD NUMBER)

(CATEGORY)

GROUP
Downgra~~~~~~ 3-year
interva~~~~~~ssified
12 y~~~

## NATIONAL AERONAUTICS AND SPACE ADMINISTRATION

## MANNED SPACECRAFT CENTER

### Houston, Texas
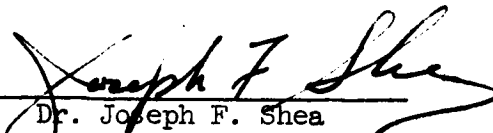
### November 13, 1963

POSTLAUNCH MEMORANDUM REPORT

FOR

APOLLO PAD ABORT I

[U]

APPROVED FOR DISTRIBUTION BY:

Dr. Joseph F. Shea
Manager, Apollo Program Office

NATIONAL AERONAUTICS AND SPACE ADMINISTRATION

MANNED SPACECRAFT CENTER

HOUSTON, TEXAS

November 13, 1963

CONTENTS

~~CONFIDENTIAL~~

Section                                                                                                                                                                                    Page

Apollo Pad Abort I

## 1.0 SUMMARY

### 1.1 Overall Mission Evaluation

The Apollo Pad Abort 1 mission was scheduled to be launched at 9:00 a.m. m.s.t. on November 7, 1963, at White Sands Missile Range, New Mexico. The launch officially occurred at 9:00:01.105 a.m. m.s.t., and was a complete success. The vehicle performance was, in general, as predicted with no significant malfunctions. Personnel supporting the mission representing White Sands Missile Range, Manned Spacecraft Center, North American Aviation, and other contractor personnel performed their assigned tasks at a high degree of competence. Based on preliminary analysis of data, all primary and secondary mission objectives were satisfied.

### 1.2 Test Objectives Evaluation

1.2.1 First order objectives.- All first-order objectives were considered satisfied. Following are the first-order objectives with brief comments on each.

(a) Determine aerodynamic stability characteristics of the Apollo escape configuration during a pad abort. Comment: The Apollo escape configuration was stable during the pad-abort flight. Indications are, however, that the vehicle stability was less than predicted during the powered phase of flight.

(b) Demonstrate the capability of the escape system to propel a command module to a safe distance from a launch vehicle during a pad abort. Comment: The command module at apogee exceeded the minimum altitude and range for a pad abort by approximately 970 feet and 1,525 feet, respectively.

(c) Demonstrate launch-escape timing sequence. Comment: The launch-escape timing sequence was demonstrated to be adequate for a pad-abort mission.

(d) Demonstrate proper operation of the launch-escape tower release device. Comment: The escape-tower released cleanly and at the proper time with little effect on spacecraft motions.

(e) Demonstrate proper operation of the tower jettison and pitch-control motors. Comment: The pitch-control motor produced the predicted initial spacecraft motions, even though the peak chamber-pressure value was slightly lower than predicted. The tower-jettison motor satisfactorily jettisoned the tower.

~~CONFIDENTIAL~~

(f) Demonstrate earth-landing timing sequence and proper operation of the parachute subsystem of the earth-landing system. Comment: The earth-landing timing sequence was demonstrated to be adequate for a pad-abort mission. The parachute subsystem performed as required, resulting in a descent velocity of approximately 24 feet per second at a 5,000-foot altitude, mean sea level. This is approximately the velocity predicted at this altitude.

1.2.2     Second-order test objectives.- All second-order test objectives were considered satisfied. Following are the second-order test objectives with brief comments on each.

(a) Determine dynamics of command module during jettisoning of escape tower. Comment: The dynamics of the command module were determined during jettisoning of the escape tower. The data indicate little effect of jettisoning the tower on the command module dynamics.

(b) Demonstrate operation of research and development instrumentation and communications equipment to be used on subsequent flights. Comment: The operation of the research and development instrumentation and communications equipment was demonstrated to be acceptable for subsequent flights.

(c) Demonstrate compatibility of prototype handling ground support equipment (GSE). Comment: The handling GSE utilized during boilerplate 6 preparation for flight was considered adequate, although many modifications were required during the field test.

(d) Determine initial separation trajectory of the launch-escape tower. Comment: The initial separation trajectory of the launch-escape tower was determined and preliminary analysis indicated that no problem existed during this phase.

(e) Determine escape-tower vibration during pad abort. Comment: Escape-tower vibrations were obtained and a preliminary investigation of the data indicated that the results are approximately as was predicted.

1.3   Problems

The most significant problem disclosed during the postflight investigation of the Pad Abort 1 mission was the rocket exhaust particles impinging on the command module.

This impingement resulted in soot deposits, the significance of which will be the subject of future study.

~~CONFIDENTIAL~~

## 2.0 INTRODUCTION

### 2.1 General

The Apollo Pad Abort 1 Mission was planned to demonstrate the capability of the Apollo spacecraft to abort from the launching pad and to recover the spacecraft crew. To perform this mission, Apollo boilerplate 6 was manufactured by North American Aviation, Downey, California, and was delivered to White Sands Missile Range, New Mexico, on July 1, 1963. Complete systems tests were performed on the vehicle at White Sands Missile Range (WSMR) prior to launch operations on November 7, 1963. This test was the first flight test of an Apollo vehicle.

Appendix A1.0 contains a brief history of the spacecraft. Details of the launch operations may be found in appendix A2.0.

### 2.2 Test Objectives

The test objectives for this test were as follows:

First-order test objectives

(1) Determine aerodynamic stability characteristics of the Apollo escape configuration during a pad abort.

(2) Demonstrate the capability of the escape system to propel a command module to a safe distance from a launch vehicle during a pad abort.

(3) Demonstrate launch-escape timing sequence.

(4) Demonstrate proper operation of the launch-escape tower-release device.

(5) Demonstrate proper operation of the tower-jettison and pitch-control motors.

(6) Demonstrate earth-landing timing sequence and proper operation of the parachute subsystem of the earth-landing system.

Second-order test objectives

(1) Determine dynamics of the command module during jettisoning of the escape tower.

(2) Demonstrate operation of research and development instrumenta-
tion and communications equipment to be used on subsequent
flights.

(3) Demonstrate compatibility of prototype ground support equip-
ment.

(4) Determine initial separation trajectory of the launch-escape
tower.

(5) Determine escape-tower vibration during a pad abort.

## 3.0  DESCRIPTION OF THE MISSION

Mission launch was initiated on November 7, 1963 at 9:00:01.105 a.m. m.s.t., when a ground-command abort signal was transmitted to the command module via hard line. The signal activated the abort relay in the launch-escape-system sequencer, which in turn sent a signal to ignite the launch-escape and pitch-control motors. These motors ignited nearly simultaneously and lifted the command module along a planned trajectory. After 15.6 seconds, a signal was sent from the launch-escape-system sequencer to ignite the escape-tower release bolts which simultaneously ignited the tower-jettison motor which separated the launch-escape tower from the command module. The signal also armed the earth-landing-system sequencer.

The drogue parachute of the command module was deployed at 18.6 seconds after launch. The drogue parachute aided in orienting the command module to the attitude required for pilot parachute deployment, which occurred at 24.0 seconds, and simultaneously released the drogue parachute. The pilot parachutes extracted the main parachutes from their bags. Main parachutes line stretch occurred at 26.1 seconds, disreef occurred at 32.3 seconds, and full open occurred at 35.0 seconds. All three main parachutes disreefed simultaneously with little or no aerodynamic interference.

The launch-escape tower followed a ballistic trajectory and impacted at 43.7 seconds.

The command module followed a normal parachute descent at a velocity of 24 feet per second. Landing of the command module occurred at 165.1 seconds.

## 4.0 TEST VEHICLE DESCRIPTION

### 4.1 Spacecraft Description

Apollo boilerplate 6 consisted of two major components, the command module and the launch-escape system (see fig. 4.1-1). These components are similar to the production Apollo vehicle in shape, size, and function and are further defined in the following sections. The reference axis system used throughout this report is presented in figure 4.1-2.

4.1 1    Launch escape system.- The general launch-escape system structure consisted of the following major structures and subsystems.

    (1)  Tower structure

    (2)  Launch-escape motor

    (3)  Pitch-control motor

    (4)  Tower-jettison motor

    (5)  Tower-release mechanism

4.1.1.1    Tower structure:- The launch-escape tower was constructed of welded tubular titanium alloy. At the top of the tower, a skirt was provided to mount the launch-escape motor. At the bottom, four explosive bolts attached the tower to the command module.

4.1.1.2    Launch-escape motor:- The launch-escape motor was used to provide the vertical displacement during an abort. This motor was a solid-propellant motor with 4 nozzles nominally canted 35°. The escape-rocket resultant thrust vector was required to be approximately 2.5° with the spacecraft centerline. The escape motor was ignited by a pyrogen type ignitor which utilized two exploding bridgewire initiators.

4.1.1.3    Pitch-control motor:- The pitch-control motor was a solid-propellant motor which was used to produce the spacecraft pitch rate required to obtain lateral displacement during an abort. Ignition was similar to that of the launch-escape motor.

4.1.1.4    Tower-jettison motor:- The tower-jettison motor was used to jettison the escape tower from the command module. This

motor was a solid-propellant motor with two nozzles canted 30° from the motor centerline. The resultant thrust axis of this motor is nominally 2.5° from the motor centerline. Ignition was similar to that of the launch-escape motor.

4.1.1.5    Tower-release mechanism:- The tower-release mechanism provided for release of the escape tower when tower jettison was required. The tower-release mechanism consisted of four explosive bolts each containing a single explosive charge with dual ignition capability. Positive release of the tower will occur when either or both of the hot wire initiators are fired. Normally, both initiators are fired.

4.1.2     Command module.- The command module of boilerplate construction consisted of the following major structures and subsystems:

(1)   Module structure

(2)   Launch-escape-system sequencer

(3)   Electrical-power system

(4)   Onboard-instrumentation system

(5)   Earth-landing system

The command module subsystems are shown in figure 4.1.2-1.

4.1.2.1    Command module structure:- The command module structure was constructed of aluminum alloy skin. There were four main longerons which were attached to the launch-escape tower. Several secondary longerons were utilized for load transfer from the forward bulkhead to the vehicle midring. The inner and center skin of the aft heat shield were resin-impregnated glass laminations.

4.1.2.2    Launch-escape-system sequencer:- The launch-escape-system sequencer controlled launch-escape and pitch-control-motor ignition, tower-jettison-motor ignition, tower separation, and initiation of the earth-landing-system sequencer.

4.1.2.3    Electrical-power system:- The electrical-power system consisted of one 1,500 watt-hour and two 140 watt-hour Eagle Picher silver-zinc batteries. The 1,500 watt-hour battery was connected to the instrumentation buses and the two 140 watt-hour batteries were connected to separate pyrotechnic busses.

4.1.2.4    Onboard instrumentation system:- The onboard instrumentation system consisted of one telemetry system and a tape recorder for acquiring inflight data.

4.1.2.5    Earth-landing system:- The earth-landing system consisted of pyrotechnics, one conical ribbon drogue parachute, three ring-sail main parachutes, three pilot parachutes, and a sequencer. The sequencer consisted of relays, dummy baroswitches, and timing devices.

## 4.2 Weight and Balance

Final weight and balance numbers of boilerplate 6 are listed in table 4.2-1. The axis system referred to in this table is presented in figure 4.1-2.

## 4.3 Test Setup

The command module with escape tower attached was mounted in a vertical position on three bearing points of a pad adapter. A photograph of the test setup is shown in figure 4.3-1. The adapter was attached to a concrete pad. There were no attachments between the command module and the adapter. An umbilical was connected to the forward heat shield of the command module to allow for application of external power to the vehicle, monitoring of systems within the command module, and transmission of external signals into the command-module sequencer.

TABLE 4.2-1.- WEIGHT AND BALANCE DATA

| Condition | Weight, lb | Center-of-gravity location, in. | | | Moments of inertia, slug-ft$^2$ | | |
|---|---|---|---|---|---|---|---|
| | | $^a$X | Y | Z | $I_{xx}$ Roll | $I_{yy}$ Pitch | $I_{zz}$ Yaw |
| Total spacecraft at launch | 15,822.05 | 1,152.75 | 0.33 | 4.29 | 5,289.1 | 70,184.8 | 70,091.8 |
| Accuracy (launch condition) | ±15.8 | ±0.21 | ±.06 | ±0.05 | | | |
| Spacecraft at launch-escape motor burnout | 12,619.15 | 1,116.35 | .41 | 5.38 | 5,203.9 | 51,064.3 | 50,937.3 |
| LES at jettison-motor burnout | 3,753.32 | 1,278.04 | -1.16 | 1.08 | 238.9 | 11,224.9 | 11,219.7 |
| Command module prior to drogue-parachute deployment | 8,659.03 | 1,039.58 | 1.10 | 7.37 | 4,939.9 | 4,012.4 | 3,906.9 |
| Command module after drogue-parachute deployment | 8,631.03 | 1,039.40 | 1.10 | 7.50 | 4,929.1 | 3,991.0 | 3,890.3 |
| Command module at landing | 8,231.25 | 1,136.95 | 1.11 | 7.56 | 4,885.6 | 3,721.6 | 3,601.5 |

$^a$The base of command module is 998.7 in. above reference plane.

Command module

Forward face of
forward bulkhead

77 rad

-1.3

$X_a$ 1000
$X_c$ = 0

c.g. burnout

c.g. CM only

84.05

$X_a$ 1082.75

Launch escape tower

Resultant thrust
vector

c.g. gross

48.8 dia

2.5°

35°

33.50

Section A-A

33.50

A      A

$X_a$ 1220.75

$X_a$ 1202.75

405.39 (Launch escape system)

26.00 dia (typ)

Aft end of exhaust hole

Launch escape motor

Split line
$X_a$ 1365.75

Tower jettison motor
$X_a$ 1367.75

Pitch control motor

$X_a$ 1416.17

$X_a$ 1434.35

Q-ball

$X_a$ 1463.33

$X_a$ 1488.14

Note   1.  All dimensions in inches unless otherwise noted.

2.  Tower structural members have been omitted.

Figure 4.1-1.- Boilerplate 6 configuration.

Head end looking toward feet

Left side looking toward right

Bottom
View looking forward

| Axis | | Moment about axis | | | Acceleration |
|---|---|---|---|---|---|
| Designation | Symbol | Designation | Symbol | Positive direction | Positive direction |
| Longitudinal | X | Rolling | L | Y→Z | +X |
| Lateral | Y | Pitching | M | Z→X | +Y |
| Normal | Z | Yawing | N | X→Y | +Z |

| Force symbol (Parallel to axis) | Angle | | Velocity | |
|---|---|---|---|---|
| | Designation | Symbol | Linear (component along axis) | Angular |
| X | Roll | $\phi$ | u | p |
| Y | Pitch | $\theta$ | v | q |
| Z | Yaw | $\psi$ | w | r |

Angle of attack, $\alpha$
Angle of sideslip, $\beta$

Vehicle orientation on launch pad

+Z axis, south
+Y axis, west
Pitch angle, $-90°$

Figure 4.1-2.- Reference axis system.

1. Main parachute cluster harness
2. Main parachute pack
3. Pilot mortar
4. Drogue mortar
5. Sequence controller
6. Forward compartment cover

Drogue chute guide assy

Dummy reaction control system pitch motor

Gyro assembly

Power control box

LES sequencer relay pkg (ref)

RF pkg telemetry

Battery

Modulation pkg telemetry

ELS sequencer relay pkg (ref)

Signal conditioner

Tape recorder

Antenna (4 places)

Transducers (40 places)

Amplifier racks (3 places)

Junction box

Battery

Timer
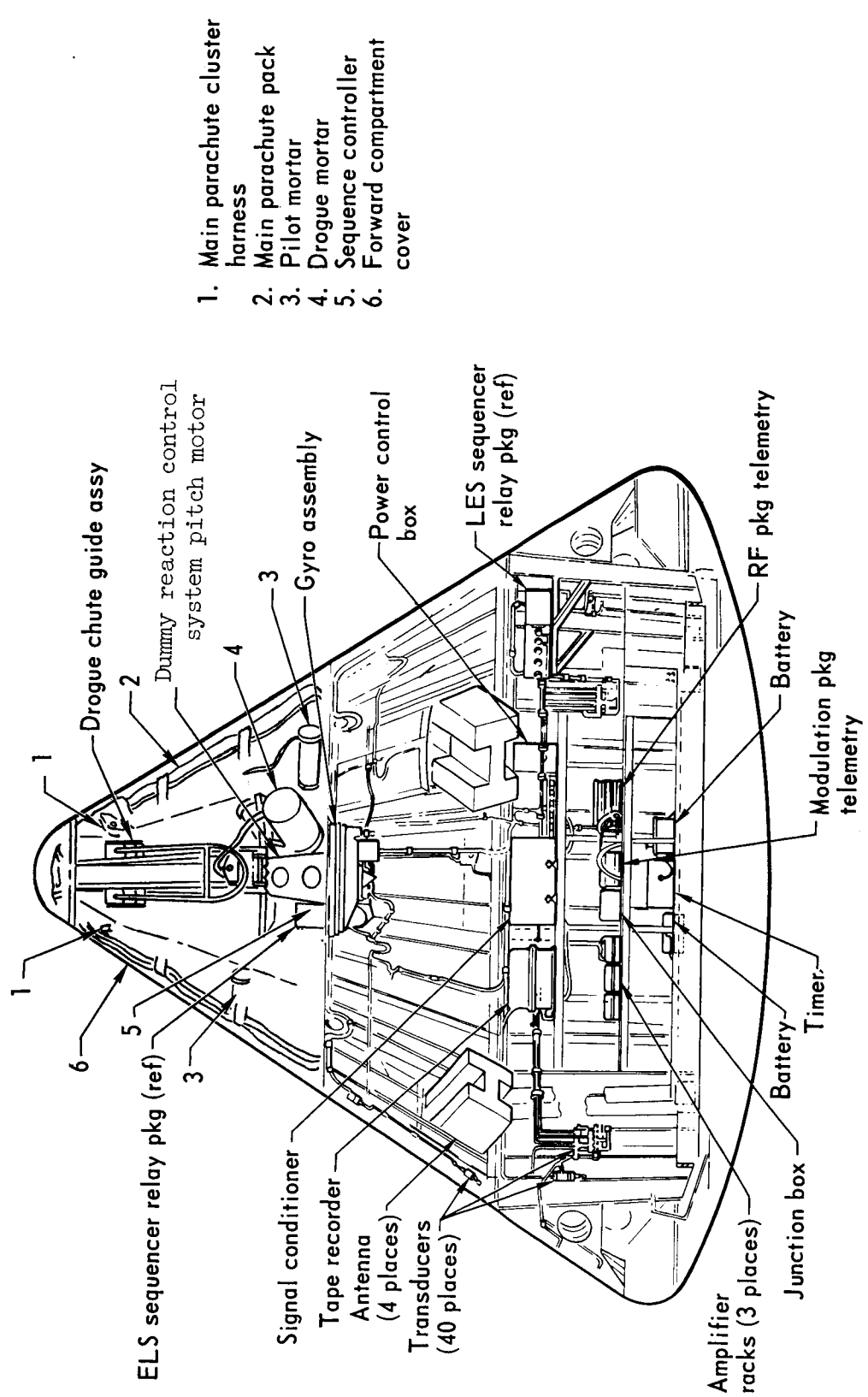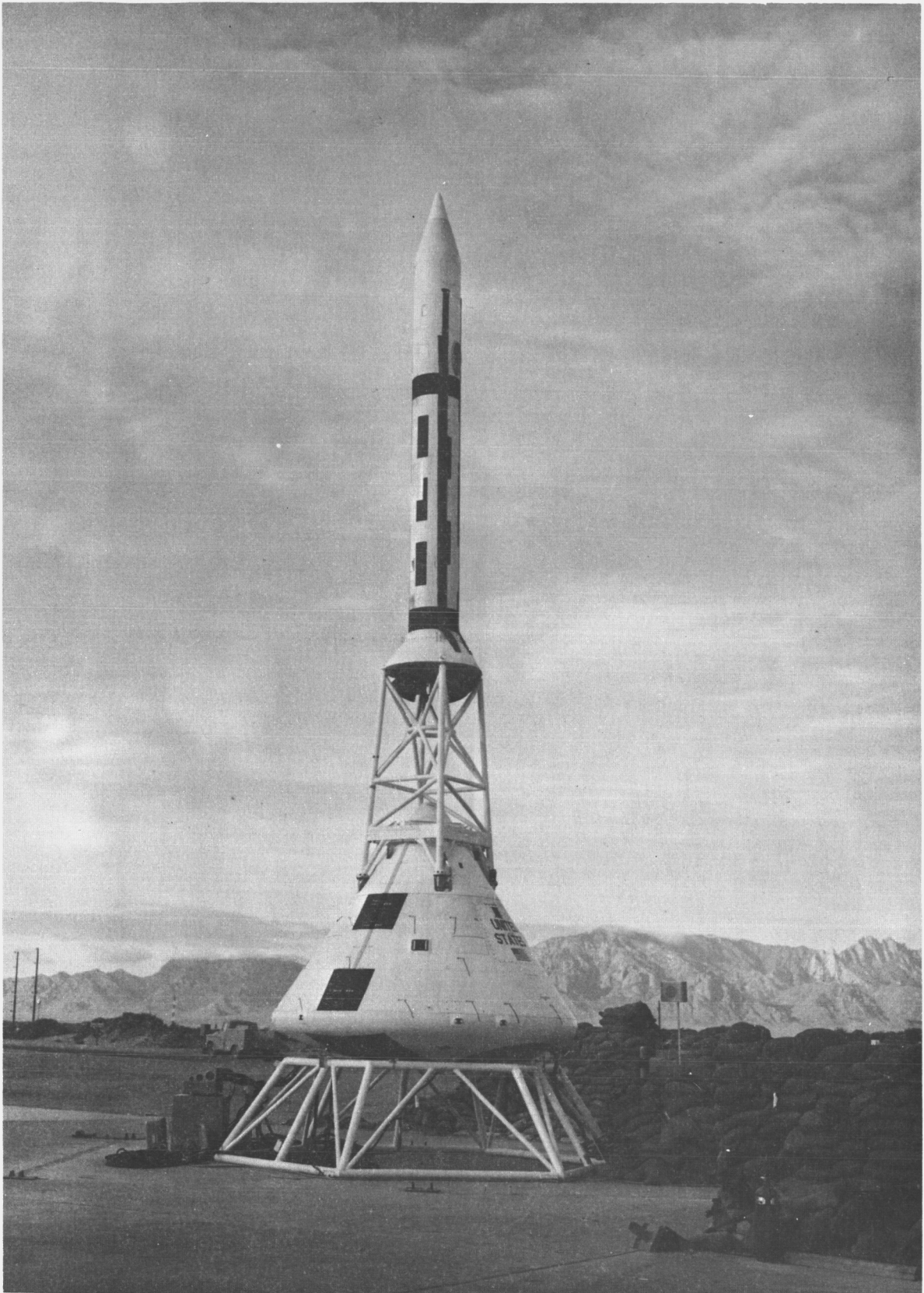
Figure 4.1.2-1.- Command Module equipment location.

Figure 4.3-1.- Test setup for Pad Abort-1 mission.

## 5.0  TRAJECTORY ANALYSIS

### 5.1  Flight Parameters

The flight parameters for the Pad Abort Test are given in
table 5.1-1.  Also included in this table are the times at which major
events occurred.  The columns headed by ACT give the actual results of
this flight as reduced from the phototheodolite cameras.  The columns
of figures headed by NOM give the results of a nominal no-wind trajec-
tory simulation.  This nominal trajectory is based on the weights data
given in table 4.2-1.

### 5.2  Trajectory

The ground track of the command module is shown in figure 5.2-1.
The average winds at the time of launch as shown in table 5.1-1 approx-
imate 15 knots.  These wind velocities are shown in figure 5.2-2.  Tra-
jectory simulated studies show that a wind of this magnitude produces
a deviation of approximately 2,500 feet in the landing of the command
module.  A trajectory simulation performed after the launch by using
near-launch winds showed a landing of the command module a few hundred
feet from the actual impact.  This deviation of landing from the nomi-
nal is almost entirely attributed to the wind effects on the command
module while it is on the parachutes.  The distance from the launch
pad to the projection of the command module on the surface of the earth
is tabulated as range in table 5.1-1.

The launch trajectory data shown in figure 5.2-3 compare the
actual flight with the nominal no-wind trajectory simulation.  The
actual flight data are reduced from data obtained from 5 Contraves
cinetheodolite sites.  The identification of these sites, and their
locations in a pad-centered coordinate system are given in figure 12.1-1.
The nominal, no-wind simulated trajectory curves in figure 5.2-3 are
based on a digital computer simulation by using the best available in-
formation on weight, balance, aerodynamics, and thrust.  The simulation
further used the 1959 ARDC atmosphere.  This atmosphere has been stated
by WSMR personnel as being fairly close to a nominal White Sands atmos-
phere.

The altitude at apogee in figure 5.2-3(a) is shown to be slightly
higher than in the no-wind simulation.  This increased altitude is an
expected result of the wind profile through which the vehicle flew be-
cause of a slight wind docking effect on the vehicle during the ascent.
Under full parachutes the rate of descent is very close to that assumed,
but the altitude at which the constant rate begins is 350 feet higher
than nominal.  After taking out the 100 feet of higher apogee, the

difference of 250 feet has to be a result of incorrect drag-time assumptions on the parachutes. This time difference is shown in table 5.1-1. Since the rate of descent started at a higher altitude, the time of landing, of course, was later. Trajectory simulations showed that tail winds also produced a lengthening of flight time and head winds produced a shorter time. By using the winds at time of the launch, trajectory simulation showed a landing at 163.4 seconds. Both figure 5.2-3 and the ground track shown in figure 5.2-1 show that the trajectory is very little affected by winds during powered flight. All parameters plotted in figure 5.2-3 show a small dependence on wind. However, as seen in figure 5.2-1, the landing of the command module is very dependent on the wind.

With reference to appendix A4.0 it may be seen that both Mach number and dynamic pressure are calculated by empirical formulas which use the true airspeed as input. True airspeed is defined as the difference between the velocity vector of a vehicle and the velocity vector of the wind. Figure 5.2-3(b) shows a true airspeed some 40 feet per second lower than nominal at apogee. This difference is caused by a 10-percent lower maximum thrust as shown in section 7.3.2-1. The other discrepancy is that of true airspeed between nominal and actual, occurring between 20 and 30 seconds. This is the result of an incorrect assumption of the parachute drag-time characteristics. The times at which the different parachute configurations were effective are shown in table 5.1-1.

The maximum Mach number was 0.05 lower than predicted; the maximum dynamic pressure was 80 lb/sq ft lower than predicted as shown in figures 5.2-3(c) and 5.2-3(d), respectively. These lower peaks were caused by a lower maximum airspeed as previously discussed. The secondary peaks are 0.02 and 15 lb/sq ft higher than nominal because of the higher airspeed at the time of the parachute deployment. These peaks occurred about 2 seconds earlier than nominal. This time is 26 seconds, the time at which the main parachutes reached full line stretch.

A comparison of the actual acceleration along the X-body axis with the acceleration in a nominal trajectory simulation is also shown in figure 5.2-3(e). The oscillations from 25 to 35 seconds resulted from the oscillations of the command module during the opening of the main parachutes as discussed in section 7.5. Figure 5.2-3(e) shows that the magnitude of the several peaks were much lower than the acceleration caused by the launch-escape motor.

The flight-path angle of the actual flight as shown in figure 5.2-3(f) was very close to the nominal until the drogue parachutes were deployed at 18.5 seconds. When the main parachutes reached the disreef condition, the flight-path angle showed a marked effect caused by the winds. Under full parachutes, the command-module had a descent rate of approximately

24 feet per second and as shown in figure 5.2-2, for most of the descent, a wind from the west southwest of about 20 feet per second was blowing. This produced a variable flight-path angle of -30° to -50°.

Figure 5.2-4 shows the altitude and range at apogee achieved by this vehicle to be 9,270 feet above mean sea level (msl) and 4,750 feet, respectively. Also shown in this figure is the range-altitude box which outlines the minimum Apollo requirements for a pad abort. These requirements are for the vehicle to achieve an apogee of 4,000 feet and a range of 3,000 feet under msl conditions. Based on an abort from WSMR which is 4,036 feet above msl, this box is at an altitude and range of approximately 8,300 feet above msl and 3,225 feet, respectively. This mission therefore exceeded the minimum requirements by 970 feet in altitude and 1,525 feet in range.

Subsequent work on this analysis will include trajectory simulations using the launch winds and the corrected values of thrust found during the test flight. A new atmosphere subroutine has been written for the 7094 digital computer simulation. Pressure and temperature data presented in figure 5.3-5 will be used for comparison of the 1959 ARDC atmosphere with the ambient atmosphere during the test.

## 5.3  Results

The vehicle exceeded the Apollo minimum altitude and range requirements for a pad abort by 970 feet and 1,525 feet, respectively. When the winds are taken into account, trajectory simulation predicted the test flight very well.
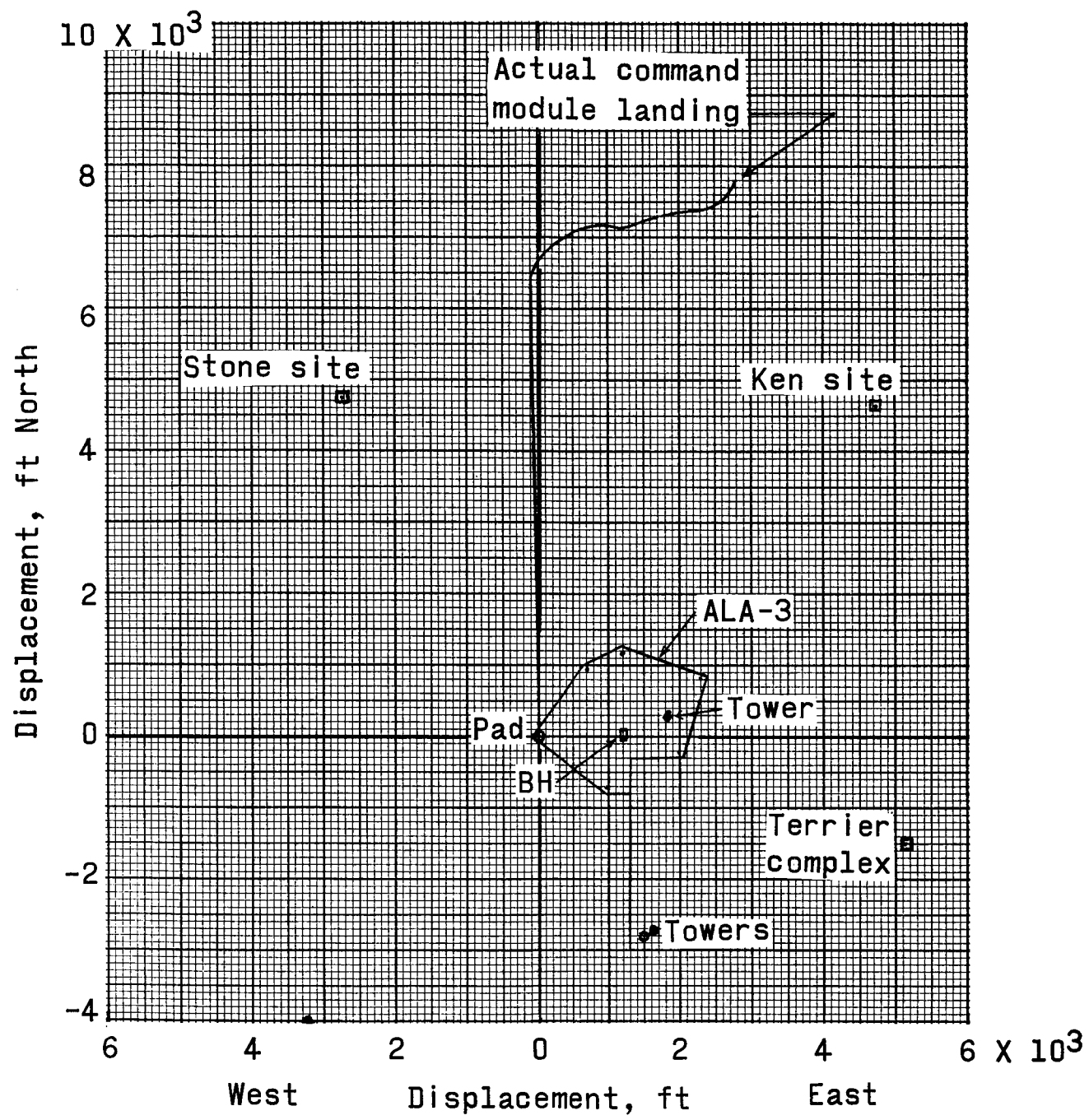
Figure 5.2-1.- Ground track for Command Module,
Pad Abort Test PA-1.
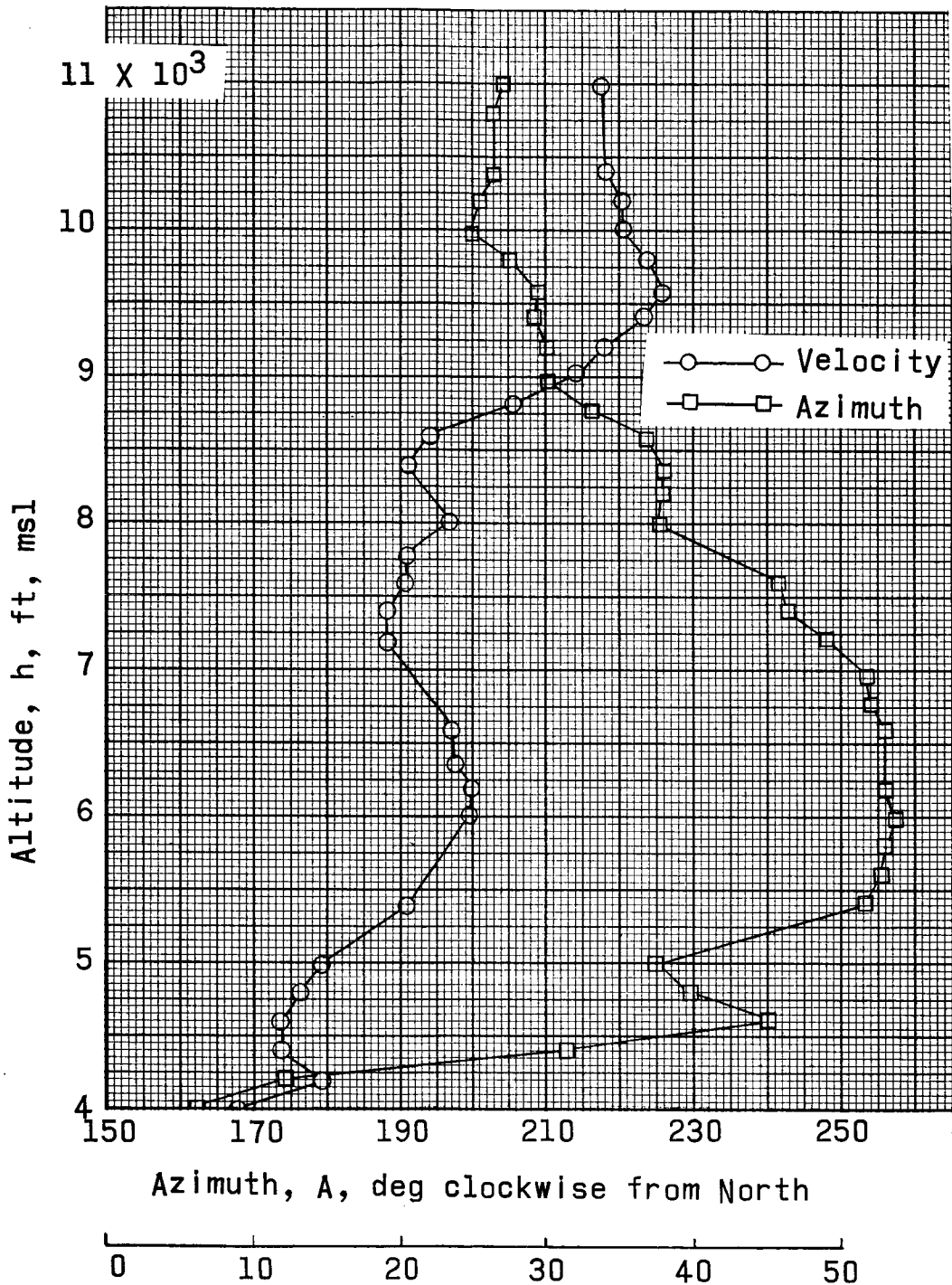
Figure 5.2-2.- Wind speed and azimuth plotted against altitude.
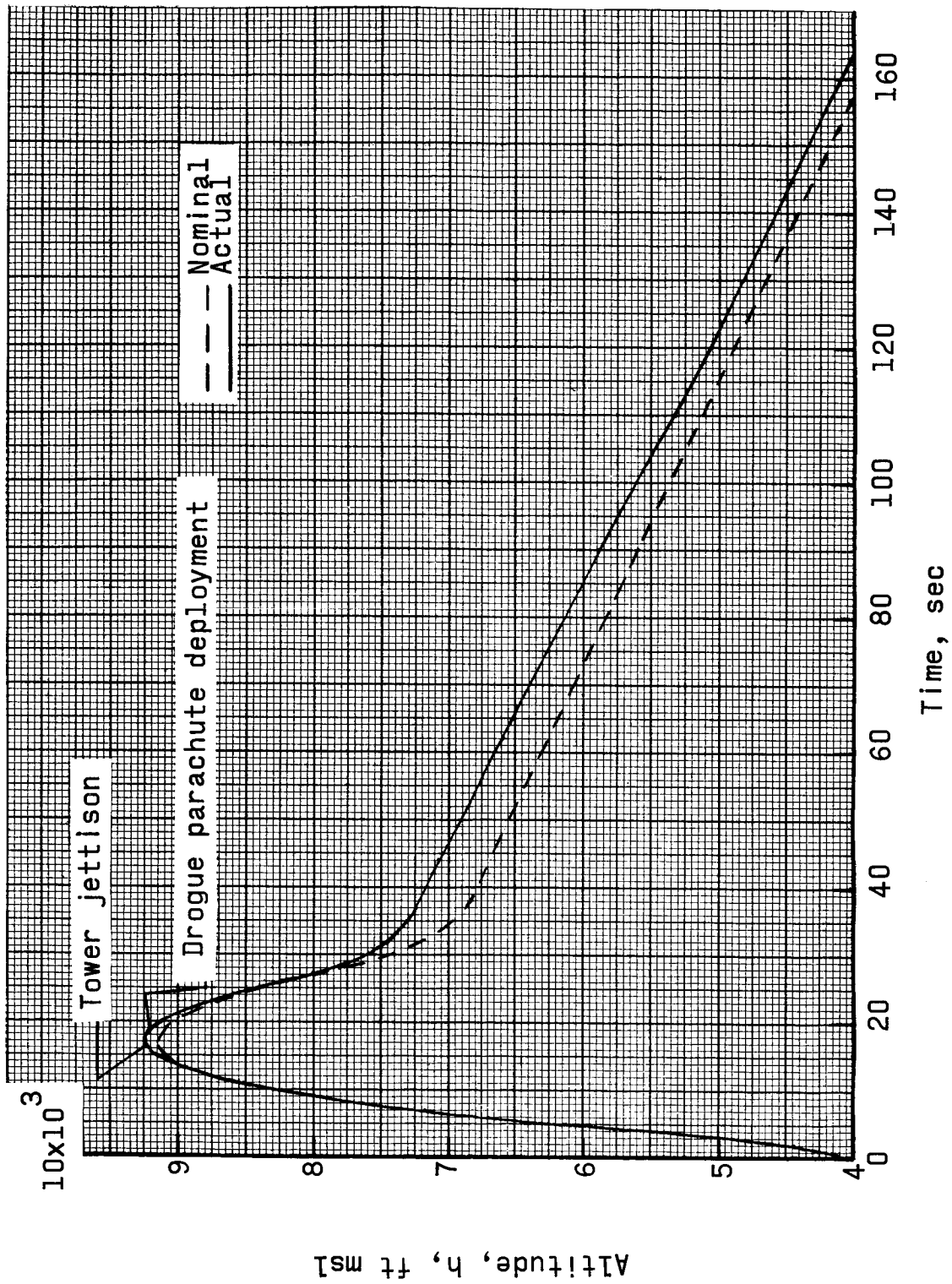
(a) Altitude plotted against time.

Figure 5.2-3. - Time histories of trajectory parameters for
Pad Abort Test PA-1.
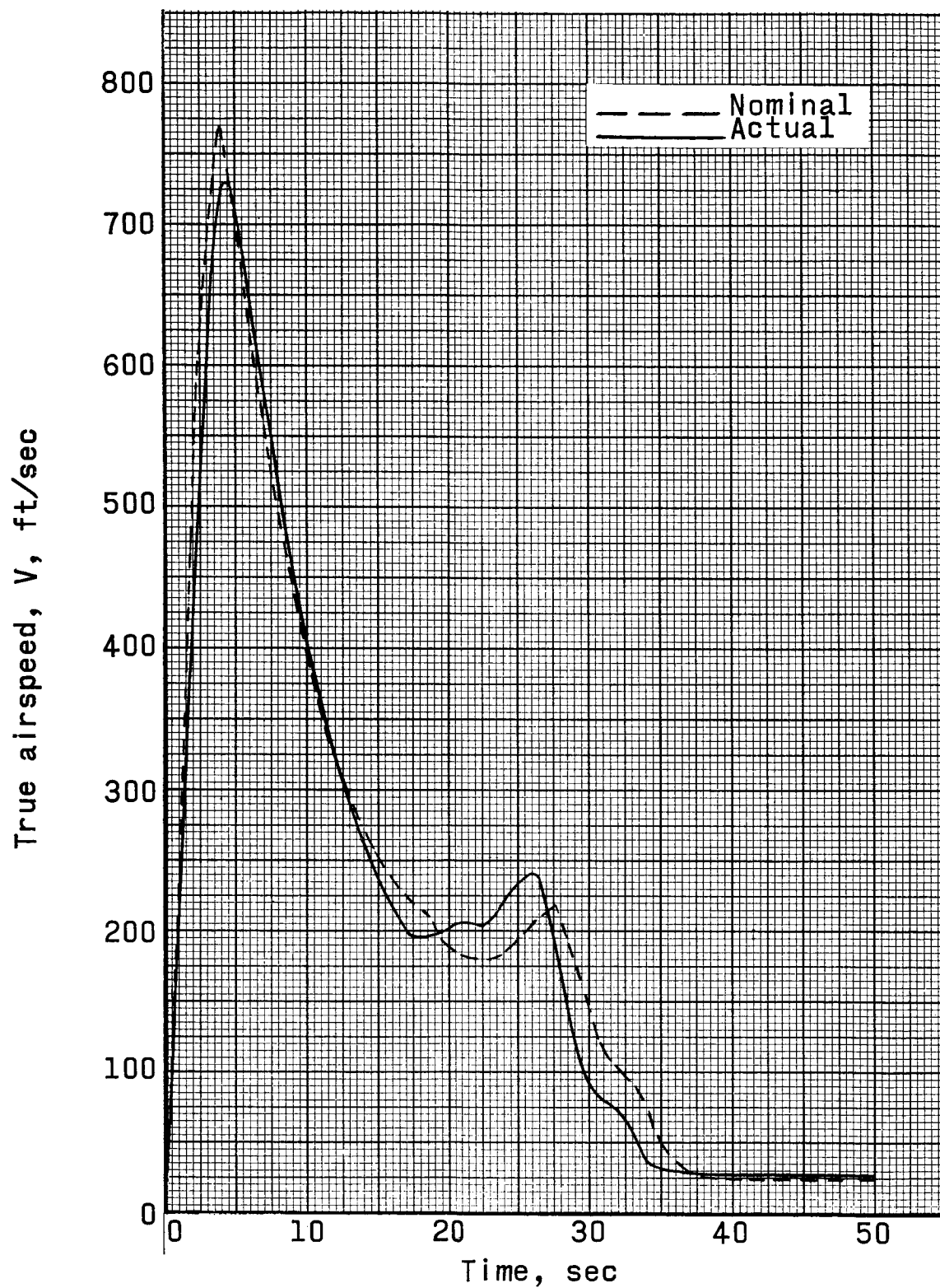
(b) True airspeed plotted against time.

Figure 5.2-3.- Continued.
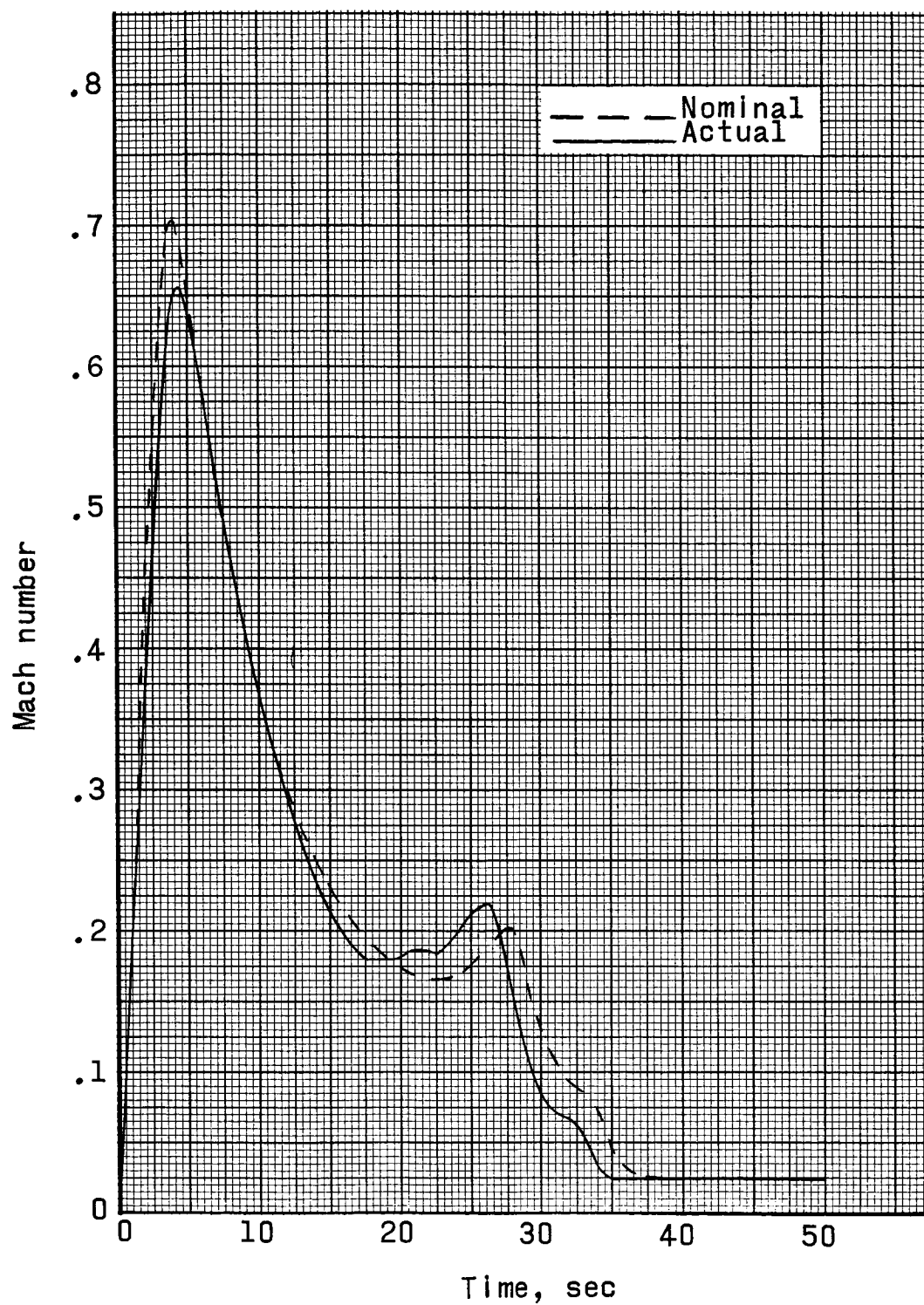
(c) Mach number plotted against time.

Figure 5.2-3.- Continued.
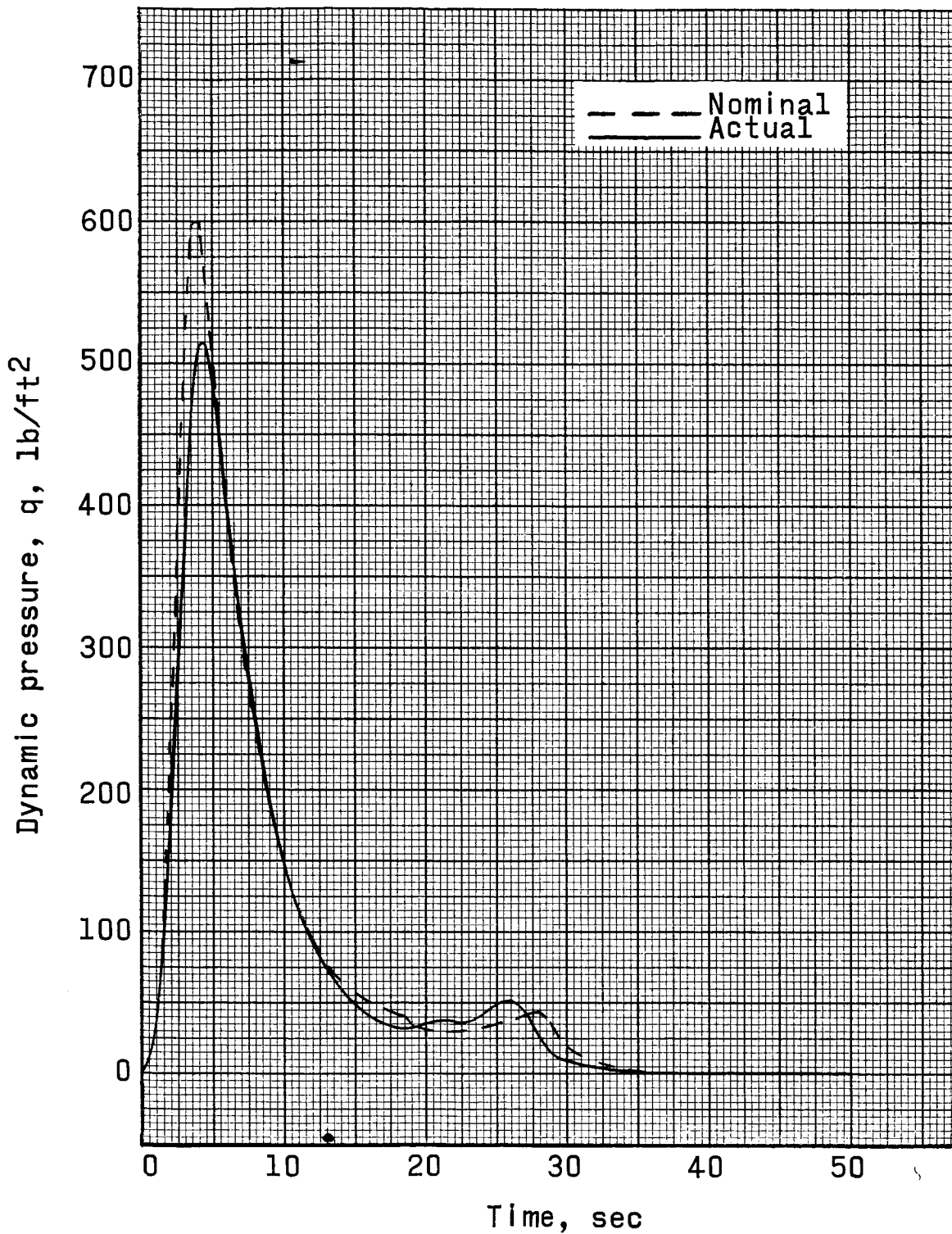
(d) Dynamic pressure plotted against time.

Figure 5.2-3.- Continued.

(e) Axial acceleration plotted against time.

Figure 5.2-3.- Continued.

(f) Flight-path angle plotted against time.

Figure 5.2-3.- Concluded.

Figure 5.2-4.- Altitude plotted against range for Pad Abort Test PA-1.

Figure 5.2-5.- Atmosphere temperature and pressure plotted against altitude.

## 6.0  STABILITY AND MOTION ANALYSIS

### 6.1  Introduction

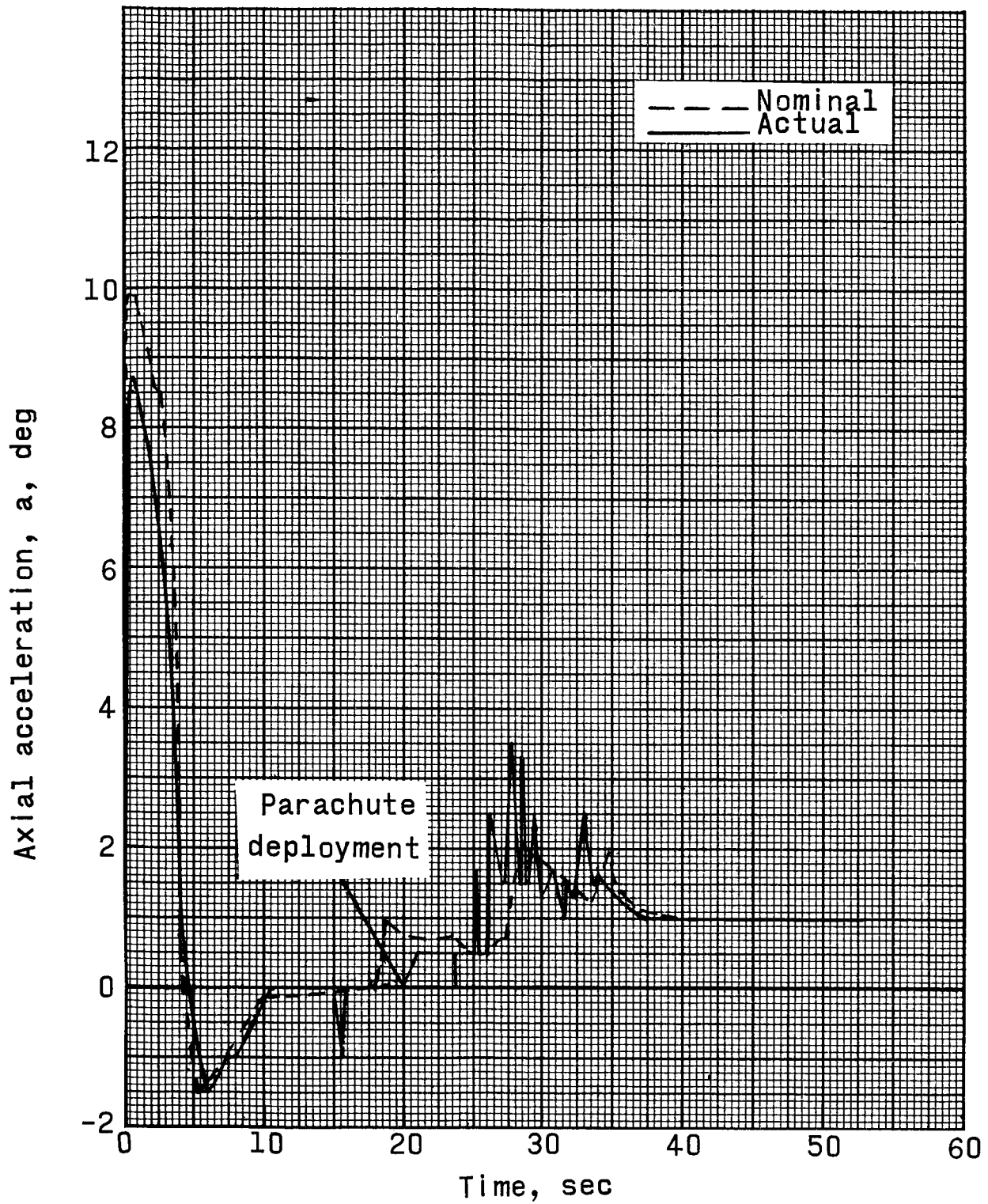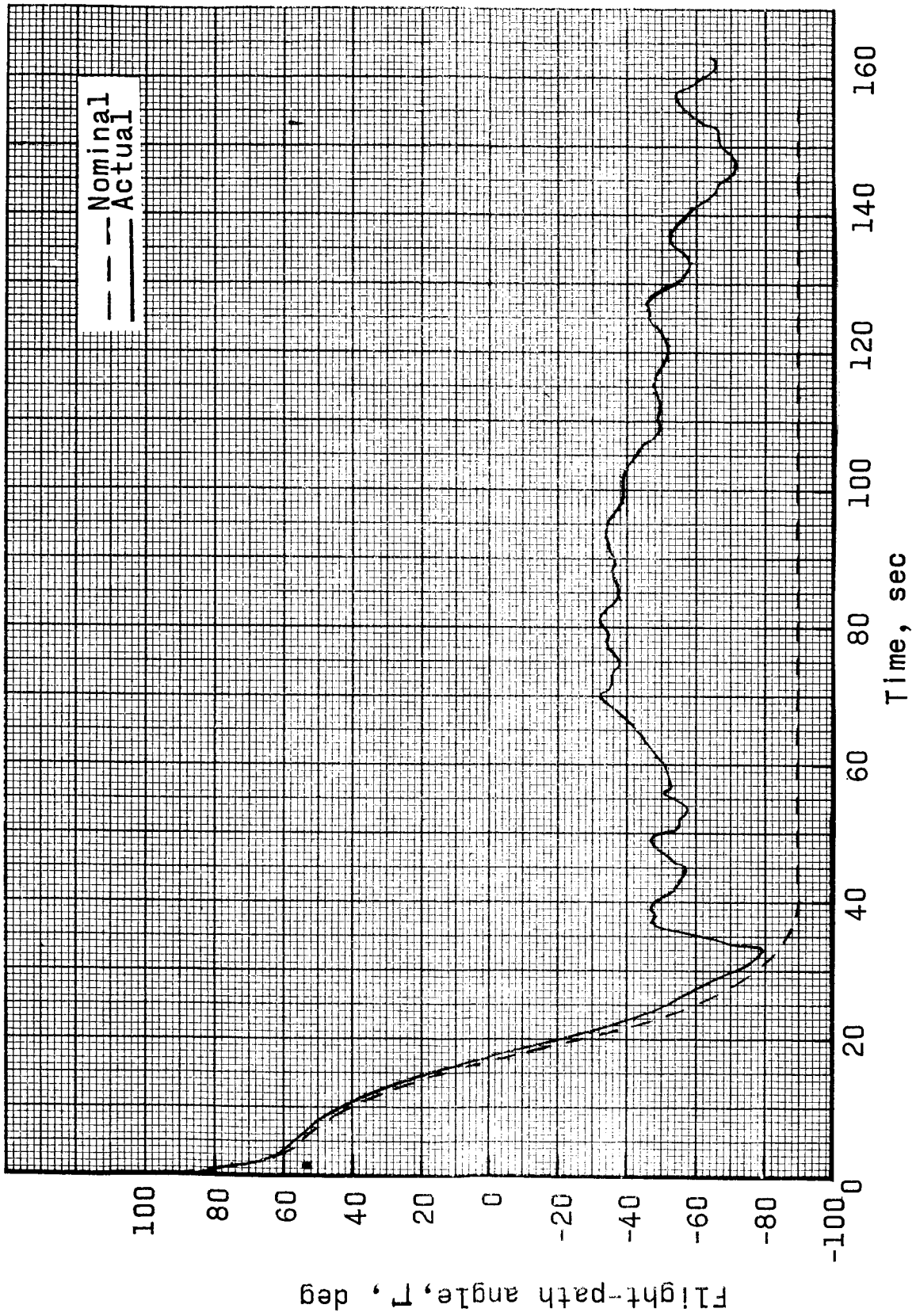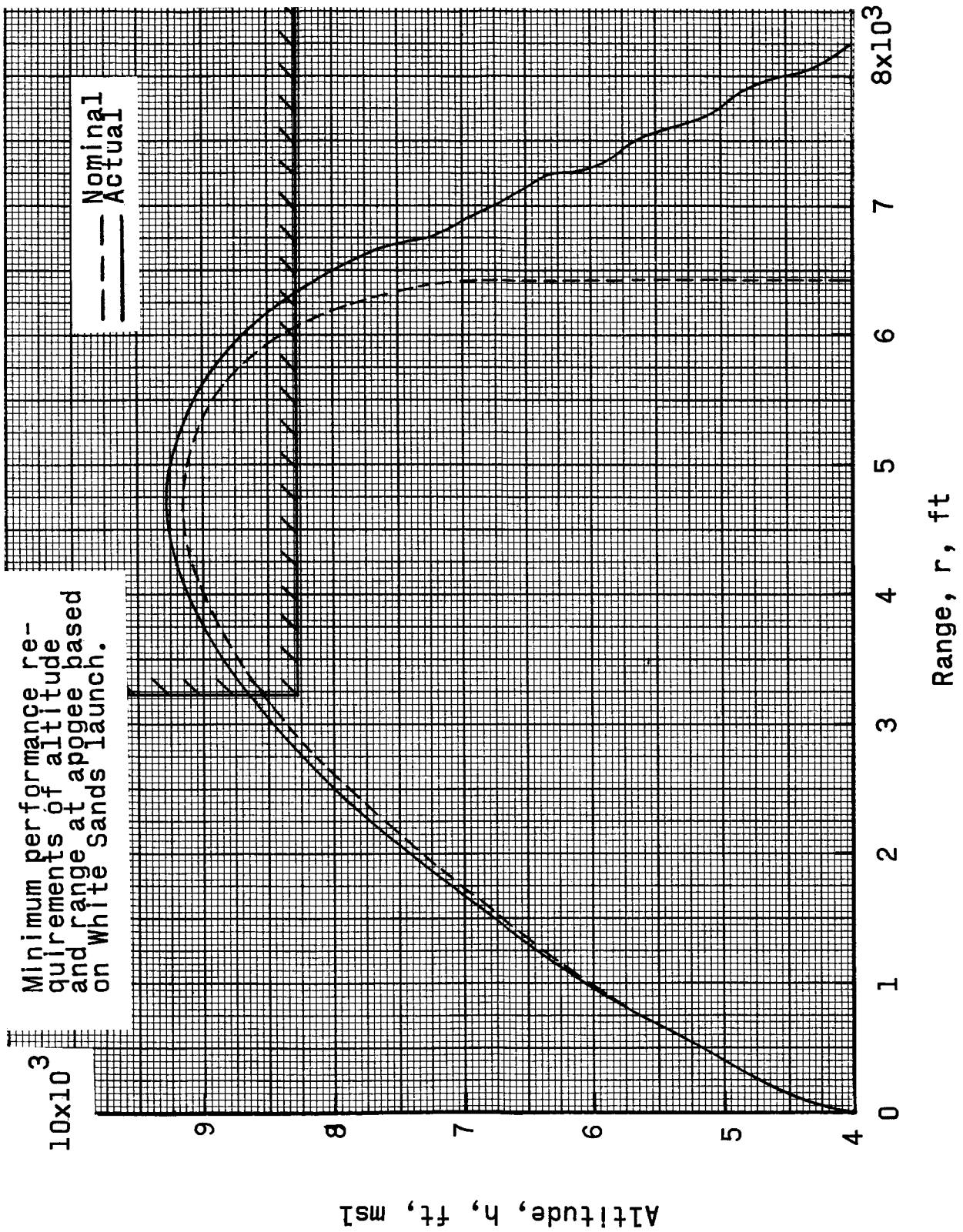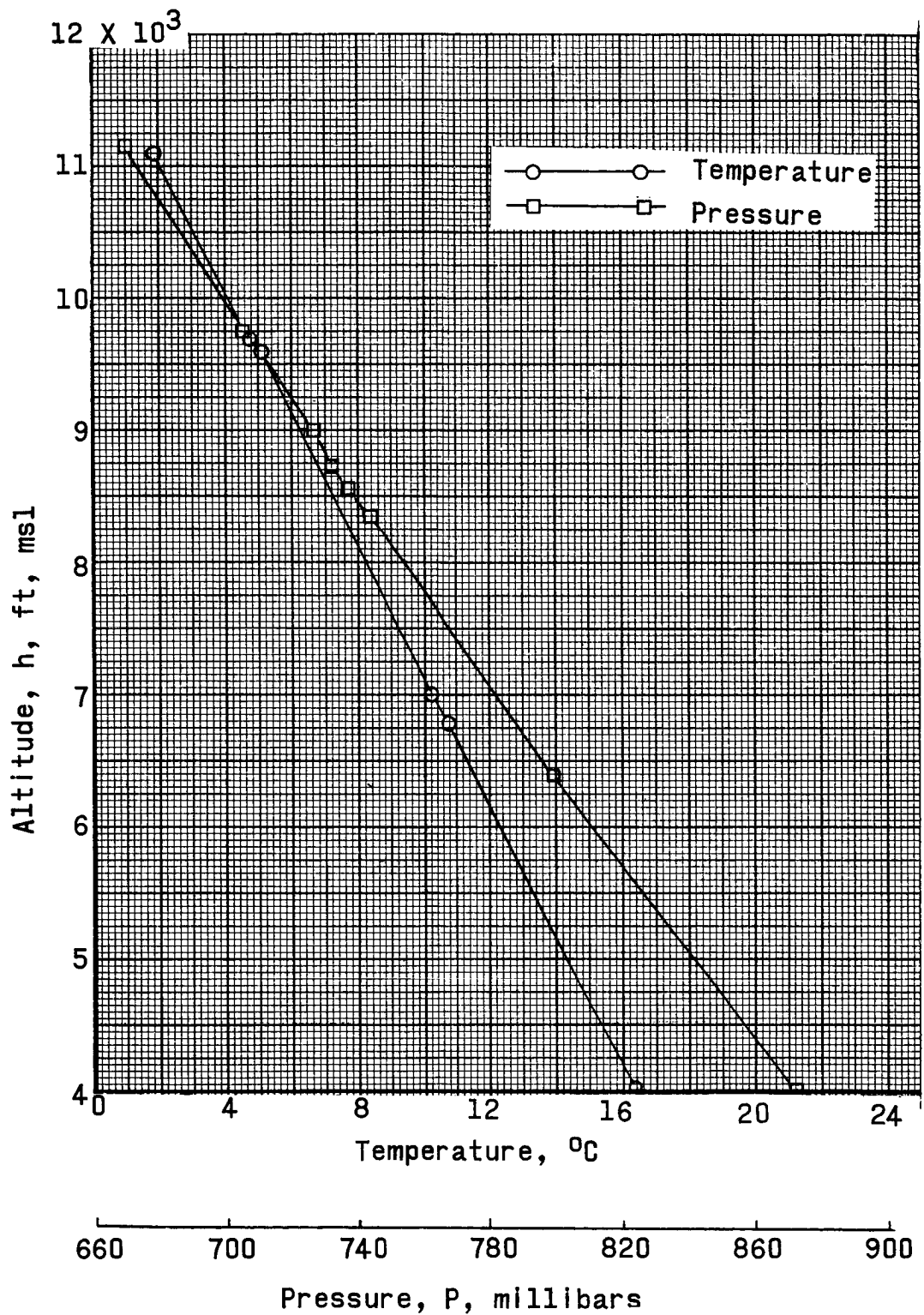The flight motions experienced during launch-escape vehicle flight resulted from a combination of many parameters. Off-nominal characteristics in any one of these parameters will have an effect on the motions which will result in a difference from predicted values. The primary factors affecting flight are aerodynamics, rocket-motor performance and thrust-vector alinement, weights, inertias, center-of-gravity location, and atmospheric characteristics.

The aerodynamic estimates used for the Pad Abort 1 flight motion predictions were obtained from results of wind-tunnel model testing. The effect of launch-escape motor burning on aerodynamic stability was derived from a model which decomposed hydrogen peroxide to simulate the rocket exhaust. Rocket-motor performance was based on the predicted boilerplate 6 motor characteristics presented in figures 7.3.2.1-1 and 7.3.2.2-1. The nominal launch-escape motor thrust-vector alinement presented in figure 8.3-1 was used in predictions of boilerplate 6 motion. Preflight estimates of weight, center of gravity, and inertias are presented in figures 8.2-1 to 8.2-6. Atmospheric properties are found in figure 6.1-1. Figure 4.1-2 defines the orientation and axes system of the launch-escape vehicle.

At abort initiation, the launch-escape motor and pitch motor are ignited. The pitch motor burns for 0.5 second and creates vehicle angular motion in the pitch plane. The purpose of the pitch motor on a pad abort is to change the vehicle's initial attitude so that the resulting trajectory achieves the minimum range and altitude requirements. These requirements are a 3,000-foot range and a 4,000-foot altitude at apogee for sea-level atmospheric conditions. The aerodynamic restoring loads are small during the first 1.0 to 1.5 seconds because of low dynamic pressure. After pitch-motor burnout, and prior to buildup of dynamic pressure, the moment from the launch-escape motor opposes the initial motion from the pitch motor. As dynamic pressure increases, a combination of launch-escape motor and aerodynamic moments overcome the initial pitch rate. An oscillatory motion is then established in the pitch plane as the vehicle seeks its aerodynamic trim point. Rocket motor misalinement in the Y and Z axes can result in undesired roll and yaw motions during the launch-escape vehicle flight.

### 6.2  Pitch Plane Motions

Angles of attack during the launch-escape vehicle flight were obtained by two independent methods (A and B) and the results compared with preflight predictions. Method A consisted of a comparison of flight-path

angle from phototheodolite data with the spacecraft attitude from the pitch-attitude gyroscope. This comparison is presented in figure 6.2-1. The angle of attack derived by this method is defined as the algebraic sum of the flight-path angle and the pitch-attitude angle. Method B used values of angle of attack calculated from differential pressure measurements at the escape-motor nose cone (Q-ball). Reduction of these Q-ball data involves dividing an incremental pressure reading from the Q-ball pressure taps by a calibration factor times the dynamic pressure $\frac{\Delta P}{Kq}$. This value $\frac{\Delta P}{Kq}$ is then used to obtain the angle of attack from calibration curves. During periods of low dynamic pressure, large errors in angle of attack can be obtained with small magnitude changes in input data. The angle of attack derived by method B is presented on an enlarged scale in figure 6.2-2 as it was obtained from the IBM Computer. It is also plotted in appendix A4-18. Data scatter is very obvious during the first 2 seconds of flight and also the last 3 seconds prior to tower jettison (time 12.5 to 15.5 sec.). The dynamic pressure was low during both these time intervals (fig. 5.2-2(c)) and the data scatter is due, in part, to this fact.

Figure 6.2-3 presents a comparison of angle of attack obtained by both methods A and B together with the preflight predictions. For this comparison, the Q-ball angle of attack has been arbitrairly offset 2° in the positive direction. This shift was made because the pressure used to compute the angle of attack was not corrected for the preflight signal bias. When the arbitrary shift was applied to the Q-ball angle of attack, results from methods A and B agreed well in amplitude and frequency through the first 12 seconds. After this time, dynamic pressure was below 100 lb/sq ft and Q-ball angle-of-attack accuracy was decreasing rapidly. The angle of attack during vehicle pitch oscillations is in agreement with the predicted nominal for the first positive peak (flight-measured value of 12° as opposed to the predicted value of 11°). However, the peak-to-peak value for the first cycle of angle of attack was 15.5° as opposed to 10.2°, predicted. The peak-to-peak magnitude for the next two cycles is also 15.5° compared to predicted values of 5.5° for the second cycle and 3.2° for the third cycle. The frequency of oscillation of angle of attack is lower than predicted — four cycles prior to tower jettison rather than five cycles. These trends indicate that the vehicle aerodynamic stability was somewhat lower than had been predicted. A positive statement to this effect cannot be made, however, until a detailed analysis is performed to isolate the aerodynamic coefficients from the other off-nominal contributing factors. These factors include the following:

(1) Launch-escape motor thrust level deviation.

(2) Center-of-gravity travel deviation.

(3)   Moments-of-inertia deviation.

(4)   Thrust-vector alinement detailed error analysis.

These factors are discussed in detail in the other sections of this report. They will be integrated into existing computer programs in an attempt to match the Pad Abort 1 launch-escape vehicle flight motions.  Long-term analysis planned subsequent to this report will allow derivation of actual flight aerodynamic coefficients.

## 6.3   Yaw Plane Motions

The launch-escape vehicle motions in the yaw plane were investigated in a manner similar to those in the pitch plane.  Because of a lack of instrument sensitivity for the low range of yaw angles experienced, few quantitative values can be derived at this time.  An attempt was made to correlate the yaw attitude gyroscope with the phototheodolite flight azimuth angle to obtain an angle of sideslip.  The yaw attitude gyroscope output was scattered between $\pm 7°$, but indicated that average yaw attitudes were low.  Inability to fair a smooth curve through the data scatter prevented direct comparison with flight azimuth to derive sideslip angles. The flight azimuth angle is presented in figure 6.3-1.  The low amplitude of the flight azimuth angle is also an indication of low sideslip angles.

The angle of sideslip obtained from IBM reduction of Q-ball differential pressures is presented in figure 6.3-2.  These data contain an initial preflight signal bias which was uncorrected.  The arbitrary shift such as that performed in the angle-of-attack analysis has not been performed for angle of sideslip since no comparison with alternate methods was made.  The Q-ball sideslip output exhibited scatter similar to that evidenced on the Q-ball angle-of-attack output.  Also similar is the indicated divergence of sideslip in the low dynamic-pressure region toward the end of launch-escape-vehicle flight.

## 6.4   Roll Motions

Roll attitude during launch-escape-vehicle flight presented in figure 6.4-1 was obtained from the roll-attitude gyroscope.  The spacecraft roll direction and amplitude are extremely sensitive to thrust-vector misalinement in the Y-Z plane.  Initial roll rate could be expected to be either positive or negative depending on the direction and magnitude of the thrust vector misalinement.  The low amount of roll experienced on Pad Abort 1 indicated that the lateral thrust-vector misalinement was small.

## 6.5 Results

The Pad Abort 1 launch-escape vehicle was stable, but the stability and motion differed somewhat from the preflight nominal predictions. Pitch-plane motions were damped less than predicted, and were lower in frequency. Indications are that the aerodynamic stability was lower than predicted. Several off-nominal factors during the flight must be investigated in more detail to confirm this prediction. Vehicle yaw motions were small, but could not be analyzed quantitatively with confidence. Roll motions were small, indicating small thrust-vector misalinement in the Y-Z plane. Long-term analysis of the flight results will allow determination of configuration aerodynamic coefficients.
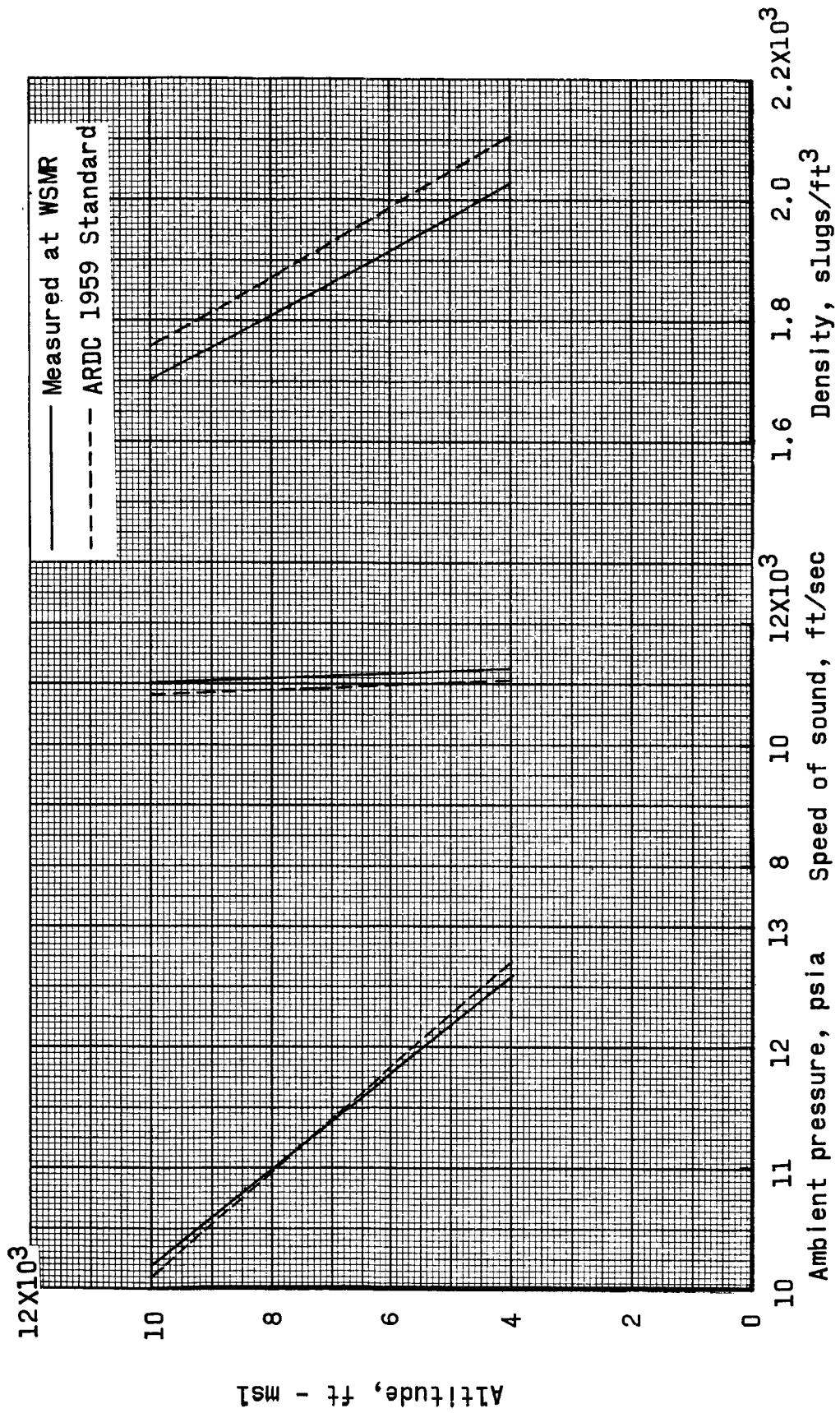
Figure 6.1-1.- Atmospheric properties during pad abort mission.
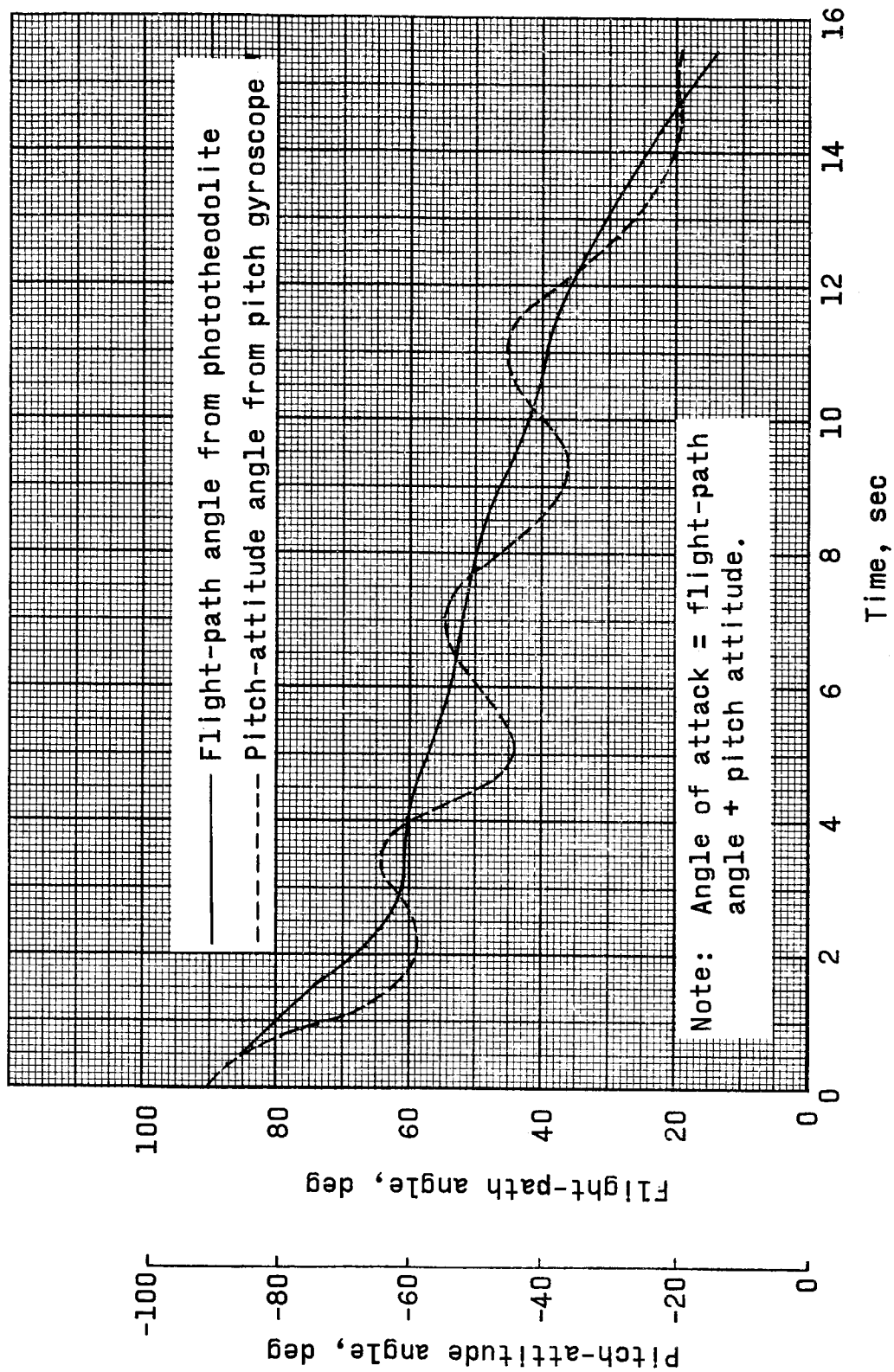
Figure 6.2-1.- Comparison of launch-escape vehicle flight path-
angle with pitch attitude to derive angle of attack. Method A.
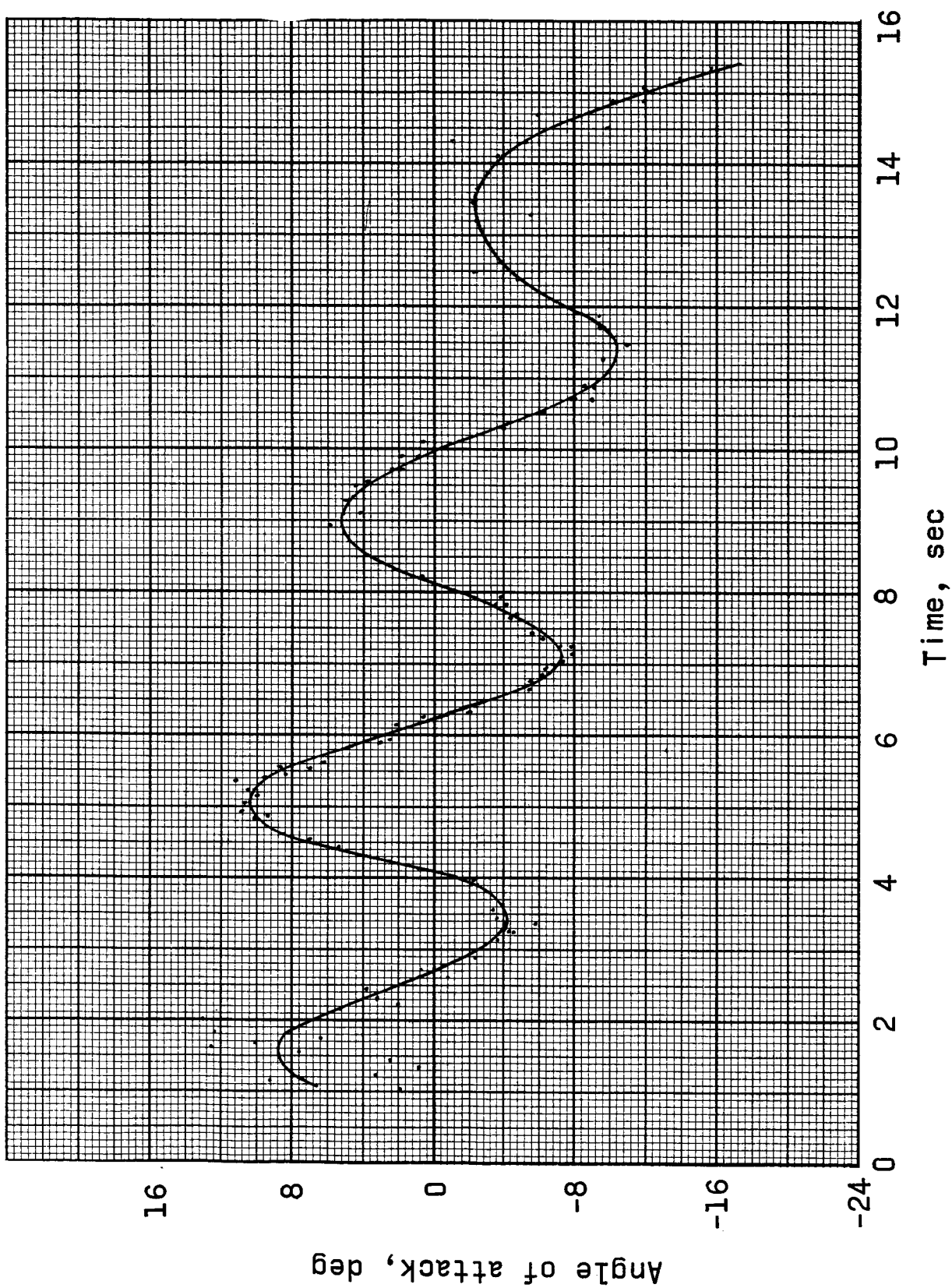
Figure 6.2-2.- Launch-escape vehicle angle of attack obtained from Q-Ball, Method B.

Photothedolite flight-path angle compared with pitch attitude gyroscope to derive angle of attack. Method A.

Predicted nominal angle of attack

Q-Ball angle of attack offset+2⁰ from IBM printout results. Method B.
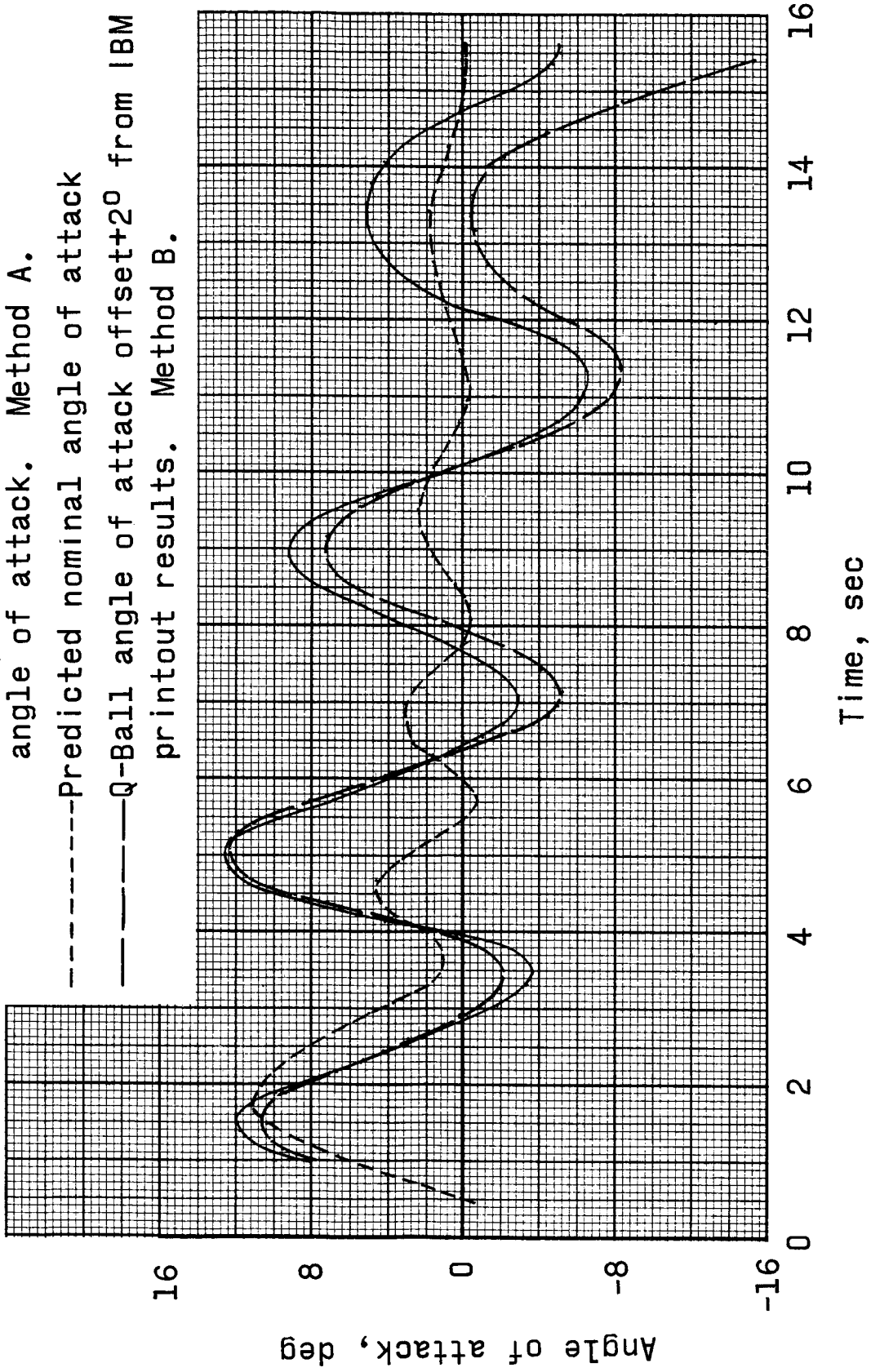
Figure 6.2-3.- Launch-escape vehicle angle of attack derived by methods A and B compared with predicted values.

Note: Low range yaw attitude gyroscope scatter did not allow comparison to derive angle of sideslip.
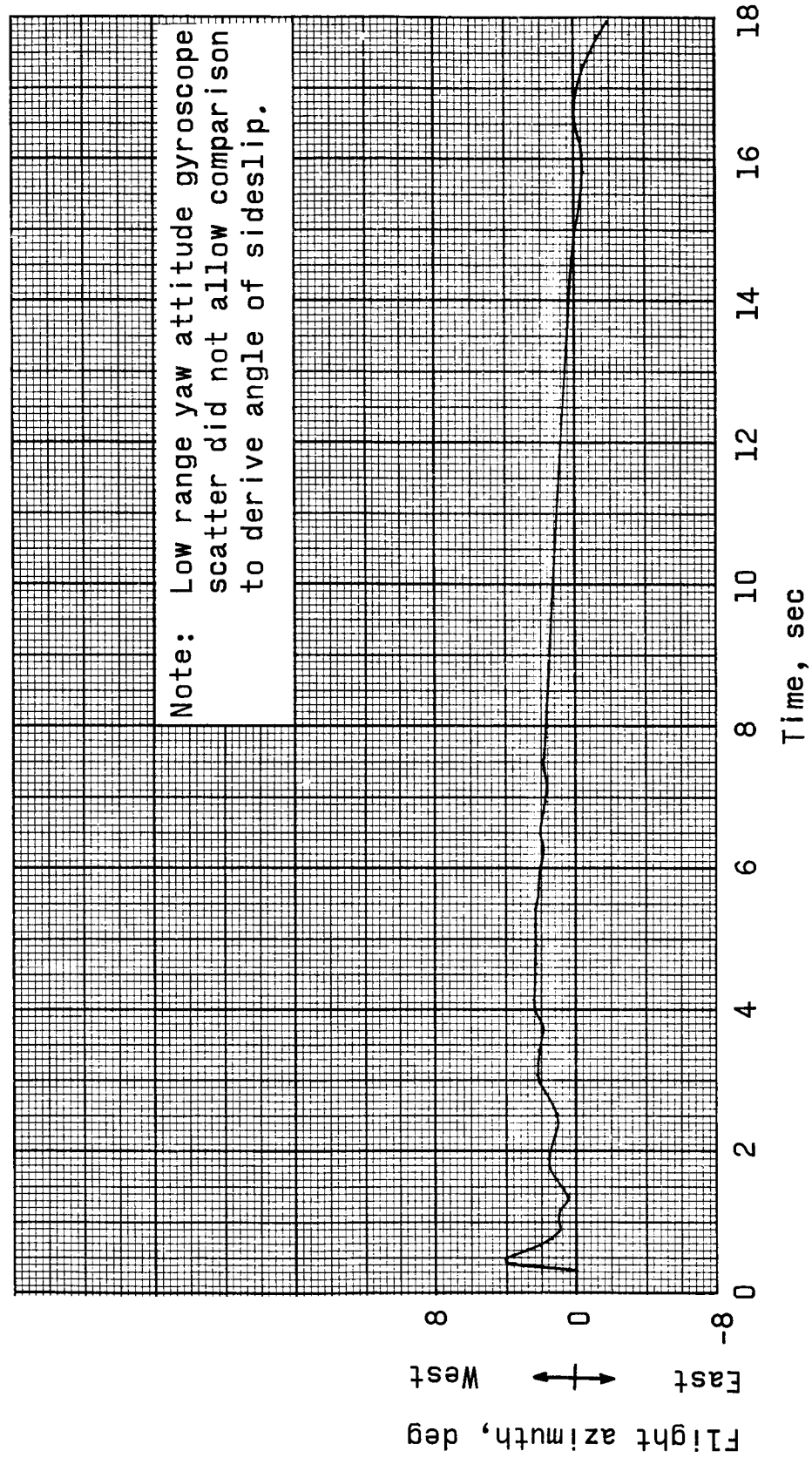
Figure 6.3-1.- Flight azimuth angle of launch escape vehicle plotted against time.
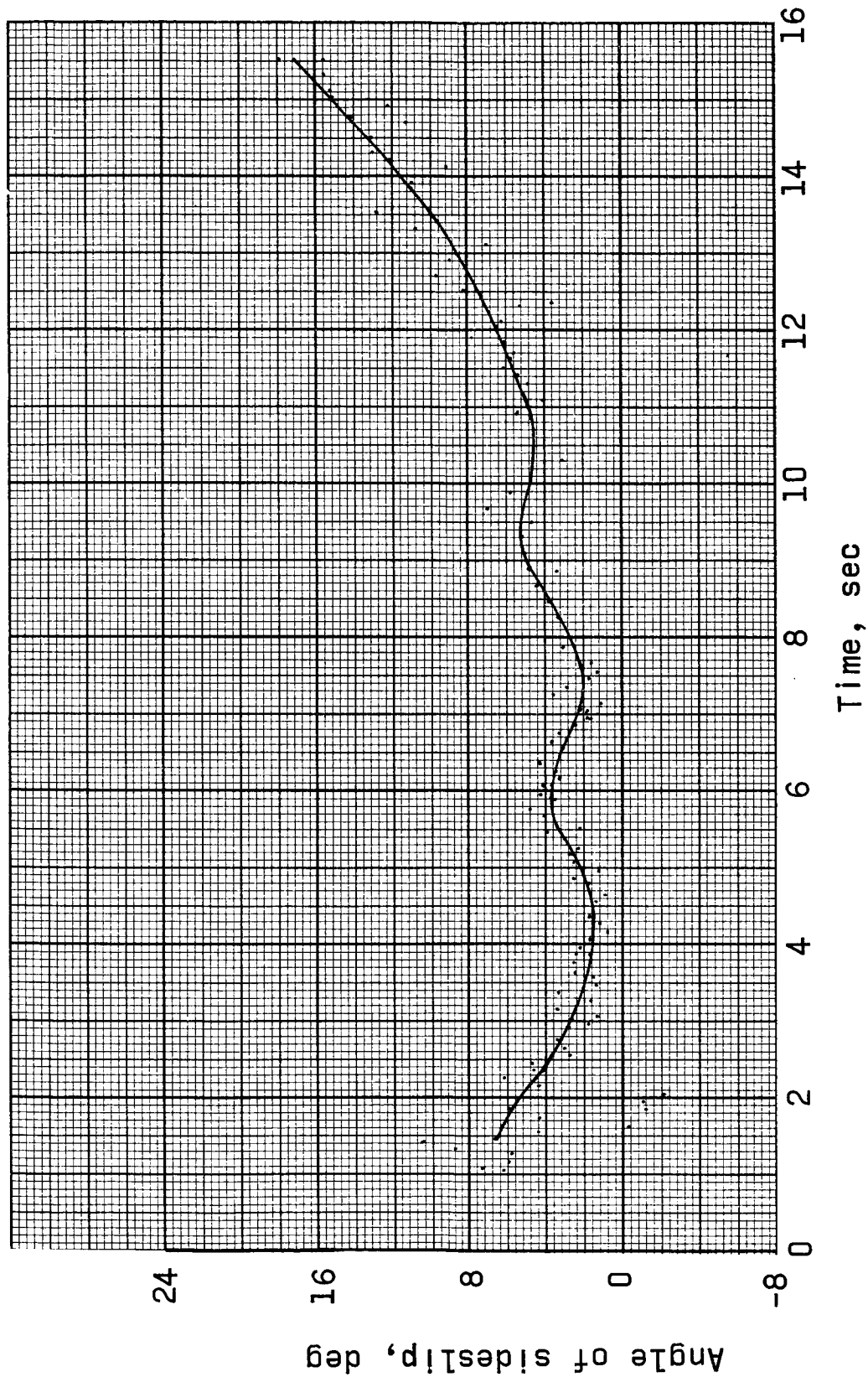
Figure 6.3-2.- Launch-escape vehicle angle of sideslip derived from Q-Ball plotted against time.
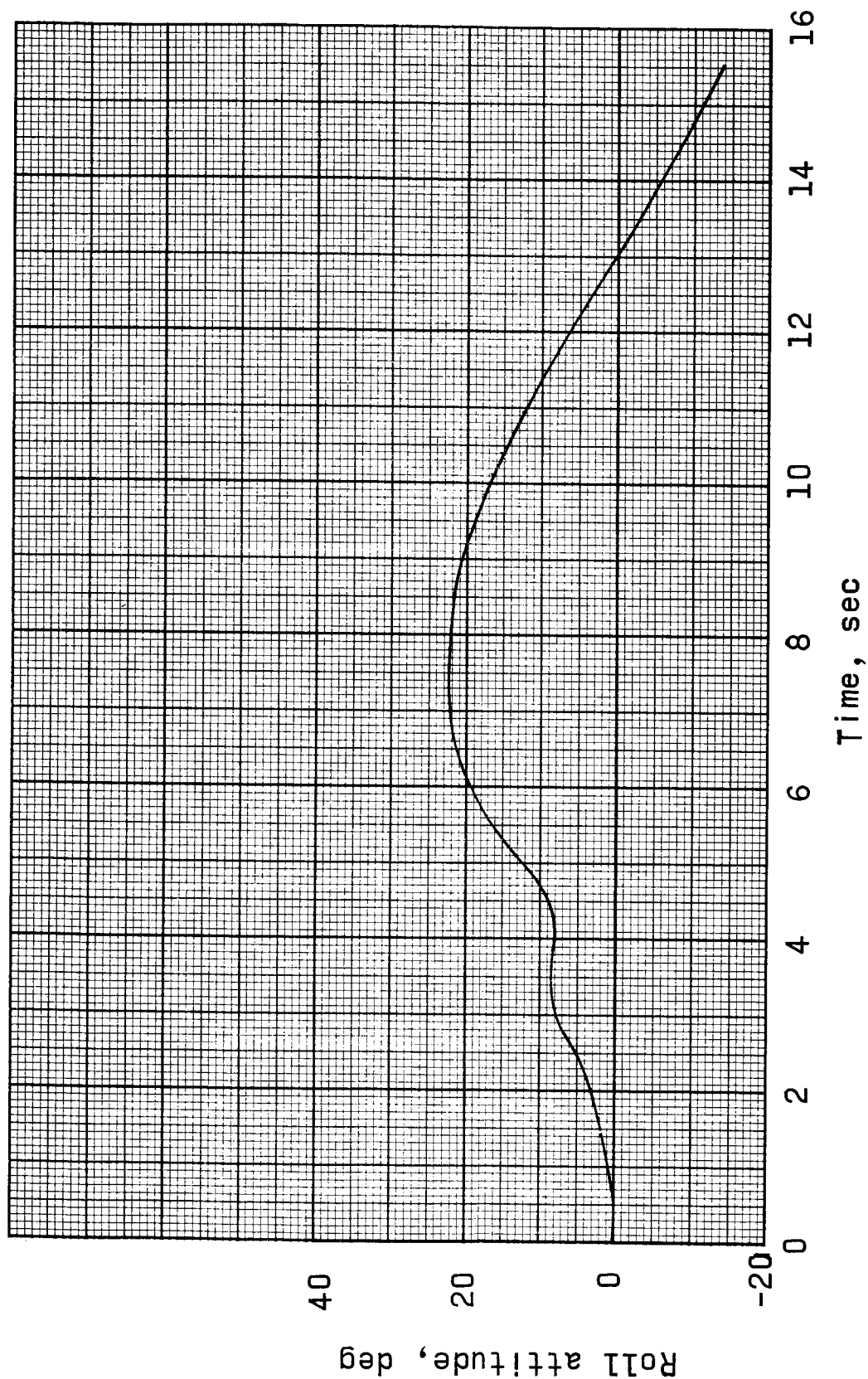
Figure 6.4-1.- Launch-escape vehicle attitude from roll attitude gyroscope plotted against time.

## 7.0  SPACECRAFT SYSTEMS PERFORMANCE

A brief discussion of each of the boilerplate 6 systems follows.
This discussion follows the general outline of introduction, system description, performance during flight, and conclusion.

### 7.1  Electrical and Sequential System

7.1.1   Introduction.- The role of the electrical and sequential system in boilerplate 6 was to provide power to the instrumentation, launch-escape system (LES), and earth-landing systems (ELS). The sequential system, utilizing relay logic, was used to program the separation and jettison of the launch-escape system and deployment of the earth-landing system parachutes. Based upon flight telemetry and visual observation, all electrical and sequential systems performed as programed.

7.1.2   System description.- The electrical and sequential systems consisted of three zinc silver oxide batteries, power and control relay box, launch-escape system relay control box, earth-landing system sequence controller, and inertia switch. Two 5-ampere-hour batteries operated the ELS, LES, and associated pyrotechnic circuitry. The LES and ELS systems containing systems A and B were completely redundant. Either side of each unit will initiate the function programed. A block diagram of the sequence of events for Pad Abort 1 mission is included in figure 7.1.2-1. One 60-ampere-hour battery provided power to all instrumentation units in the spacecraft. (See fig. 7.1.2-2.) The inertia switch was used to sense spacecraft landing.

7.1.3   System performance.- At lift-off, main buses A and B were at approximately 29.0 volts direct current under a 13-ampere load. (See appendix A4-9(a), seg. 54, 64, and 51.) The bus voltage and current remained constant until T+15.4 seconds, at which time tower jettison occurred. Tower instrumentation and Q-ball electronics were removed from the bus A load causing a 1.5 ampere decrease in load at tower jettison. At lift-off pyrotechnic buses A and B were at 28 volts; however the voltage of bus B decreased to 14 volts direct current at T+24 seconds and remained at this potential for 3.8 seconds. (See appendix A4-9(a), seg. 53 and 52.) This time was coincident to the time of drogue parachute disconnect and pilot parachute deployment functions. Postlaunch tests of the ELS sequencer revealed that the fuse-resistor in series with the drogue release initiator, system B, was blown, and the initiator on the drogue release, System B, was shorted. It is thought that upon firing of the initiator during flight the initiator shorted to ground and the resulting high power

drain caused the bus voltage to drop to 14 volt direct current. Subsequently the resistor blew after 3.8 seconds, removing the short circuit.

Investigation of the recovered launch-escape motor skirt indicated the area under the skirt was subjected to flame impingement. This area contains launch-escape system wiring which was protected with high-temperature tape. Inspection indicated that the wiring was adequately protected by the tape for this mission.

Onboard data indicate that only one side of the landing relay was activated at landing. This anomaly is being investigated during postlaunch tests and further finding will be published in subsequent reports. The actual time of sequence actuations is shown in table 7.1.3-1. System B leads system A by approximately 0.3 second. This time lead was observed during preflight tests.

7.1.4    Conclusions.- During the flight sequence, all functions occurred at the proper time with system A lagging behind system B by approximately 0.3 second. A similar time differential was observed during preflight checkout and is within the tolerances of the system.

TABLE 7.1.3-1.- SEQUENCE OF EVENTS

| Event | Time, sec |
|---|---|
| Abort initiate relay closure | 00.0 |
| Launch-escape motor EBW discharge (B) | 00.0 |
| Launch-escape motor EBW discharge (A) | 00.0 |
| Pitch-control motor EBW discharge (B) | 00.0 |
| Pitch-control motor EBW discharge (A) | 00.0 |
| Jettison-motor relay closure (B) | 15.1 |
| Jettison-motor relay closure (A) | 15.4 |
| Jettison motor fire and tower separation relay closure (B) | 15.6 |
| Jettison motor fire and tower separation relay closure (A) | 15.9 |
| Jettison motor EBW discharge (B) | 15.6[a] |
| Jettison motor EBW discharge (A) | 15.6[a] |
| ELS sequencer start relay closure (B) | 18.6 |
| ELS sequencer start relay closure (A) | 18.9 |
| Drogue deployment (B) | 18.6 |
| Drogue deployment (A) | 18.9 |
| Drogue release, pilot parachute deployment (B) | 24.0 |
| Drogue release, pilot parachute deployment (A) | 24.3 |
| Landing relay closure (B) | 165.1 |

[a]This indication is not necessarily the time of this event.
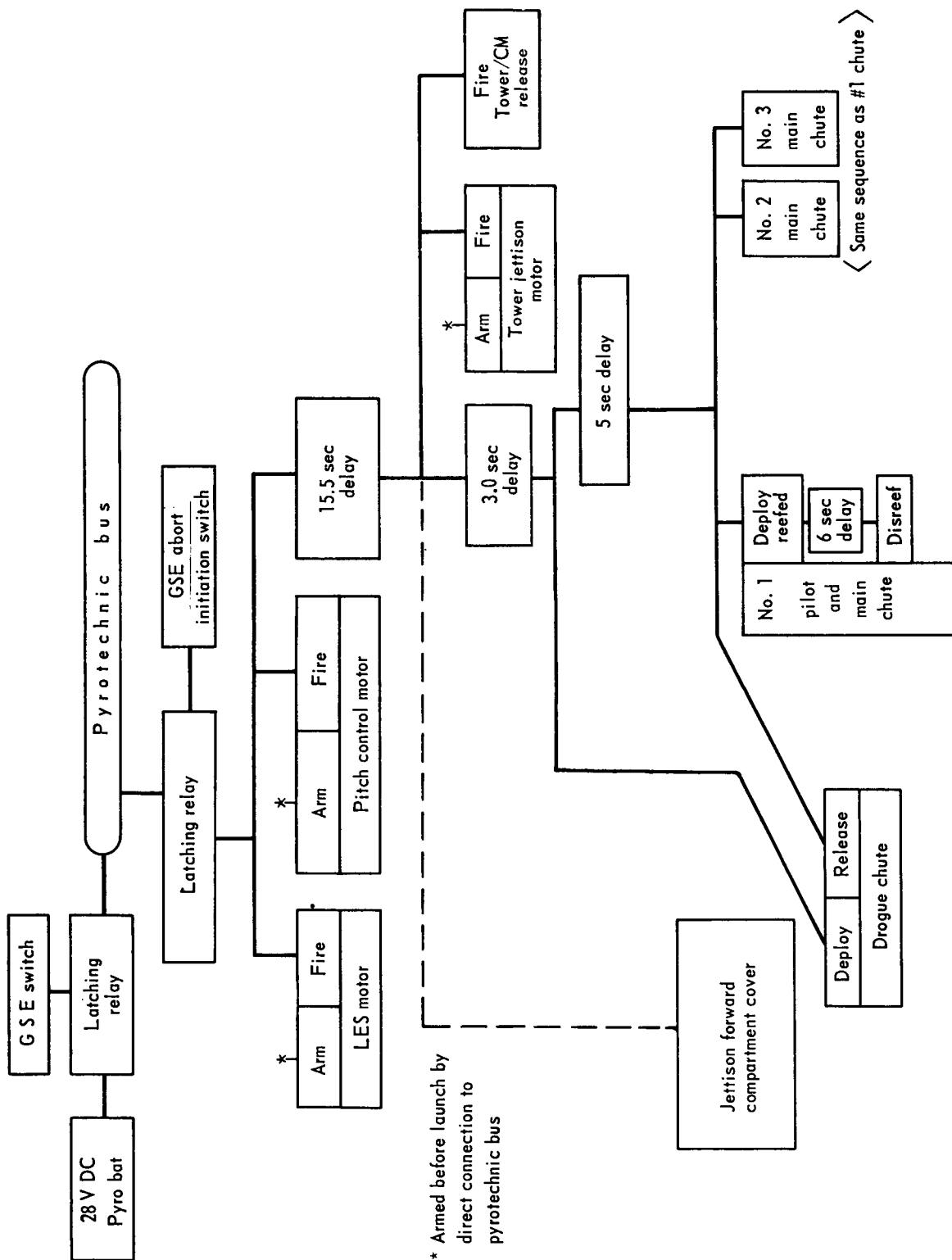
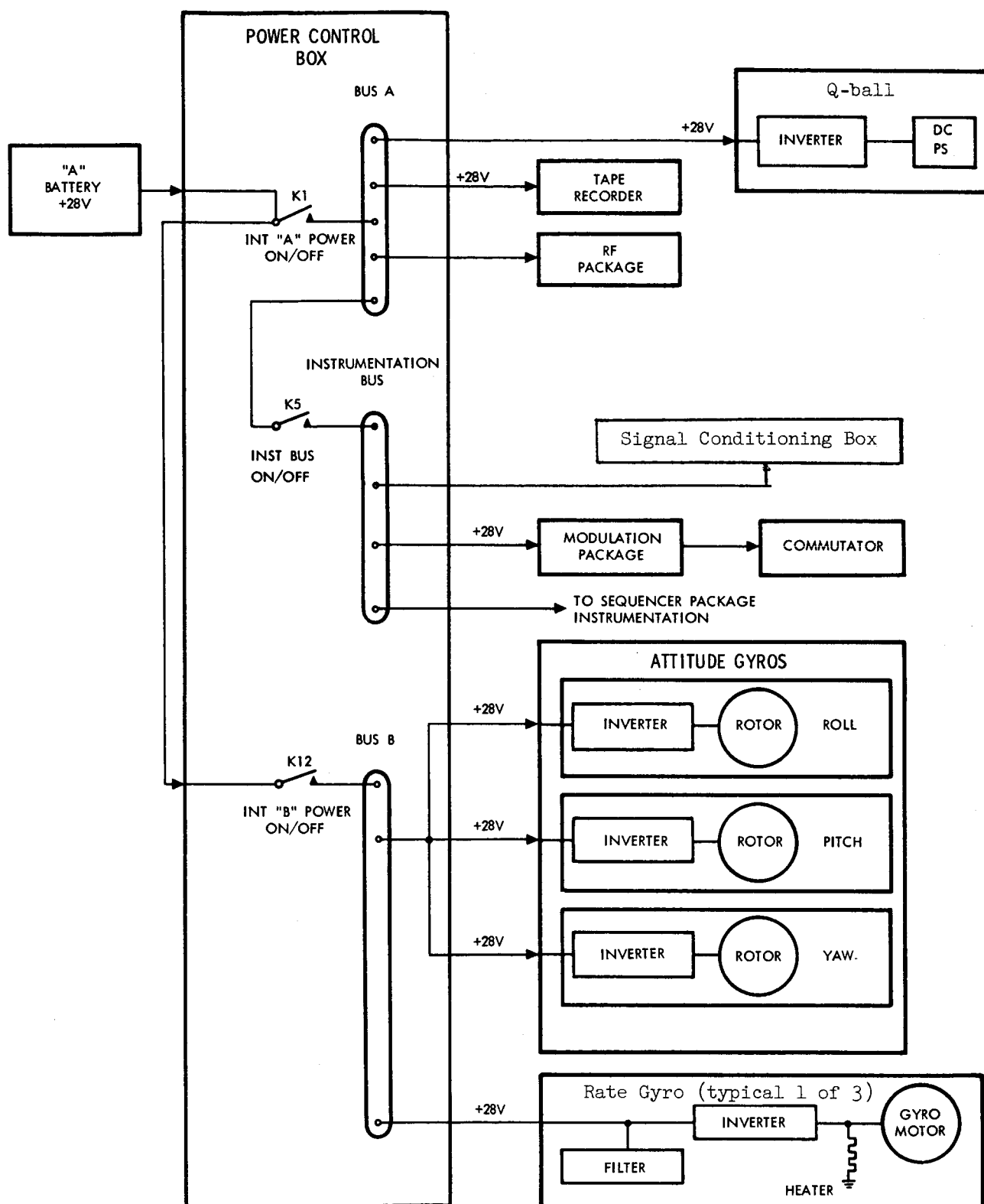Figure 7.1.2-1.- Sequence of events during Pad Abort-1 launch.

Figure 7.1.2-2.- Power distribution to instrumentation system.

## 7.2 Instrumentation and Communications

7.2.1   System description.- The telemetry (TM) system used on boiler-
plate 6 was a standard PAM/FM/FM system consisting of a 90 X 10
commutator, modulator, transmitter, 10-watt power amplifier,
and antenna system.  The telemetry system used 72 commutator
segments and 12 continuous channels.  A total of 98 data points
were obtained utilizing step functions on the commutator.  All
13 subcarrier oscillators were standard IRIG channels and the
total deviation used was 125 kc.

A 14-track onboard tape recorder was used on boilerplate 6.
Six wideband frequency modulation channels were used for high-
frequency vibration data.  The differentiated PDM output of
the commutator was recorded on a direct input track.  The mod-
ulator video output, excluding channel E, was also recorded.
Tape speed compensation was supplied by a 50 kc reference oscil-
lator in the modulation package.

Figures 7.2.1-1 to 7.2.1-4 describe the measurement locations;
figure 7.2.1-5 shows the installation configuration for the
command module; and figure 7.2.1-6 represents the block diagram
of the instrumentation system.  Measurements description and
telemetry loading are contained in table A3-1 in appendix A3.0.

7.2.2   Prelaunch checks.- With the exception of the Q-ball, which is
used to measure the angle of attack, angle of sideslip, and
dynamic pressure, and the antennas, the instrumentation system
was procured, qualified, and breadboard-tested by Manned Space-
craft Center, Houston, Texas.  The Q-ball and antenna system
were procured by North American Aviation, Inc.  Breadboard-
testing of the NASA furnished instrumentation and the Q-ball
was repeated at North American Aviation, Inc., Downey, Cali-
fornia.  After instrumentation installation, individual and
integrated system testing was performed at Downey, California,
before shipment to WSMR.  The systems also underwent individual
and integrated system testing at WSMR prior to flight.

7.2.3   Flight performance.- In general, the telemetry system performed
satisfactorily during the flight and after command module land-
ing.  A telemetry disturbance of a 0.09-second dropout was noted
immediately after LES ignition by telemetry receiving station 44.
This station noted a signal dropout occurring at T+0.18 second.
Station 56 and the telemetry trailer did not detect a signal
dropout.  Records from telemetry receiving stations 3 and 5

have not been reduced. A similiar dropout occurred on the on-
board tape recorder at a slightly different time. The onboard
tape had a signal dropout of 0.13 second at T+0.12 second.
The record which was examined had not been compensated. The
onboard tape recorder acquired good data on all tracks through-
out its running time of 9.03 minutes except for the momentary
dropout.

The pitch-rate gyro range of ±100°/sec was exceeded during the
command module turnaround at drogue parachute deployment. The
roll and yaw rate gyro indications were within range.

The attitude gyros performed satisfactorily until T+19.6 sec-
onds at which time the pitch and yaw attitude gyros tumbled
when the command module turned around after drogue parachute
deployment.

During the flight, all but two surface and base pressure trans-
ducers performed satisfactorily. The output voltage of measure-
ment CA 0060 P, conical surface pressure 33, dropped to zero at
T+1 second but at T+5 seconds the output voltage returned to
its expected value. All data from this transducer with the ex-
ception of the aforementioned 4 seconds appeared good. Measure-
ment CA 0049 P, conical surface pressure 22, appeared to have a
shift in its output of approximately 1 psia at the ambient con-
dition after landing.

All other instrumentation performed satisfactorily and trans-
mission continued for 16 minutes after landing. Transmission
was terminated by the recovery team by removing spacecraft
power.

7.2.4    Recommendations.- Several desirable but not mandatory instru-
mentation design changes should be investigated and resolved
for future flights. They are as follows:

(1)    The 5-volt calibration should be eliminated from the com-
mutated channel E. During checkout the switching opera-
tion for calibration removes the commutator input which in
turn disables the decommutation equipment at the receiving
stations. This sudden removal of the decommutation signal
from the real-time recorders requires resynchronization
and calibration of the decommutation equipment.

(2)    False indications of gyro cage and uncage positions should
be eliminated by circuit changes in gyro monitors. These
false indications were observed during power up and power
down sequences.

(3)   The bus A and bus B voltage metering circuits should be placed in the checkout trailer on isolated lines from the signal conditioning box in the command module to the checkout trailer. At present the meter circuit and the remote sensing of the power supply in the checkout trailer are on the same lines. The remote sensing current causes a voltage drop in the lines which in turn causes an erroneous reading of the voltage of bus A and bus B.

(4)   The run-time indicators in the checkout trailer should be utilized on critical run-time components. The utilization of these indicators will provide a more accurate run-time record to determine the life of critical equipment.

7.2.5    Results.- The performance of the instrumentation system was satisfactory throughout flight. Good data were received on all channels with the possible exception of one pressure transducer. Telemetry transmission continued for 16 minutes after landing at which time transmission was terminated by the recovery team.

LEGEND:
1  X AXIS SPACECRAFT ACCELERATION
2  Y AXIS SPACECRAFT ACCELERATION
3  Z AXIS SPACECRAFT ACCELERATION
4  Y AXIS TOWER ACCELERATION
5  Z AXIS TOWER ACCELERATION
6  ANGLE OF ATTACK
7  ANGLE OF SIDE SLIP
8  DYNAMIC PRESSURE
9  PITCH RATE GYRO OUTPUT
10  YAW RATE GYRO OUTPUT
11  ROLL RATE GYRO OUTPUT
12  PITCH ATTITUDE GYRO OUTPUT
13  ROLL ATTITUDE GYRO OUTPUT
14  YAW ATTITUDE GYRO OUTPUT
15  CM INTERIOR TEMPERATURE
16  PITCH CONTROL MTR CHAMBER PRESSURE
17  ESCAPE MOTOR CHAMBER PRESSURE

Figure 7.2.1-1.- Command module and tower measurement locations.
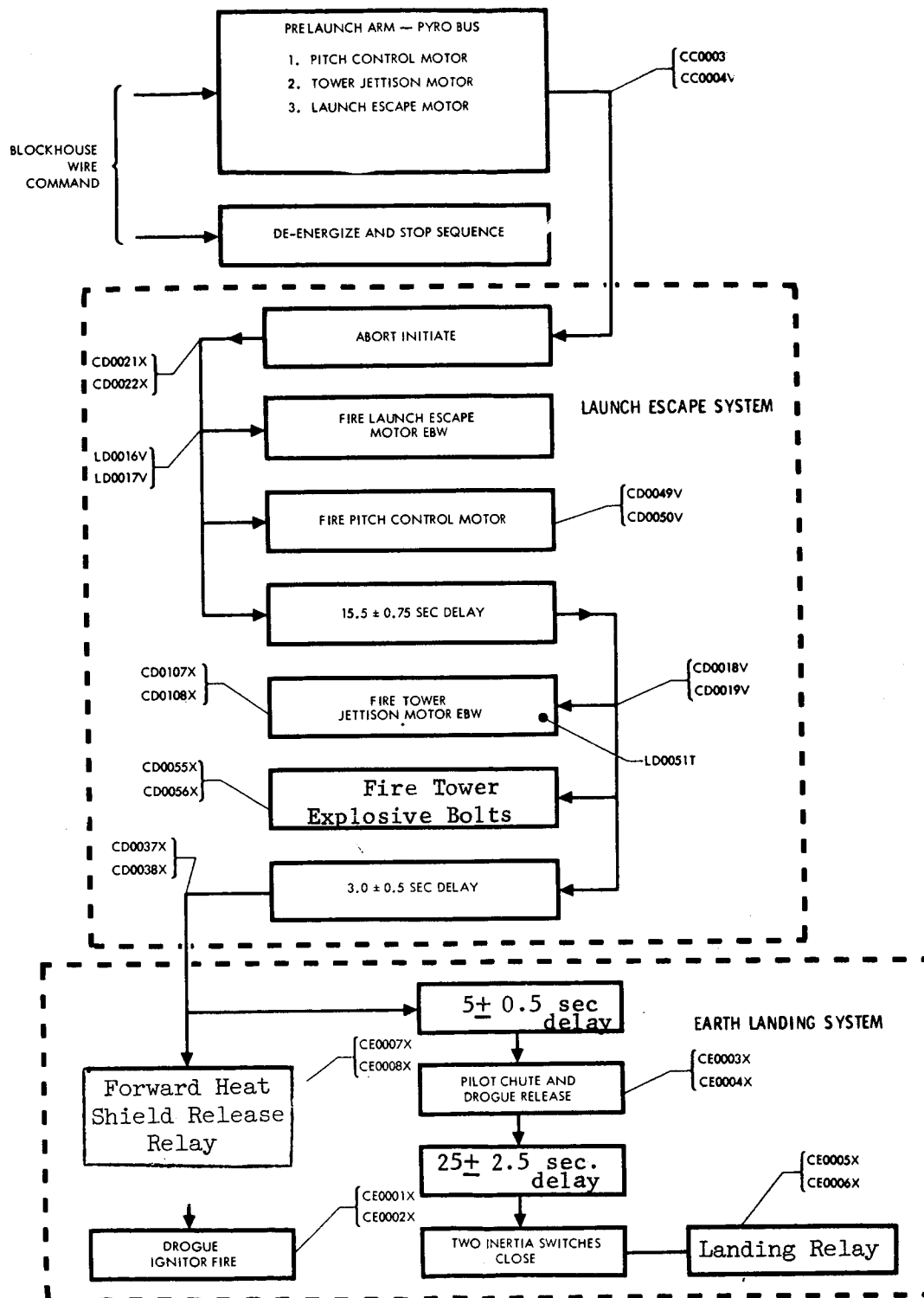
Figure 7.2.1-2.- Launch-escape system and earth-landing system measurements.

LEGEND:

① X, Y, Z, AXIS TOWER VIBRATION, LOWER (3)

② X, Y, Z AXIS TOWER VIBRATION, UPPER (3)

LA0013D
LA0014D ② 
LA0015D

$X_L$ 116.0

$X_L$ 87.9

$X_L$ 59.8

$X_L$ 34.1

$X_L$ 10.0

① LA0016D
LA0017D
LA0018D

$X_L$ 0

+X

+Y

+Z
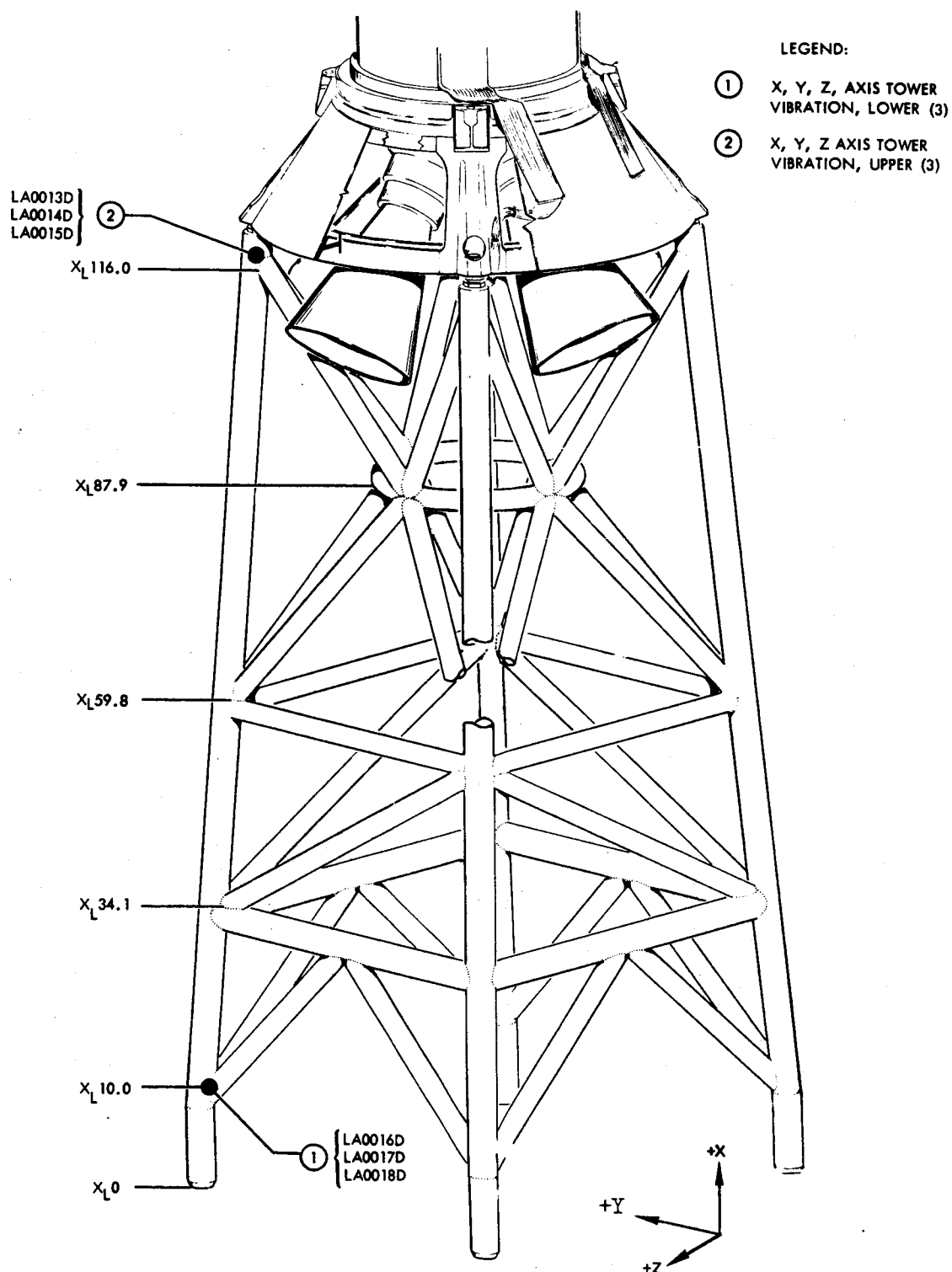
Figure 7.2.1-3.- LES tower vibration
measurement locations.

CA0043P
CA0042P
CA0050P
CA0030P

CA0055P
CA0041P

CA0029P

CA0040P
CA0060P
CA0049P
CA0028P

+Z=0°

CA0059P
CA0048P
CA0039P

CA0046P

CA0047P
CA0054P
CA0038P
CA0058P

CA0037P
CA0036P

+Y=90°          CA0031P

CA0051P

CA0061P

X$_C$ 79
X$_C$ 71
X$_C$ 50
X$_C$ 30

CA0062P

CA0032P

-Z=180°

CA0056P

CA0033P

CA0044P

CA0045P
CA0052P
CA0034P

CA0057P
CA0035P
CA0063P

-Y=270°          CA0053P

X$_C$100

X$_C$79
X$_C$71

X$_C$50

X$_C$30

0°          F                                    F          180°

CA0101P

270°                      CA0103P

BACK: CA0100P
FRONT: CA0102P

LEGEND
↓ BASE PRESSURES (4)
○ CONICAL SURFACE PRESSURES (36)

NOTE: DIAGRAM IS NOT DRAWN TO SCALE.

Figure 7.2.1-4.- Command module static pressure
measurement locations.

Figure 7.2.1-5.- Instrumentation system installation in the command module.

Figure 7.2.1-6.— Instrumentation system block diagram.

## 7.3  Rocket Propulsion

### 7.3.1    System Description.-

#### 7.3.1.1    Launch-escape motor:- 

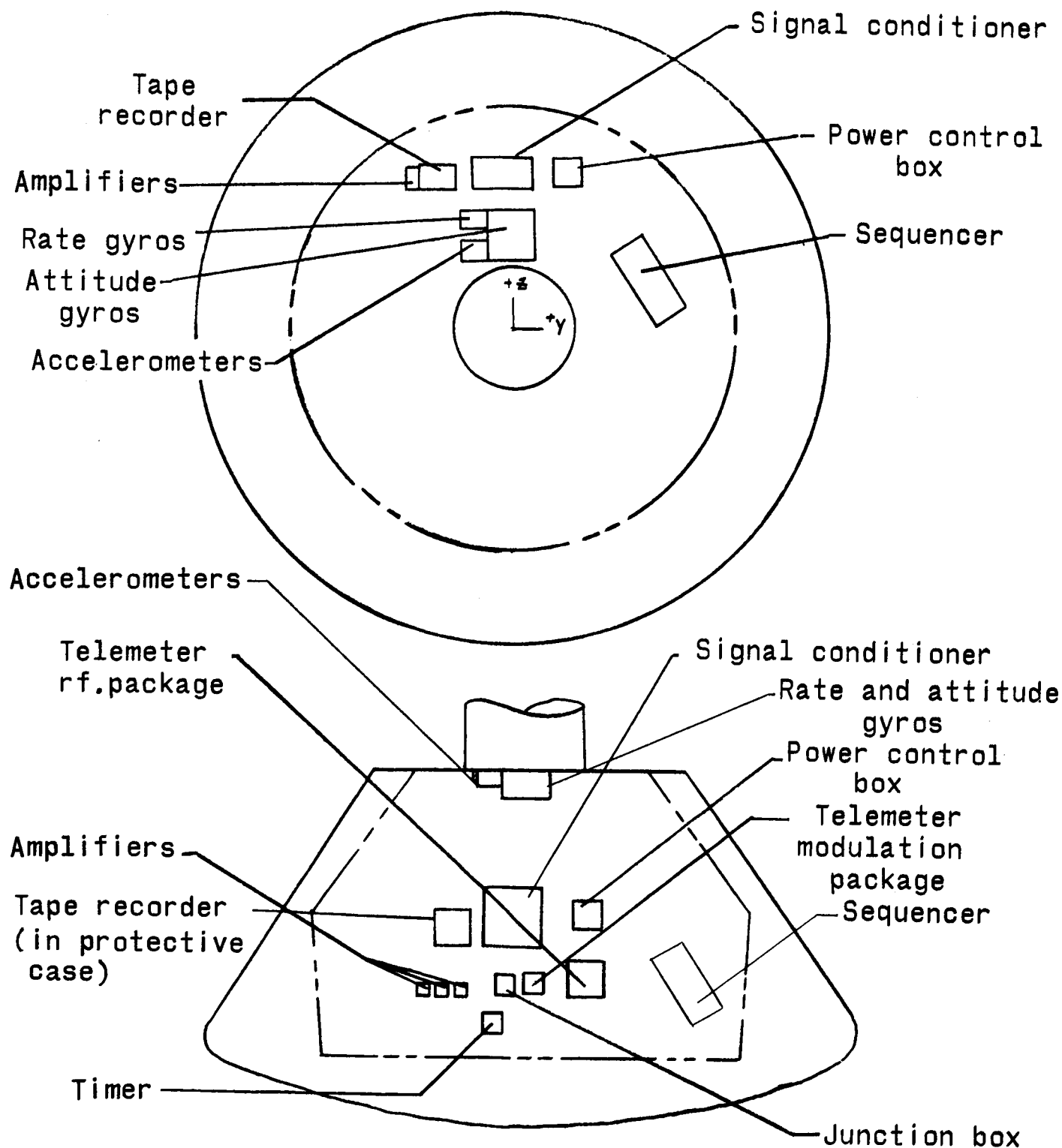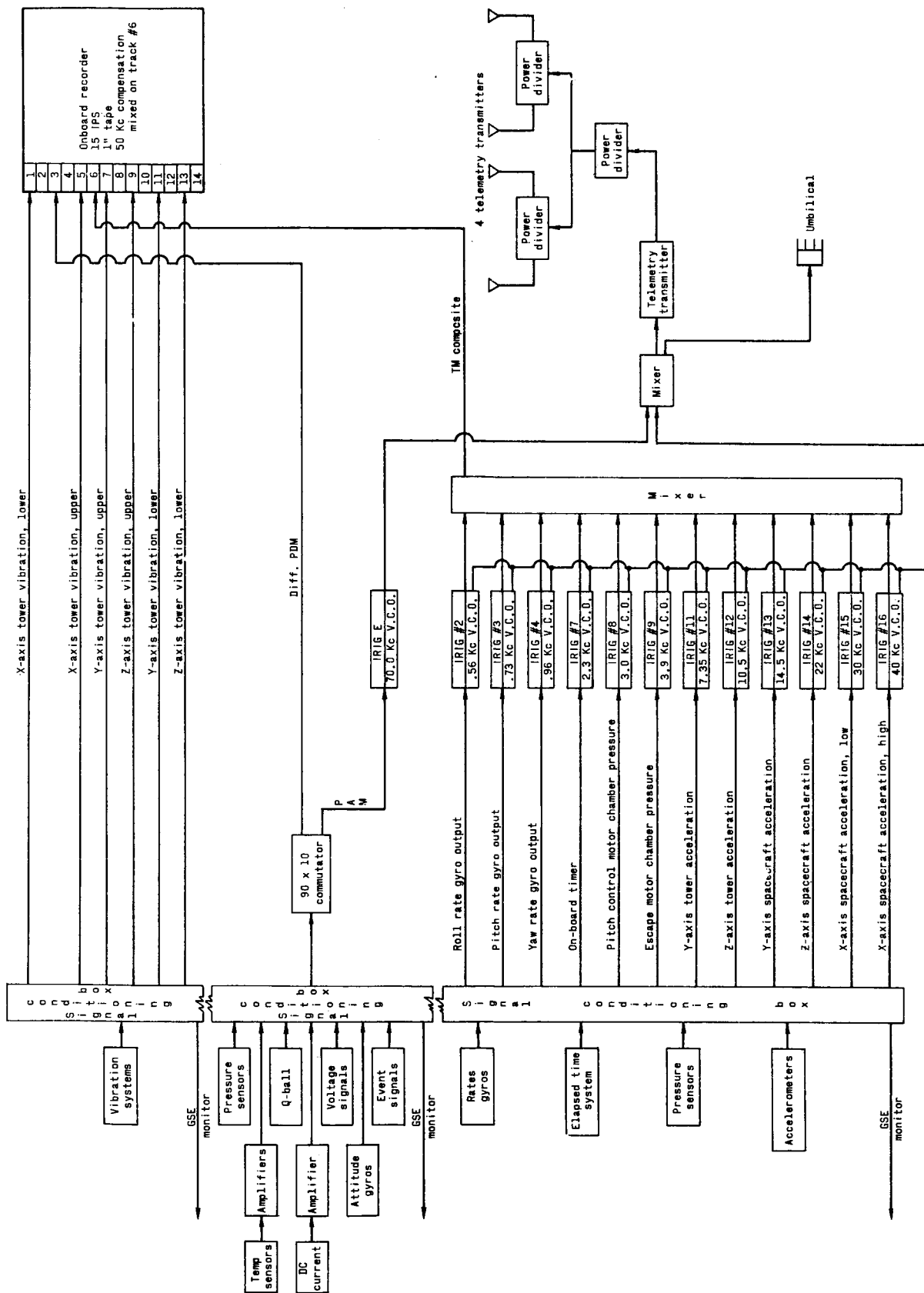The launch-escape motor was designed to provide the propulsive force for carrying the command module safely away from the launch vehicle for an abort during the period from final countdown until approximately 20 seconds after Saturn second-stage burning.  The location of the motor in the launch escape system (LES) is shown in figure 4.1.1. Motor characteristics are shown in figure 7.3.1.1-1.  The average thrust level is 155,000 pounds at 70° F at an altitude of 36,000 feet during the first 2 seconds of burning.  Nominal web burning time was 3.5 seconds, and total operating time was 8 seconds.  (The definition of ballistic parameters used in this section is shown in fig. 7.3.1.1-2.)  The escape motor utilizes a case-bonded solid propellant of polysulfide fuel binder and ammonium perchlorate oxidixer in an 8-point, internal-burning star configuration.  The motor has four nozzles spaced 90° apart and canted 35° outward from the longitudinal axis.  The nozzle cant reduces flame impingement on the command module.  A thrust vector offset of 2° 45' from the motor centerline is provided by an oversize and an undersize nozzle in the pitch plane.  The four nozzles have graphic throat inserts and fiberglass-phenolic exit skirts. Nozzle blowout closures of polyurethane foam are glued in each nozzle throat to provide a sealed, controlled environment inside the motor during storage and handling.

A pyrogen igniter is mounted in the forward end of the motor case, concentric with the longitudinal axis.  The igniter propellant is a polysulfide/ammonium perchlorate formulation identical to that used in the rocket motor.  Redundant pyrotechnic initiators (exploding bridge wire) are used to ignite boron-potassium nitrate pellets which, in turn, ignite the ingniter propellant charge.

#### 7.3.1.2    Pitch-control motor:- 

The pitch-control motor provides a positive pitching moment to change the initial attitude of the vehicle that downrange distance requirements for the abort trajectory are achieved.  Location of the motor in LES is shown in figure 4.1-1 and motor configuration is shown in figure 7.3.1.2-1.  The nominal thrust level is 2,700 pounds at 70° and sea-level atmospheric pressure and total impulse is 1,700 lb-sec.  Nominal web burning time is 0.5 sec and total operating time is 1.3 seconds.  The pitch-control motor utilizes a case-bonded solid propellant of polysulfide/ammonium perchlorate in a 14-point, internal-burning star configuration.

The nozzle has a graphite throat insert housed in a steel structural shell. A nozzle blowout closure of polyurethane foam is glued in the nozzle throat to provide a sealed, controlled environment inside the motor during storage and handling.

A pellet-type igniter is mounted in the forward end of the motor case, concentric with the longitudinal axis. Redundant pyrotechnic initiators (exploding bridgewire) are used to ignite the boron-potassium nitrate pellets which, in turn, ignite the main motor propellant charge.

7.3.1.3    Tower-jettison motor:- The tower-jettison motor provides the propulsive force for removing the LES from the command module. Location of the tower-jettison motor in the LES is shown in figure 4.1-1, and motor configuration is shown in figure 7.3.1.3-1. The nominal thrust level is 33,000 pounds at 70° F and sea-level atmospheric pressure. Nominal web burning time is 1 second and total operating time is 1.3 seconds. The tower-jettison motor utilizes a polysulfide/ammonium perchlorate propellant in a case-bonded, internal-burning, 10-point star configuration.

The motor has two scarfed nozzles spaced 180° apart and canted 30° outward from the motor longitudinal axis. The nozzles are scarfed for aerodynamic considerations on the LES. A thrust-vector offset of 2°30' from the motor centerline is provided by a 10-percent larger throat area in one nozzle. This vector produces a negative pitching moment to remove the LES from the flight path of the command module.

The nozzles have graphite throat inserts and bare steel exit skirts. Nozzle blowout closures of polyurethane foam are glued in each nozzle throat to provide a sealed, controlled environment prior to motor use. The motor has an integral interstage structure which houses the canted nozzles.

A pyrogen type igniter is mounted in the aft end of the motor between the nozzles and concentric with the motor centerline. The igniter propellant is a polysulfide/ammonium perchlorate formulation identical to that used in the rocket motor. Redundant pyrotechnic initiators (exploding bridgewire) are used to ignite boron-potassium nitrate pellets which in turn ignite the igniter propellant charge.

7.3.2      System operation.- Rocket-motor thrust level was calculated from the recorded chamber pressure by the following equation:

$$F = C_D C_F \left(P_c + P_o\right) A_t \cos \theta$$

$$= C_D\left(1.722 - \frac{P_o \epsilon}{P_c + P_o}\right)\left(P_c + P_o\right) A_t \cos \theta$$

Where:

F   thrust, pounds

$C_D$   motor discharge coefficient

$C_F$   thrust coefficient

$P_c$   recorded chamber pressure, psig

$P_o$   atmospheric pressure, psia

$\epsilon$   average nozzle expansion ratio

$A_t$   total throat area, square in.

$\theta$   nozzle cant angle, deg

The numerical value and source of thrust calculation parameters are shown in table 7.3.2-1. During thrust buildup and tailoff when chamber pressure was insufficient to provide full nozzle flow the value of ($\epsilon$) were modified to the point where separation occurred. This was estimated to be at the point where internal nozzle gas pressure was $\frac{1}{3}$ $P_o$ (that is slightly overexpanded).

Estimates were made for the effects of rocket-motor temperature on performance. These estimates were obtained from the vendor's motor specification. Estimates for altitude effects were made on a comparison of $C_F$ for different ambient pressures resulting from the change in altitude.

7.3.2.1   Launch escape motor:- The motor operated satisfactorily and performed its intended function. Maximum thrust was 131,900 pounds (10 percent lower than predicted) and average thrust during the first 2 seconds of burning was 128,375 pounds (8 percent lower than predicted). The calculated and predicted

~~CONFIDENTIAL~~

thrust time histories as well as average thrust and total impulse performance values are presented in figure 7.3.2.1-1. The recorded chamber pressure is shown in figure A4-13. The thrust rise time (zero to 90 percent full thrust) 90 milliseconds compared favorably with the prediction of 110 milliseconds.

The reasons for the lower actual thrust level are not immediately known. Motor temperature at the time of launch is partially responsible but this would account for only approximately a 2-percent loss in thrust if the motor temperature was assumed as 55° F (based on motor environmental exposure while on the launch pad).

Total impulse was obtained from a graphical integration of the calculated thrust-time curve (fig. 7.3.2.1-1). The total impulse obtained was 568,000 lb-sec. This is within 0.5 percent of both the predicted total impulse and impulse from graphical integration of the vendors predicted thrust-time curve. The motor temperature effects on total impulse would lower impulse by approximately 0.3 percent. The effects of increasing altitude (during flight) would increase total impulse by approximately 0.2 percent so that the temperature and altitude effects would tend to cancel each other.

7.3.2.2     Pitch-control motor:- The pitch-control motor operated satisfactorily and successfully performed its intended function. Maximum thrust was 2,550 pounds (7 percent lower than predicted) and total impulse was 1,692 lb-sec (2 percent lower than predicted, but within 0.5 percent of nominal). Motor thrust and total impulse performance is presented in figure 7.3.2.2-1.

A 2-percent decrease in predicted thrust may be attributed to the assumed motor temperature of 55° F, but altitude could account for a 0.2-percent increase.

The effects of motor temperature and altitude on total impulse would tend to cancel out. The 2-percent difference between actual and predicted impulse is within the normal manufacturing tolerance of ±3 percent.

The thrust rise time was 95 milliseconds to 70 percent maximum thrust and compares with the prediction of 100 milliseconds. Pitch motor ignition occurred at 0.018 second before launch-escape motor ignition, and thrust rose to approximately 400 pounds within this time. No adverse effects on the vehicle motions were noted because of this occurrence.

~~CONFIDENTIAL~~

7.3.2.3    Tower-jettison motor:- The tower-jettison motor operated
as planned and successfully performed its intended function.
Since no telemetry capability was provided for the LES after
jettisoning, it was not possible to monitor the motor perform-
ance.  Tower jettison was satisfactorily accomplished and the
LES cleared the flight path of the command module.  Trajectory
data indicate that nominal performance was met or exceeded.
The predicted thrust performance is shown in figure 7.3.2.3-1.

7.3.3    Postflight analysis.- At ground impact of the launch-escape
system, the forward section and jettison motor were telescoped,
badly deformed, and separated from the escape motor.  The
escape-motor forward closure was also separated and the motor
case was deformed and torn at the forward end.  The aft
closure and tower skirt were intact.  The fiberglass nozzle
skirts were broken off (apparently from tower breakup) but
the graphite throat inserts were in very good condition.  No
structurally or operationally deficient areas were noted on
any of the launch-escape system solid rocket motors.

The escape-motor nozzle compartment under the tower skirt was
generally covered with soot, indicating base recirculation.
Electrical wiring in the area appeared to be adequately
protected.  The escape tower paint was generally blistered
but no evidence of severe overheating was observed.  Tempera-
tures on the command module skin from the rocket motor exhausts
were near or below 250° F (see paragraph 7.6.2.4 for additional
information).

A potential problem with the solid rocket motors is evidenced
by the large amount of soot deposited on the command module
(including apex cover) during motor operation.  The soot
deposites are shown in figure 9.3-3.  The soot deposites are
alined under each of the escape-motor nozzles and are more
concentrated in the Z plane.  Paint on the aft heat shield
was scorched in the +Z plane only (see fig. 9.3-3).  This is
probably a result of the higher mass flow (thrust) produced
by the escape-motor nozzle in this location which provides
a thrust-vector offset.  The glass window samples were clouded
but an estimate of light transmissibility could not be
accurately made.

Analysis of the flight motion pictures indicates that major
soot deposition occurred during escape motor thrust-tailoff
(from about 5 sec to tower separation).  During this period,
the motor continued to burn and expelled significant amounts
of smoke, apparently from motor-liner combustion.  The deposits

in the Z-plane are believed to have been caused by the normal vehicle pitch excursions in that plane. Soot was also deposited on the tower-skirt by the jettison motor.

The problem with soot deposition may be stated as follows:

(1) Soot deposits may cloud windows.

(2) The time period, rate, and amount of soot deposition is unknown at this time.

7.3.4    Conclusions.- The capability of the launch escape and pitch control motors to propel a command module to a safe distance from a launch vehicle during a pad abort was demonstrated.

The capability of the tower jettison motor to propel the escape system safely away from the command module was demonstrated.

The problem of soot deposition on the command module and service module from the launch-escape system rocket-motors should be further investigated.

TABLE 7.3.2-1.- PARAMETERS USED FOR THRUST CALCULATION

| Symbol | Parameter | Launch-Escape Motor (serial LE-9) | Pitch-Control Motor (serial PC-20) | Source |
|---|---|---|---|---|
| $C_D$ | Motor discharge coefficient | .934 | .940 | Average of vendor development test data |
| $C_F$ | Thrust coefficient | Varies with altitude and mission time | Varies with mission time | Calculation using $C_p/C_v = 1.22$ (from vendor design data) |
| $P_c$ | Chamber pressure (psig) | Varies with mission time | Varies with mission time | Onboard-tape oscillograph record |
| $P_O$ | Atmospheric pressure (psia) | Varies with altitude and mission time | 12.6 | WSMR meteorological data |
| $\epsilon$ | Averaged nozzle expansion ratio | 9.35 | 1.60 | Vendor design data and motor log book |
| $A_t$ | Total throat area (sq. in.) | No. 1 nozzle = 18.079<br>No. 2 nozzle = 21.245<br>No. 3 nozzle = 24.454<br>No. 4 nozzle = 21.237<br>Total 85.015 | 1.04 | Vendor motor log book |
| $\theta$ | Nozzle cant angle (deg) | 35° | 0° | Motor design specification |
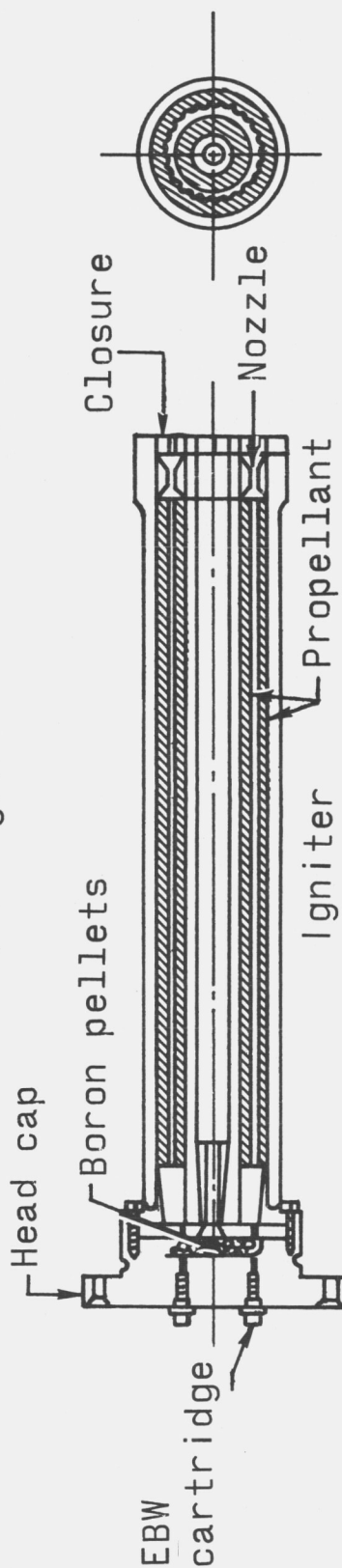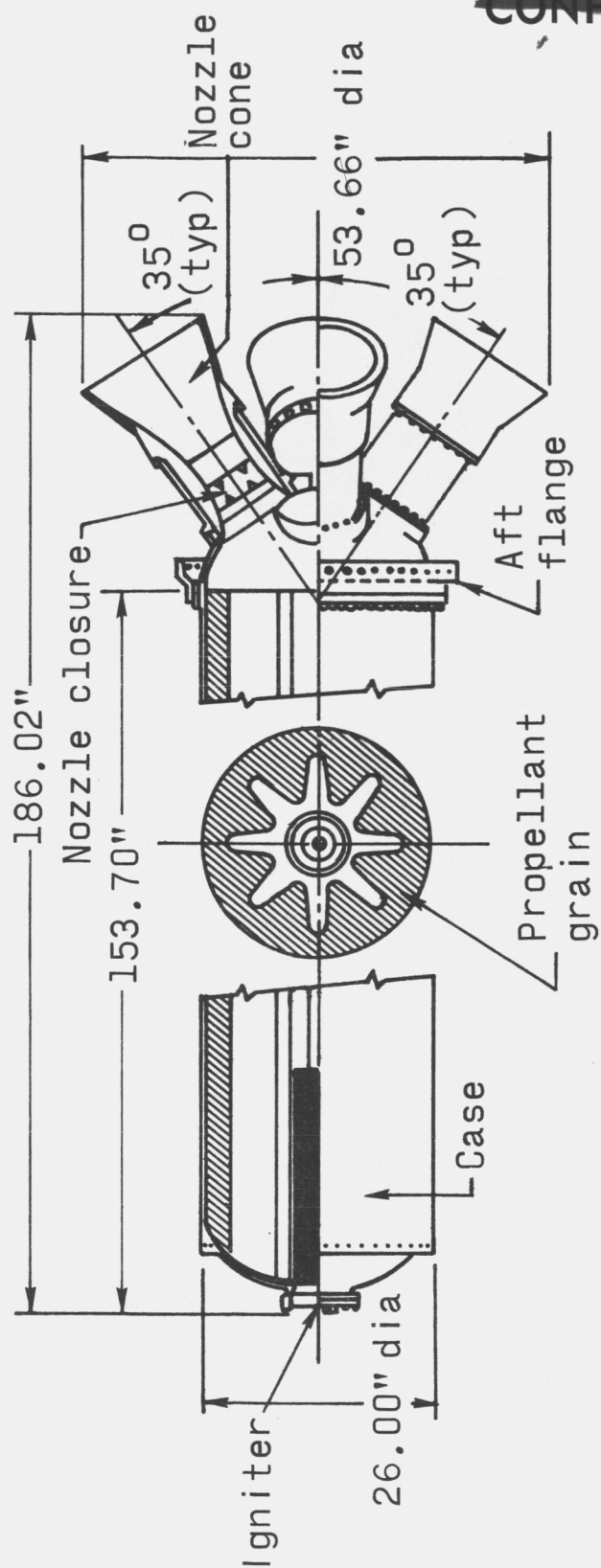
Propellant wgt          3,170 lb
Loaded wgt              4,764 lb
Case material           4,335V steel
Min yield strength      200K, psi
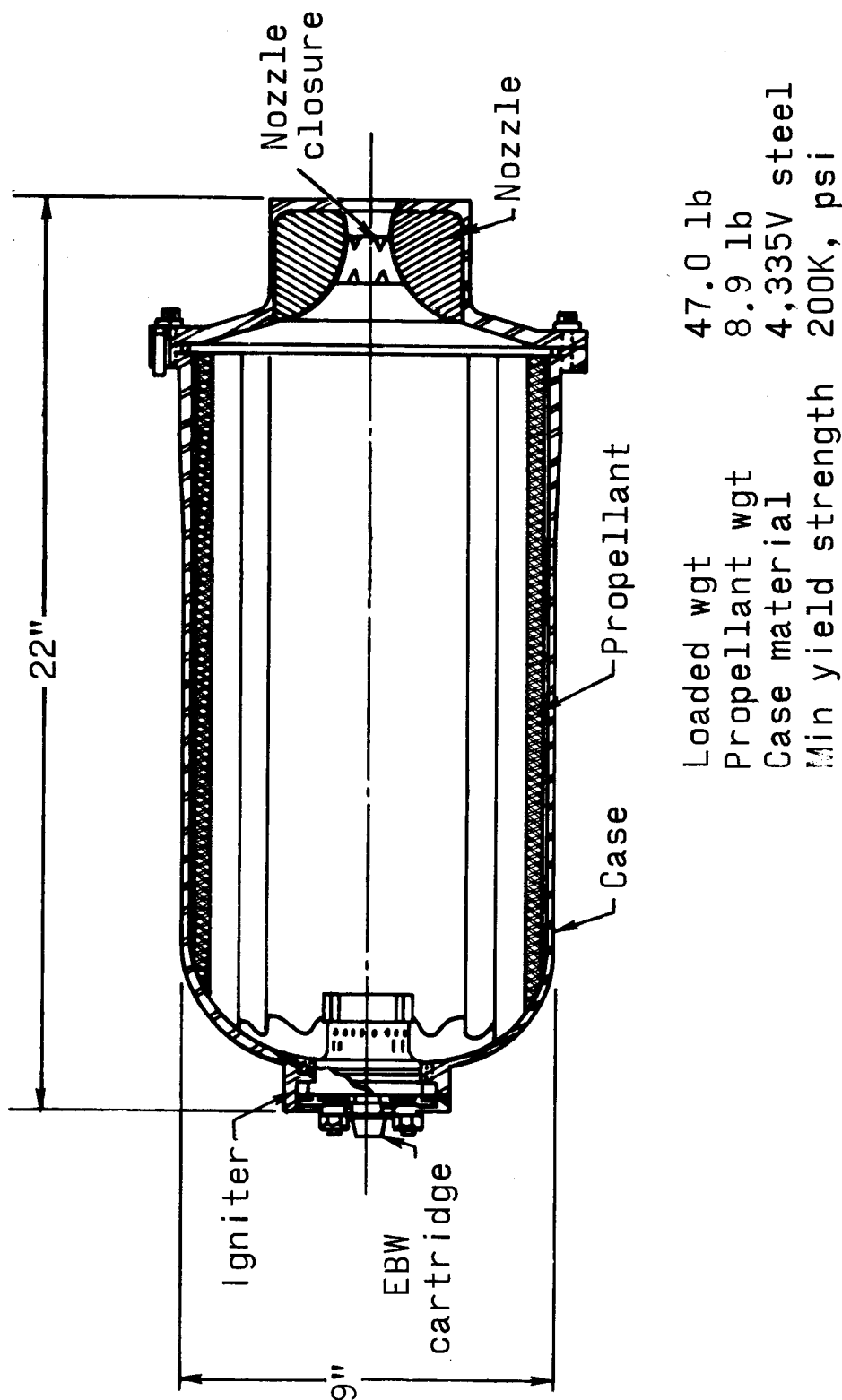
Figure 7.3.1.1-1.- Launch escape motor.

Nozzle cone

53.66" dia

35° (typ)

35° (typ)

Aft flange

Nozzle closure

186.02"

153.70"

Propellant grain

Case

26.00" dia

Igniter

Closure

Nozzle

Propellant

Igniter

Head cap

Boron pellets

EBW cartridge

| | |
|---|---|
| Loaded wgt | 47.0 lb |
| Propellant wgt | 8.9 lb |
| Case material | 4,335V steel |
| Min yield strength | 200K, psi |

Figure 7.3.1.2-1.- Pitch control motor.
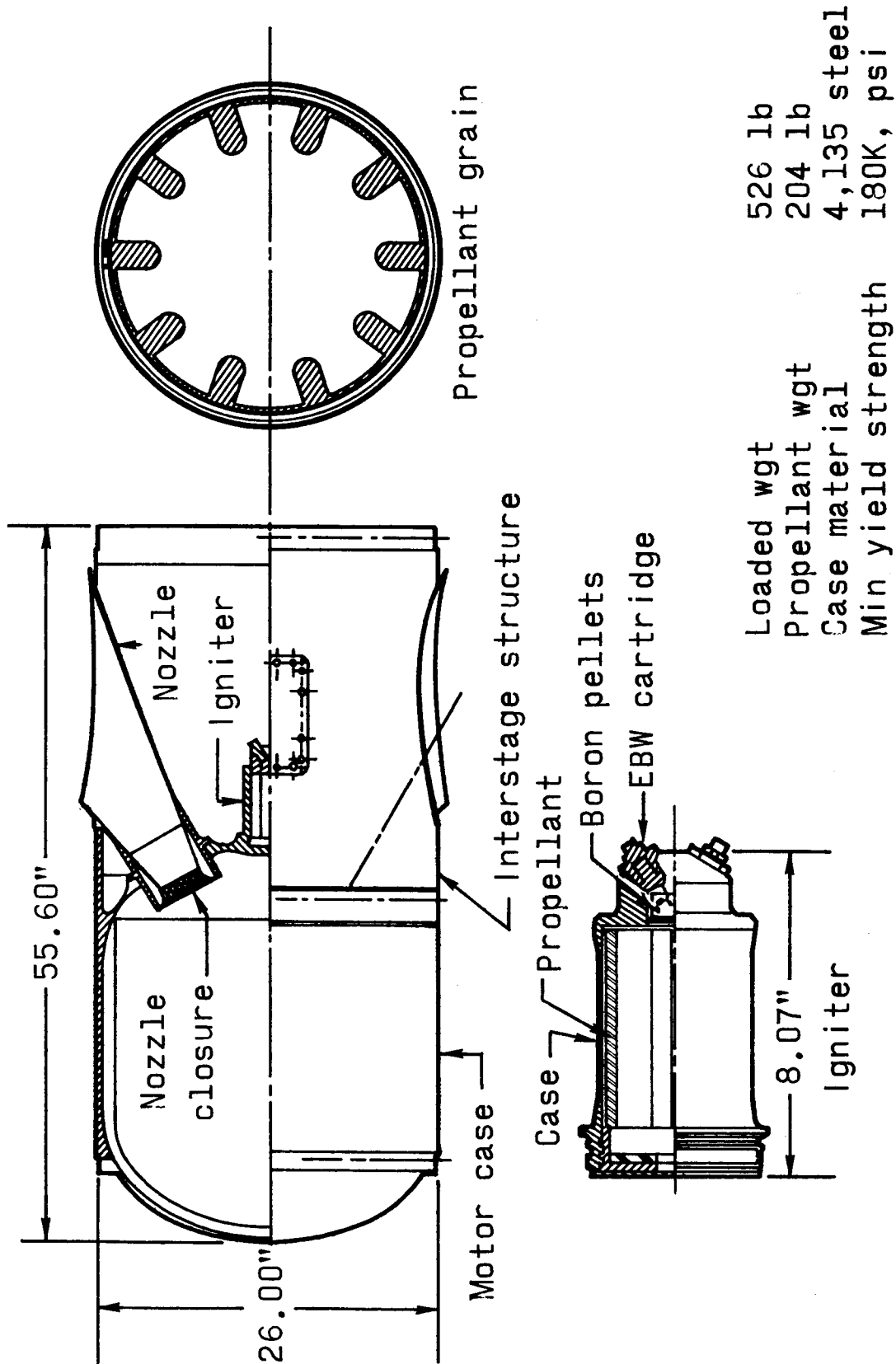
Figure 7.3.1.3-1.- Tower jettison motor.

| Parameter | Calculated | Predicted | Difference percent |
|---|---|---|---|
| Max, thrust, lb | 131,900 | 151,200 | -10.0 |
| Average thrust, lb (0-2 sec) | 128,375 | 139,650 | - 8.0 |
| Total impulse, lb-sec | 568,000 | 564,950 | + 0.5 |
| Thrust rise time, sec (0-90% ignition thrust) | 0.90 | 0.085 | + 5.0 |

Calculated (55°F, nominal trajectory
Predicted (70°F, 4000 ft)

Launch escape motor thrust, lb

Burning time, sec
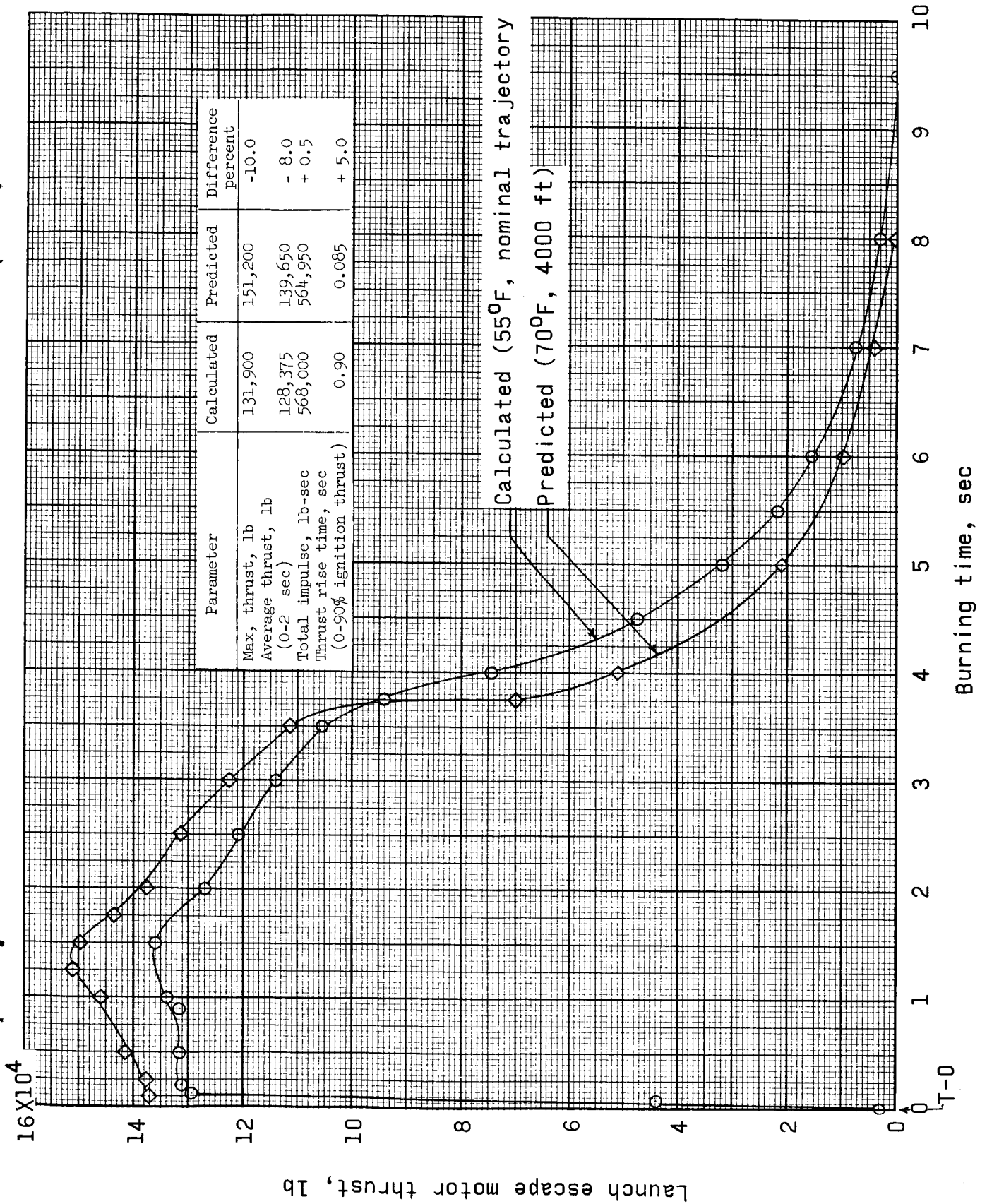
Figure 7.3.2.1-1.- Launch-escape motor performance.
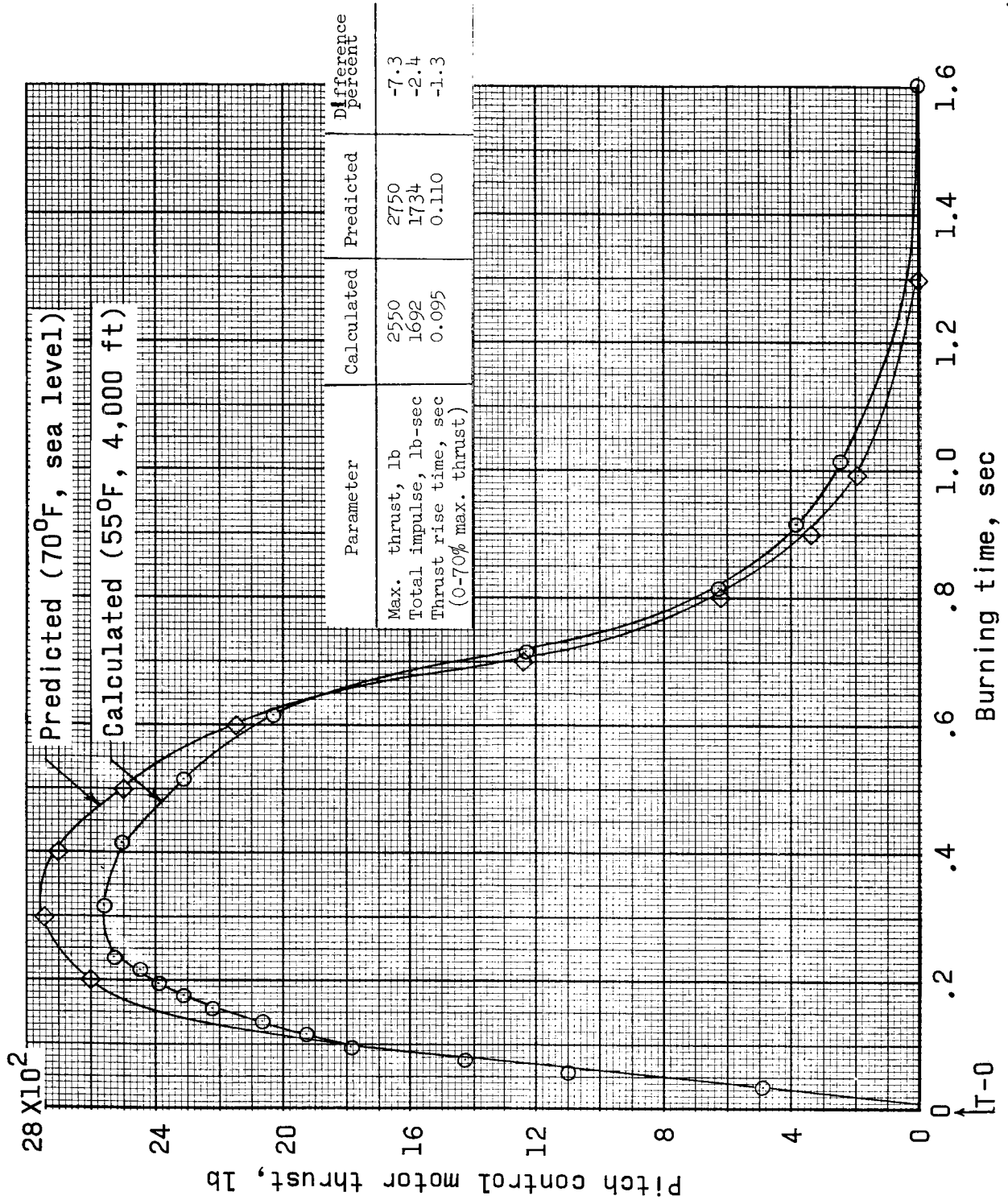
Figure 7.3.2.2-1.- BP-6 pitch-control motor performance.

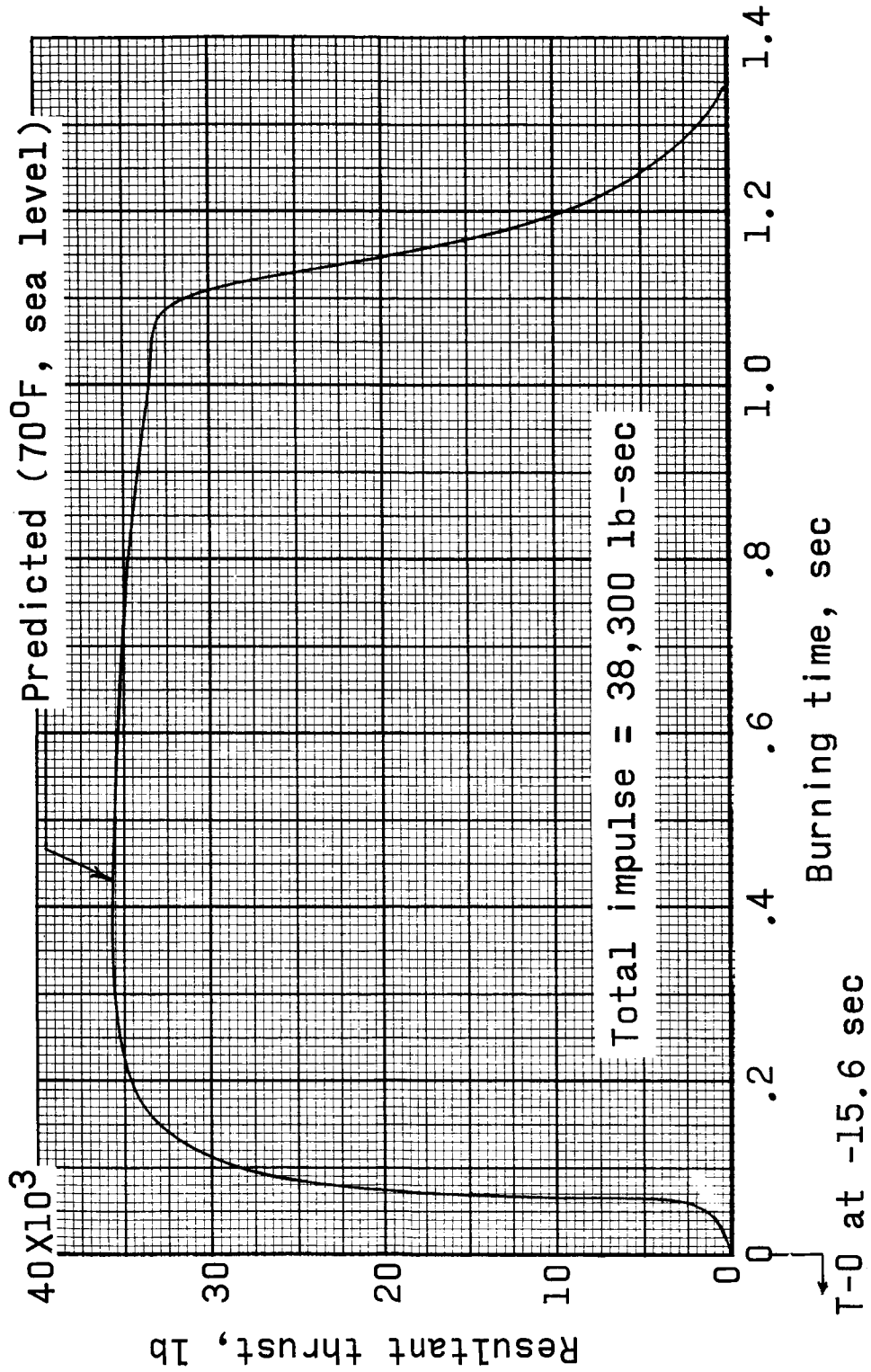| Parameter | Calculated | Predicted | Difference percent |
|---|---|---|---|
| Max. thrust, lb | 2550 | 2750 | -7.3 |
| Total impulse, lb-sec | 1692 | 1734 | -2.4 |
| Thrust rise time, sec (0-70% max. thrust) | 0.095 | 0.110 | -1.3 |

Figure 7.3.2.3-1.- BP-6 predicted tower-jettison motor performance.

## 7.4  Pyrotechnics

7.4.1  Introduction.- The pyrotechnics of the launch-escape system on boilerplate 6 provide for ignition of the launch-escape motor, pitch-control motor, the tower jettison motor; and the energy to part the separation bolts connecting the launch-escape tower to the command module.

The earth-landing system pyrotechnics provide the explosive energy which deploy the drogue parachute, release the drogue parachute, and deploy the three pilot parachutes. The forward heat-shield pyrotechnic system and the main parachutes disconnect were deleted as a result of modifications after boilerplate 3 drop test 5.

The pyrotechnics used in this test were not the type to be used in the production Apollo vehicle.

7.4.2  System description.- The pyrotechnic devices used on boilerplate 6 Apollo Pad Abort Test 1 consisted of hotwire initiators and exploding bridgewire initiators. The difference between the hotwire initiator and the exploding bridgewire initiator is that in the latter, no detonating material is required - the wire itself generates the shock wave and the high temperatures necessary for igniting the secondary booster explosive. The hotwire initiators used on the explosive separation bolts had no-fire ratings of 1 ampere-1 watt. The hotwire initiators used on the earth-landing system had no-fire rating of 0.5 ampere. The exploding bridgewire initiators utilized to ignite the launch-escape motors were hand picked for this particular test out of over 60 qualification test devices.

The pyrotechnic batteries provided the 28 volts through the sequencer to the EBW firing units. Within the EBW firing unit an oscillator started charging the capacitor up to 2,200 to 2,300 volts. When the firing signal was received the capacitor discharged and the voltage went to the EBW initiator bridgewire initiating the charge.

7.4.3  System performance.- The exploding bridgewire (EBW) initiators ignited both the launch-escape motor and the pitch-control motor at approximately T-0 second. At T+15.6 seconds the tower-jettison motor and the explosive cartridge within the tower separation bolts were ignited. The drogue parachute pyrotechnic devices fired at T+18.6 seconds and ejected the drogue parachute. At T+24.0 seconds the pyrotechnic devices in the pilot parachute mortars fired and ejected the three pilot parachutes.

Also at T+24.0 seconds the drogue disconnect cartridges fired and detonated the linear-shaped charge, thus cutting the drogue parachute from the command module. Telemetry data (appendix A 4-9 (a) ) indicate that at T+24 seconds the pyrotechnic voltage on pyrotechnic bus B dropped from 28 volts down to 14 volts for approximately 4 seconds, then rose again to 28 volts. During postflight inspection and close examination of the drogue parachute disconnect it was found that one of the hotwire initiators was shorted pin-to-pin. This would explain the drop in voltage picked up by telemetry in that there was a high power drain on the pyrotechnic bus until the fusing resistor blew, disconnecting the short from the bus. The exploding bridgewire (EBW) firing units utilized on boiler-plate 6 functioned properly by charging up to approximately 2,200 volts and discharging, per sequencer time, within the allowable time tolerance.

7.4.4    Conclusions.- All pyrotechnic devices with the exception of one drogue disconnect initiator functioned properly according to sequencer time. The drogue disconnect initiator shorted during drogue disconnect and caused a high power drain on the pyrotechnic bus until the fusing resistor blew removing this short from the bus. All exploding bridgewire (EBW) firing units functioned as expected and discharged properly.

7.5  Landing System

7.5.1  System description.-

7.5.1.1  Sequencing:- The sequencing system on boilerplate 6 was based on timing compatible with the tower-flap concept for abort and recovery. The drogue-parachute mortars were fired 3 seconds after tower jettison. Five seconds later, the drogue parachute was released and at the same time the three pilot-parachute mortars were simultaneously fired. The three pilot parachutes then deployed the three main parachutes.

7.5.1.2  Drogue parachute:- Boilerplate 6 had one 13.7-foot-diameter, FIST robbon, 25° conical, drogue parachute with a geometric porosity of 23 percent. The canopy was permanently reefed by use of pocket bands to an apparent 12.2-foot diameter. The drogue parachute riser was 56 feet long and was attached to a shaped-charge-type disconnect. The lower 15 feet of the riser was protected with Thermo Fit Sleeving, a plastic which is resistant to abrasion and cutting. The drogue parachute was deployed by a mortar which incorporated redundant initiators.

7.5.1.3  Pilot parachutes:- Boilerplate 6 had three simultaneously deployed, 10-foot-diameter, ringslot pilot parachutes. The pilot parachute risers were 43 feet long and were protected with Thermo Fit Sleeving on the lower 5 feet. The pilot parachutes were deployed by mortars which incorporate redundant initiators.

7.5.1.4  Main parachutes:- The main parachutes were 88.1-foot diameter ringsails (PDS 1543) which were independently deployed by the 10-foot-diameter pilot parachutes. The three main parachutes were sized such that proper operation of two parachutes would give a rate of descent of less than 33 ft/sec at a pressure altitude of 5,000 feet. The main parachutes were reefed to 13 percent of the nominal diameter for a period of 6 seconds. Three pyrotechnic cutters, mechanically initiated at line stretch of the main parachutes, were used to sever each reefing line. One reefing line was installed in each main parachute and operation of any one cutter per line would have resulted in normal disreefing.

The three main parachute risers were attached to a common clevis, and  5  feet of each riser were covered with Thermo Fit sleeving. based on the failure analysis of boilerplate 3 and subsequent rigging requirements, the main parachute disconnect and upper harness legs had been removed. Four lower

harness legs were attached to the clevis and to the main parachute attachment fittings located near the top egress tunnel, just above each deck gusset. The lower harness legs were approximately 60 inches long and were protected with Thermo Fit Sleeving. The bridle was designed to hang the command module at a cant angle of -5°.

The installation of the parachutes on the parachute deck is shown in figure 7.5.1.4-1.

7.5.2     System performance.-

7.5.2.1   Events:- All events in the earth landing system (ELS) occurred within specification tolerances. The following times were recorded and are compared with those expected.

| Event | Elapsed time, sec | |
|---|---|---|
| | Expected | Actual |
| Tower and forward heat-shield jettison (timer) | 15.5 | 15.6 |
| Drogue-parachute deployment (timer) | 18.5 | 18.6 |
| Drogue-parachute release and pilot parachute mortar initiation (timer) | 23.5 | 24.0 |
| Main-parachute line stretch | 27.5 | 26.1 |
| Main-parachute disreef | 33.5 | 32.3 |

The specification for the ELS timer functions is +10 percent to 0 percent.

7.5.2.2   Drogue parachute performance:- The drogue parachute was deployed by mortar at T+18.6 seconds; the command module was at an angle of attack of approximately 64°. The drogue parachute reached full inflation and became effective in 1.2 seconds and achieved reorientation of the command module before main-parachute deployment, as described in detail in paragraph 7.5.3.1. The

drogue mortar functioned normally with no apparent indication of excessive recoil loads. The drogue parachute was undamaged and there was no scuffing or abrasion of the drogue riser or the Thermo Fit sleeving. The Thermo Fit sleeving was parted in the area where it had been necessary to sew through the sleeving for attaching the deployment bag closure tie break loop. The drogue parachute was disconnected and the three pilot parachutes were deployed by mortars at T+24.0 seconds. There was no detremental effect on performance.

7.5.2.3    Pilot parachute performance:- The three pilot parachutes were deployed by mortars; the angle of attack of the command module was approximately 160°. All pilot parachutes inflated normally and provided clean deployment of all main parachutes. The pilot parachutes and risers, including the Thermo Fit sleeving, were undamaged. Each of the pilot-parachute mortars functioned normally with no apparent indication of excessive recoil loads.

7.5.2.4    Main parachute performance:- The main-parachute deployment bags were extracted from the parachute deck when the command module was at an angle of attack of approximately 230° which was near the maximum angle of attack of the command module during main-parachute deployment. During main-parachute deployment, the angle of attack of the command module decreased to a minimum of approximately 150° at main line stretch. The oscillation of the command module then damped very rapidly as the main parachutes inflated. The three parachutes disreefed at approximately the same time, and full inflation was quite uniform. No load data on individual parachutes were obtained, but qualified observers reported that all main parachutes inflated normally, with little or no aerodynamic interference. Descent on the main parachutes was uneventful and terminated in a nominal landing. At landing the command module remained upright. There was no inflight damage to the main parachutes, risers, or harness. A minor tear was found in the deployment bags. This damage was caused by the attachment fittings of the pilot parachute bridle as the deployment bags turned inside out after main parachute deployment. The damage had no effect on system operation.

Terminal descent rate on the main parachutes was reached at a pressure altitude of 7,300 feet, or approximately 3,300 feet above launch-pad altitude. The preliminary trajectory data indicate that the descent rate at pressure altitudes below 5,000 feet was approximately 24 ft/sec, which is within nominal design conditions. The total velocity at a pressure altitude of 5,000 feet was 30 ft/sec and at landing was 27 ft/sec.

7.5.3    Results.-

7.5.3.1    Performance comparisons:- Figure 7.5.3.1-1 shows a comparison of the time histories of angle of attack and dynamic pressure for boilerplate 6 from tower jettison through main-parachute line stretch. Also shown on the figure are predictions for nominal conditions for boilerplate 6 and the results of the simulation test for boilerplate 19. The dynamics of the command modules while on the drogue parachute agree very well through drogue parachute release.

The data shown in figure 7.5.3.1-1 for the boilerplate 6 test were obtained from data film and a combination of trajectory data and telemetered attitudes.

7.5.4    Conclusions.- It is concluded that the ELS was successful in all phases of operation. The command module dynamics after tower jettison agree very closely with those predicted. The minor damage to the main-parachute bags and the Thermo Fit sleeving on the drogue-parachute riser was not detrimental to the operation of the systems. Because of the angles of attack and dynamics of the command module at drogue and pilot parachute deployment, no abrasion or cutting of the protective sleeving was experienced.
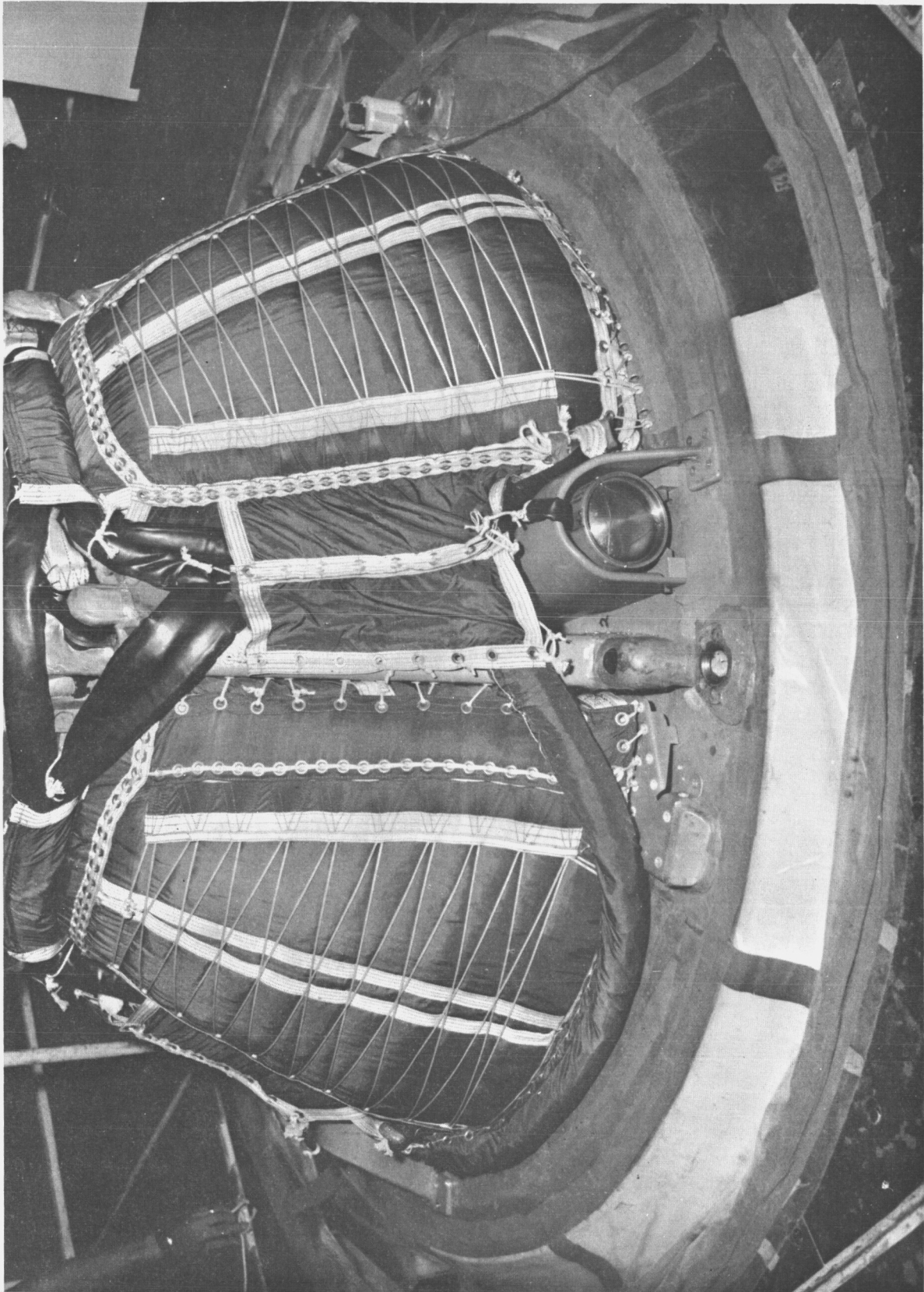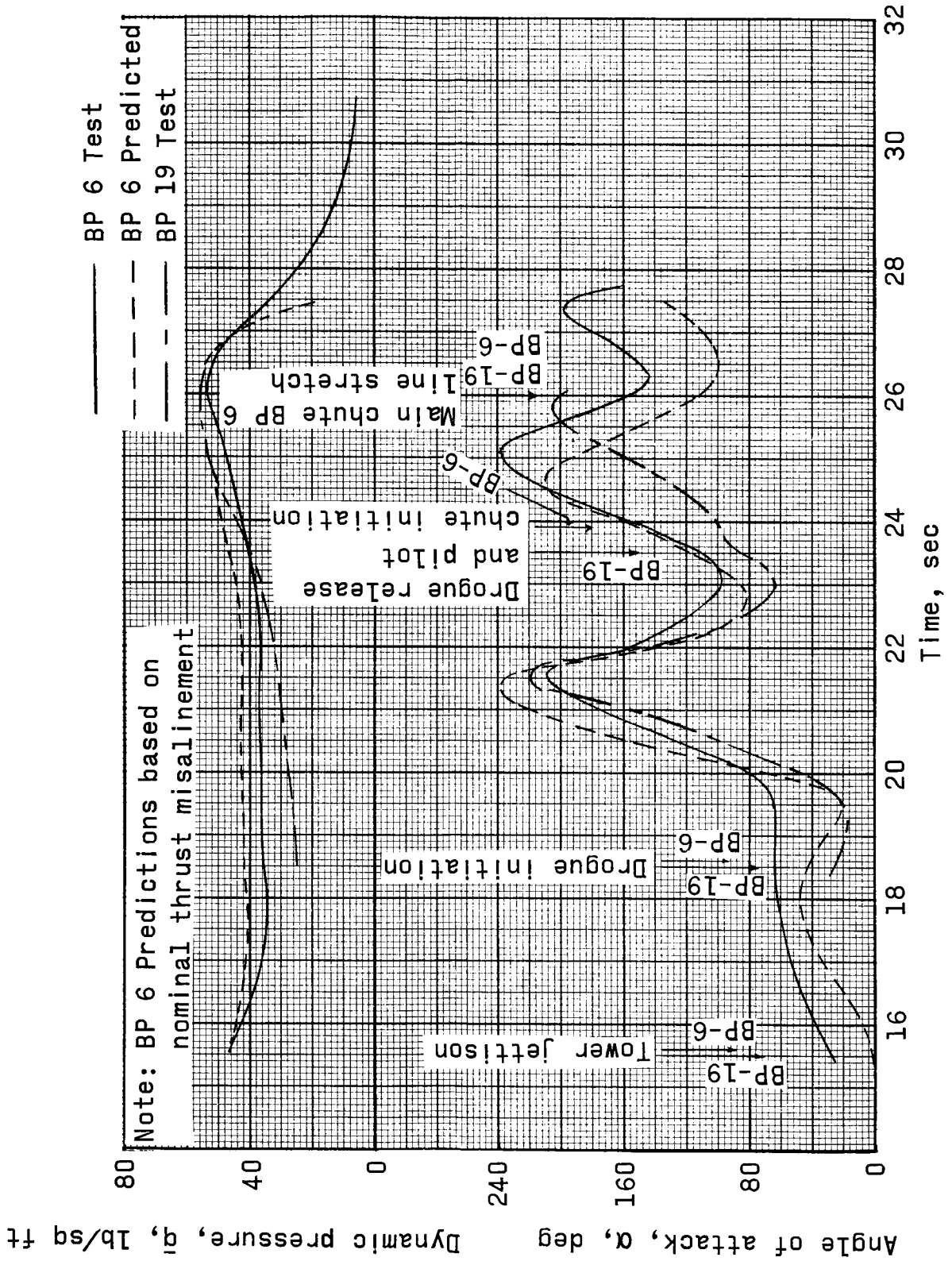
Figure 7.5.1.4-1.- Parachute deck prior to flight.

Figure 7.5.3.1-1. – Angle of attack and dynamic pressure time history comparison.

## 7.6  Structures

The structure for Pad Abort 1 flight-test vehicle consists of a production launch-escape system in combination with a simulated (boiler-plate) command module.  Since the command module is not representative of the actual spacecraft, no instrumentation was provided to determine structural loads.  Measurements of such characteristics as vehicle accelerations, angle of attack, Mach number, and dynamic pressure enabled a determination of the inflight loads resulting from external environment or vehicle dynamics.  The magnitude of the loads encountered by the vehicle during flight are discussed in this section.

The vehicle was instrumented with 40 pressure transducers for the purpose of determining the effects of escape-motor jet-plume impingement on the aerodynamic stability characteristics and on the structure.  A thorough analysis of these pressures was not possible for this report; however, some trends and comparisons with wind-tunnel jet-effect data are discussed.

A second-order test objective was to establish the tower vibration during a pad abort.  Six high-range, high-response accelerometers were placed on the escape tower for this purpose.  A preliminary evaluation of these data indicates that the objective was met.

7.6.1    Flight loads.- A preliminary investigation of the flight loads encountered by the vehicle indicated that the loads were much less than spacecraft design loads.  Table 7.6.1-1 shows a comparison of the flight parameters for two of the worst loading conditions with some representative design values.  The external pressure distribution for design is based on a tumbling condition.  Since this vehicle did not attain high angles of attack (>30°), the external pressures were less than design pressures. Postflight inspection of the command module showed no structural damage attributed to loads encountered during flight.

7.6.2    Pressure measurements.- A preliminary investigation was made of the command module local pressures obtained during powered flight.  The primary purpose of this instrumentation was to provide detailed pressure distributions on the command module for eventual correlation with vehicle stability characteristics and for structural evaluation.  The local pressure distribution and vehicle aerodynamic stability are interrelated and affect the loads accordingly.  The stability characteristics determine the flight parameters which affect the overall loads, and the local pressure distributions affect the design of the local structure.  The local pressures are affected considerably by the jet plumes from the four escape-motor nozzles.  The data obtained from this flight will allow a detailed analysis of

pressures and stability characteristics for a range of subsonic
Mach numbers and low angles of attack.

7.6.2.1   Command module pressures:- Figure 7.2.1-4 shows the location of
the pressure transducers on the command module. The data indi-
cate that good information was obtained from all except 2 of
the 40 measurements.

Figure 7.6.2.1-1 shows time histories of the measurements ob-
tained during the early portion of the flight. These pressure
measurements are presented to give an indication of the varia-
tion in data scatter with measurement location. Base pressure
measurement CA 0100 P (base pressure no. 1) is typical of the
four base measurements obtained. This transducer gave smoother
data than the other measurements on the heat shield. Four con-
ical pressures are shown in the figure. Pressures CA 0053
(no. 26) and CA 0063 (no. 36) were measured along a ray dir-
ectly opposite a jet axis. The scatter is greater for these
pressures during escape-motor thrusting than for measurements
CA 0052 (no. 25) and CA 0048 (no. 21), which are positioned
between jet plumes. This trend is evident formost of the pres-
sure measurements. The increased scatter opposite the plumes
is attributed to the highly turbulent jet mixing layer.

7.6.2.2   Comparison of measured pressures with wind-tunnel data:- This
section contains a preliminary analysis of the pressures. Two
conditions have been investigated which correspond closely to
available preliminary wind-tunnel data (ref. FSJ-1 jet effects
wind-tunnel test dated August 8, 1963) which has not yet been
published in report form. The following table shows the con-
ditions chosen and the comparable wind-tunnel data. The con-
dition at T+2.6 seconds corresponds to early trajectory indica-
tions of a sideslip angle $\beta$ of $\approx 2°$ at M=0.5. Angle of attack
at this time was essentially zero $(\alpha \approx 0°)$.

| Flight time, sec | Mach number | | Angle of sideslip, deg | |
|---|---|---|---|---|
| | Flight | Wind tunnel | Flight | Wind tunnel |
| 4.0 | 0.65 | 0.70 | 0 | 0 |
| 2.6 | 0.50 | 0.50 | $\approx 2.5$ | 2 |

Figure 7.6.2.2-1 shows pressure distributions which are located on rays between jet plumes. Figure 7.6.2.2-1(a) shows the distribution for M=0.65 at β=0°, and the distribution for M=0.5 at β=2.5° is shown in figure 7.6.2.2-1(b). Both figures show that pressure coefficients for the wind-tunnel and flight tests are in fair agreement. At these low angles of sideslip, there is no predominant trend except that the pressures from flight are slightly higher over the aft portion of the command module.

Figure 7.6.2.2-2 shows pressure distributions which are located on rays opposite jet plumes. Figure 7.6.2.2-2(a) and (b) are for MO=0.65 and M=0.5, respectively. Again, agreement with wind-tunnel data is good. Both figures show that the jet-on pressures are higher than jet-off pressures except over the aft portion of the command module at M=0.5.

The agreement of the flight-test data is very good. For β=0° agreement between rays 90° apart is excellent as shown in 7.6.2.2-1(a). In addition, the angle-of-sideslip effect at M=0.5 is apparent in figures 7.6.2.2-1(b) and 7.6.2.2-2(b). From this limited investigation at low angles of sideslip, it appears that there were no large errors in the wind-tunnel-measured pressure distributions. The vehicle stability and motion analysis (section 6.0) indicated a less stable pitching-moment coefficient than predicted. No positive indication of this was observed from the limited amount of pressure data analyzed. Analysis at higher angles of attack or sideslip may show decreased pitching-moment stability.

Figure 7.6.2.2-3 is a plot of the peripheral pressure distribution at station $x_c$ 50.5. Comparable wind-tunnel data show excellent agreement peripherally at this station. However, from the plots of pressures along the rays, agreement seems to be better in this region of the command module than elsewhere.

7.6.2.3    Base-pressure measurement:- Four base-pressure measurements were made on the command-module heat shield. All measurements indicate about the same magnitude of pressure throughout flight. Figure 7.6.2.3-1 shows a time history of the base-pressure coefficient, and for comparison, wind-tunnel data at two discrete Mach numbers, M=0.5 and M=0.7 are shown. This analysis shows that the base-drag flight data are in good agreement with wind-tunnel data.

7.6.2.4    Jet impingement:- A brief analysis of the photographic coverage of the flight shows that no direct jet impingement of the escape-

motor plumes on the command module occurred during the high-level thrust period. This may be seen in figure 7.6.2.4-1. A small amount of impingement occurred during thrust tail-off but should not be significant to the command module pressure. Photographs during tail-off also show that most of the soot was deposited at this time. Figure 9.3-3 shows the sooted + Z quadrant of the command module, which was the most heavily sooted portion. There were four distince sooted areas along the escape-motor nozzle axis. In comparison, figure 4.3-1 shows the clean command module prior to flight.

Temperature-sensitive points located on the $\pm$Y- and $\pm$Z-axes of the command module showed that surface temperatures did not exceed 250° F during the flight. A small portion of the heat shield in the +Z quadrant close to the maximum diameter was scorched during the flight. This scorching may have occurred because this area is opposite the nozzle with the greatest mass flow or because the plume was forced closer to this portion of the command module during one of the relatively large positive angle-of-attack excursions.

7.6.3  Tower vibration accelerometers.- Oscillograph records of the tower vibration accelerometers, whose locations are shown in figure 7.2.1-3, indicate the accelerations on the order of 40g to 50g were measured. More detailed results must await a spectral analysis of the data obtained.

7.6.4  Concluding remarks.- The flight loads encountered during pad Abort 1 were less than design values. There was no evidence that structural damage occurred during flight. Data obtained from the pressure measurements should permit a thorough analysis of detailed pressure distributions over the command module for the flight regime encountered. Tower vibration data were obtained, but no analysis has been made at this time.

TABLE 7.6.1-1.- COMPARISON OF DESIGN LOAD PARAMETERS

WITH PAD ABORT 1 FLIGHT TEST

| Parameter | Approximate design values for tumbling Pad Abort[a] | PA-1 flight | |
|---|---|---|---|
| | | q max | α max |
| Time, sec | --- | 4.14 | 5.00 |
| Mach number | 0.7 | 0.66 | 0.64 |
| Angle of attack, deg | 90 | $\approx 4$ | $\approx 12.5$ |
| Dynamic pressure, lb/sq ft | 500 | 519 | 485 |
| Pitching acceleration, radians/sec$^2$ | 2.6 | $\approx 0$ | $\approx 0.4$ |
| Z-axis acceleration, g | -4.9 | -1.0 | -1.3 |
| X-axis acceleration, g | 1.9 | $\approx 1.0$ | $\approx 0$ |

[a]From NAA document ARM-6, dated June 4, 1963.
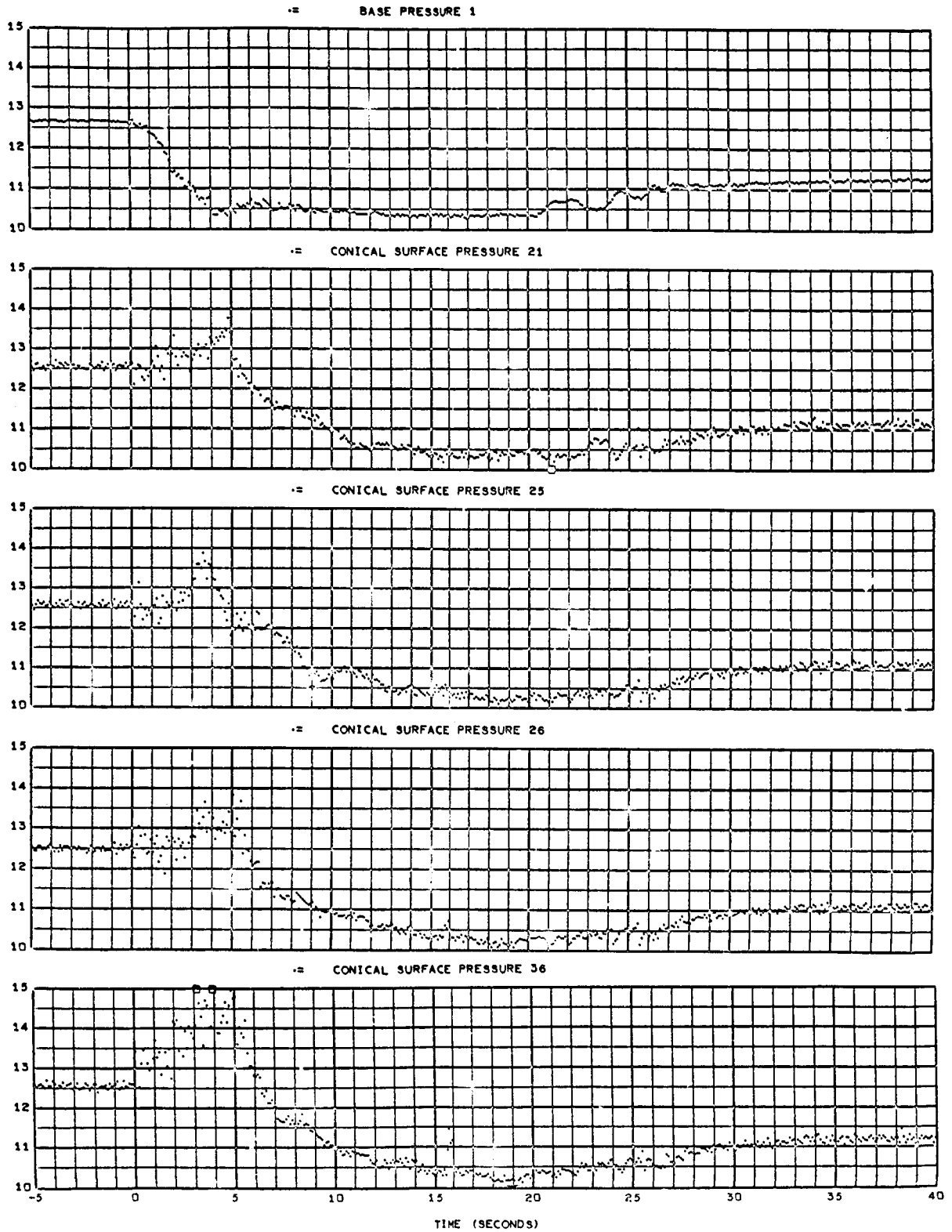
Figure 7.6.2.1-1.- Representative pressure histories of unsmoothed
data.
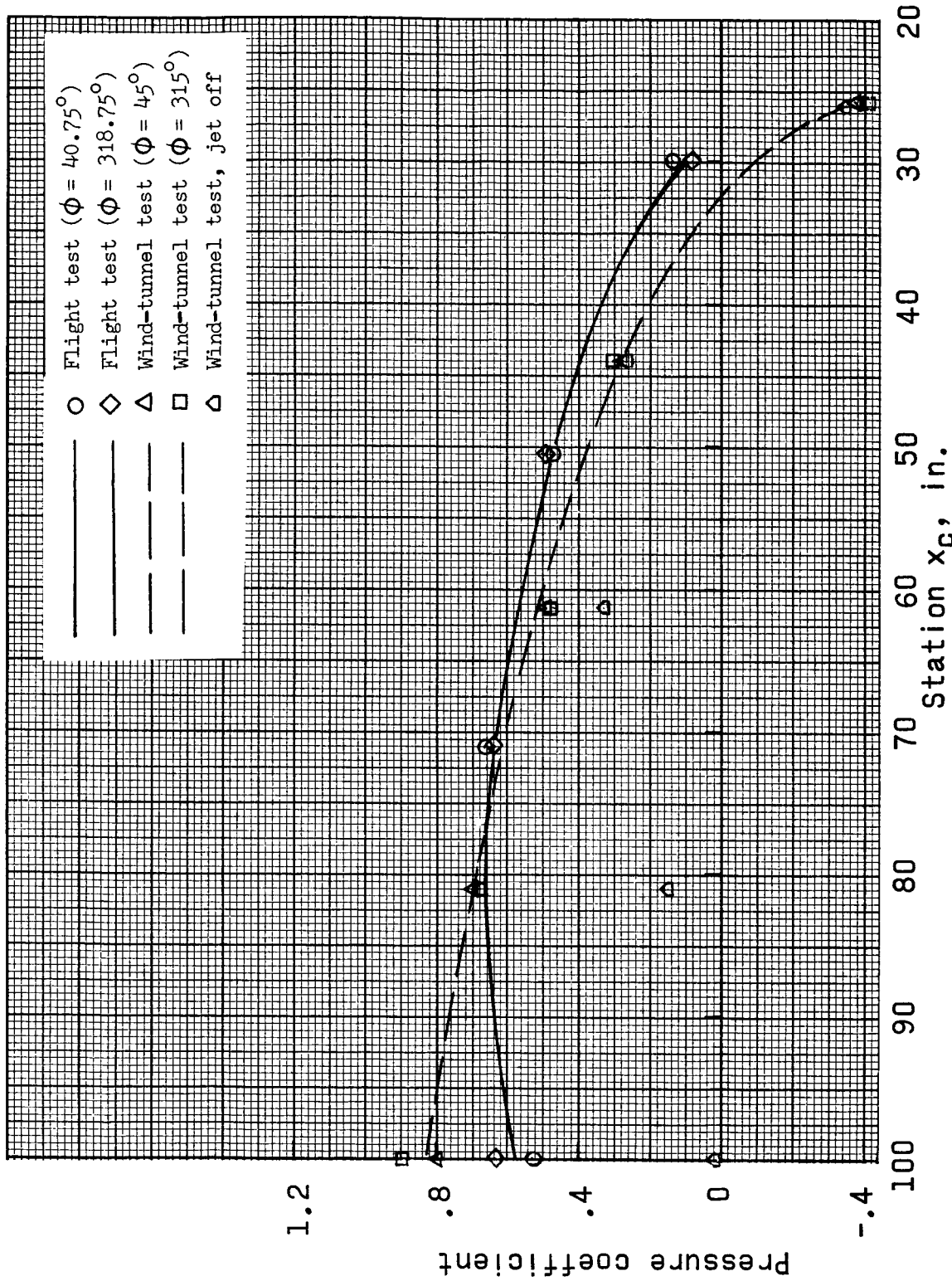
(a) M = 0.65, β ≈ 0°, α ≈ 0°. Pressure coefficient along a ray between jets.
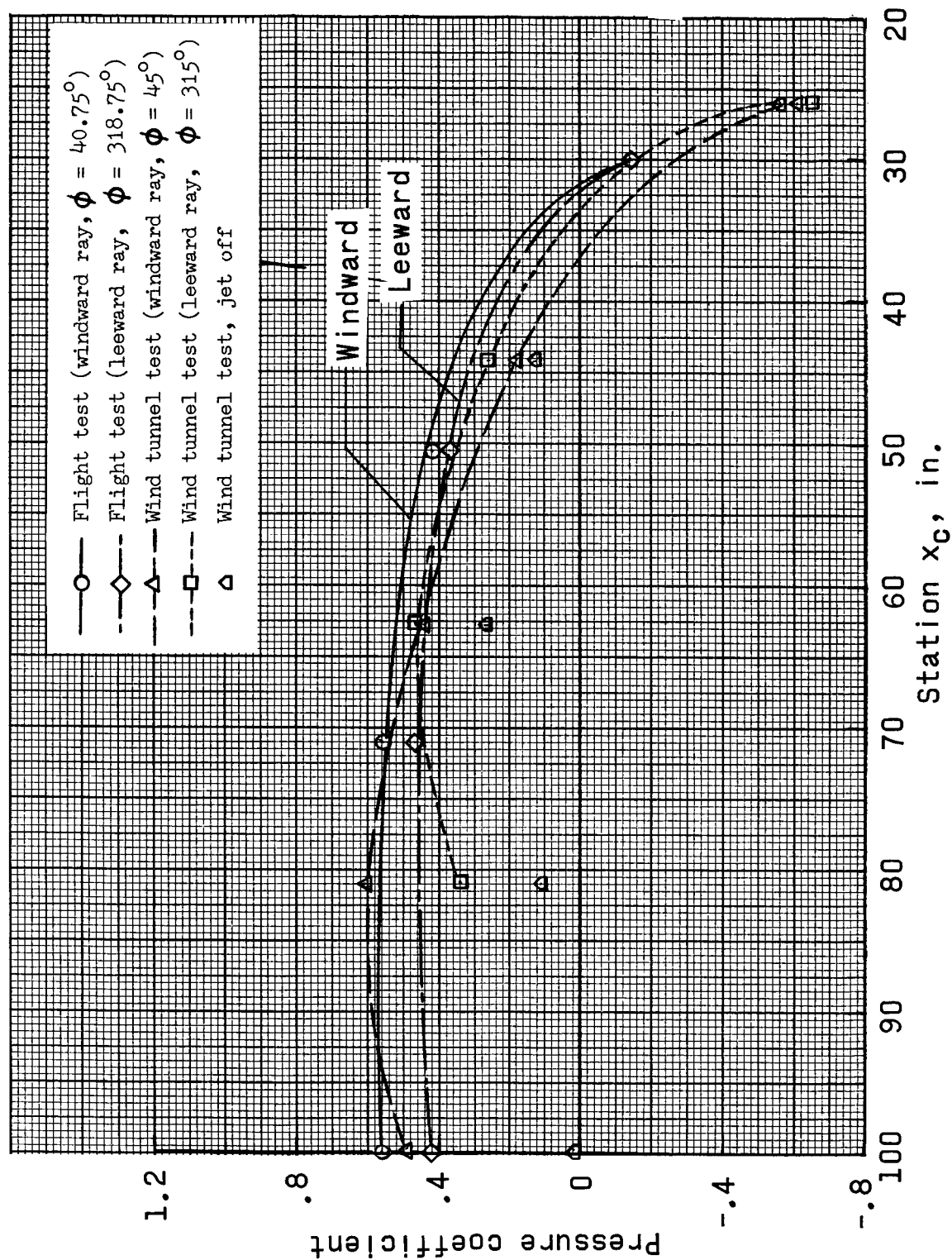
Figure 7.6.2.2-1.-

(b) M = 0.50, β = 2.5°, α ≈ 0°.

Figure 7.6.2.2-1.- Concluded.
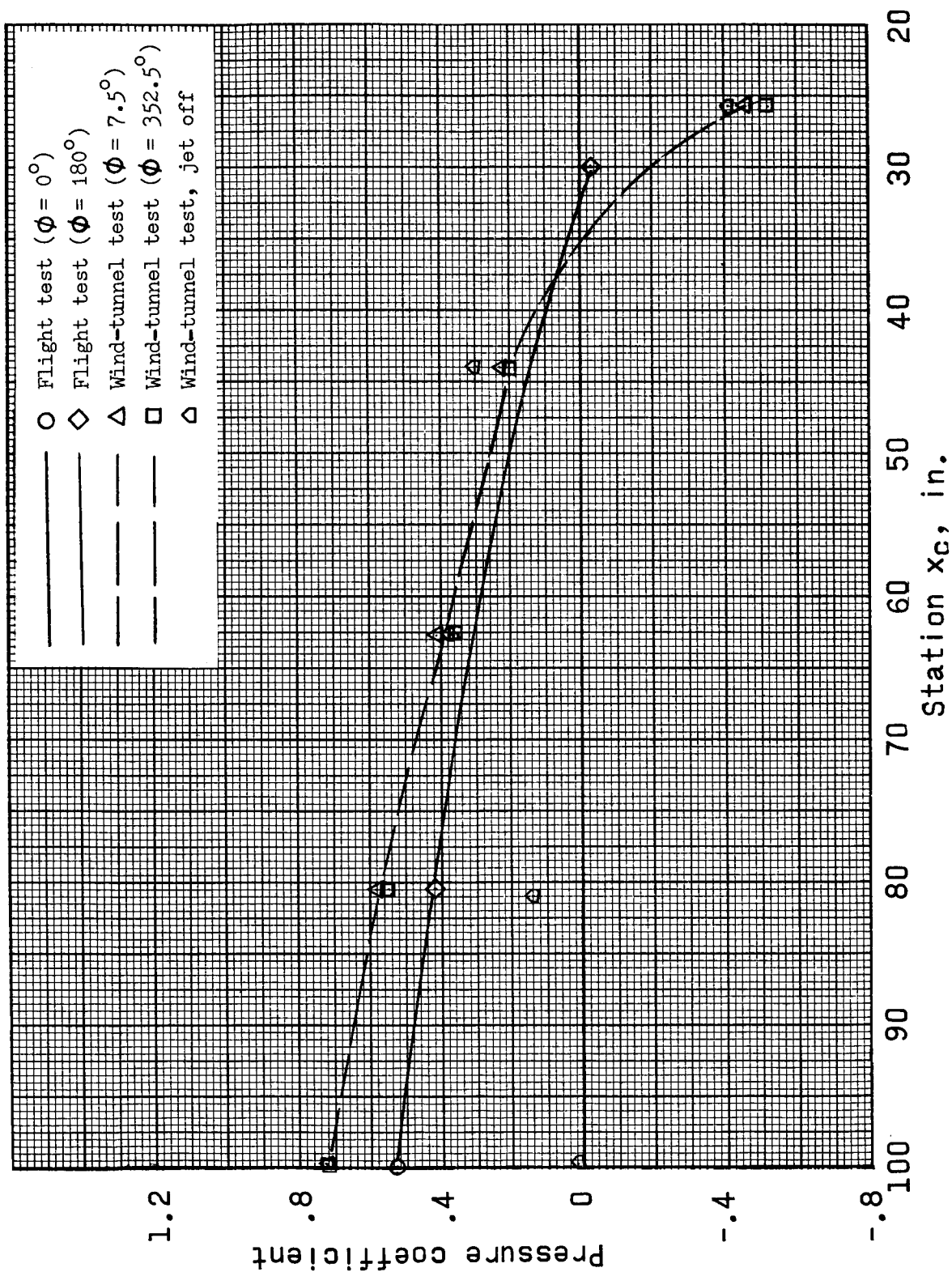
(a) $M = 0.65$, $\beta \approx 0°$, $\alpha \approx 0°$.

Figure 7.6.2.2-2.- Pressure coefficient along a ray opposite a jet plane axis.
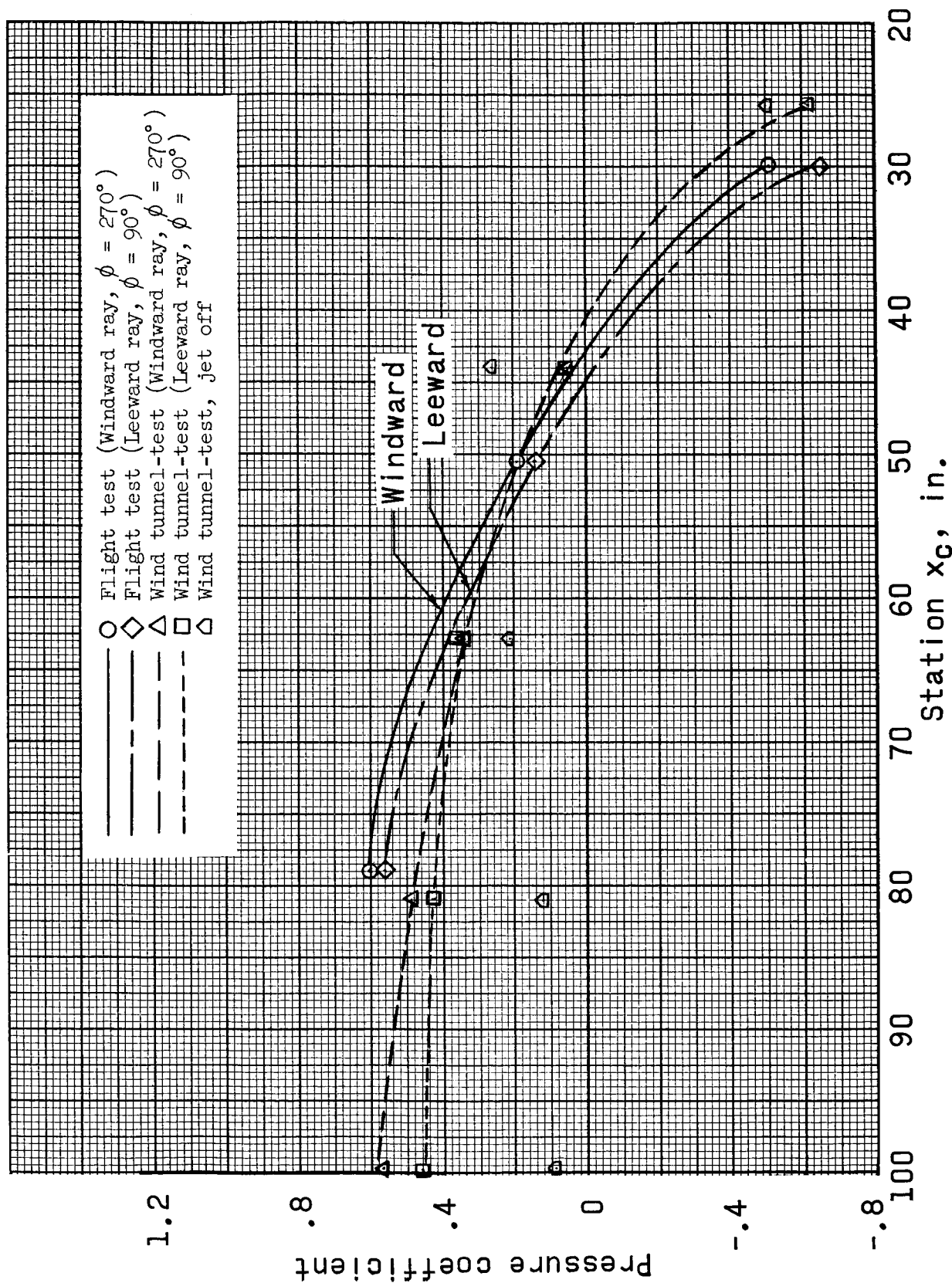
(b) M = 0.5, β≈2.5, α≈0°.

Figure 7.6.2.2-2.- Concluded.
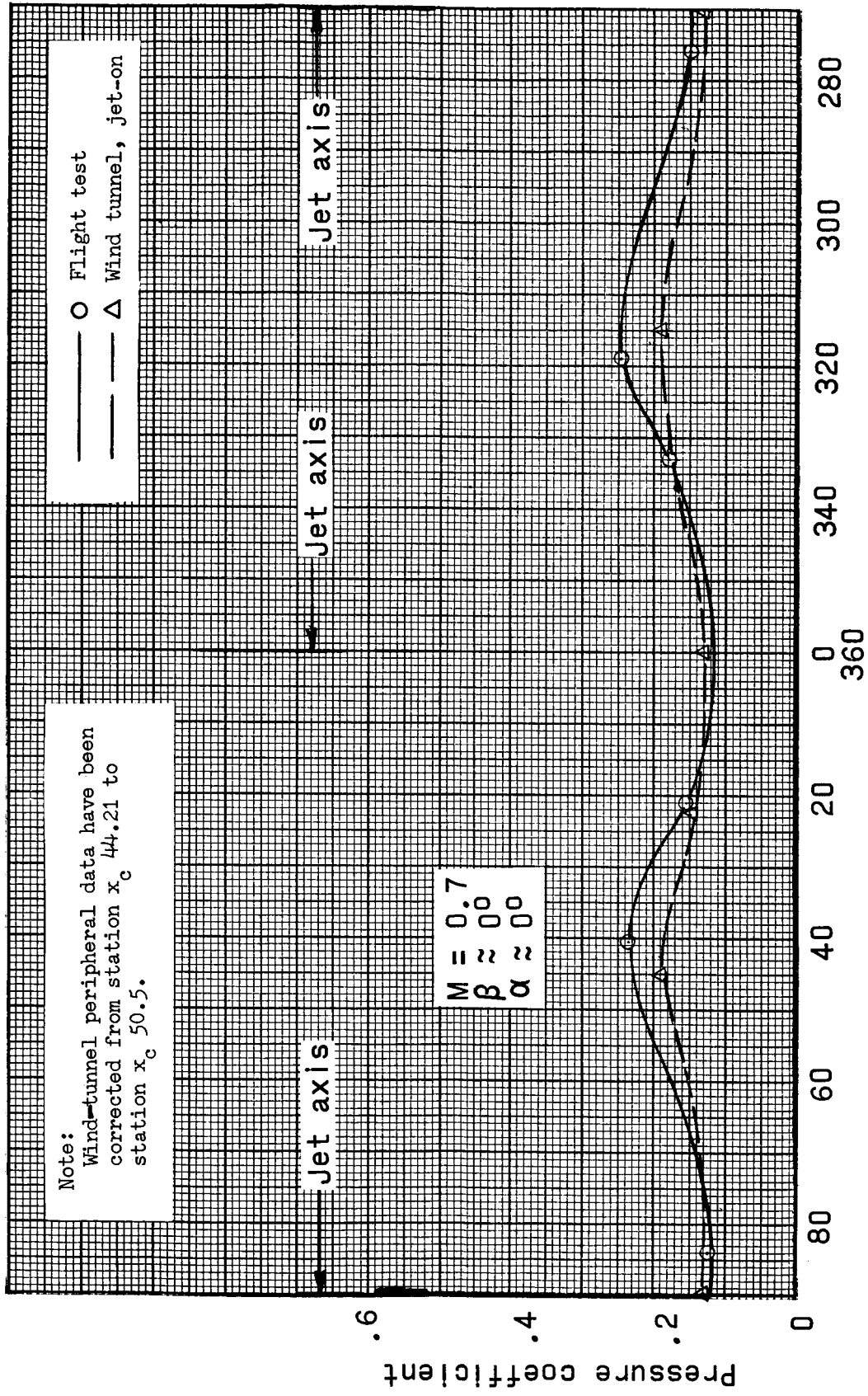
Figure 7.6.2.2-3.— Peripherial pressure coefficient distribution at BP-6 station $x_c$ 50.5.
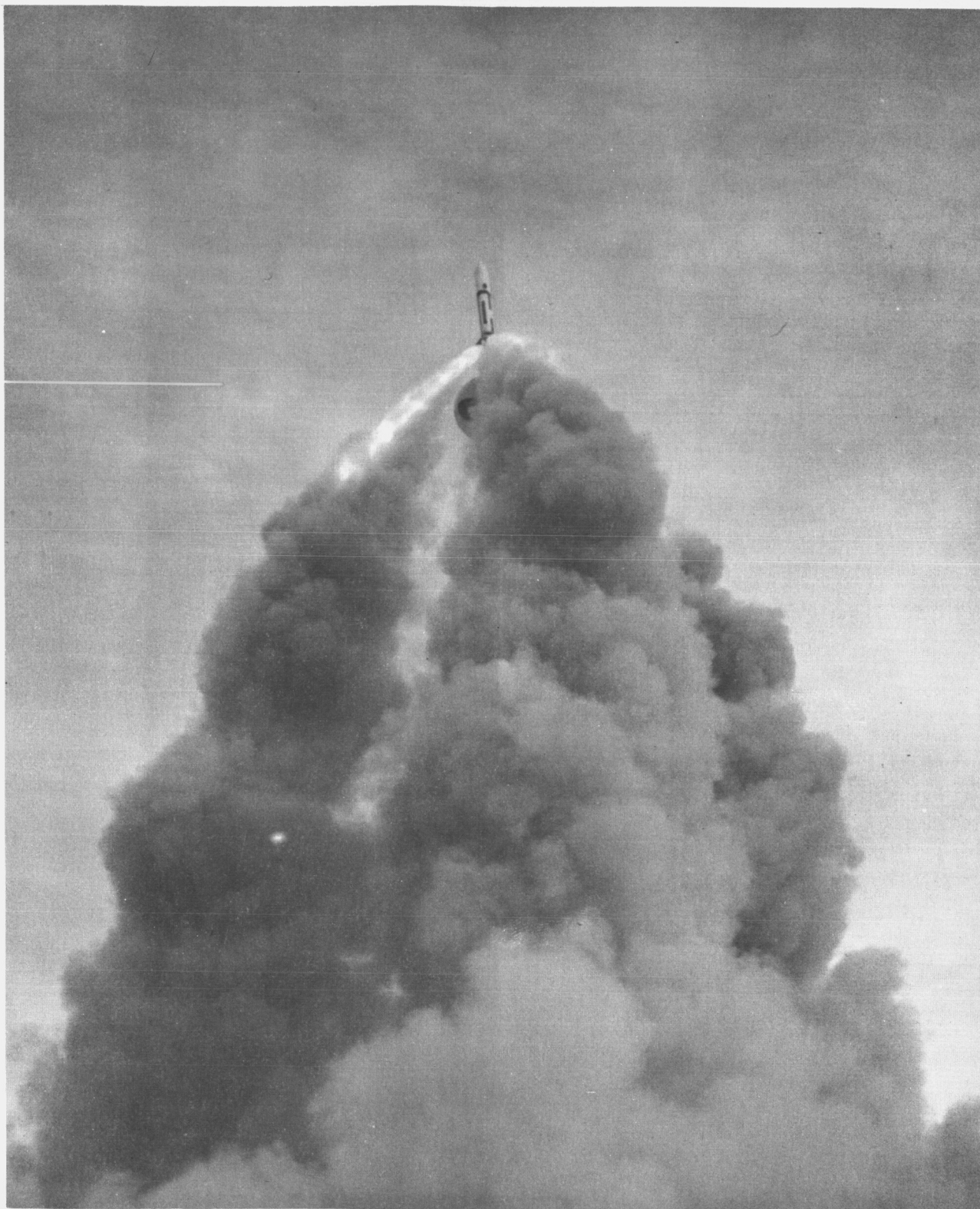
Figure 7.6.2.4-1.- Flight during high level thrust
period showing no direct impingement.
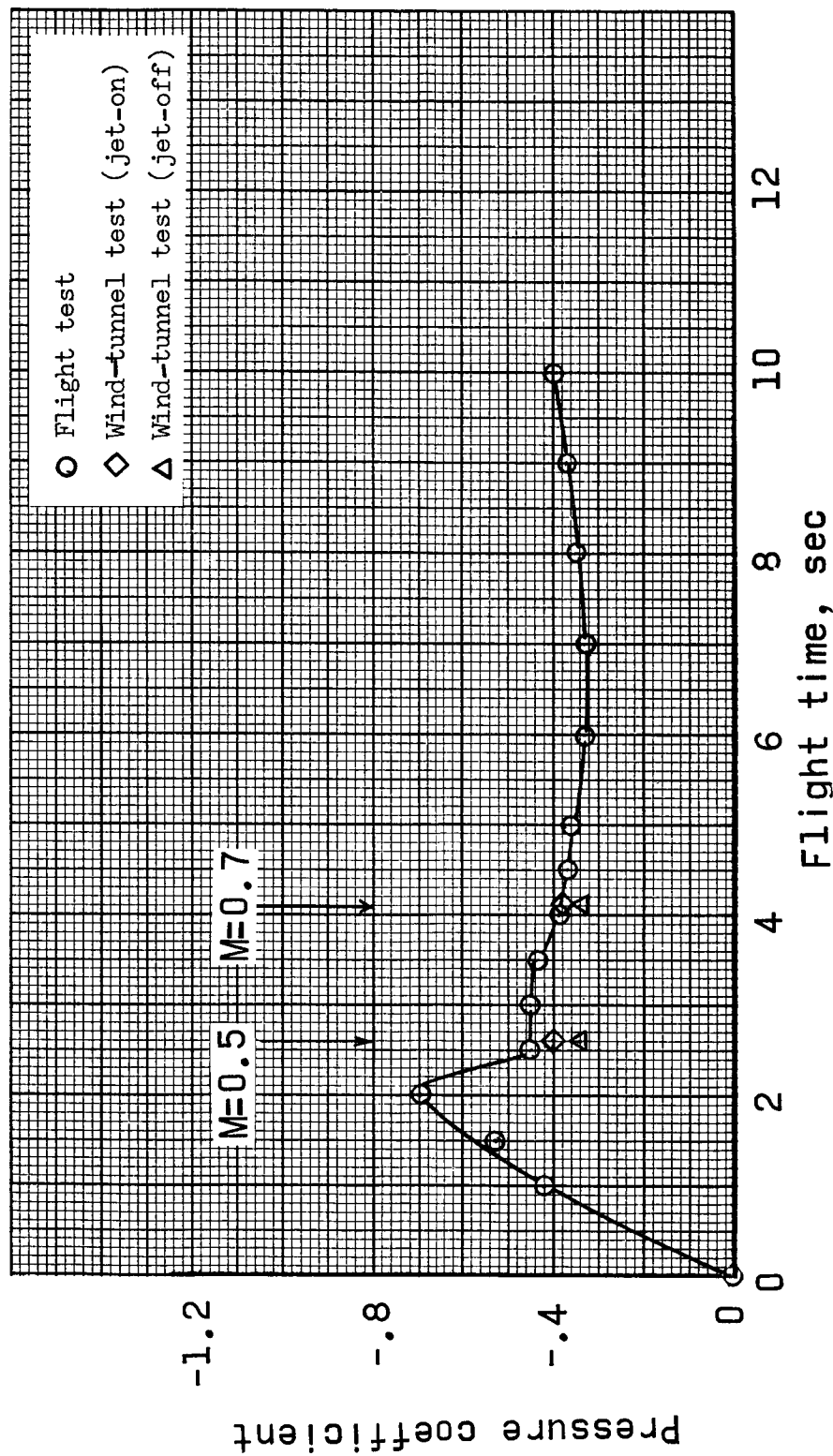
Figure 7.6.2.3-1.- Base pressure coefficient time history from base pressure measurement #1.

## 8.0  MASS CHARACTERISTICS AND THRUST-VECTOR ALINEMENT DURING FLIGHT

During flight the mass characteristics of the vehicle changed as the launch-escape motor burned.  In order to ascertain the changes in mass characteristics, the actual change in propellant weight as a function of time had to be determined.

### 8.1  Propellant Weight

During launch-escape motor operations, propellant mass was expelled through the nozzles.  The propellant mass expelled during any period of time can be determined by using the following expression:

$$W = \frac{A_t g}{c^*} \int_0^t P_c \, dt$$

where:

$A_t$ = throat area, assumed constant

$g$ = gravitational constant

$c^*$ = characteristic velocity, assumed constant

$P_c$ = chamber pressure

$t$ = time

Therefore, the propellant weight expelled in a given time can be determined by integrating the curve of the rocket-motor chamber pressure $P_c$ plotted against time $t$.

In order to determine the variation of propellant weight with time, the percentage of area under the curve for $P_c$ plotted against time at a given time increment  was determined.  The total expended weight $W_t$ is proportional to the total area under the curve.  Likewise, the incremental weight $W_i$ expended is proportional to the incremental area under

the curve at any time.  This relationship is expressed as follows:

$$\frac{W_i}{W_t} = \frac{\dfrac{A_t g}{c^*} \displaystyle\int_0^t P_c \, dt}{\dfrac{A_t g}{c^*} \displaystyle\int_0^T P_c \, dT}$$

$$\equiv \frac{W_i}{W_t}$$

$$= \frac{\text{Incremental area}}{\text{Total area}}$$

where:

  $i$ = incremental unit

  $t$ = incremental time

  $T$ = total time

The total area and incremental areas under the curve for $P_c$ plotted against time were determined by graphical integration.  The percentage area at each time is proportional to the percentage weight expended. The propellant weight remaining at each time was taken as the difference between the initial loaded weight and that expended during the time period being considered.  The actual motor propellant weight presented as a function of time for the boilerplate 6 flight is shown graphically in figure 8.1-1.

## 8.2  Spacecraft Mass Characteristics

Based upon actual weight data and the propellant time curve shown in figure 8.1-1, the variation of spacecraft mass characteristics with time was computed.  All the mass characteristics deviated from the predicted values.  This discrepancy is attributed to the weight time history of launch-escape motor propellant deviating from the predicted.

Figure 8.2-1 presents a time history of the spacecraft weight.  The weight of the pitch-control motor propellant has been removed.  At burn-out of the launch-escape motor the vehicle weight was computed to be 12,619.15 pounds.  This weight includes the jettison-motor propellant.

Figure 8.2-2 shows the flight and predicted longitudinal location of the center of gravity with respect to time.  Flight data indicate

that burnout occurred when the longitudinal location of the center of gravity was at 1,116.35 inches as compared with the predicted location of 1,116.00 inches. The initial (launch) center-of-gravity was predicted to be at a longitudinal location of 1,152.6 ±0.5 inches. The actual initial center of gravity determined during weight and balance operations was 1,152.75 inches. The flight center of gravity based on the above computations was forward of the predicted positions, which would tend to produce a more stable condition.

Figure 8.2-3 shows the actual and predicted center-of-gravity location in the Z direction with respect to time. The values actually attained for the center of gravity in the Z direction, 4.29 and 5.38 inches at launch and burnout, respectively, were the nominal values desired. The rate of change of the center-of-gravity location in the Z direction deviated slightly from the predicted.

Figure 8.2-4 presents the center-of-gravity location in the Y direction with respect to time. As can be seen from this figure, the actual center-of-gravity location in the Y direction did not vary significantly from predicted values.

Figures 8.2-5 and 8.2-6 present the moments of inertia with respect to time. The actual moments of inertia were slightly lower than the predicted values. Moments of inertia are calculated since no actual determinations of these parameters were performed. All inertia data have been corrected to account for the tilting of the launch-escape-system (LES) motor as a result of the thrust-vector misalinement.

Table 4.2-1 presents the mass characteristics of the spacecraft at various significant events. The jettisoned weights (that is, apex cover and drogue, pilot, and main parachutes) are all actual values, the items having been weighed prior to flight.

### 8.3 Thrust-Vector Alinement

The thrust-vector alinement of the launch-escape motor was performed on October 18, 1963. The thrust-vector angle was set at 2° 23.8'. Prior to launch, on T-1 day, the thrust-vector angle was checked on the launch pad and found to be 2° 25.8', which was within set tolerances.

The initial thrust-vector angle was checked by two independent methods. These methods are as follows:

1. The distance between the skirt and the tower leg adjustment bolts was measured. The thrust-vector angle was calculated from these distances and found to be 2° 23'.

    2.  Based upon the center-of-gravity shift caused by the angular displacement of the LES, the thrust-vector angle was calculated and found to be 2° 27.0'.

    Figure 8.3-1 shows a graphical representation of the thrust-vector angle.
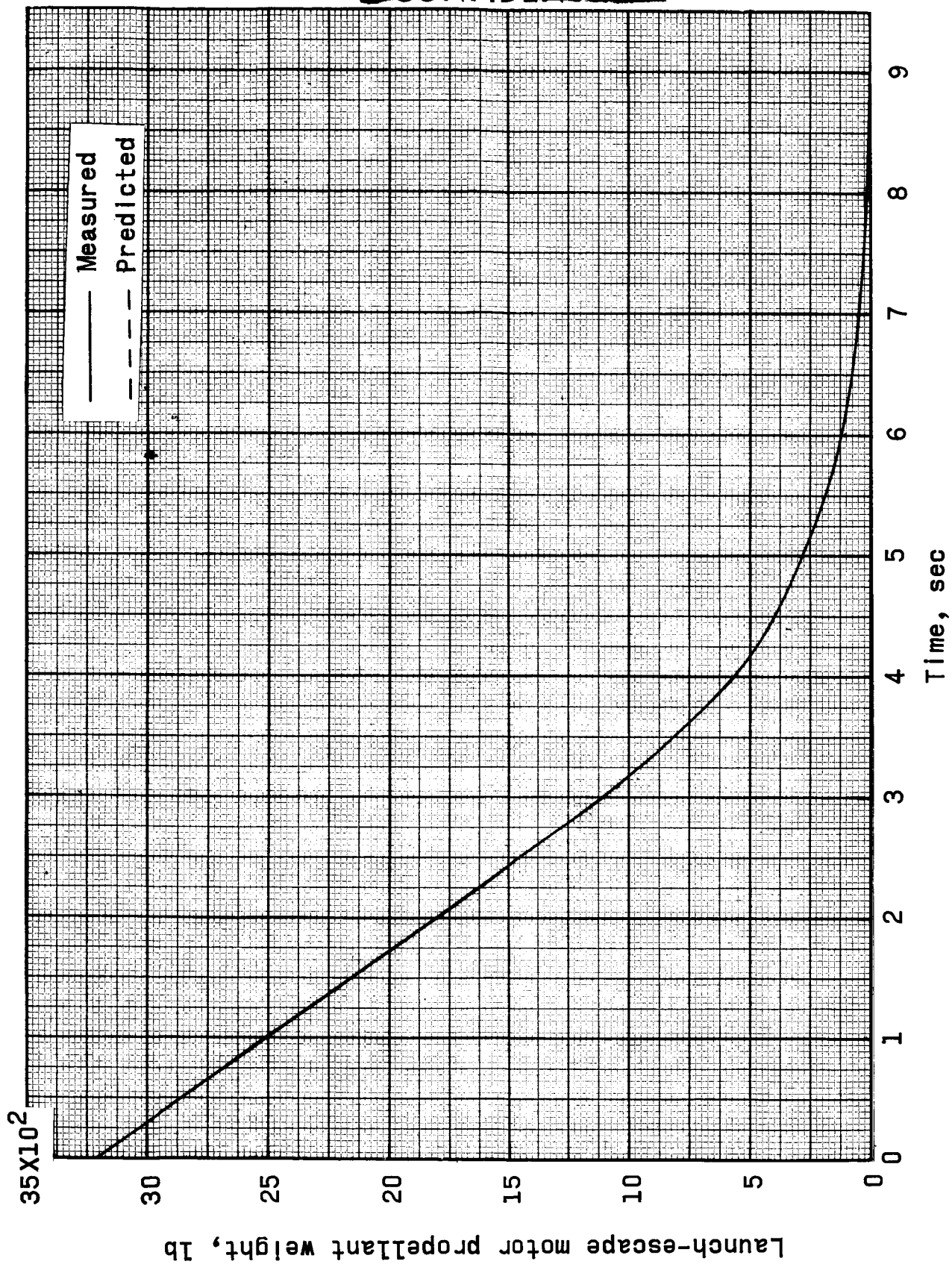
Figure 8.1-1.- Launch-escape motor propellant weight plotted against time, motor LE-9.

Figure 8.2-1.- Spacecraft weight plotted against time.
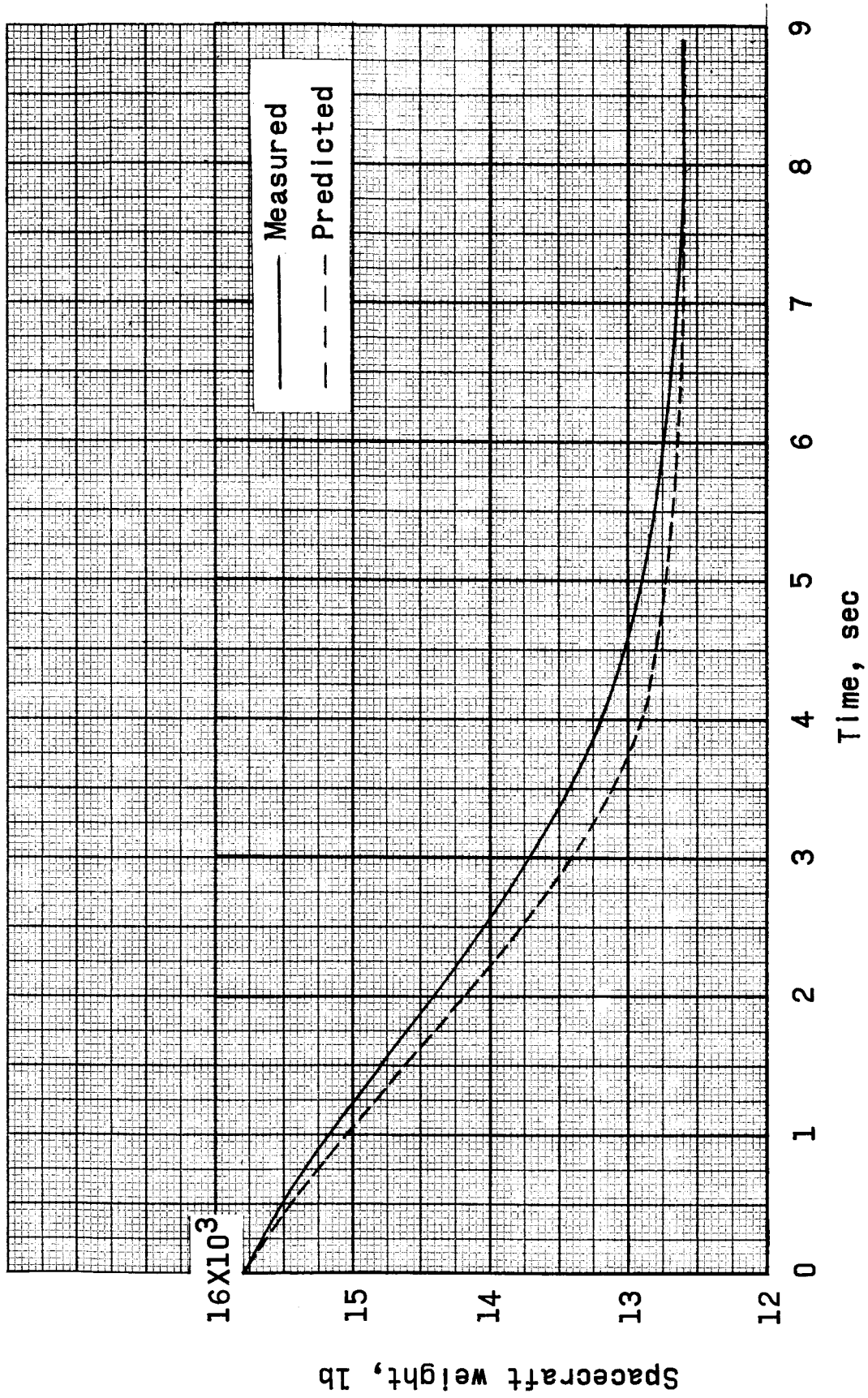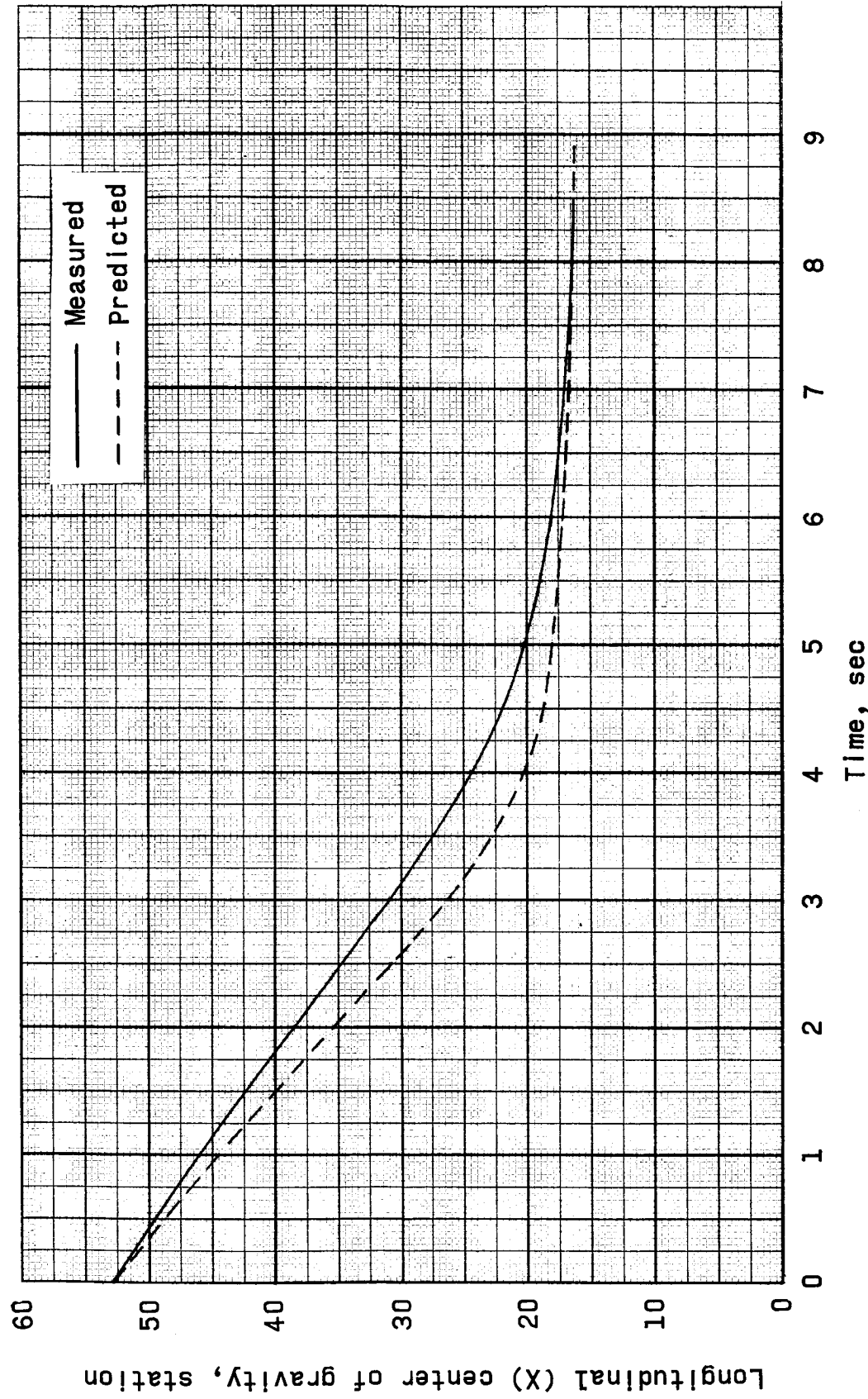
Figure 8.2-2.- Center of gravity in longitudinal (X) direction plotted against time.
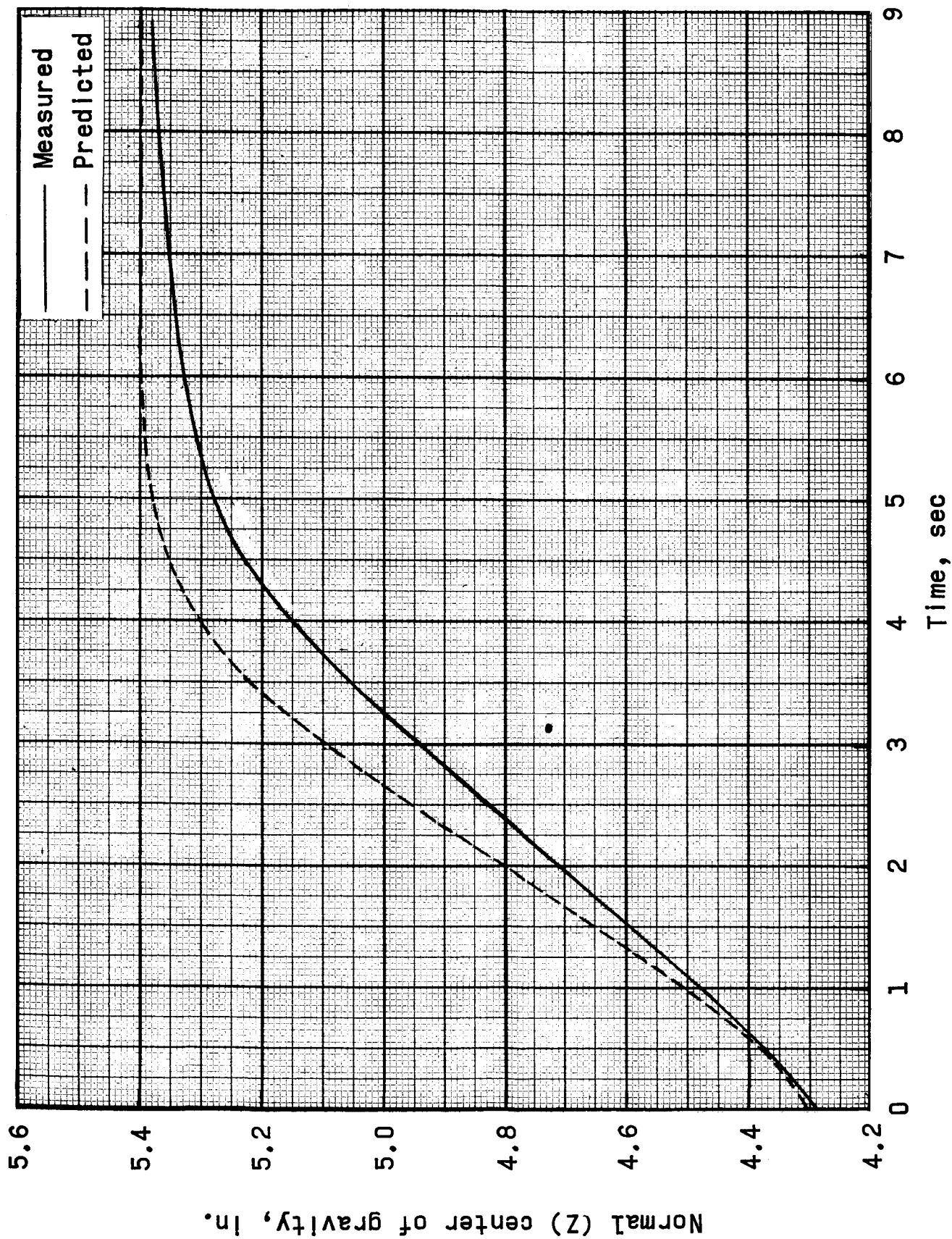
Figure 8.2-3.- Pad Abort 1, center of gravity in normal (Z) direction plotted against time.
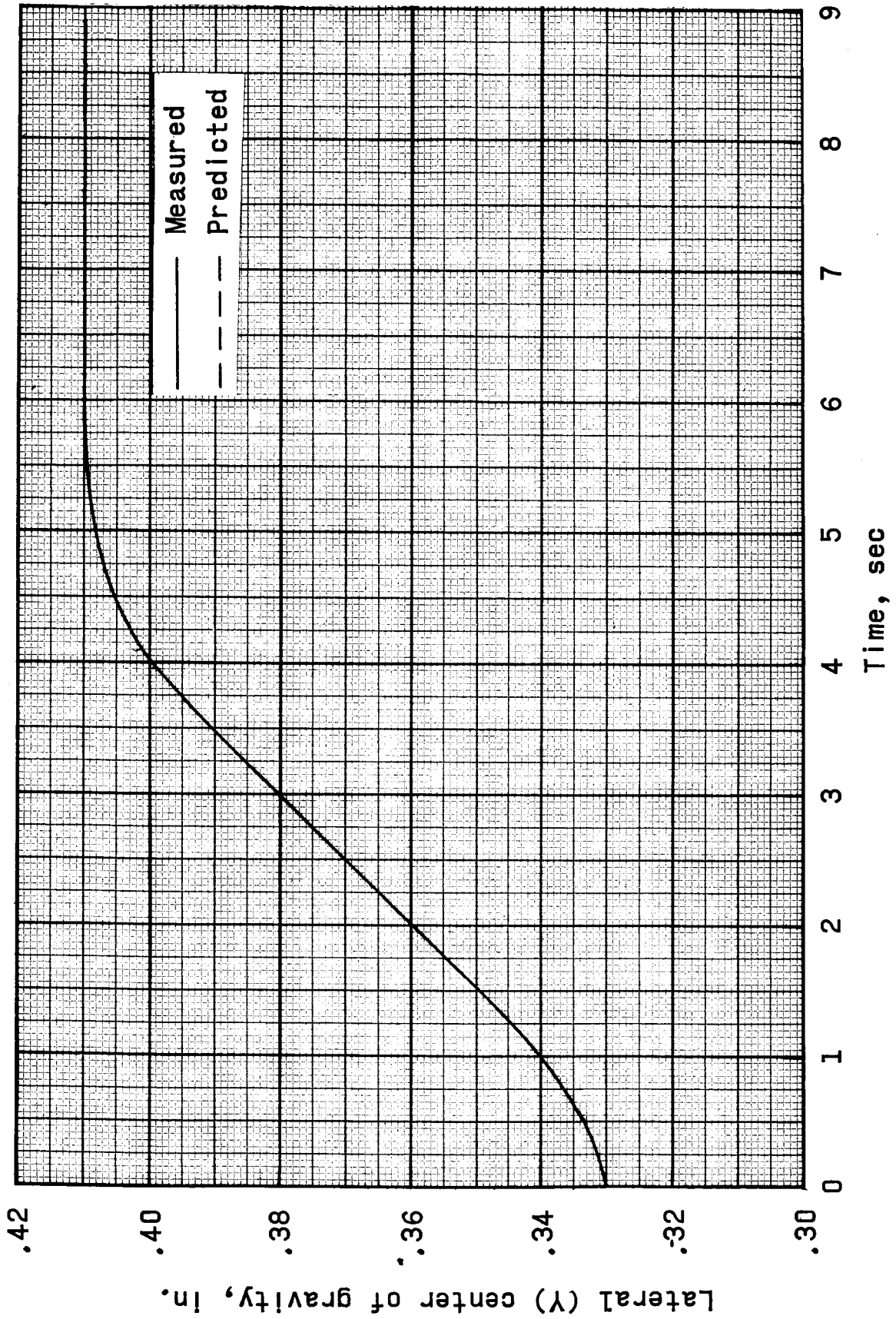
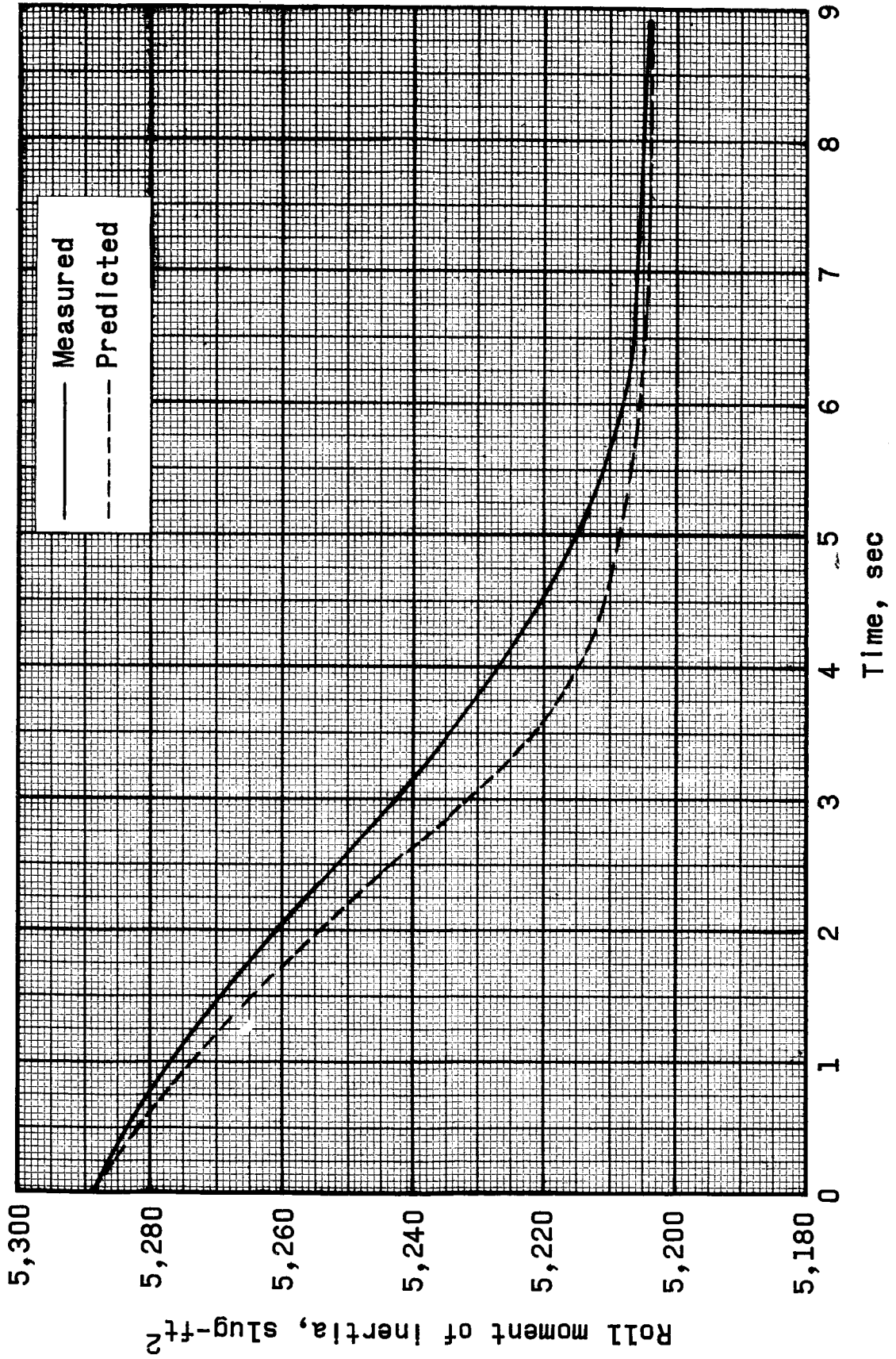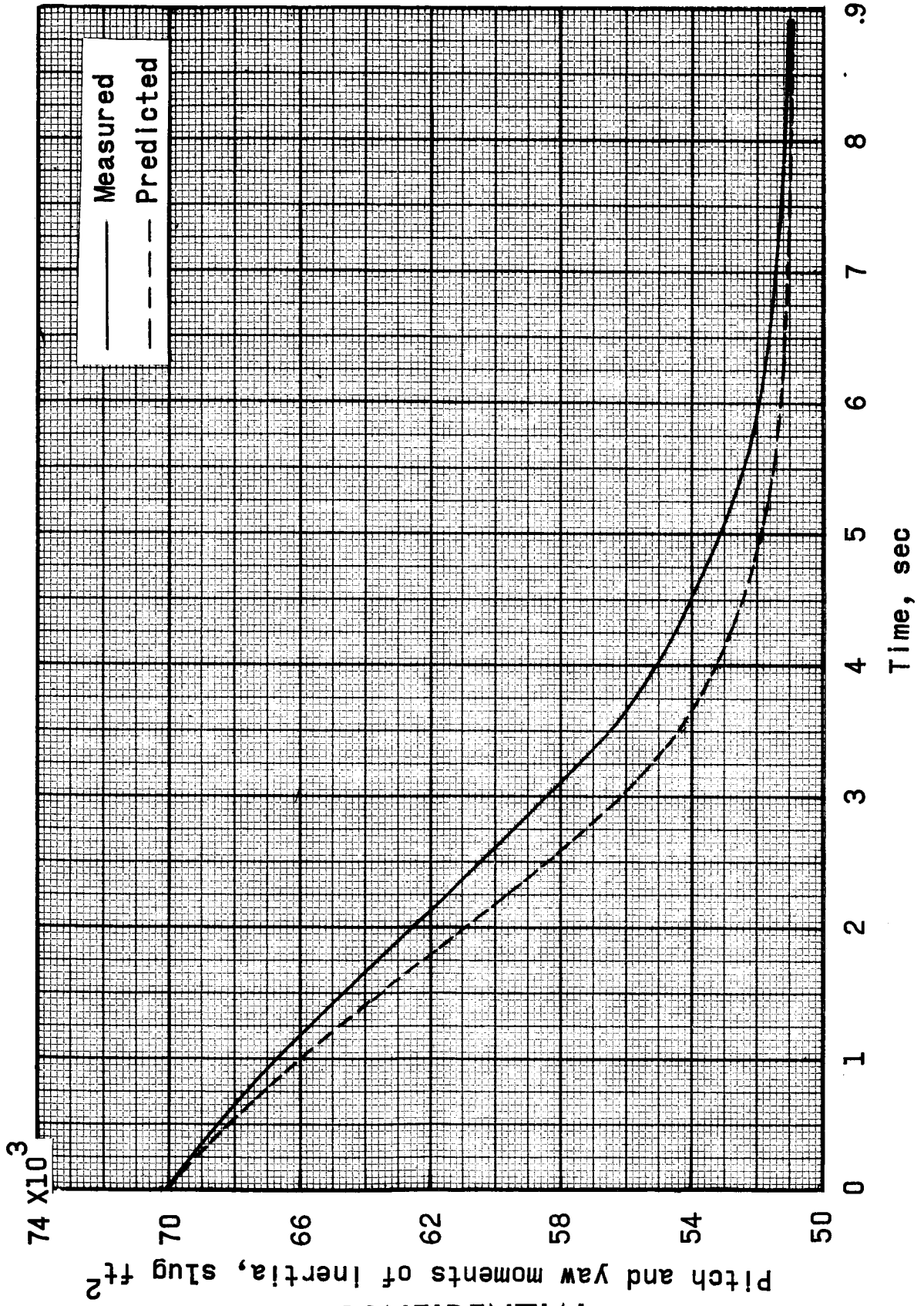Figure 8.2-4.- Center of gravity in lateral (Y) direction plotted against time.

Figure 8.2-5.- Roll moment of inertia plotted against time.
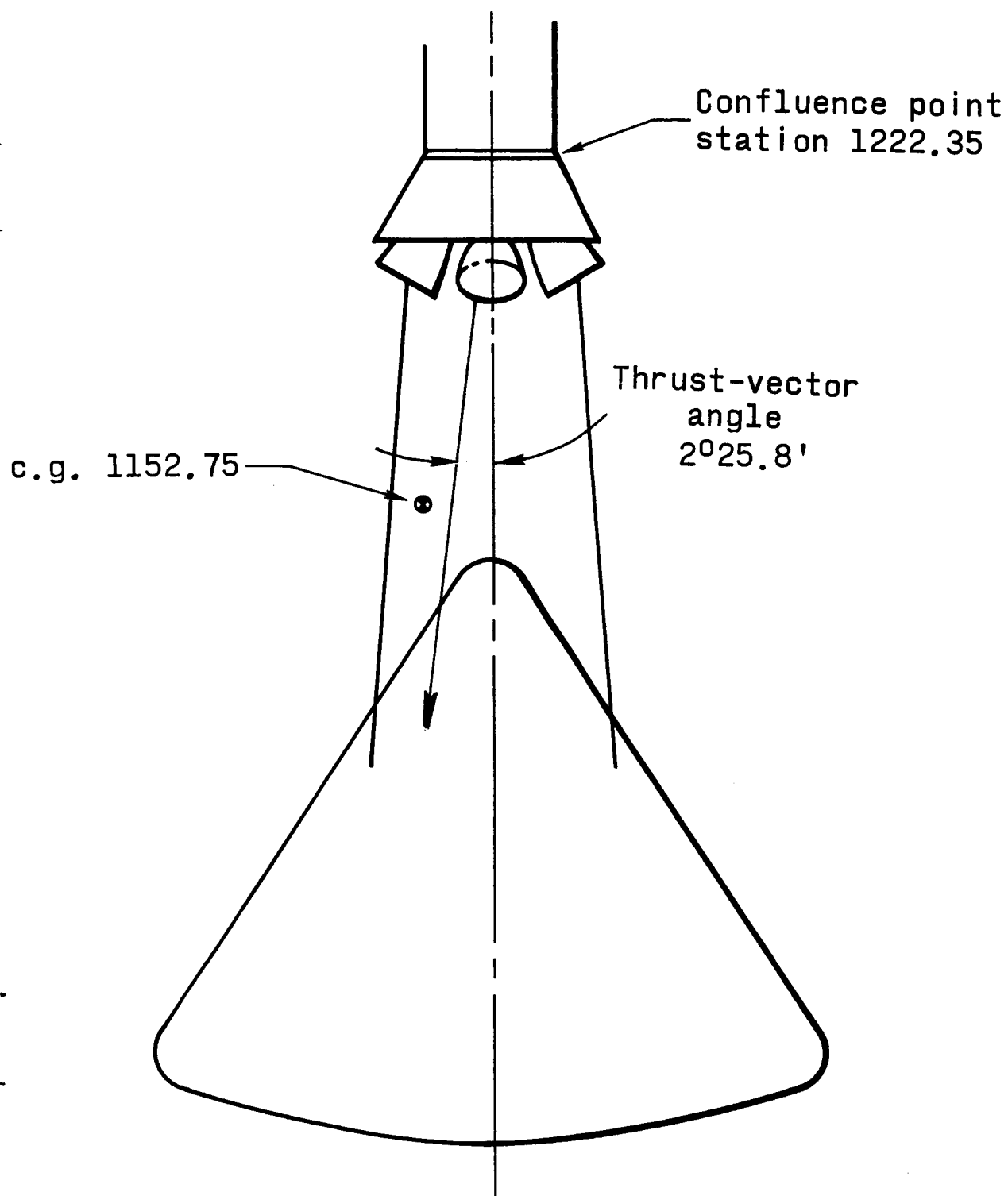
Figure 8.2-6.- Pitch and yaw moments of inertia plotted against time.

Figure 8.3-1.- Diagram showing thrust-vector angle.

## 9.0  RECOVERY OPERATIONS

### 9.1  Introduction

Recovery teams were established to supply rapid inspection and recovery of all flight hardware.  The teams were pre-positioned downrange to afford optimum utilization of time and equipment for the recovery operations.

### 9.2  Recovery Teams and Equipment

The recovery force consisted of two recovery teams organized and equipped for downrange recovery operation.  Team number one was assigned the responsibility for the recovery of the command module, and team number two, the launch-escape tower.

Prior to launch, the recovery teams were positioned in the vicinity of the expected landing and impact areas.  A helicopter from the WSMR Recovery Branch was positioned downrange to direct the recovery teams to the landing and impact areas.  A photographic helicopter was on station to photograph the descent and landing of the command module, the recovery-team movements, and the general landing and impact area scenes.  The recovery teams were equipped to conduct salvage operations in the event of any flight anomalies.  Equipment necessary for all required inspections and the preservation of scientific data were also included.  Team number one was equipped with an MM-1 balloon-tired "Terracruiser" vehicle for retrieving the command module.

Team number one reported on station at T-60 minutes and team number two at T-70 minutes.

Updated predicted landing points based on prevailing winds were passed to the recovery teams at T-60 minutes and T-30 minutes.

### 9.3  Recovery Procedure

Upon inflation of the main parachutes, team number one proceeded to the expected landing point of the command module and arrived on scene at T+7 minutes or about 4 minutes after the command module landing.

After general area photographs were taken (figs. 9.3-1 to 9.3-3) and pyrotechnic devices had been examined, the command module was entered through the side hatch.  Main batteries and pyrotechnic batteries were powered down at T+17 minutes 30 seconds and T+18 minutes 25 seconds, respectively.  The onboard tape recorder was removed and dispatched to the checkout trailer at T+35 minutes.  All parachutes were examined and packed.

Glass samples placed on the command module for evaluating rocket-motor exhaust impingement and heat-sensitive paint were photographed and covered for protection. The hatch was reinstalled, and the lifting bridles were attached to the command module. At T+2 hours 8 minutes, the command module was lifted and placed in the transportation dolly secured to the rear of the MM-1 balloon-tired Terracruiser. Loading and tie-down were completed at T+2 hours 45 minutes, and the vehicle with the command module proceeded to the NASA Vehicle Assembly Building. The command module arrived at the Vehicle Assembly Building at T+3 hours 38 minutes where the command-module–dolly combination was off loaded.

Team number two, with direction from the recovery helicopter, proceeded to the launch-escape tower immediately after impact and arrived on scene at T+9 minutes. The team completed their inspection, photographed the launch-escape tower (fig. 9.3-4), and retrieved all hardware from the tower. The hardware was returned to the Vehicle Assembly Building, arriving at T+2 hours 12 minutes.

## 9.4 Postflight Inspection

There was no obvious damage to the drogue or main parachutes. The main parachutes collapsed shortly after landing. The only obvious damage to the command module was an approximate 0.25-inch displacement of the heat shield in the -Z direction. There were also some exhaust deposits on the upper hatch cover of the command module. It has not been determined whether the deposits on the hatch cover originated from the tower-jettison motor or from the continued burning of the launch-escape motor. The command module landed with little roll, bounce, or slide. The module came to rest in an upright position at a slightly inclined angle.

Personnel from WSMR Geodetic Branch made surveys of the landing site of the command module and the impact point of the launch-escape system. The results of this survey indicated that the command module landed on an azimuth of 19°31'00", 8,220 feet downrange from the launch pad and the launch-escape tower impacted 11,979 feet, bearing 357°45'39" from the launch pad. (See fig. 9.4-1.)

## 9.5 Concluding Remarks

There were no difficulties encountered in locating, recovering, or retrieving the mission hardware. Especially valuable in transporting the command module from the landing area was the MM-1 Terracruiser vehicle. This vehicle easily traversed the sandy hummocks in the area of command-module landing.

There was some delay in the photographic coverage of events and hardware at the site of the command module landing because the photographers who were assigned to team number one were given the additional requirement of filming flight events from their downrange vantage point. Therefore, they were not ready to move with the team when it started toward the landing area. Still photography coverage was also inadequate at the command module because of the insufficient amount of film provided for the photographers. These deficiencies will be rectified for the next recovery operation.

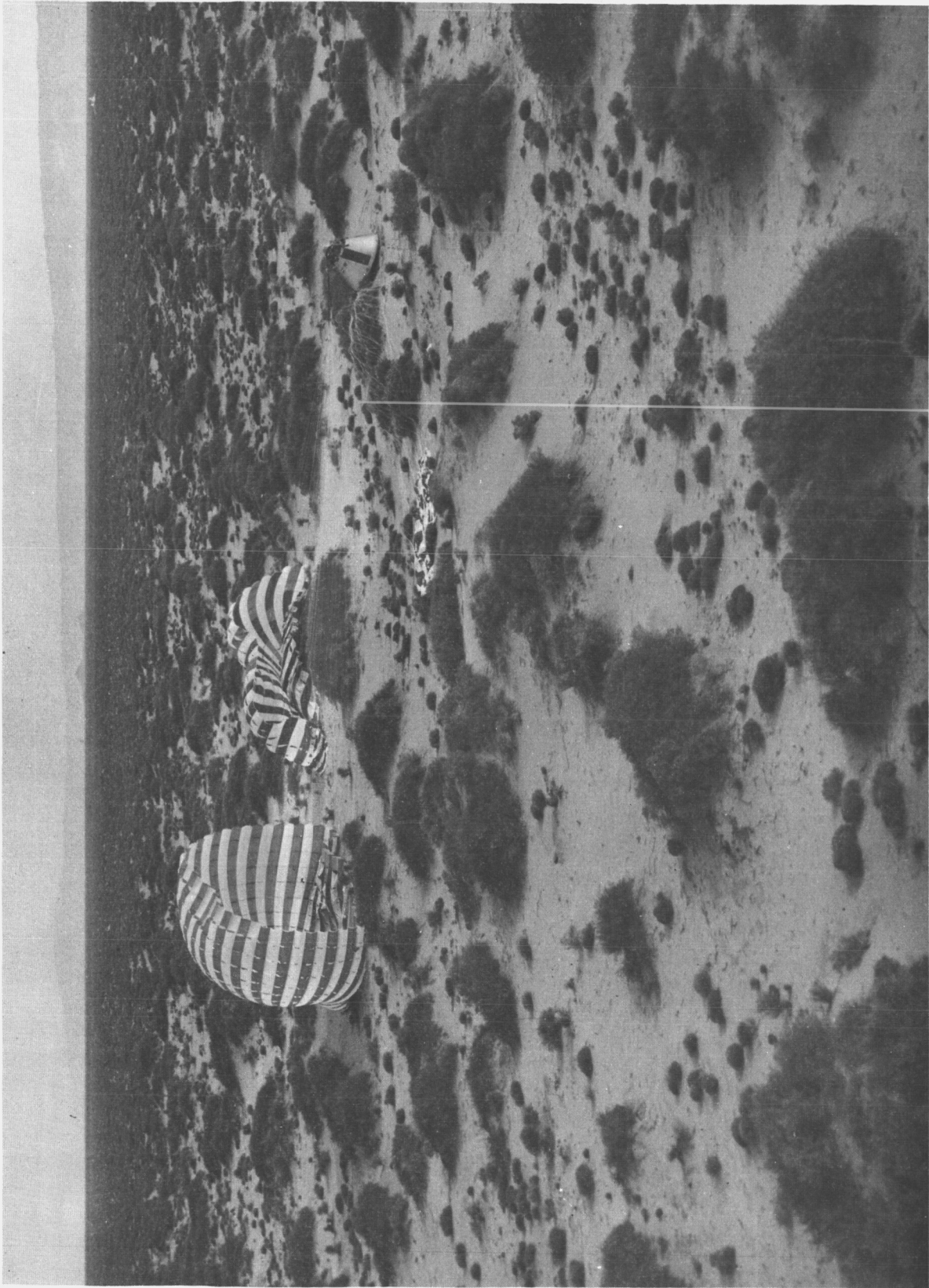Figure 9.3-1.- Command module and main parachutes after landing.

Figure 9.3-2. - Command module after landing.

Figure 9.3-3.- Closeup view of command module after landing.
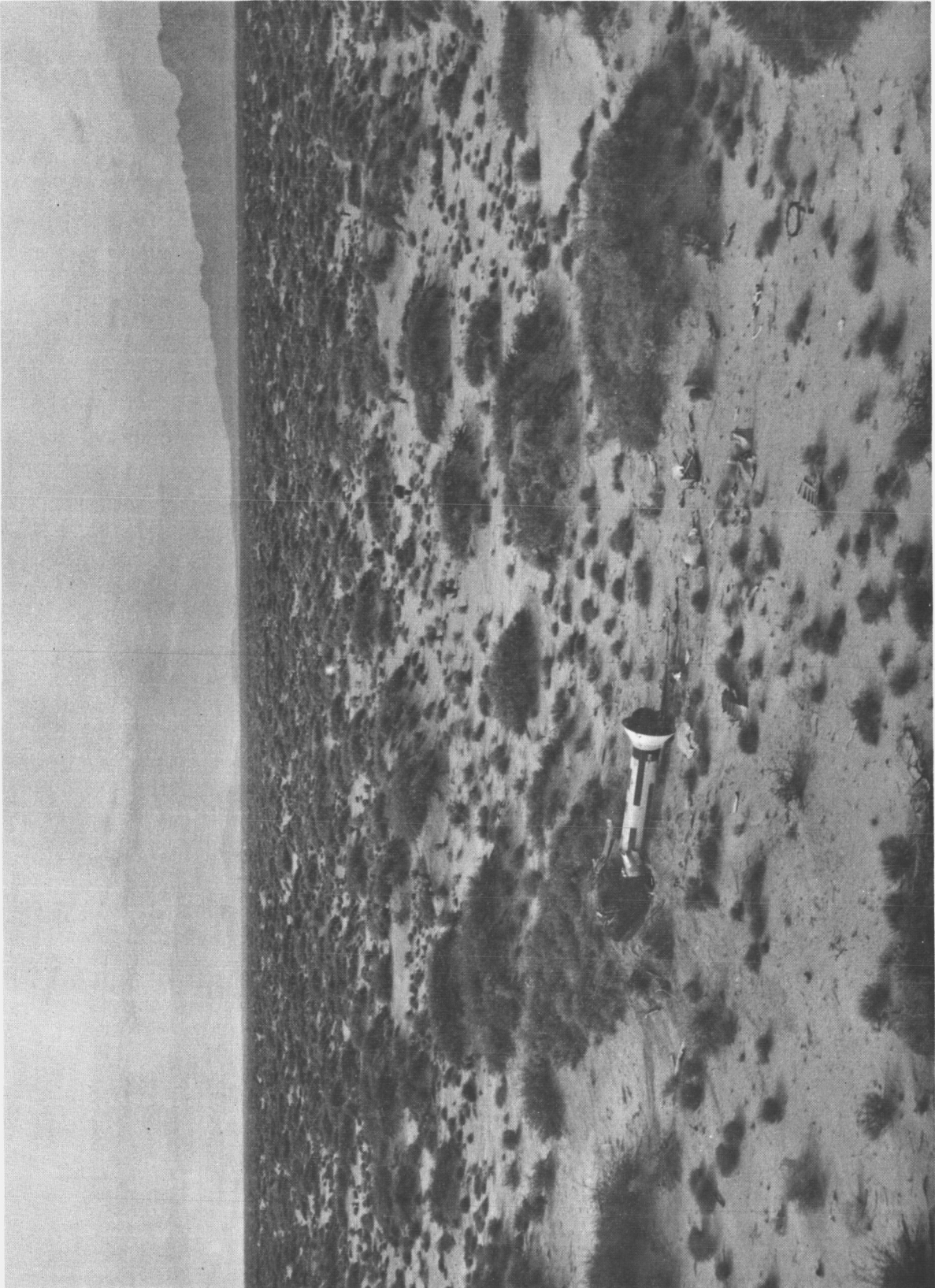
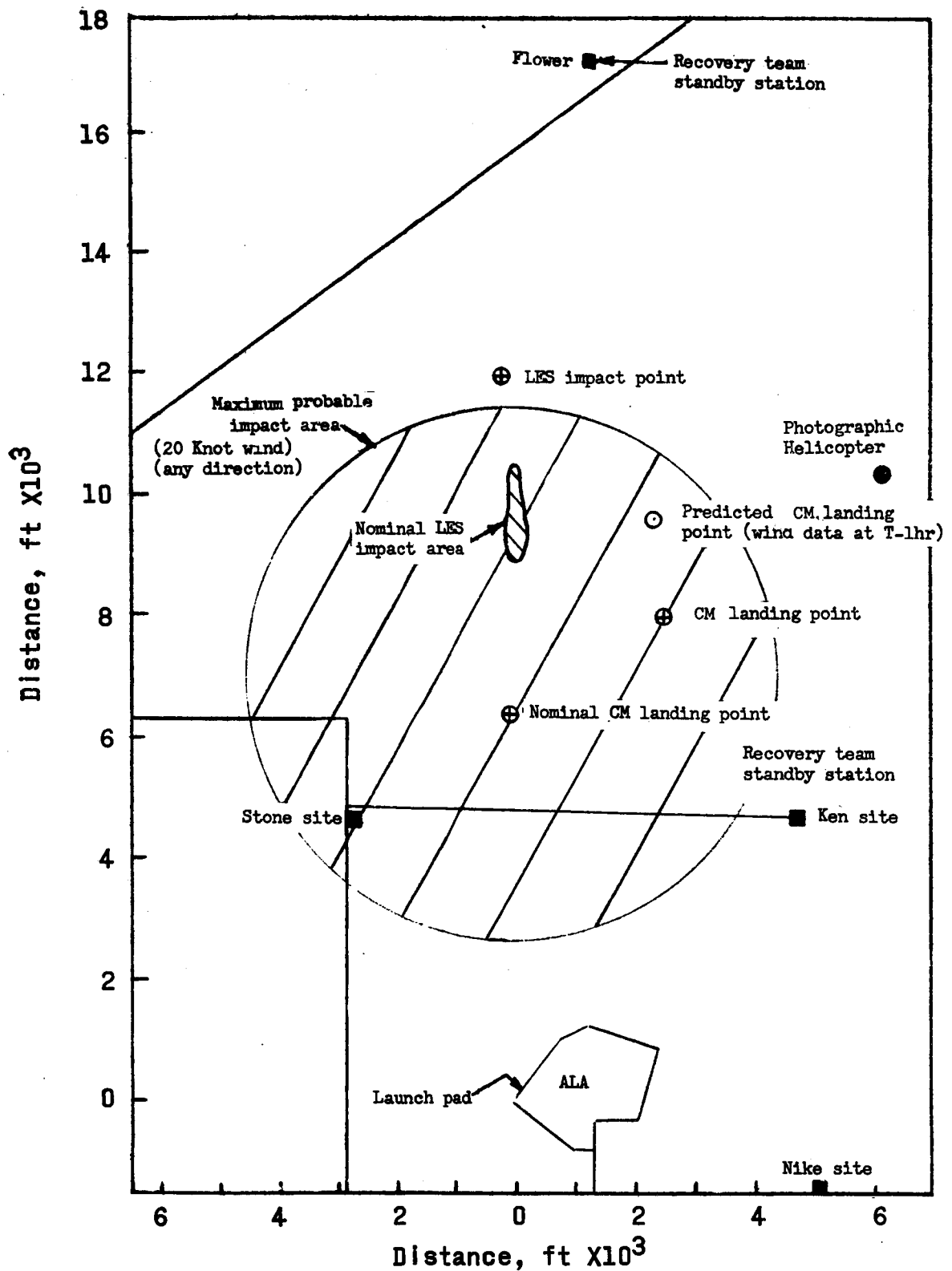Figure 9.3-4.- Photograph of launch escape tower at impact.

Figure 9.4-1.- Plot of landing area, position of recovery teams.

## 10.0  SPACECRAFT POSTFLIGHT INSPECTION AND TESTS

The postflight inspection plan outlines only those requirements for postflight inspection that were conducted at WSMR.  The purpose of the postflight inspection was to provide information which may be lost as a result of spacecraft handling and transportation or which must be investigated to provide additional data to aid in the evaluation of flight data.  The results of these tests were to be well documented.

During the postflight inspection, precautions were taken to insure that the flight equipment was not unnecessarily touched, moved, disconnected, or changed in order to preserve its postflight condition.  Continuous camera coverage was made available to take any pictures requested.

### 10.1  Types of Postflight Tests

The initial postflight activities were as follows:

(1)  Verify that all pyrotechnics were expended.

(2)  Check safety wires on pyrotechnic devices.

(3)  Remove batteries and start investigation.

The following items were also requested:

(1)  Sideview photographs of command module from 90° along +Y- and +Z-axes and photographs taken directly overhead looking down on the command module.

(2)  Photographs of tower, forward heat shield, and apex cover.

(3)  Analysis of all heat-resistant paint samples with estimated flight temperatures.

(4)  Photographs of the tower skirt to evaluate heat damage to the tower jettison wire harness.

(5)  Visual inspection as well as continuity and resistance checks of pyrotechnic wire harnesses.

(6)  Visual inspection of putty on the command module top deck.

~~CONFIDENTIAL~~

(7) Visual inspection of the electrical connectors and wiring harness condition.

(8) Visual inspection of the nozzles on all motors.

(9) Visual inspection of the parachute flaps on the top deck.

(10) Visual inspection of the exploding bridge wire (EBW) firing cables in the interface between the launch-escape motor and the tower-jettison motor.

(11) Verification of the condition and length of tower adjustment bolts.

(12) Visual inspection of the condition of LES tower skirt.

(13) Analysis of samples of mystic tape, exhaust deposits, and glass samples for rocket impingement.

(14) Visual inspection of drogue and pilot parachute mortar mounts for signs of over-stressing.

(15) Visual inspection of parachute risers and main harnesses.

(16) Visual inspection of main parachute bags for damage.

(17) Photographs of the thermo fit separation on the drogue parachute riser at the point where the bag tie loop is sewn to the riser.

(18) Analysis of exhaust deposits on outside of spacecraft.

(19) Bench tests of earth-landing system (ELS) and LES sequencers.

(20) Command module was powered by battery source to perform the following activities:

   (a) Check center frequency of telemetry transmitter.

   (b) Actuate R and Z calibration buses.

   (c) Actuate 5-point calibration.

   (d) Trouble-shoot X-axis high-range accelerometer circuit.

~~CONFIDENTIAL~~

(e) Rate and attitude gyros as well as the accelerometers were removed from their supports and moved to observe dynamic change.

(f) The following conical pressure transducer circuits were checked:

| Pressure transducer | Instrumentation channel assignment |
|---|---|
| 31 | A-E-41 |
| 33 | A-E-84 |
| 36 | A-E-87 |
| 22 | A-E-28 |
| 24 | A-E-30 |
| 28 | A-E-34 |

## 10.2 Results of Postflight Tests

The tasks outlined for the postlaunch inspection and tests have been accomplished. Photographs were taken and visual inspections were made as required. The electrical tests were completed. A telemetry tape was made while radiating from the command module and while conducting the electrical tasks outlined.

The results of these tests are being documented. This report contains some of the results under the respective system descriptions. The photographs and the rest of the postlaunch analysis are planned to be included in the final report.

## 11.0 RANGE PERFORMANCE

### 11.1 Communications

11.1.1   Description.- The range provided the following communications services:

(1)  Range Command-Ready-Hold Network:  This is the formal communications channel between range users and range personnel for transmitting support readiness and countdown information.

(2)  Range Telemetry Network:  This is the intercom network linking all range telemetry stations with the telemetry systems controller at the Range Control Station.  Recording of pre-launch calibrations and telemetry checkouts were coordinated over this network.

(3)  Tower Observer to Blockhouse Intercom Network:  Reports on test events (parachutes open, impact, et cetera) were transmitted to the Blockhouse and over the launch-complex intercom system by the visual observer positioned on the NASA Telemetry Antenna Tower.

(4)  Voice Recorder:  A tape recording of channels 1 and 2 of the launch-complex intercom system, the range telemetry network, and the Range Command-Ready-Hold Network was made.

(5)  Telephones.

(6)  An emergency maintenance team to repair any range communications systems malfunctions.

11.1.2   Performance.- All communications systems performed satisfactorily.

### 11.2 Radio Frequency Radiation Control

11.2.1   Description.- Control of electromagnetic energy on the launch pad from T-5 hours to completion of the test was required since electromagnetic interference checks were not made.  All high-powered pulse radars in the southern half of the range were either turned off or operated without radiating in the general direction of the launch pad.  Range frequency-monitoring stations continuously monitored the frequency spectrum to detect any violations of the control.

11.2.2    Performance.- No violations of the radiation-control antenna were noted.

### 11.3  Closed-Loop Television

11.3.1    Description.- Three closed-loop television systems were used to provide three views of the launch pad.  One camera was located near the pad to give a closeup view of the vehicle. One camera was located south of the launch pad to provide general launch-pad surveillance.  The third camera was located approximately 4,000 feet northwest of the pad for general launch-pad surveillance.  The three monitor sets were located in front of the control console in the blockhouse.

11.3.2    Performance.- The television system performed satisfactorily.

### 11.4  Timing

11.4.1    Description.- The range timing system supplied IRIG standard codes to all range support stations, the NASA telemetry station, and to the NASA checkout trailer.

11.4.2    Performance.- The timing system performed satisfactorily.

### 11.5  Meteorological

11.5.1    Description.- Two general categories of meteorological support were provided:  real-time prelaunch data and postlaunch data for conditions at time of firing.

(1)  Real-time meteorological data on surface and upper atmospheric winds were collected periodically from T-3 hours at the launch site.  Conditions from the surface to an altitude of 500 feet were obtained from instrumentation located on a 500-foot tower adjacent to the blockhouse.  Balloons were tracked to obtain data from altitudes of 500 feet to 7,000 feet. The data were processed in the blockhouse by range meteorological personnel and given to the NASA Meteorological Coordination.

(2)  Meteorological conditions at the time of launch were recorded and published in a postlaunch report received by NASA on the day after the launch.

11.5.2    Performance.- All meteorological support requirements were met.

## 11.6 Geodetics

11.6.1   Description.- Surveys of the launch-pad adapter, command-module landing, and launch-escape-system impact were requested.   Range surveys are made in the White Sands Tranverse Mercator (WSTM) Coordinate System and converted first into the White Sands Cartesian System (WSCS).   Data in the WSCS system are then converted into a Cartesian coordinate system with the launch point as the origin.   Geodetic data on the requested points were provided in all three coordinate systems.

11.6.2   Performance.- Performance was satisfactory.

## 11.7 Telescopes

A detailed discussion of the telescope-cine-camera coverage is included in section 12.0.   Coverage of the test was as requested except for one item.   Because of the small field of view of the optical systems used, photographs of the command module did not include some of the parachute action during the period from pilot-parachute inflation to main-parachute full blossom.

## 11.8 Contraves Cinetheodolites

A detailed discussion of cinetheodolite coverage is included in section 12.0.   Coverage was satisfactory.   Copies of boresight films from some of the instruments are being obtained because the films include some of the parachute action missed by the tracking telescopes.

## 11.9 Fixed Cameras

Data film was obtained from four engineering-sequential cameras and four position-data cameras as specified in section 12.0.   Coverage from the position-data cameras (F 1195, F 1196, F 1197, and F 1198) was requested in order to have high sample-rate data (60 samples per sec) available in case of an abnormality early in the flight.   Since there was no abnormal occurrence early in the flight, reduction of the data from these cameras was not requested.

11.9.1   Performance.- Fixed camera coverage was satisfactory.

## 11.10 Telemetry

Telemetry support as set forth in section 12.0 was provided. After the launch the magnetic tape recordings from telemetry stations 5, 44, and 56 were brought by range personnel to telemetry station 3 in the White Sands Headquarters area. This station 3 is the only range telemetry station with the tape "dubbing" capability. A total of 16 tapes were made available by the range personnel from 3 to 7 hours after launch. The tapes were requested in 4 hours. Exact cause of the loss of decommutator synchronization during the mission at telemetry station 56 has not yet been determined. Information to date indicates that the probable cause was in the countdown procedure used in calibrating the subcarrier oscillator on the commutated channel. Closer coordination with the range will be maintained on future tests to avoid the recurrence of this problem by exercising the instrumentation system with full range support on simulated missions and thoroughly analyzing the results. Range performance on the telemetry support was satisfactory.

# 12.0 DATA AND FILM COVERAGE

## 12.1 Film Coverage

Table 12.1-1 is a compilation of all range camera coverage during the PA-1 mission. Figure 12.1-1 shows the relative location of the telemetry and range camera sites with respect to the launcher.

12.1.1 Engineering sequential.- Four clock cameras, spaced at approximately 90° intervals around the periphery (approximately 300 feet from launcher), covered the first 200 feet of flight at 500 frames per second.

Sixteen mm reprints of the 35 mm original telescopic tracking camera film were provided from the following range stations: T-7, T-126, T-127, T-128, T-151, T-152, T-155, T-198, T-253, and G-110. The locations of these stations are shown in figure 12.1-1.

12.1.2 Position and derivative data.- The following table is an itemization of the coverage obtained for position and derivative data.

| Item | Time coverage | Range station used | Rate, samples per sec |
|---|---|---|---|
| Command module | Launch to 8 sec | G-101,107,110,112,154 | 20 |
| Command module | 8 sec to 60 sec | G-107,109,110,112 | 5 |
| Command module | 60 sec to landing | G-101,107,109,110,112 | 1 |
| LES | Launch to 8 sec | G-101,108,109,152,154 | 20 |
| LES | 8 sec to impact | G-101,108,152,154 | 5 |

12.1.3 Attitude data.- The following table shows the expected data coverage for pitch, yaw, and roll obtained by the range. The actual data coverage is not fully known at this time. Roll data will depend on the base of the command module being in full view of the camera.

~~CONFIDENTIAL~~

| Item | Time coverage | | Rate, samples per sec |
|------|---------------|---|------------------------|
| Pitch, yaw, and roll | Launch to 8 sec | | 20 |
| | 8 sec to 60 sec | | 5 |
| | 60 sec to landing | | 1 |

## 12.2 Meteorological Data

Meteorological data of the conditions existing at the time of launch were received in increments of 200 feet up to an altitude of 12,000 feet msl. These data consisted of scratch listings, final reports, and IBM card decks containing the following:

(1)  Wind direction in degrees from true North

(2)  Wind velocity in knots

(3)  Temperature in degrees Centigrade

(4)  Pressure in millibars

(5)  Altitude in feet msl

(6)  Relative humidity in percent

(7)  Index of refraction

(8)  Density in grams per cubic meter

## 12.3  Event Data

The event times as recorded by range tracking telescopes are shown in the following table. All times noted are derived from the tracking telescope film data and are with respect to zero time.

| Event | Source | Time, sec |
|---|---|---|
| LES motor ignition | T-152 | 0.0651 ± 0.0020 |
| Pitch control motor ignition | T-127 | 0.0227 ± 0.0022 |
| Pitch control motor burnout | T-127 | 1.3984 ± 0.0022 |
| LES motor burnout | T-127 | 9.567 ± 0.008 |
| Jettison motor ignition | T-151 | 15.5579 ± 0.0020 |
| Command-module—LES separation | T-151 | 15.5579 ± 0.0020 |
| Jettison motor burnout | T-127 | 19.8320 ± 0.0020 |
| Drogue-parachute deployment | T-152 | 18.6073 ± 0.0020 |
| Drogue-parachute release | T-151 | 23.9841 ± 0.0020 |
| Pilot parachute, first appearance | T-151 | 23.9841 ± 0.0020 |
| Main parachute, full-line stretch | T-152 | 26.3375 ± 0.0024 |
| LES impact | T-126 | 43.757 ± 0.008 |
| Command-module landing | T-127 | 165.057 ± 0.008 |

## 12.4  Geodetic Data

Geodetic surveys of the pad abort fixture, command-module landing, and LES impact were received.  The direction and range from the launch point to the command-module and LES impact locations are as follows:

| Event | White Sands Transverse Mercator System, azimuth heading | Range, feet |
|---|---|---|
| Launcher to LES impact | 357° 45' 39" | 11,980 |
| Launcher to command module landing | 19° 31' 00" | 8,220 |

In the White Sands Transverse Mercator System (WSTM):

X is measured in feet along a line passing through the point in question which crosses the central meridian, longitude 160° 20' 00.000" W., at a right angle and increases positively to the East.

Y is measured in feet along the central meridian, longitude 106° 20' 00.000" W., increasing positively to the North.

H is measured in feet along a radius of the earth at the point in question, above mean seal level, 1929 datum, positive upwards.

The origin of this system is the intersection of latitude 32° 10' 00.000" N. and longitude 106° 20' 00.000"W. This origin has a value of X - 500,000.00 feet and Y - 100,000.00 feet.

The White Sands Cartesian System (WSCS) and launcher tangent plane coordinates of these locations are listed in the following table:

| Location | WSCS, ft | Launcher tangent plane, ft. |
|---|---|---|
| Pad abort fixture | E = 502,495.54 | E = 0 |
| | N = 257,470.45 | N = 0 |
| | Z = 2,625.38 | Z = 0 |
| LES impact | E = 501,991 | E = -468 |
| | N = 269,443 | N = 11,973 |
| | Z = 2,737 | Z = -28 |
| Command module landing | E = 505,206 | E = 2,747 |
| | N = 265,219 | N = 7,749 |
| | Z = 2,688 | Z = -28 |

In the White Sands Cartesian System (WSCS):

E is measured in feet in the plane along a line passing through the point in question, crossing the North-South axis at a right angle, and increasing positively eastward.

N is measured in feet in the plane along a line passing through the point in question crossing the East-West axis at a right angle, and increasing positively northward.

Z is measured positively upward from and normal to the plane.

The origin of this system is the intersection of latitude 33° 05' 00.00" N. and longitude 106° 20' 00.00" W. This origin has a

value of E - 500, 000.00 feet and N - 500,000.00 feet.  At this point, the plane is tangent to Clarke's spheroid of 1866 at sea level.

## 12.5  Telemetry Data

A total of five telemetry receiving sites were used to record telemetry data from Mission Pad Abort 1.  Four of these sites were the WSMR telemetry stations J-3, J-5, J-44, and J-56.  The fifth station used to record telemetry was the NASA telemetry trailer.

Real-time telemetry displays of all continuous data and 47 of the 72 commutated data channels were obtained from telemetry stations J-44 and J-56.

The remaining 25 commutated data channels were played back at telemetry station J-56 immediately after the flight.  Real-time displays of commutated data recorded at telemetry station J-56, from T-5 minutes to the end of RF transmission, provided only qualitative data.  This apparently resulted when the ground-station decommutator lost synchronization during the subcarrier oscillator (SCO) step calibration at T-5 minutes and the zero-volt reference drifted before synchronization was reestablished.  This loss of synchronization caused the data traces to be correct in trends but not necessarily in value.  This problem did not appear on the data from telemetry station J-44.

Real-time data displays made at the NASA telemetry trailer were used for the T+1 hour postlaunch critique in the blockhouse.

## 12.6  Onboard Data

The NASA telemetry trailer provided tape copies and analog playbacks for support of the posttest analysis effort at WSMR.

## 12.7  Summary of Data Flow

Figure 12.7-1 shows the planned and actual delivery times of the major data items for Pad Abort Mission 1.  In practically all cases, planned data-delivery times were either met or exceeded.

TABLE 12.1-1.- RANGE CAMERA COVERAGE

| Station | Film | Frame rate | Focal length | Image | Time coverage | Quality | |
|---------|------|-----------|--------------|-------|---------------|---------|---------|
| | | | | | | Images | Film |
| T-7 | B&W | 60 | 96 in. | LES&CM | Launch to 164.395 sec | Fair | Hazy |
| T-126 | B&W | 60 | 60 in. | LES&CM | Launch to 164.800 sec | Good | Good |
| T-127 | Color | 60 | 24 in. | LES&CM | Launch to 165.049 sec | Good | Good |
| T-127 | Color | 250 | 48 in. | LES | Launch to 59.455 sec | Very good | Very good |
| T-128 | Color | 60 | 60 in. | LES&CM | Launch to 164.765 sec | Fair to good | Fair |
| T-151 | Color | 250 | 48 in. | LES | Launch to 58.885 sec | Very good | Very good |
| T-151 | Color | 60 | 48 in. | LES&CM | Launch to 162.730 sec | Good | Dark |
| T-152 | Color | 250 | 48 in. | LES | Launch to 62.695 sec | Very good | Good |
| T-152 | Color | 60 | 80 in. | LES&CM | Launch to 164.595 sec | Good | Dark — timing bad |
| T-154 | B&W | 60 | 91 in. | LES&CM | 6.0005 to 164.795 sec | Fair to poor | Dark |
| T-155 | Color | 60 | 48 in. | LES&CM | 1.478 to 165.038 sec | Good | Good |
| T-198 | Color | 60 | 96 in. | LES&CM | Launch to 164.746 sec | Good | Good |
| F 1195 | Color | 60 | 80mm | LES&CM | 1st 700 ft | | |
| F 1196 | Color | 60 | 80mm | LES&CM | 1st 700 ft | | |
| F 1197 | Color | 60 | 80mm | LES&CM | 1st 700 ft | | |
| F 1198 | Color | 60 | 80mm | LES&CM | 1st 700 ft | | |
| 0300F | Color | 500 | 80mm | LES&CM | 1st 200 ft | Good | Good |
| 0730F | Color | 500 | 80mm | LES&CM | 1st 200 ft | Good | Good |
| 0930F | Color | 500 | | LES&CM | 1st 200 ft | Good | Good |
| 1230F | Color | 500 | | LES&CM | 1st 200 ft | Good | Good |
| G-80 | B&W | 20 | 50 in. | Not usable | | Film dark and blurred | |
| G-82 | B&W | 20 | 50 in. | Not usable | | Film dark and blurred | |
| G-101 | B&W | 20 | 60 in. | LES&CM | Launch to 164.695 sec | Good | Fair |
| G-107 | B&W | 20 | 60 in. | LES&CM | Launch to 162.395 sec | Good | Fair |
| G-108 | B&W | 20 | 60 in. | LES&CM | Launch to 16.395 sec | Good | Fair |
| G-109 | B&W | 20 | 60 in. | LES&CM | Launch to 163.945 sec | Good | Fair |
| G-110 | B&W | 20 | 60 in. | LES&CM | Launch to 164.945 sec | Good | Fair |
| G-111 | B&W | 20 | 60 in. | LES&CM | Launch to 164.845 sec | Good | Fair |
| G-112 | B&W | 20 | 60 in. | LES&CM | Launch to 164.145 sec | Good | Fair |
| G-152 | B&W | 20 | 60 in. | LES&CM | Launch to 16.045 sec | Good | Fair |
| G-154 | B&W | 20 | 60 in. | LES&CM | Launch to 164.245 sec | Good | Fair |
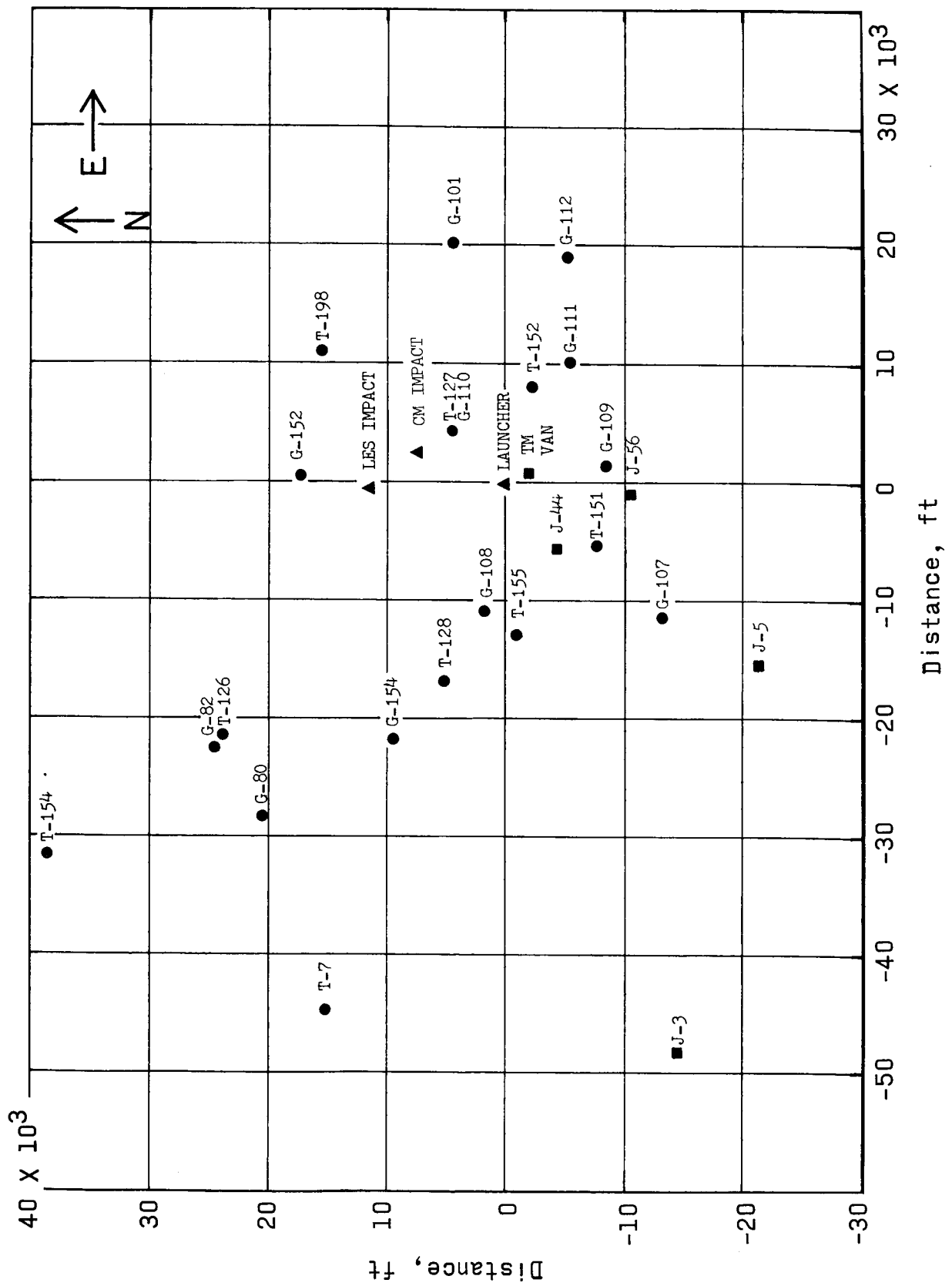
Figure 12.1-1.- Telemetry and range camera station location.
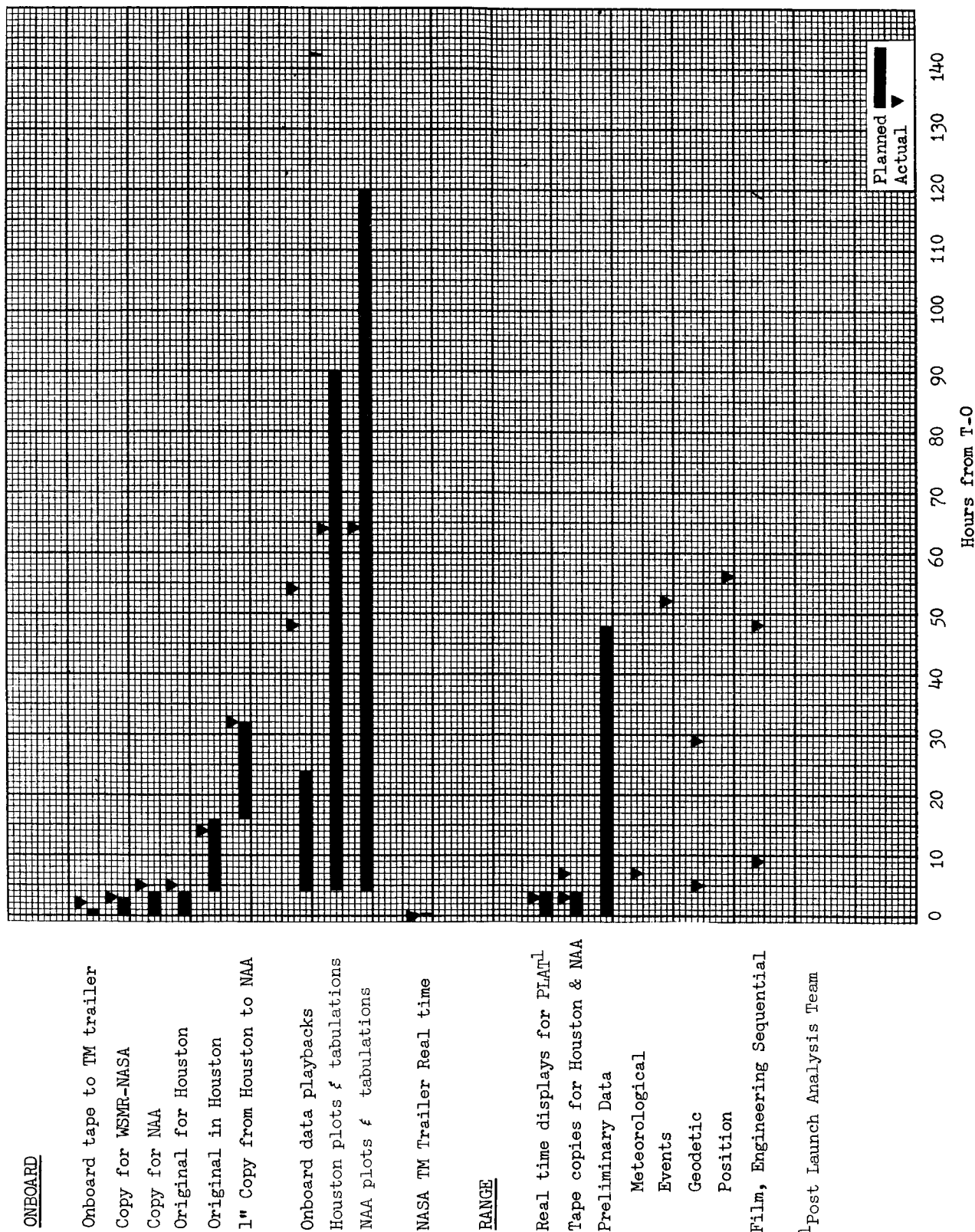
Figure 12.7-1.- Data flow schedule.

APPENDIX A1.0

SPACECRAFT HISTORY

This history includes the activities on boilerplate 6 from the time it entered the test preparation area at North American Aviation, Inc., Downey, Calif. on March 8, 1963, through launch at White Sands Missile Range, New Mexico, on November 7, 1963. A bar chart which depicts the major milestone events during this period is shown in figure A1.0-1.

A1.1    North American Aviation, Inc.

The command module was received from manufacturing final assembly in the Test Preparation Interim area at 9:30 p.m. on March 8, 1963, at North American Aviation, Inc., Downey, California. It was received in a "shell" configuration without equipment or harness in the forward compartment. The forward heat shield and a major portion of the onboard equipment were also missing.

The pad adapter was received on March 11, 1963, and subsequently was mated to the command module on March 12, 1963.

Because of extensive and repetitive rework in both the test preparation and manufacturing areas, the forward compartment cover was not delivered to the test area until approximately 1 month after the command module. During rework on the command-module structure and top deck area, operational test procedures were conducted on the command module wiring, electrical system, and instrumentation components. These procedures required approximately 1 week, at the end of which time the command-module instrumentation was removed to facilitate removal of the wiring harness.

The first command-module wiring harness was removed because of the failure of crimp-pin samples to pass the required pull test. At this time, the installation of strakes was begun and the mechanical rework continued. Strake installation and rework was completed on March 27, 1963.

The launch-escape-system motors (inert) were delivered on March 26, 1963, and the nose cone, interstage structure, and motor skirt, 2 days later. Assembly of the LES motors was completed on March 30, 1963, and the weight and balance measurements began the following day.

On April 3, 1963, the installation of wiring harness no. 2 began and proceeded concurrently with the installation of the forward-compartment-cover jettison system and top-deck equipment installation. The

installation of the harness was completed on April 6, 1963. The forward-compartment equipment and reinstallation of the command-module instrumentation was completed on April 17, 1963. Also during this period, the forward-compartment cover was received; the launch-escape tower and the Apollo instrumentation test-console escape tower were delivered and weighed; and the functional verifications for the Apollo-instrumentation-test console, data recording group, junction box and cables, and the signal-conditioner console were completed.

Weight and balance measurements were performed between May 3 and May 7, 1963, for the command module in the horizontal and vertical positions, the command module and LES combination in the vertical position, launch-escape tower in the horizontal position, and the launch-escape motor in the horizontal position. All launch-escape-system rocket motors were inert. An attempt was made to weigh the assembled LES, but problems in design of the fixture prevented obtaining acceptable weight readings. All weight readings at North American Aviation were obtained by using a Revere Weighing Kit. The thrust-vector alinement for boiler-plate 6 was first performed with inert motors. Following this alinement, the command module and LES were demated, driven around the facility for 1 hour, and remated. The thrust vector was then checked and found to fall within 0.015 inch of its original position.

The Apollo Instrumentation Test Console was the only ground-support equipment available for checkout when the command module was received in the test preparation area. Because of the lack of the forward deck harness, a temporary harness was installed. Discrepancies found in the interim sequencers precluded making an accurate check at that time (March 23, 1963) and the sequencers were subsequently returned to the vendor for rework.

A series of instrumentation operational test procedures were accomplished utilizing the Test Console and the telemetry ground station. These tests were made for the sole purpose of verifying compatiblity of the no. 2 wiring harness. The Test Conductor's Console and the Junction Box to be located at North American Aviation were delivered on April 7, 1963, and the Pyrotechnics Devices Substitute Unit, for test only, was delivered on April 24, 1963. The Data Recording Group, minus recorders, was delivered on April 10, 1963.

After completion of individual systems checkout, the first Integrated System Test was performed on April 30, 1963.

In early May, Operation "Little WSMR," simulating the field configuration and conditions, was conducted by using WSMR assigned ground-support equipment.

The command module and LES were mated in the Navaho tower, the thrust vector was alined, and then the CM and LES were demated. The command module was loaded on a "low boy" trailer and transported for 1 hour around the local area to simulate transport from the "Honest John" building (WSMR) to the launch pad. The LES was placed on a handling trailer and transported in the same manner as the command module. The command module and LES were remated and a thrust-vector verification was conducted which confirmed that the resulting deviation was well within tolerance. The WSMR telemetry trailer was not used during this operation; an interim telemetry station was substituted. The command module wiring harness no. 2 was removed May 9, 1963, and replaced by wiring harness no. 3 on May 18, 1963.

Several Operational Test Procedures were rerun for wiring harness no. 3 compatibility. The boilerplate suffered schedule slippage during this period because of numerous malfunctions encountered while running these procedures.

The electromagnetic interference (EMI) test was conducted during a minimum interference condition time, with the command module and LES mated electrically.

The final integrated system test was successfully completed on June 27, 1963, and shipping preparations to White Sands Missile Range were initiated.

Two pieces of ground support equipment (GSE), the LES intermodule substitute unit and the command module substitute unit, were not shipped for test operations at White Sands Missile Range. Boilerplate 6, immediately vital GSE, and related equipment were air shipped to Holloman Air Force Base, Alamogordo, N. M. Departure time from Long Beach, Calif., was at 8:29 a.m. P.d.t., July 1, 1963, and arrival time was 11:20 p.m. m.s.t. for an elapsed flight time of 2 hours 51 minutes.

A1.2  White Sands Missile Range, N. Mex.

The command module, launch-escape tower, and attendant GSE arrived at White Sands Missile Range on July 2, 1963. The flight hardware was shipped without the ordnance devices which were preshipped from the respective vendors and stored in a bunker on the base. All equipment was subject to a receiving inspection. Some GSE was shipped to the launch pad for installation and all flight components were delivered to the Honest John Building for assembly.

The launch-escape motor was returned to the vendor for nozzle modifications to provide more bearing strength on the carbon insert. The motor was reshipped to White Sands Missile Range and passed a satisfactory grain inspection on July 5, 1963. Desiccant bags were added

inside the motors, and satisfactory leak tests were performed. This motor received another satisfactory grain inspection on August 14, 1963.

The tower-jettison motor after being received at White Sands Missile Range was returned to the vendor for nozzle modifications. The modification included a redesign of the nozzle blow-out and a redesign to provide more strength for the carbon insert. The motor was reshipped to White Sands Missile Range on July 2, 1963. At this time it was modified to provide more strength to the interstage structure. After installation of the parachutes, it was found that the rings on the parachute risers were of questionable reliability because of possible structural failure. Since a design fix was anticipated, the recovery system pyrotechnics were not installed. However, weight and balance operations were completed as scheduled, and the airborne equipment was moved to the launch pad for facility compatibility and preliminary electrical checks. Weight and balance measurements were conducted in the Honest John Building and consisted of separate determinations of the LES tower motor assembly. A horizontal weighing of the command module was also performed. An additional determination of the command-module weight was made by means of a single cell in tension between the lifting hook of the crane and lifting sling. No command module, vertical or stacked, weight and balance measurement was performed because of difficulties encountered with the overhead crane.

Following preliminary pad checks, completed on August 7, 1963, the modules were demated and transported to the new Vehicle Assembly Building. The parachutes were removed, the launch-escape motor was reinspected, and the forward compartment rework was started. This rework consisted of deactivating the cover jettison system, attaching the cover to the tower, and removing and installing upperdeck components to reduce the probability of cutting the parachute-risers.

Command module buildup was delayed by two major items: The changes to the earth-landing system (ELS) because of a failure at El Centro, Calif., on boilerplate 3 and the decision to use $\frac{1}{2}$-amp pyrotechnics in the earth-landing system. Following procurement of the necessary hardware, the command module was assembled. Final weight and balance measurements were conducted in the Vehicle Assembly Building during the period October 14 to October 17, 1963.

The horizontal weighing of the command module was repeated to achieve better accuracy. A single load cell weighing was also performed. The command module and the stacked configuration in the vertical position were weighed and balanced. A weight and balance measurement of the complete LES was achieved as a result of modification to the weight and balance fixture. A minimum of four readings was taken for each test, and excellent repeatability was achieved. The final weight and balance

measurement was performed by utilizing an interim readout for the load cell transducers.  This interim readout was utilized because of malfunctions of the normal system.

The final thrust-vector alinement prior to flight was performed on October 18, 1963.  The vehicle was demated, transported to the launch pad, and reassembled.  The thrust vector was found to be within 0.050 inch of its original position.  As an additional check, the thrust vector was checked prior to launch at T-1 day.  It was found to be within the acceptable tolerances.

System tests began on October 19, 1963; and employed a building block checkout concept, it concluded with Integrated Systems Test no. 1 which included the firing of live pyrotechnics, a simulated countdown, and Integrated Systems Test no. 2.  Launch pad checks were completed on November 4, 1963.

Launch countdown and launch were completed on November 7, 1963.
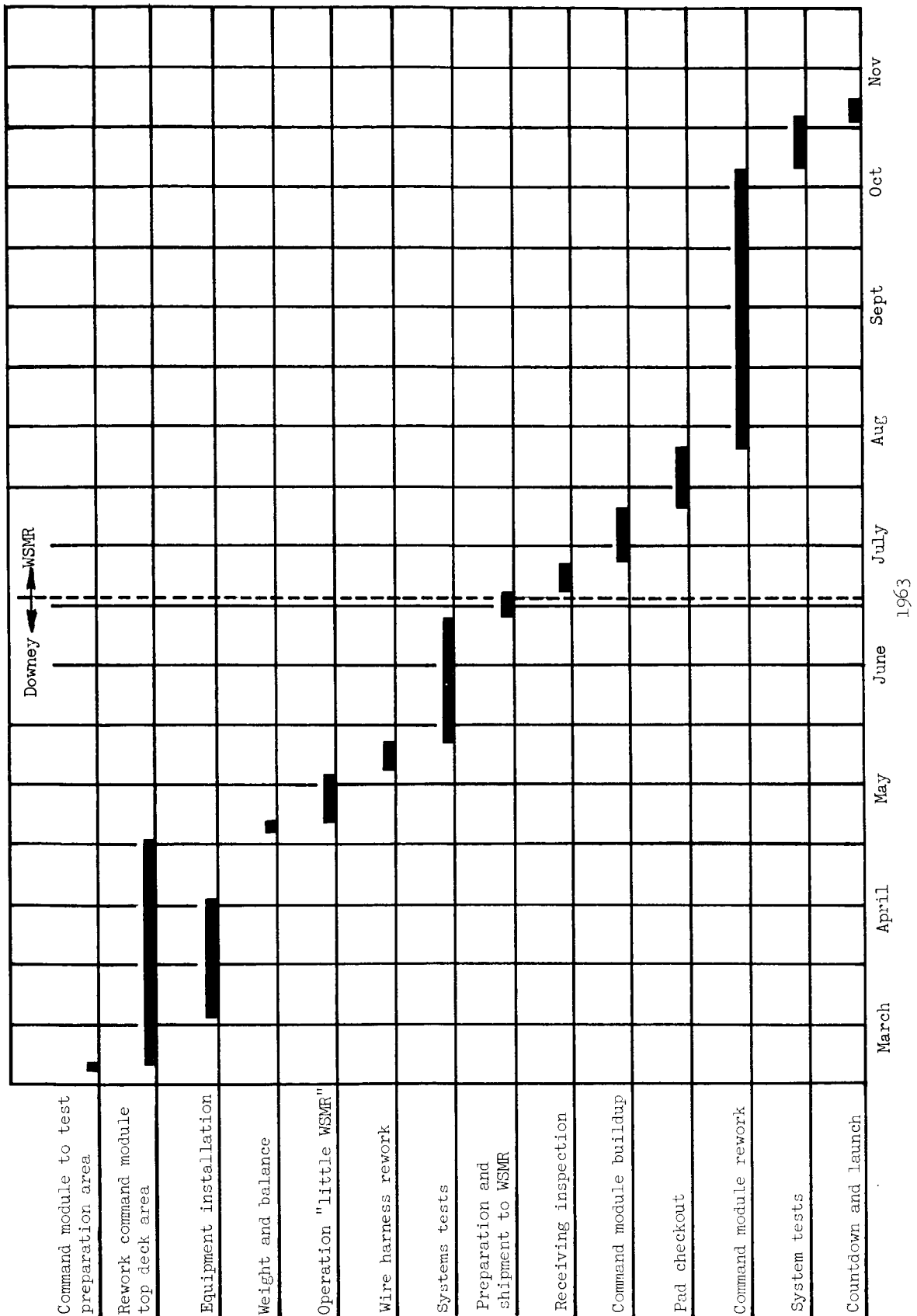
Figure A1.0-1.- Major milestone events in BP-6 history.

APPENDIX A2.0

LAUNCH OPERATIONS

Launch operations for Apollo Pad Abort 1 began at 7:00 a.m. m.s.t. on November 6, 1963 (T-1 day) with the installation of all ordnance items and the flight batteries. In addition, cranes and trucks were positioned on either side of the building, commonly known as the Tiki hut, which is used to house the test vehicle. General pad clean-up was also accomplished during this period.

The 7-hour launch countdown began as scheduled at 2:00 a.m. m.s.t., November 7, 1963, and proceeded without any major problems. The schedule is presented in figure A2.0-1. Ordnance connection and the installation of the cable connectors and cover plates began 48 minutes early at T-255 minutes. The time required for this operation was underestimated, and the actual operation consumed an extra 38 minutes. In addition, because of the large number of visitors and participating WSMR range support personnel, the pad clearing efforts took more time than anticipated. The blockhouse was secured at T-30 minutes and the terminal count proceeded as planned. T-0 occurred at exactly 9:00 a.m. m.s.t. by the blockhouse clock. Actual launch time was 9:00:01.105 a.m. m.s.t.
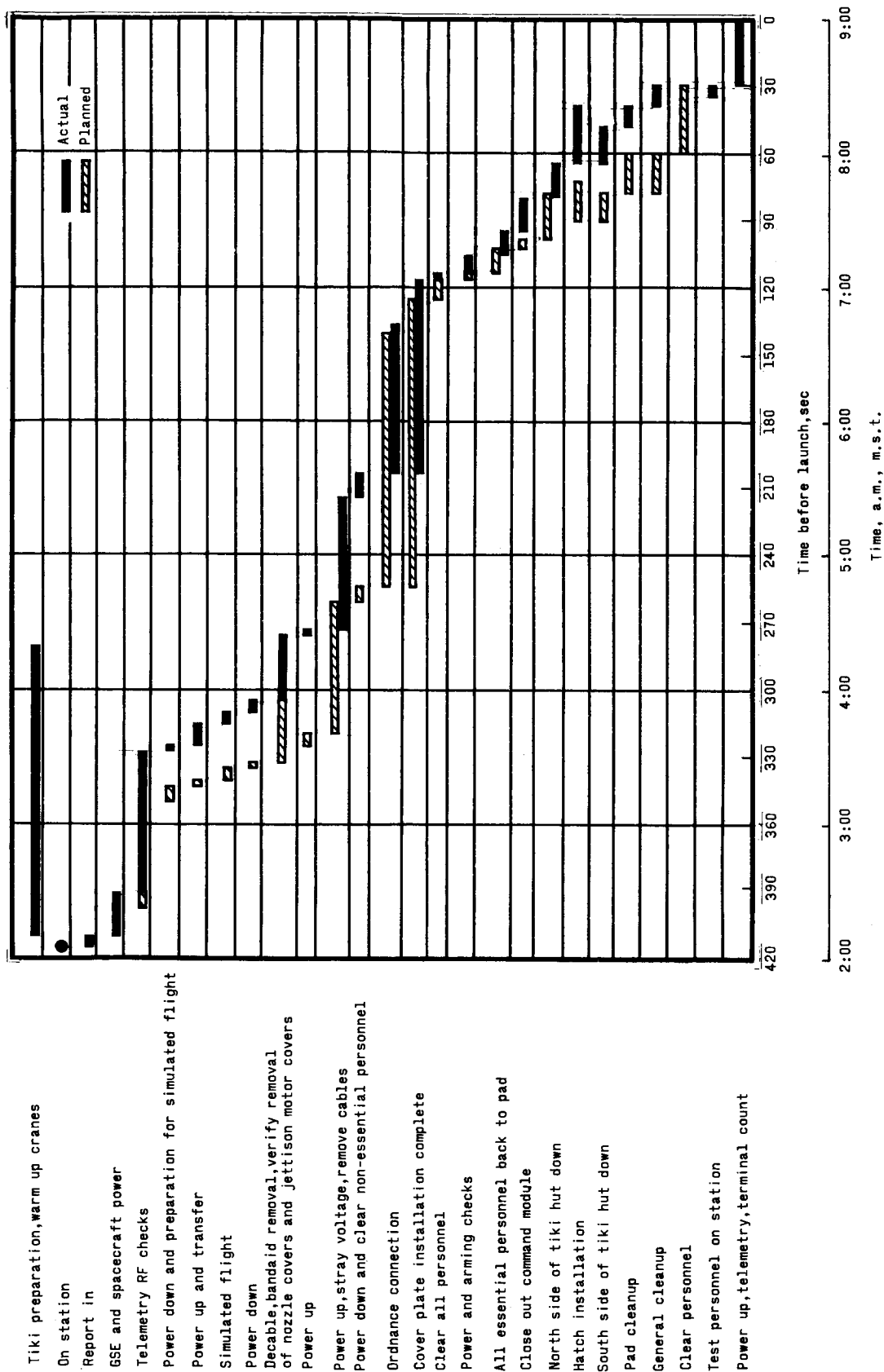
Figure A2.0-1.- Planned and actual prelaunch countdown.

APPENDIX A3.0

INSTRUMENTATION LISTINGS

A3.1  General

This appendix defines the onboard instrumentation and contains a list of measurements made for the evaluation of the flight. The test measurement list is included as table A3.1-1, which lists all of the measurements by channel and segment assignment and by system. The priority of each measurement is also indicated on the tabulations.

A.3.1.1  Table A3.1-1 legend.- Table A3-1 is coded to agree with the computer program established by NAA for Apollo measurements.

A3.1.2  Measurement identification.- The coding for this column consists of seven discrete alpha-numeric characters.

(1)  The first character designates the measurement location by module.

C - Command module

L - Launch escape tower

(2)  The second letter denotes the system within which the measurement originates.

A - Structures

C - Electrical

D - Launch escape

E - Earth landing

K - Flight technology

T - Communications and instrumentation

(3)  The four digits are assigned sequentially for numerical identification.

(4)  The seventh character denotes measurement classification

A - Acceleration

B - Current

D - Vibration

H - Position

P - Pressure

R - Rate

T - Temperature

V - Voltage

W - Time

X - Discrete event

A3.1.3  **Measurement description**.- This column is a brief definitive title given to each measurement which is unique and descriptive.

A3.1.4  **Channel**.- The channel identification for the telemetry system is a 14-digit alpha-numeric system.

This identification specifies:

(1) The telemetry RF link (LK); TRK designates onboard tape recorder assignment.

(2) Subcarrier assignment (SC no.)

(3) Commutator segment number (com-seg)

A3.1.5  **Data range**.- The data range denotes, in engineering units, the minimum and maximum ranges of the instrumentation system, including the transducer signal conditioner and telemetry system.

A3.1.6  **Priority**.- The priority column indicates the criticality of the measurement as follows:

P - Primary denotes those measurements which must be available at launch for mission success and/or to meet the flight objectives.

S - Secondary denotes those measurements which are highly desirable, but for which the mission will not be aborted or delayed.

M - Designates a group of related measurements of which no
more than a specified percentage may be inoperative
(80 percent, primary; 20 percent, secondary).

A3.1.7    Response.- The response column denotes the rate and units
required to provide satisfactory data resolution to time or
wave form.  Response for continuous data monitoring (telemetry
or recorder) is specified in cycles per second (cps).  Response
for commutated data monitoring is measured in samples per
second (s/s).

A3.1.8    Location.- The location coordinates denote the physical location
within the spacecraft at which the measurement is taken.  The
location is given either in polar or linear coordinates.

TABLE A3.1-1.- APOLLO BOILERPLATE MEASUREMENT LIST

[See sections A3.1.1 to A3.1.8 for explanation of notation used in table]

(a) Structures system for boilerplate 6

| Measurement identification | Measurement description | Channel LK | Channel SC no. | Com. seg. | Data range Low | Data range High | Data range Unit | Priority | Response Rate | Response Unit | Location |
|---|---|---|---|---|---|---|---|---|---|---|---|
| C A0001 A | X-axis, spacecraft accel., high | A | 16 | | -10 | +20 | g | P | 0 to 30 | cps | XC78, YC0, ZC21 |
| C A0002 A | X-axis, spacecraft accel., low | A | 15 | | - 2 | + 2 | g | P | 0 to 30 | cps | XC78, YC0, ZC21 |
| C A0005 A | Y-axis, spacecraft accel. | A | 13 | | -10 | +10 | g | P | 0 to 20 | cps | XC78, YC0, ZC21 |
| C A0007 A | Z-axis, spacecraft accel. | A | 14 | | -10 | +10 | g | P | 0 to 20 | cps | XC78, YC0, ZC21 |
| L A0011 A | Y-axis, tower accel. | A | 11 | | -10 | +10 | g | P | 0 to 30 | cps | XL380, YL0, ZL6 |
| L A0012 A | Z-axis, tower accel. | A | 12 | | -10 | +10 | g | P | 0 to 30 | cps | XL380, YL6, ZL0 |
| L A0013 D | X-axis, tower vibration, upper | TRK | | 5 | -200 | +200 | g | M | 20 to 2,500 | cps | XL120, YL25, ZL25 |
| L A0014 D | Y-axis, tower vibration, upper[a] | TRK | | 9 | -200 | +200 | g | M | 20 to 2,500 | cps | XL120, YL25, ZL25 |
| L A0015 D | Z-axis, tower vibration, upper[a] | TRK | | 7 | -200 | +200 | g | M | 20 to 2,500 | cps | XL120, YL25, ZL25 |
| L A0016 D | X-axis, tower vibration, lower | TRK | | 1 | -200 | +200 | g | M | 20 to 2,500 | cps | XL10, YL24, ZL26 |
| L A0017 D | Y-axis, tower vibration, lower | TRK | | 11 | -200 | +200 | g | M | 20 to 2,500 | cps | XL10, YL24, ZL26 |
| L A0018 D | Z-axis, tower vibration, lower | TRK | | 13 | -200 | +200 | g | M | 20 to 2,500 | cps | XL10, YL24, ZL26 |
| C A0028 P | Conical surface pressure 1 | A | E | 7 | + 2 | +22 | psia | M | 10 | s/s | XC30, 359 deg |
| C A0029 P | Conical surface pressure 2 | A | E | 8 | + 2 | +22 | psia | M | 10 | s/s | XC30, 21.5 deg |
| C A0030 P | Conical surface pressure 3 | A | E | 9 | + 2 | +22 | psia | M | 10 | s/s | XC30, 40.75 deg |
| C A0031 P | Conical surface pressure 4 | A | E | 10 | + 2 | +22 | psia | M | 10 | s/s | XC30, 84 deg |
| C A0032 P | Conical surface pressure 5 | A | E | 11 | + 2 | +22 | psia | M | 10 | s/s | XC30, 179.5 deg |
| C A0033 P | Conical surface pressure 6 | A | E | 12 | + 2 | +22 | psia | M | 10 | s/s | XC30, 203.75 deg |
| C A0034 P | Conical surface pressure 7 | A | E | 13 | + 2 | +22 | psia | M | 10 | s/s | XC30, 221.25 deg |
| C A0035 P | Conical surface pressure 8 | A | E | 14 | + 2 | +22 | psia | M | 10 | s/s | XC30, 246.5 deg |
| C A0036 P | Conical surface pressure 9 | A | E | 15 | + 2 | +22 | psia | M | 10 | s/s | XC30, 276 deg |
| C A0037 P | Conical surface pressure 10 | A | E | 16 | + 2 | +22 | psia | M | 10 | s/s | XC30, 293.25 deg |
| C A0038 P | Conical surface pressure 11 | A | E | 17 | + 2 | +22 | psia | M | 10 | s/s | XC30, 318.75 deg |
| C A0039 P | Conical surface pressure 12 | A | E | 18 | + 2 | +22 | psia | M | 10 | s/s | XC30, 335.5 deg |
| C A0040 P | Conical surface pressure 13 | A | E | 19 | + 2 | +22 | psia | M | 10 | s/s | XC100, 357 deg |
| C A0041 P | Conical surface pressure 14 | A | E | 20 | + 2 | +22 | psia | M | 10 | s/s | XC50.5, 21.5 deg |
| C A0042 P | Conical surface pressure 15 | A | E | 21 | + 2 | +22 | psia | M | 10 | s/s | XC71, 41.916 deg |

[a] During launch preparation it was noted that the tower vibrations on the Y- and Z-axes were inadvertently reversed. This has been corrected on this list.

TABLE A3.1.1.- APOLLO BOILERPLATE MEASUREMENT LIST - Continued

[See sections A3.1.1 to A3.1.8 for explanation of notation used in table]

(a)  Structures system for boilerplate 6 - Concluded

| Measurement identification | Measurement description | Channel | | | Data range | | | Priority | Response | | Location |
|---|---|---|---|---|---|---|---|---|---|---|---|
| | | LK | SC no. | Com. seg. | Low | High | Unit | | Rate | Unit | |
| C A0043 P | Conical surface pressure 16 | A | E | 22 | +2 | +22 | psia | M | 10 | s/s | XC100, 40.75 deg |
| C A0044 P | Conical surface pressure 17 | A | E | 23 | +2 | +22 | psia | M | 10 | s/s | XC100, 221.25 deg |
| C A0045 P | Conical surface pressure 18 | A | E | 24 | +2 | +22 | psia | M | 10 | s/s | XC71, 221.25 deg |
| C A0046 P | Conical surface pressure 19 | A | E | 25 | +2 | +22 | psia | M | 10 | s/s | SC100, 318.75 deg |
| C A0047 P | Conical surface pressure 20 | A | E | 26 | +2 | +22 | psia | M | 10 | s/s | XC71, 318.75 deg |
| C A0048 P | Conical surface pressure 21 | A | E | 27 | +2 | +22 | psia | M | 10 | s/s | XC50.5, 335.5 deg |
| C A0049 P | Conical surface pressure 22 | A | E | 28 | +2 | +22 | psia | M | 10 | s/s | XC50.5, 359 deg |
| C A0050 P | Conical surface pressure 23 | A | E | 29 | +2 | +22 | psia | M | 10 | s/s | XC50.5, 40.75 deg |
| C A0051 P | Conical surface pressure 24 | A | E | 30 | +2 | +22 | psia | M | 10 | s/s | XC50.5, 84.0 deg |
| C A0052 P | Conical surface pressure 25 | A | E | 31 | +2 | +22 | psia | M | 10 | s/s | XC50.5, 221.25 deg |
| C A0053 P | Conical surface pressure 26 | A | E | 32 | +2 | +22 | psia | M | 10 | s/s | XC50.5, 276 deg |
| C A0054 P | Conical surface pressure 27 | A | E | 33 | +2 | +22 | psia | M | 10 | s/s | XC50.5, 318.75 deg |
| C A0055 P | Conical surface pressure 28 | A | E | 34 | +2 | +22 | psia | M | 10 | s/s | XC71, 21.5 deg |
| C A0056 P | Conical surface pressure 29 | A | E | 39 | +2 | +22 | psia | M | 10 | s/s | XC71, 203.75 deg |
| C A0057 P | Conical surface pressure 30 | A | E | 40 | +2 | +22 | psia | M | 10 | s/s | XC71, 246.5 deg |
| C A0058 P | Conical surface pressure 31 | A | E | 41 | +2 | +22 | psia | M | 10 | s/s | XC71, 293.25 deg |
| C A0059 P | Conical surface pressure 32 | A | E | 42 | +2 | +22 | psia | M | 10 | s/s | XC71, 335.5 deg |
| C A0060 P | Conical surface pressure 33 | A | E | 84 | +2 | +22 | psia | M | 10 | s/s | XC79, 359 deg |
| C A0061 P | Conical surface pressure 34 | A | E | 85 | +2 | +22 | psia | M | 10 | s/s | XC79, 84 deg |
| C A0062 P | Conical surface pressure 35 | A | E | 86 | +2 | +22 | psia | M | 10 | s/s | XC80.3, 179.5 deg |
| C A0063 P | Conical surface pressure 36 | A | E | 87 | +2 | +22 | psia | M | 10 | s/s | XC79, 276 deg |
| C A0100 P | Base pressure 1 | A | E | 3 | +8 | +15 | psia | M | 10 | s/s | BOT, 50R, 90 deg |
| C A0101 P | Base pressure 2 | A | E | 4 | +8 | +15 | psia | M | 10 | s/s | BOT, 50R, 0 deg |
| C A0102 P | Base pressure 3 | A | E | 5 | +8 | +15 | psia | M | 10 | s/s | BOT, 50R, 270 deg |
| C A0103 P | Base pressure 4 | A | E | 6 | +8 | +15 | psia | M | 10 | s/s | BOT, 50R, 180 deg |
| C A0610 T | CM interior temperature | A | E | 76 | +0 | +150 | °C | S | 10 | s/s | CM interior |

TABLE A3.1-1.- APOLLO BOILERPLATE MEASUREMENT LIST - Continued

[See sections A3.1.1 to A3.1.8 for explanation of notation used in table]

(b) Electrical system for boilerplate 6

| Measurement identification | Measurement description | Channel | | | Data range | | | Priority | Response | | Location |
| | | LK | SC no. | Com. seg. | Low | High | Unit | | Rate | Unit | |
|---|---|---|---|---|---|---|---|---|---|---|---|
| C C0001 V | d-c voltage main bus A | A | E | 51 | +22 | +32 | vd-c | P | 10 | S/S | Power control box |
| C C0002 V | d-c voltage main bus B | A | E | 64 | +22 | +32 | vd-c | P | 10 | S/S | Power control box |
| C C0003 V | d-c voltage pyro bus A | A | E | 52 | + 0 | +32 | vd-c | P | 10 | S/S | LES sequencer |
| C C0004 V | d-c voltage pyro bus B | A | E | 53 | + 0 | +32 | vd-c | P | 10 | S/S | LES sequencer |
| C C0005 C | Total d-c current | A | E | 54 | + 0 | +25 | amps | P | 10 | S/S | Power control box |

(c) Launch-escape system for boilerplate 6

| Measurement identification | Measurement description | Channel | | | Data range | | | Priority | Response | | Location |
| | | LK | SC no. | Com. seg. | Low | High | Unit | | Rate | Unit | |
|---|---|---|---|---|---|---|---|---|---|---|---|
| L D0012 P | Pitch-control motor chamber pressure | A | 8 | | + 0 | +2,500 | psid | P | 0 to 45 | cps | XL345, YL0, ZL-1 |
| L D0013 P | Escape-motor chamber pressure | A | 9 | | + 0 | +2,500 | psid | P | 0 to 45 | cps | XL290, YL0, ZL0 |
| L D0016 V | Escape-motor EBW A charge | A | E | 44 | + 0 | +2,500 | vd-c | P | 10 | S/S | EBW module |
| L D0017 V | Escape-motor EBW B charge | A | E | 45 | + 0 | +2,500 | vd-c | P | 10 | S/S | EBW module |
| L D0018 V | Tower-jettison motor EBW A charge | A | E | 48 | + 0 | +2,500 | vd-c | P | 10 | S/S | EBW module |
| L D0019 V | Tower-jettison motor EBW B charge | A | E | 49 | + 0 | +2,500 | vd-c | P | 10 | S/S | EBW module |
| C D0021 X | Abort initiate relay close A | A | E | 55 | | | step | P | 10 | S/S | LES sequencer |
| C D0022 X | Abort initiate relay close B | A | E | 55 | | | step | P | 10 | S/S | LES sequencer |
| C D0057 X | ELS sequence start relay close A | A | E | 63 | | | step | P | 10 | S/S | LES sequencer |
| C D0038 X | ELS sequence start relay close B | A | E | 63 | | | step | P | 10 | S/S | LES sequencer |
| L D0049 V | Pitch-control motor EBW A charge | A | E | 46 | + 0 | +2,500 | vd-c | P | 10 | S/S | EBW module |
| L D0050 V | Pitch-control motor EBW B charge | A | E | 47 | + 0 | +2,500 | vd-c | P | 10 | S/S | EBW module |
| L D0051 T | Tower-jettison motor EBW module temperature | A | E | 80 | -50 | + 175 | °C | P | 10 | S/S | EBW module |
| C D0055 X | Tower-jettison motor fire relay close A | A | E | 62 | | | step | P | 10 | S/S | LES sequencer |
| C D0056 X | Tower-jettison motor fire relay close B | A | E | 62 | | | step | P | 10 | S/S | LES sequencer |
| C D0107 X | Tower-jettison motor fire relay close A | A | E | 61 | | | step | P | 10 | S/S | LES sequencer |
| C D0108 X | Tower-jettison motor fire relay close B | A | E | 61 | | | step | P | 10 | S/S | LES sequencer |

TABLE A3.1-1.- APOLLO BOILERPLATE MEASUREMENT LIST – Concluded

[See sections A3.1.1 to A3.1.8 for explanation of notation used in table]

(d) Earth landing system for boilerplate 6

| Measurement identification | Measurement description | Channel LK | Channel SC no. | Channel Com. seg. | Data range Low | Data range High | Data range Unit | Priority | Response Rate | Response Unit | Location |
|---|---|---|---|---|---|---|---|---|---|---|---|
| C E0001 X | Drogue deploy relay close A | A | E | 65 | | | step | P | 10 | S/S | ELS sequencer |
| C E0002 X | Drogue deploy relay close B | A | E | 65 | | | step | P | 10 | S/S | ELS sequencer |
| C E0003 X | Main parachute deploy-drogue release relay A | A | E | 66 | | | step | P | 10 | S/S | ELS sequencer |
| C E0004 X | Main parachute deploy-drogue release relay B | A | E | 66 | | | step | P | 10 | S/S | ELS sequencer |
| C E0005 X | Landing relay close A[b] | A | E | 67 | | | step | P | 10 | S/S | ELS sequencer |
| C E0006 X | Landing relay close B[b] | A | E | 67 | | | step | P | 10 | S/S | ELS sequencer |
| C E0007 X | Forward heat shield release relay close A[c] | A | E | 60 | | | step | P | 10 | S/S | ELS sequencer |
| C E0008 X | Forward heat shield release relay close B[c] | A | E | 60 | | | step | P | 10 | S/S | ELS sequencer |

(e) Flight technology system for boilerplate 6

| Measurement identification | Measurement description | Channel LK | Channel SC no. | Channel Com. seg. | Data range Low | Data range High | Data range Unit | Priority | Response Rate | Response Unit | Location |
|---|---|---|---|---|---|---|---|---|---|---|---|
| C K0001 R | Pitch rate gyro output | A | 4 | | -100 | +100 | deg/sec | P | 0 to 10 | cps | XC78, YC0, ZC21 |
| C K0002 R | Yaw rate gyro output | A | 3 | | -100 | +100 | deg/sec | P | 0 to 10 | cps | XC78, YC0, ZC21 |
| C K0003 R | Roll rate gyro output | A | 2 | | -100 | +100 | deg/sec | P | 0 to 10 | cps | XC78, YC0, ZC21 |
| C K0016 H | Pitch attitude gyro output | A | E | 74 | -175 | +175 | deg | P | 10 | S/S | XC78, YC0, ZC21 |
| C K0017 H | Roll attitude gyro output | A | E | 73 | -175 | +175 | deg | P | 10 | S/S | XC78, YC0, ZC21 |
| C K0018 H | Yaw attitude gyro output | A | E | 75 | -175 | +175 | deg | P | 10 | S/S | XC78, YC0, ZC21 |
| L K0023 H | Angle of attack | A | E | 35 | -40 | +40 | deg | P | 10 | S/S | XL399, YC0, ZC0 |
| L K0024 H | Angle of sideslip | A | E | 36 | -40 | +40 | deg | P | 10 | S/S | XL399, YC0, ZC0 |
| L K0025 P | Dynamic pressure | A | E | 37 | 0 | +1,250 | psf | P | 10 | S/S | XL399, YC0, ZC0 |

(f) Communications and instrumentation system for boilerplate 6

| Measurement identification | Measurement description | Channel LK | Channel SC no. | Channel Com. seg. | Data range Low | Data range High | Data range Unit | Priority | Response Rate | Response Unit | Location |
|---|---|---|---|---|---|---|---|---|---|---|---|
| C T0001 W | Onboard timer | A | 7 | | | | | P | 0 to 35 | cps | CM interior |
| C T0007 X | R and Z calibration monitor | A | E | 88 | | | step | P | 10 | S/S | SIG cond box |
| C T0020 V | Link A diff. PDM (90 × 10 comm) | TRK | | 3 | | | | P | | PDM | TM comm |
| C T0021 V | Link A mixer no. 2 output | TRK | | 6 | | | | P | 20 to 2,500 | cps | TM mod bus |
| C T0201 T | TM RF transmitter A, temperature | A | E | 78 | + 0 | +150 | °C | S | 10 | S/S | TM RF transmitter A |
| C T0202 T | TM RF Amp A, temperature | A | E | 77 | + 0 | +150 | °C | S | 10 | S/S | TM RF Amp A |

[b] The main parachute release relays A and B were changed to landing relay closures A and B since recent design changes eliminated the release system.

[c] The heat-shield release relay was instrumented, but this system was inactive because of a recent design change. The forward heat shield was firmly attached to the tower and separated from the CM during tower jettison.

APPENDIX A4.0

TEST DATA COMPILATION

A4.1  General

The data contained in this appendix are in two major categories:

(a)  Direct recorded onboard magnetic tape data

(b)  Computed data, utilizing the onboard magnetic tape data and WSMR preliminary range tracking data.

Launch-escape-tower vibration data, contained on the onboard magnetic tape, are not presented in this appendix since reduced results from these data will be dependent upon spectral analysis processing. However, it is planned to include the data in the final NASA report on this mission.

A4.2  Primary Data Source

The primary data source for this mission was the 14-track onboard magnetic tape recorder.  The data contained on the onboard magnetic tape consisted of continuous and commutated information.  (Refer to section 7.2 for system details and appendix A3.0 for instrumentation listings.)

A4.3  Data Plot Discussion

Each plot of the commutated onboard data included in the report (figs. A4-1 to A4-33) consisted of two portions.  For the initial portion of the mission (0 to 40 sec), each data point was plotted.  During the latter portion of the flight (25 sec to 165 sec), only every fifth point was plotted.  The measurement number and description coding are defined in appendix A3.0.  Each measurement location portrayed on the miniature space vehicle on each plot shows the relative position of the transducer. The closed circle indicates a measurement on the far side of the sketch while an open circle indicates a measurement on the near side of the sketch.

A4.3  Data Scaling

Pulse differential modulation (PDM) data are linear in nature and are converted to telemetry volts by using the slope and offset method

$$\text{Slope} = m = \frac{5}{D_2 - D_1}$$

Where $D_1$ is digital value of the 0-volt segment and $D_2$ is digital value of the 5-volt segment.

$$\text{Offset} = B = - m(D_1)$$

The offset and slope of the system were computed for every frame. Data calibrations recorded prior to the flight test were used to convert continuous data to telemetry volts. These calibrations consisted of five voltage steps (0, 1.25, 2.50, 3.75, and 5.0 volts). Digital values of each step were edited and the best average was determined.

The slope and offset method was then applied to these calibrations:

$$\text{Slope} = m = \frac{5\left[1.25(C_2) + 2.5(C_3) + 3.75(C_4) + 5.0(C_5)\right] - 12.5\sum_{i=1}^{5} C_i}{5\sum_{i=1}^{5}\left(C_i^2\right) - \left(\sum_{i=1}^{5} C_i\right)^2}$$

$$\text{Offset} = B = \frac{12.5\sum C_i - \left(\sum C_i\right)\left[1.25(C_2) + 2.5(C_3) + 3.75(C_4) + 5.0(C_5)\right]}{5\sum_{i=1}^{5}\left(C_i^2\right) - \left(\sum_{i}^{5} C_i\right)^2}$$

Where $C_1$, $C_2$, $C_3$, $C_4$, $C_5$ are digital average values of the respective calibration steps. PDM and continuous data are converted to engineering units by using the following equation:

$$V_i = B + mD_i$$

where $V_i$ is telemetry volts, and $D_i$ is the ith data word in the frame.

Then

$$F_i = A_o + A_1 V_i \ldots\ldots\ldots + A_n V_i^n$$

where  F  is function value in engineering units, n  is the degree of
the respective calibration curve, and  A  is coefficient of the poly-
nominal.

Total acceleration is computed (comp) as the magnitude of the vector
sum of the component accelerations (X-axis, high; Y-axis; and Z-axis).

Pitch, yaw, and roll rates were computed by evaluating the first
derivative of the second-degree least-squares curve fitted to seven
consecutive attitude readings.

No corrections were made to the data for R and Z calibrations or
for known ambient values.

A4.4  Cinetheodolite Computation Procedures

The White Sands Missile Range Processing Facility computed position
data by using an N-station solution.  This solution determines line-of-
sight for each station from observed azimuth and elevation angles.
These observed angles were corrected for atmospheric refraction and
systematic errors of the instrumentation; then an N-station least-squares
solution is used to compute position data.  The computed position was
determined as that point for which the sum of the squares of the per-
pendicular distance to each line-of-sight is minimum.

In the right-hand Cartesian coordinate system, the origin was the
surveyed location of the launch pad (longitude 106°19'31.315", lati-
tude 32°25'0.066", and altitude above mean sea level  H, 4,036 ft).  The
X-axis is positive in the direction of the intended flight path, true
North; the Y-axis is positive upward.  Altitude  H  above mean sea level
is computed for each position.  The equation used is

$$H = Z + 4,036 + \frac{X^2 + Y^2}{2r + (Z + 4,036)}$$

where  r  is the average radius of the earth at the launch vicinity,
(20,897,038 ft) and X, Y, and Z are position coordinates in the afore-
mentioned coordinate system.

Each component velocity and acceleration is obtained by evaluating
the first and second derivative, respectively, of the second-degree
least-squares curve fitted to seven consecutive position points, having
their midpoint at the position of desired velocity and acceleration.

Total velocity is computed as the magnitude of the vector sum of
the component velocities.  Total acceleration is computed by evaluating

the first derivative of total velocity.

Flight-path and heading angles are computed from the component velocities and define the direction of the total velocity vector. Heading angle is measured positive counterclockwise from the positive X-axis to the projection of the total velocity vector on the XY-plane. Flight-path angle is measured positive above this XY-plane.

Ground range is computed as the magnitude of the vector sum of the displacement along the X- and Y-axes. Slant range is computed as the magnitude of the vector sum of the displacement along the X-, Y-, and Z-axes.

Upper air data are correlated with flight data by relating the corresponding altitude components. The altitude component of the flight data is taken as altitude H above mean sea level. The altitude component of upper air data is a corrected altitude computed from pressure information. All interpolations are linear.

True airspeed V is computed as the absolute value of the vector differences of the velocities of wind and vehicle. Vertical component of the wind velocity is assumed to be zero.

Dynamic pressure q in lb/sq ft is computed by using the equation

$$q = 97 \ V^2 \ \rho \ 10^{-8}$$

where ρ is density in slugs/ft$^3$.

Mach number M is computed by using the equation

$$M = 0.0152(V)/(T)^{\frac{1}{2}}$$

where T is temperature in degrees Kelvin.

Zero wind-position data (u, v, w) are computed by adding the vector components of wind velocity, summed over the respective time increment to original position data.

Position angles are computed from zero wind position data. Azimuth angle is the angle from the positive U-axis to the projection, in the UV-plane, of the line-of-sight from the origin to the vehicle. Elevation angle is the angle from the U-axis to the projection of the line-of-sight in the VW-plane.

Relative position is computed as the differences of the component positions of tower and the command module. Total relative position is computed as the vector sum of the component relative positions.

Relative velocity and acceleration are computed by using relative position in the previously described manner.
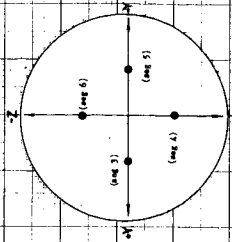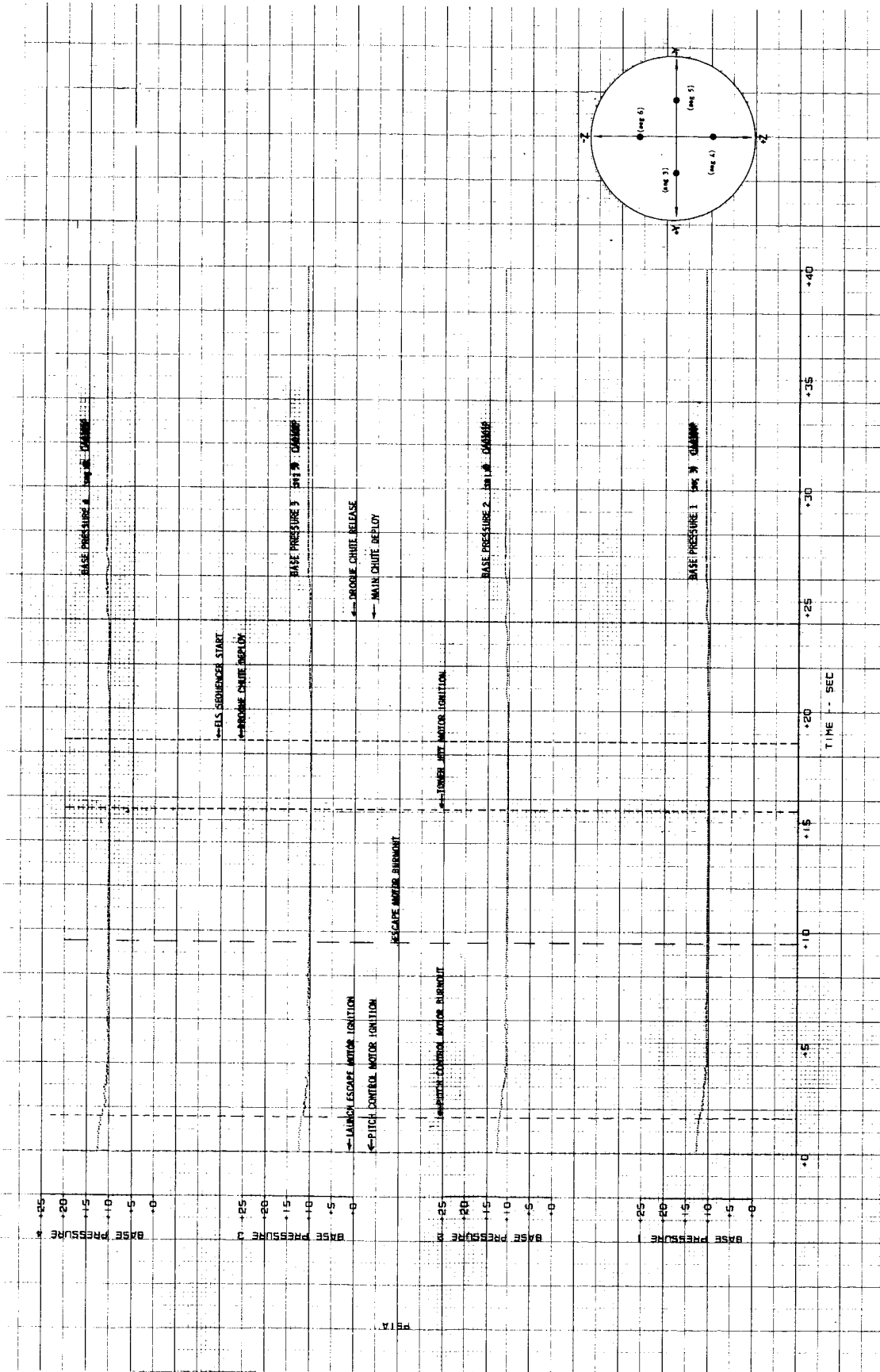
(a)  0 through 40 seconds.

Figure A4-1.- Pressures measured at base of command module.
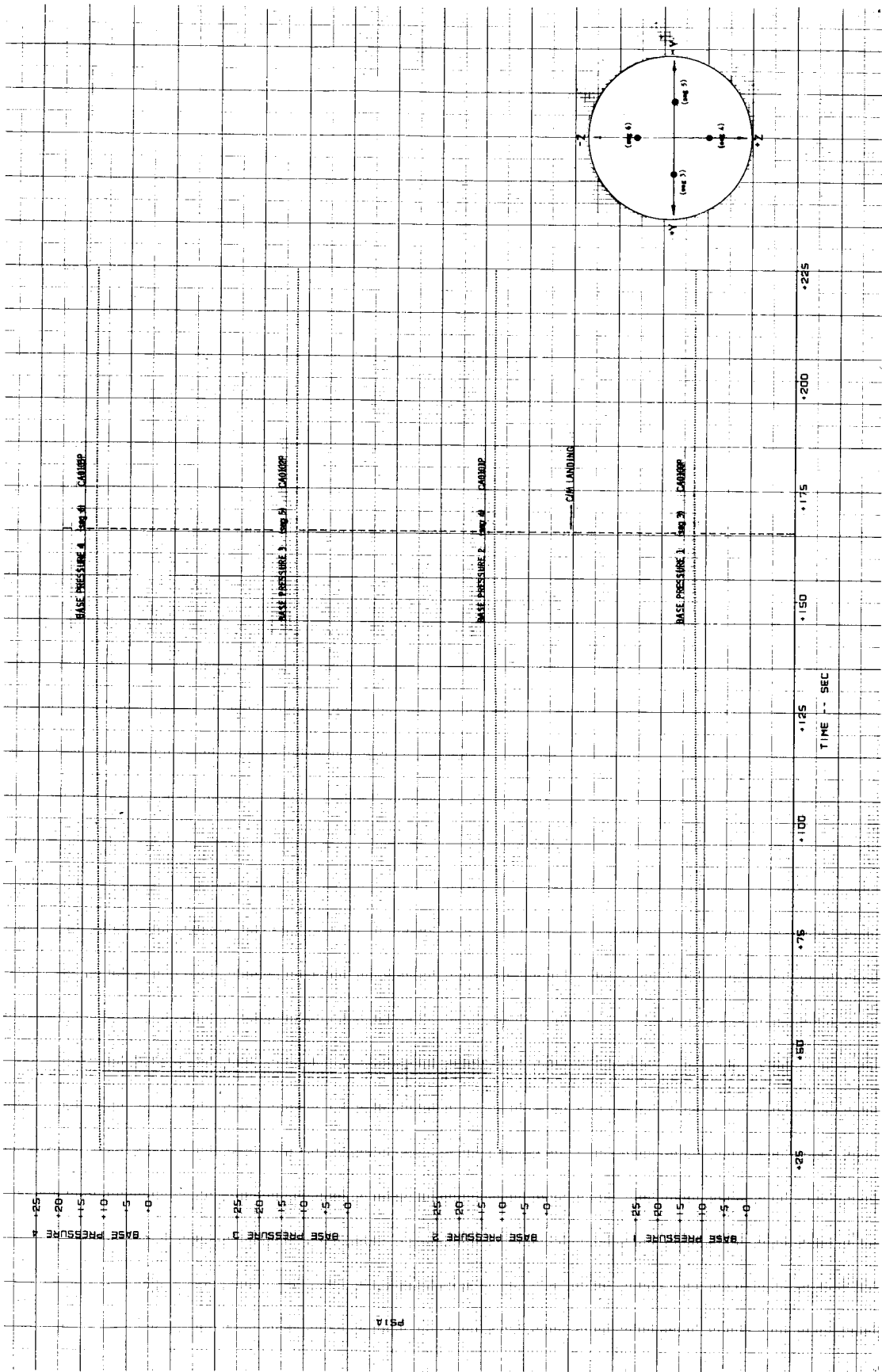
(b)  25 through 225 seconds.

Figure A4-1.- Concluded.
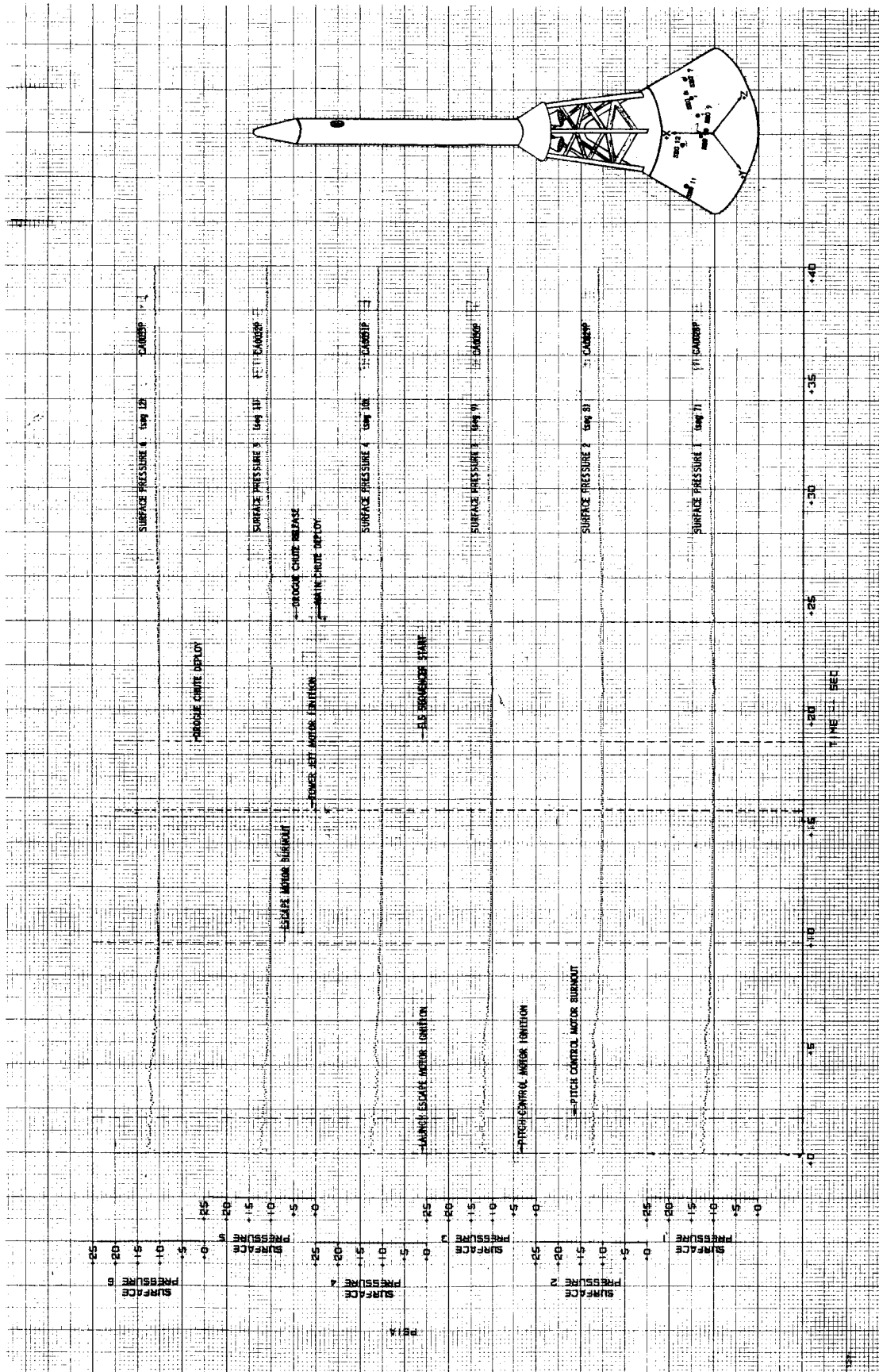
(a)  0 through 40 seconds.

Figure A4-2.- Command module conical surface pressures.
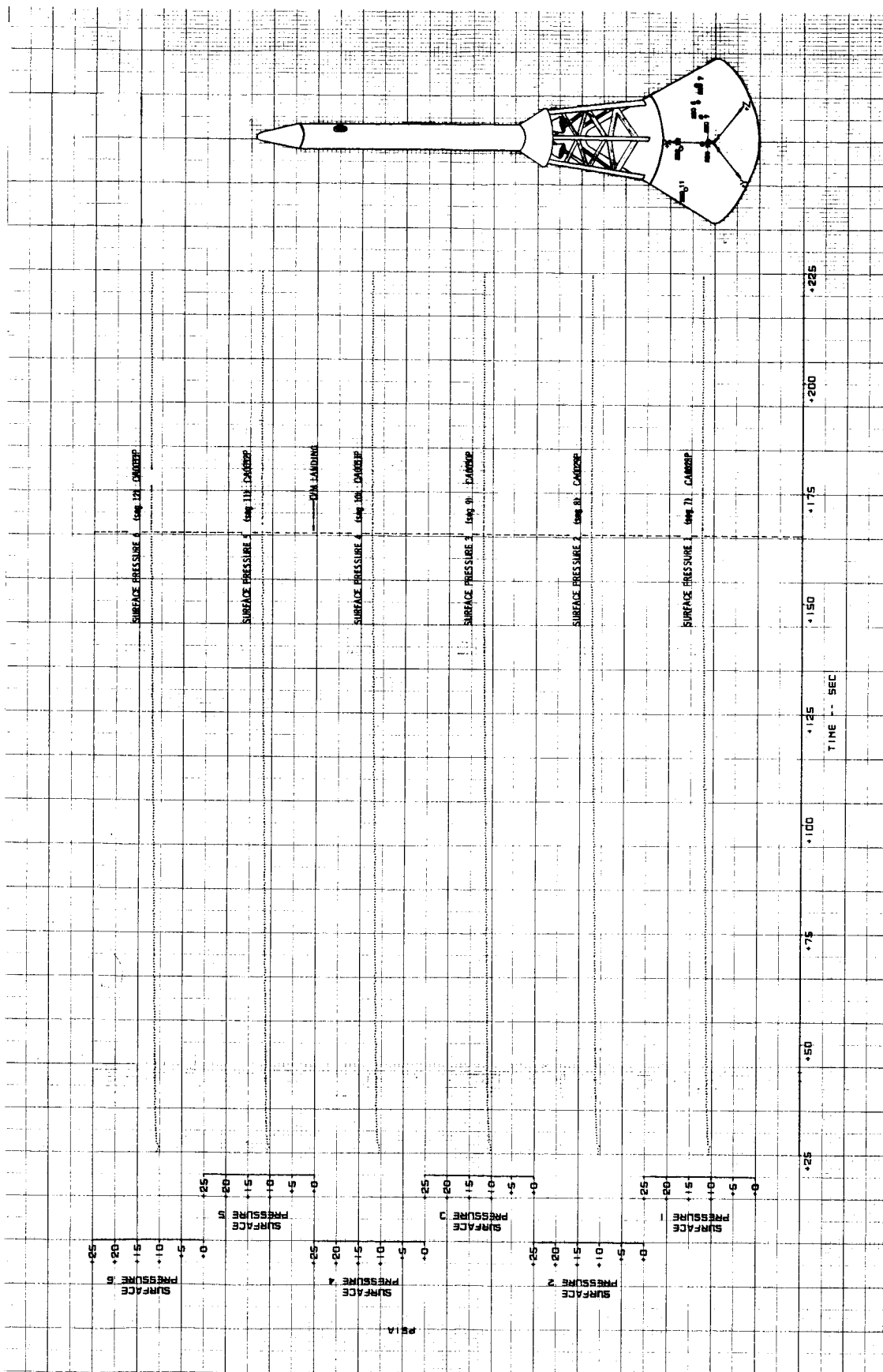
(b) 25 through 225 seconds.

Figure A4-2.- Concluded.
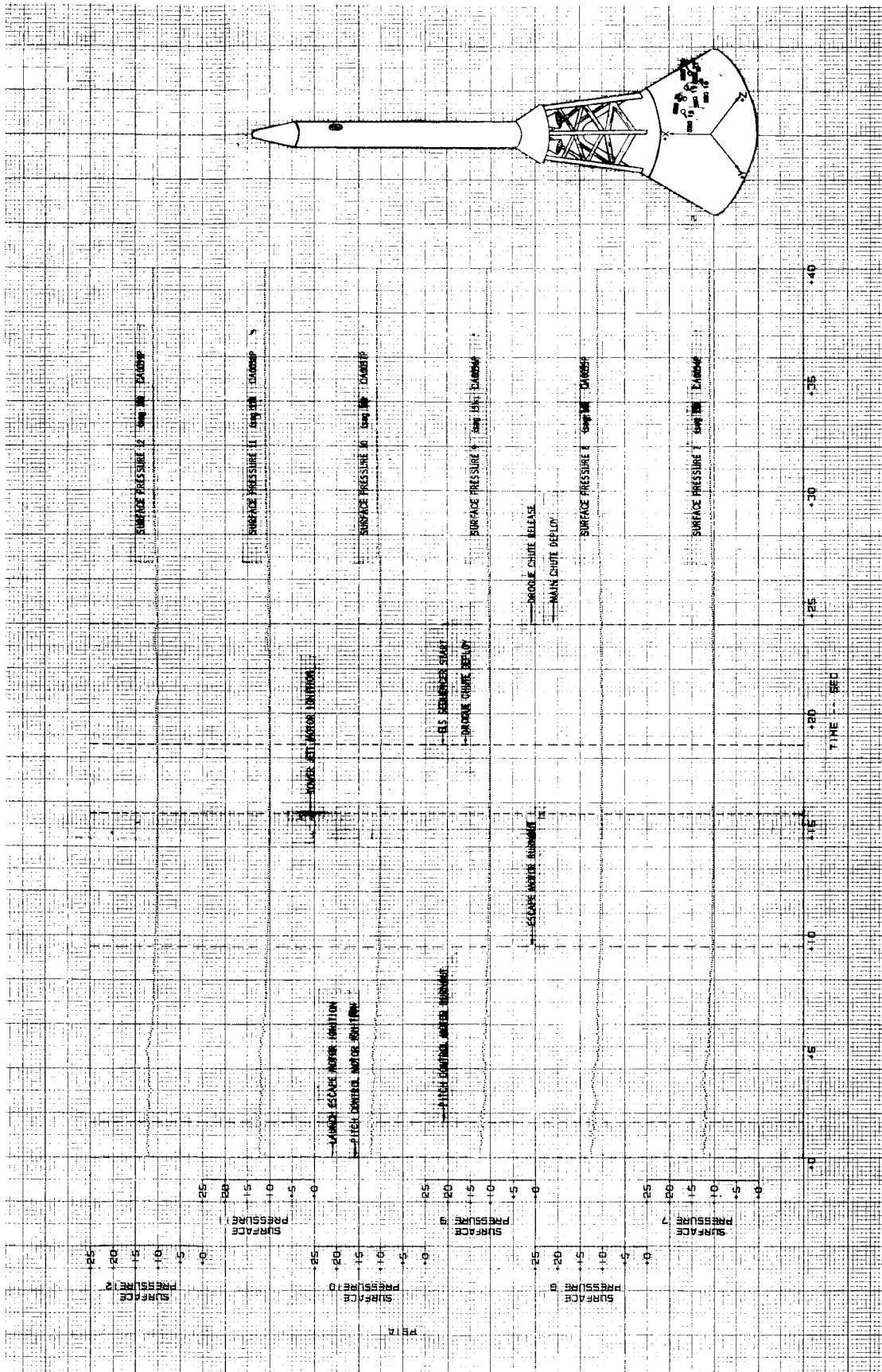
(a) 0 through 25 seconds.

Figure A4-3.- Command module conical surface pressures.
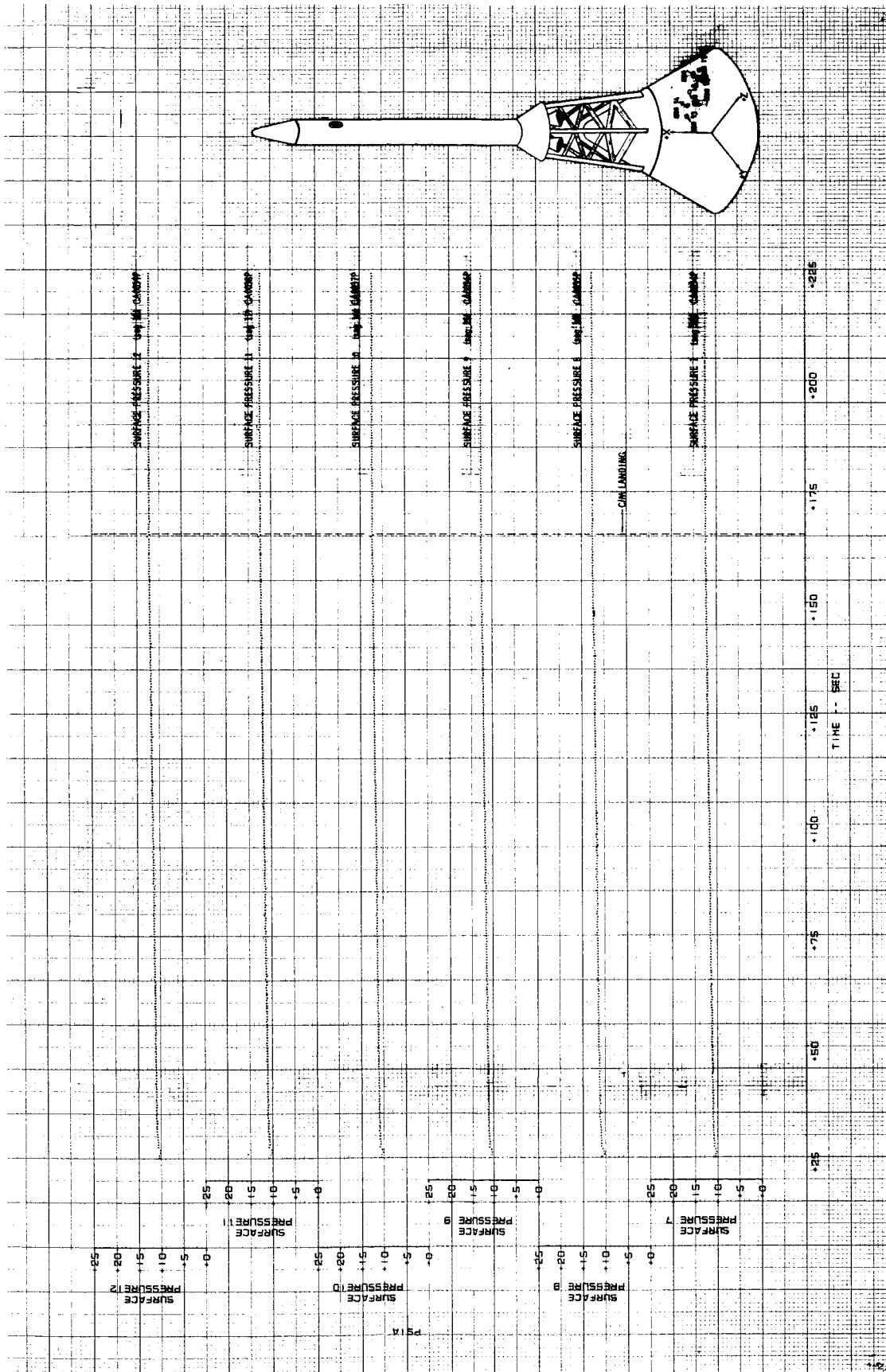
(b) 25 through 225 seconds.

Figure A4-3.- Concluded.
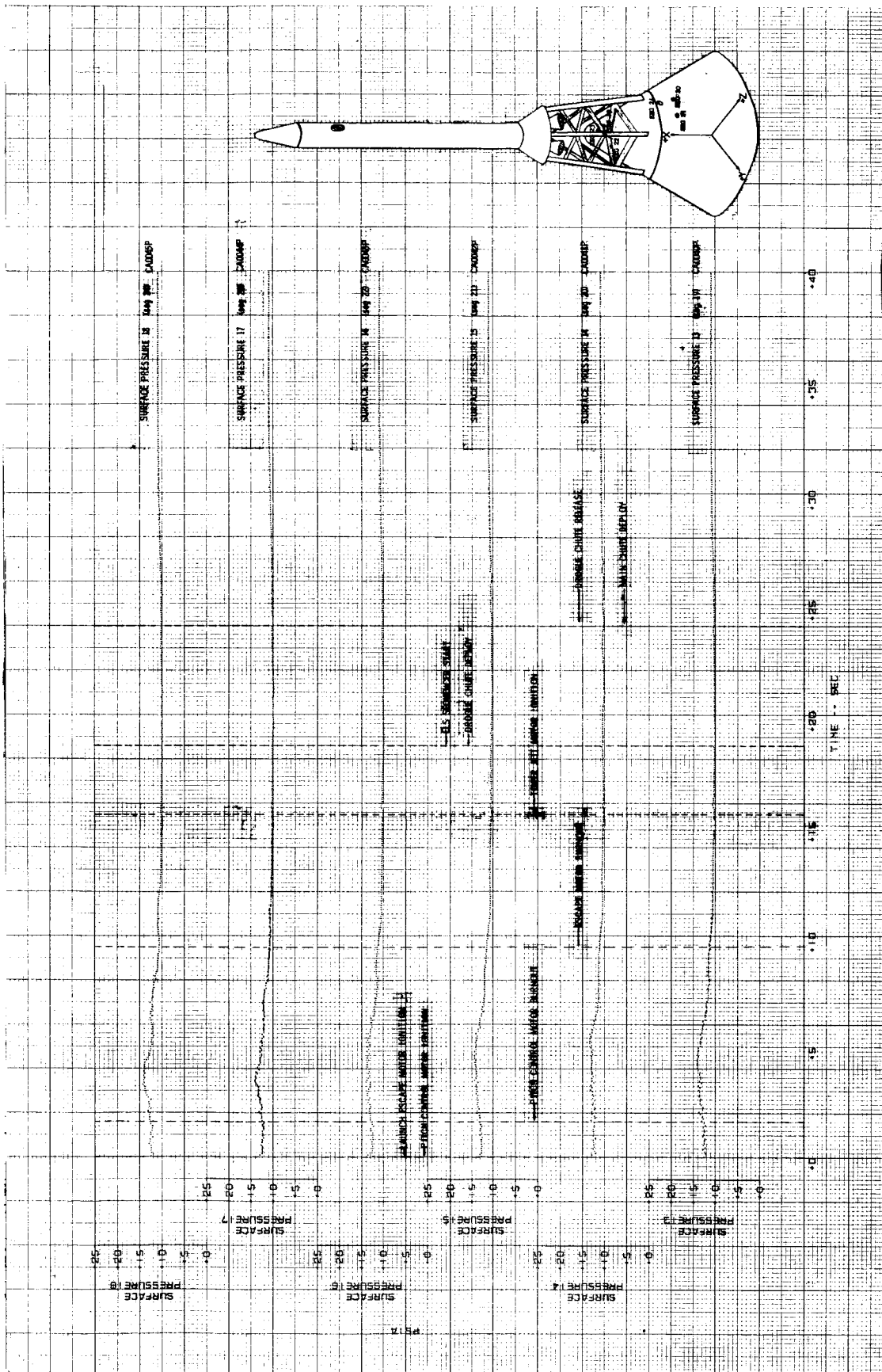
(a)  O through 40 seconds.

Figure A4-4.- Command module conical surface pressures.
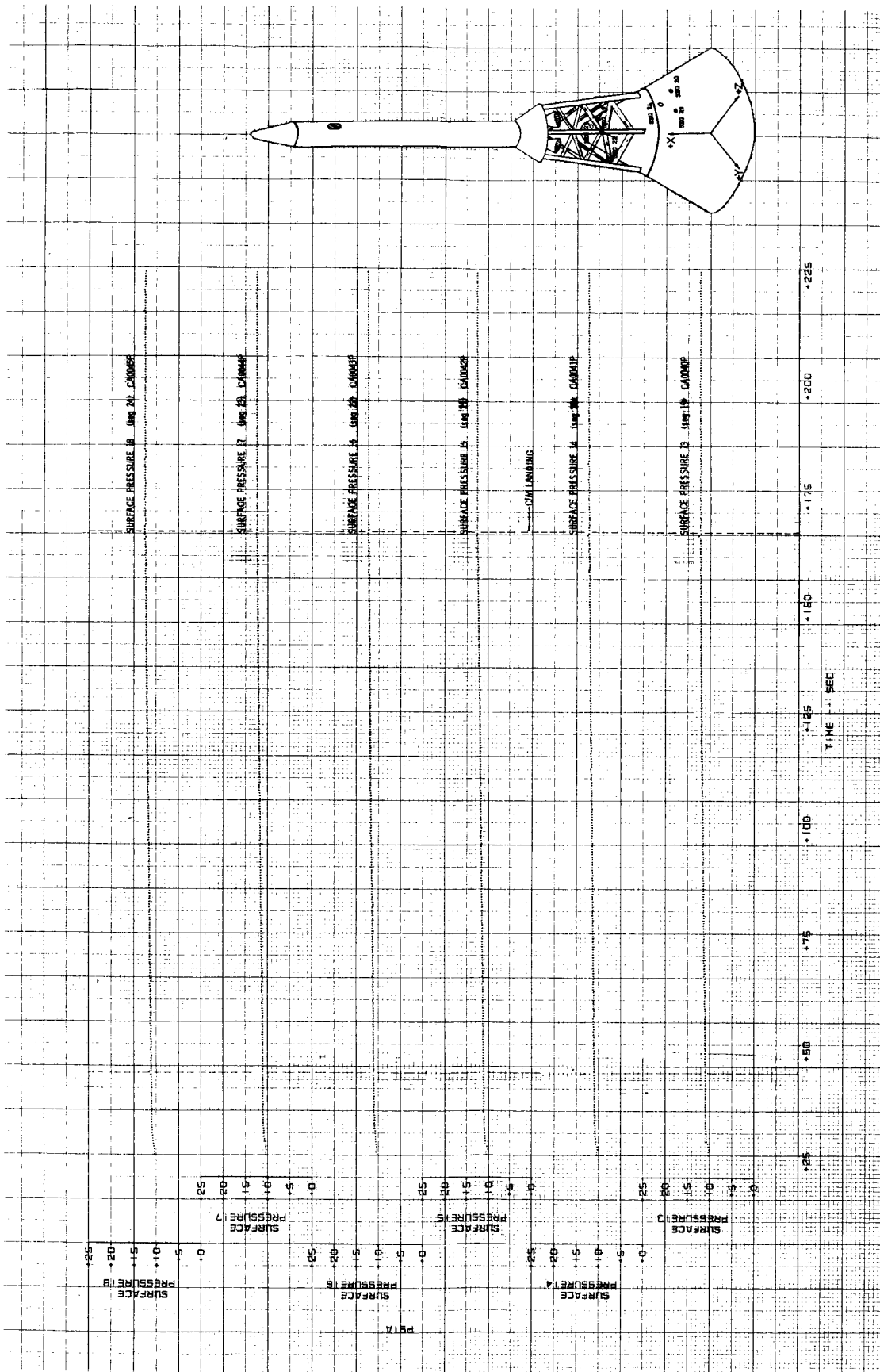
(b) 25 through 225 seconds.

Figure A4-4.- Concluded.
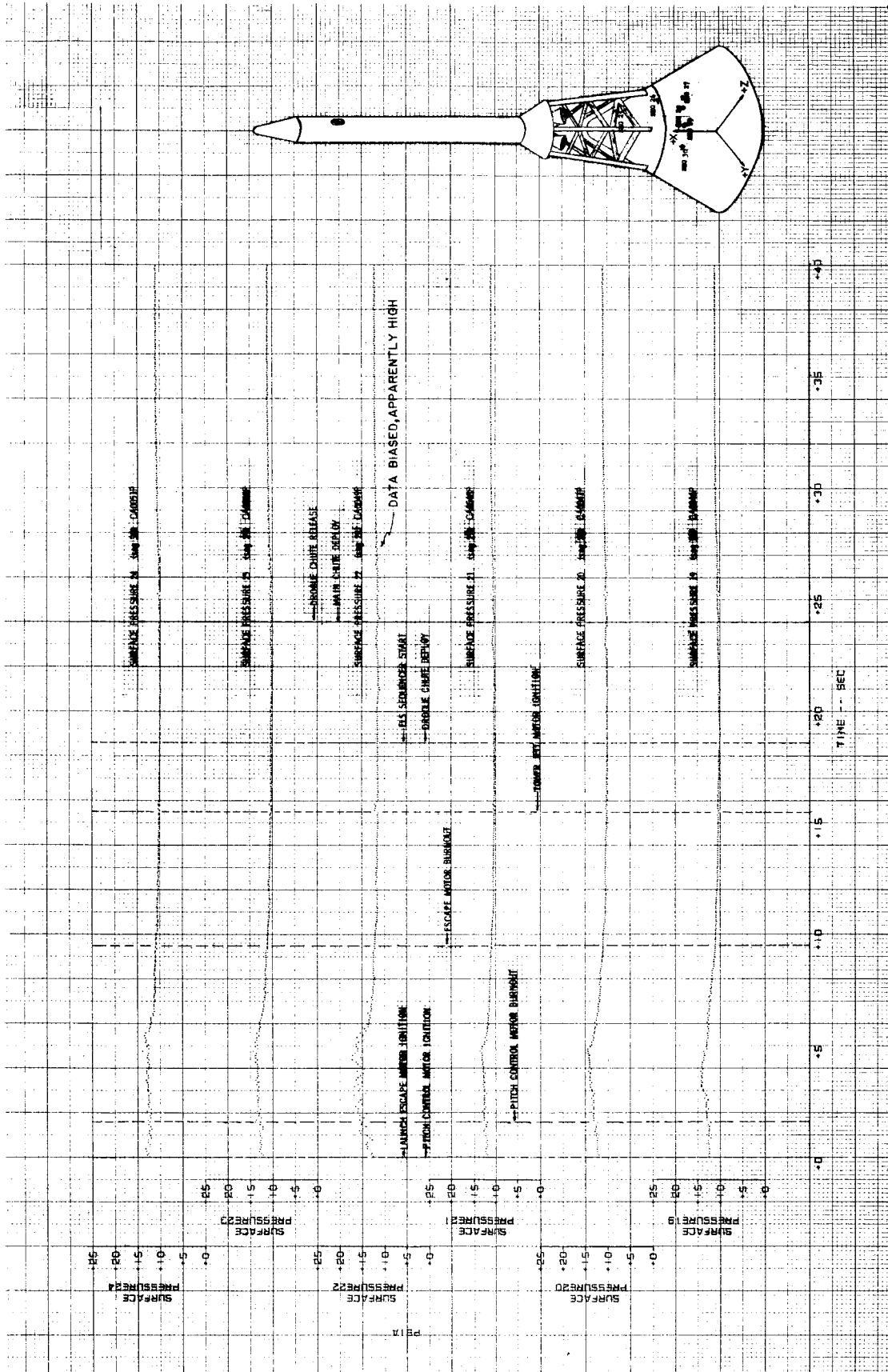
(a) 0 through 40 seconds.

Figure A4-5.- Command module conical surface pressures.
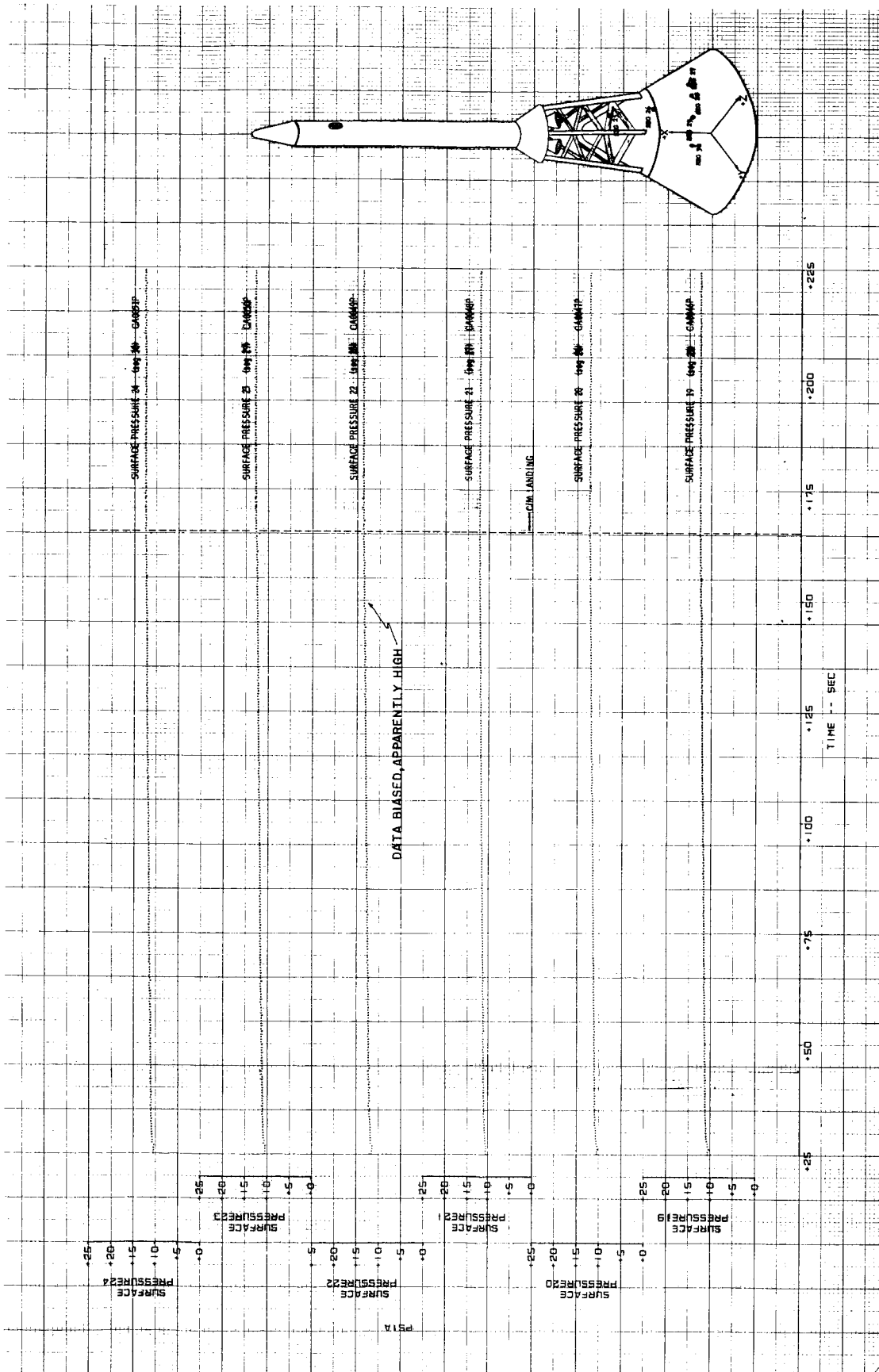
(b) 25 through 225 seconds.

Figure A4-5.- Concluded.
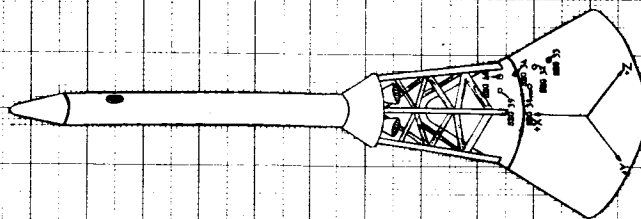
(a) 0 through 40 seconds.

Figure A4-6.- Command module conical surface pressures.
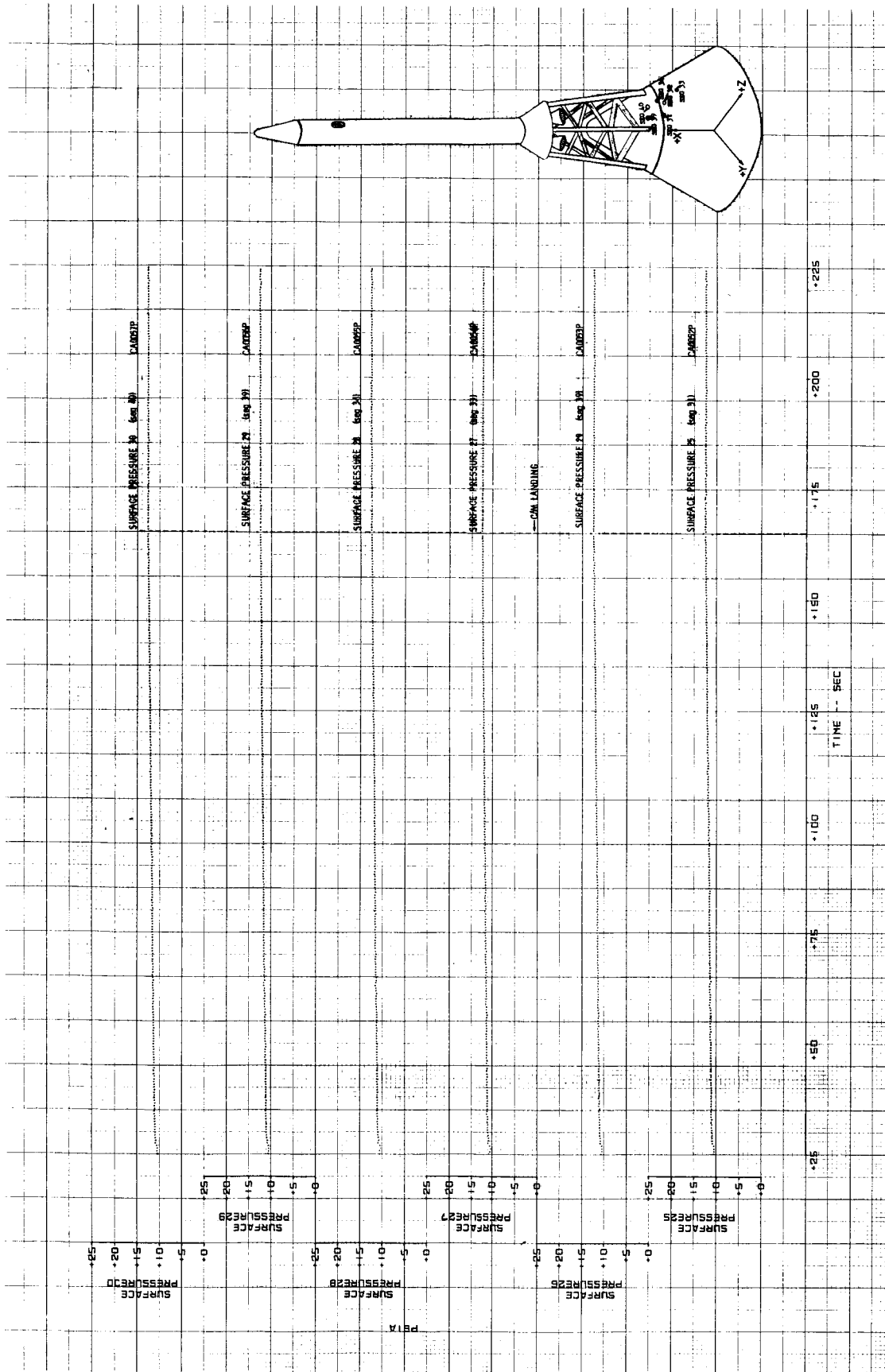
(b) 25 through 225 seconds.

Figure A4-6.- Concluded.
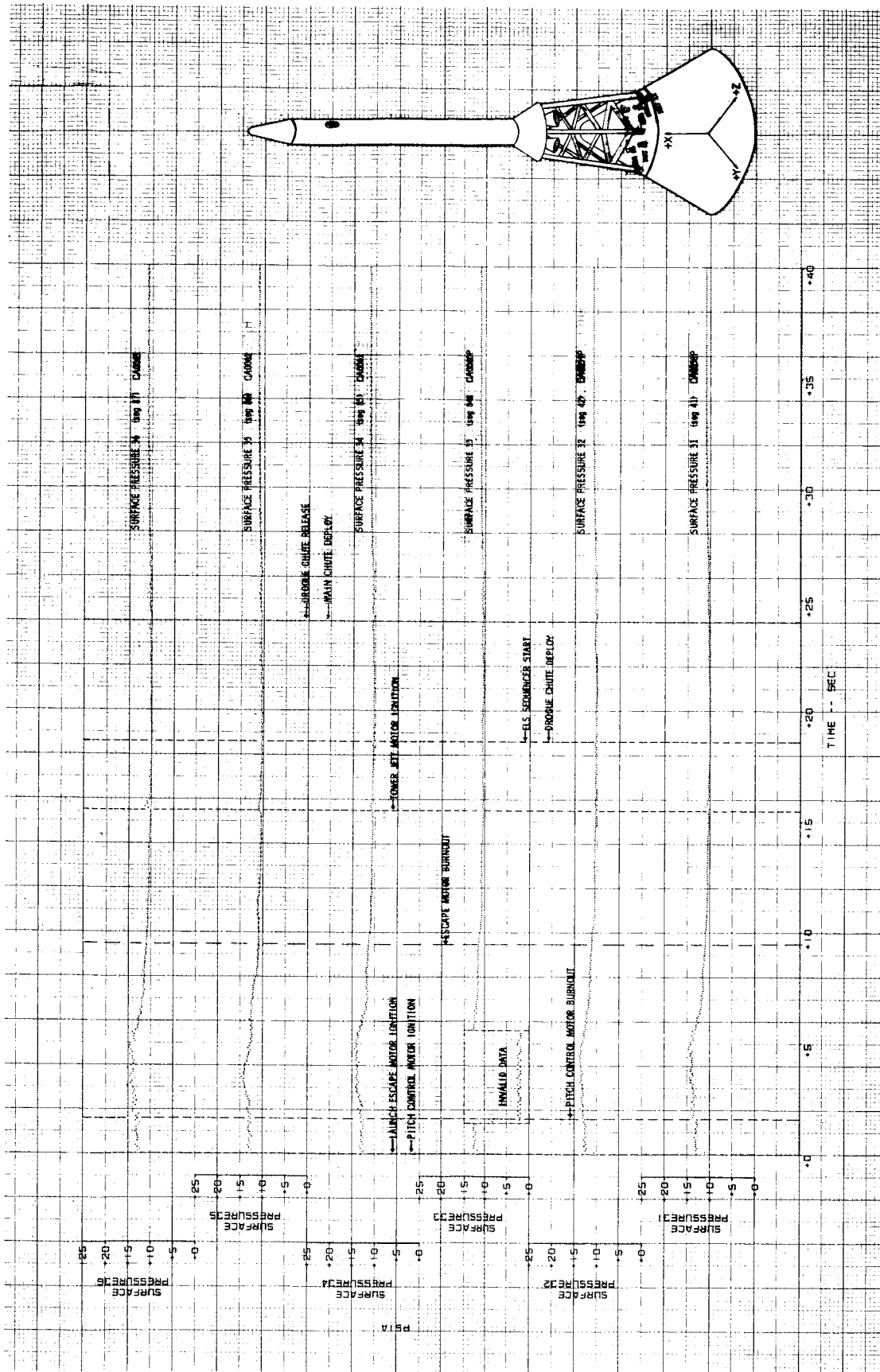
(a)   0 through 40 seconds.

Figure A4-7.- Command module conical surface pressures.
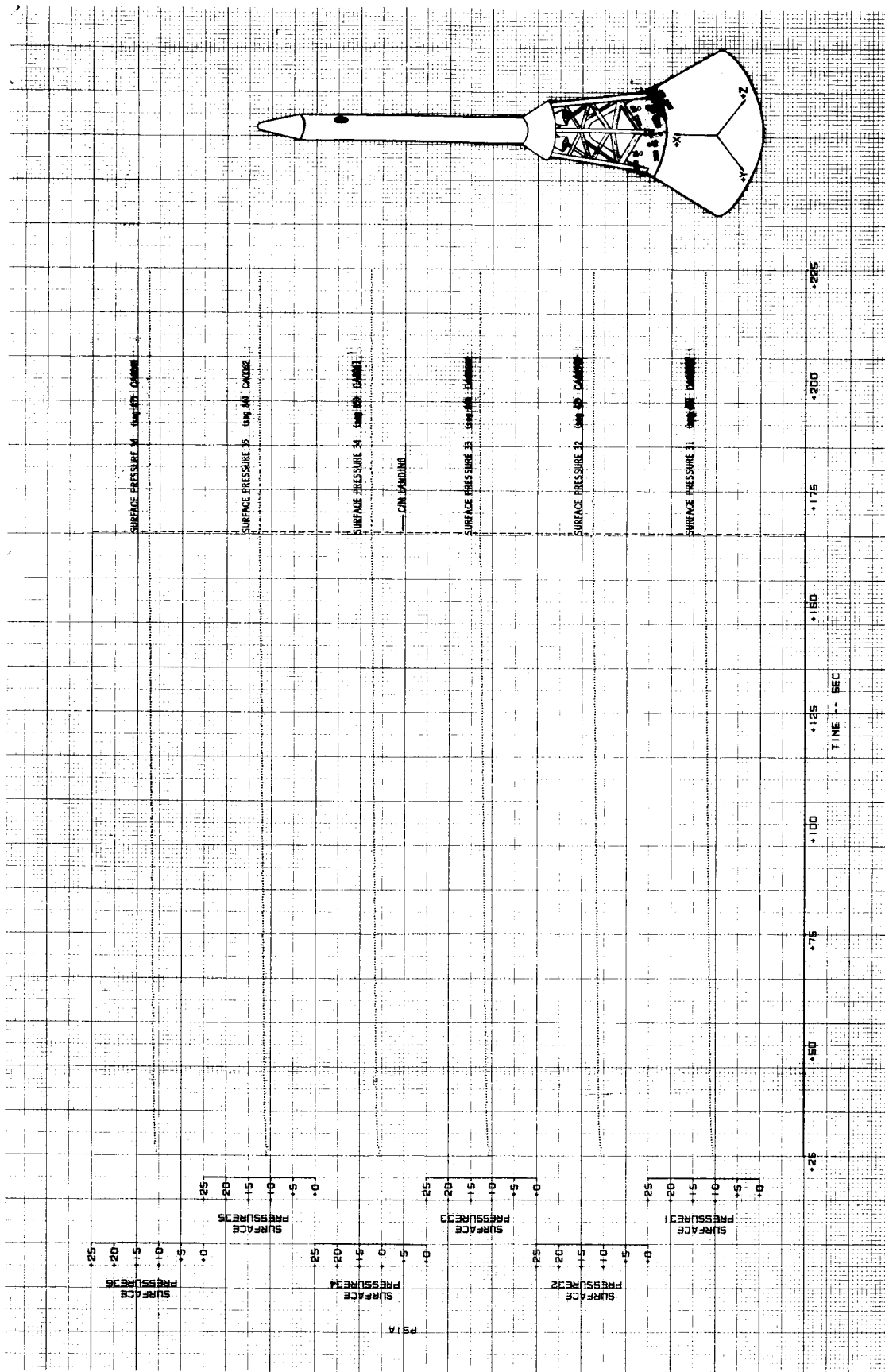
(b) 40 through 225 seconds.

Figure A4-7.- Concluded.
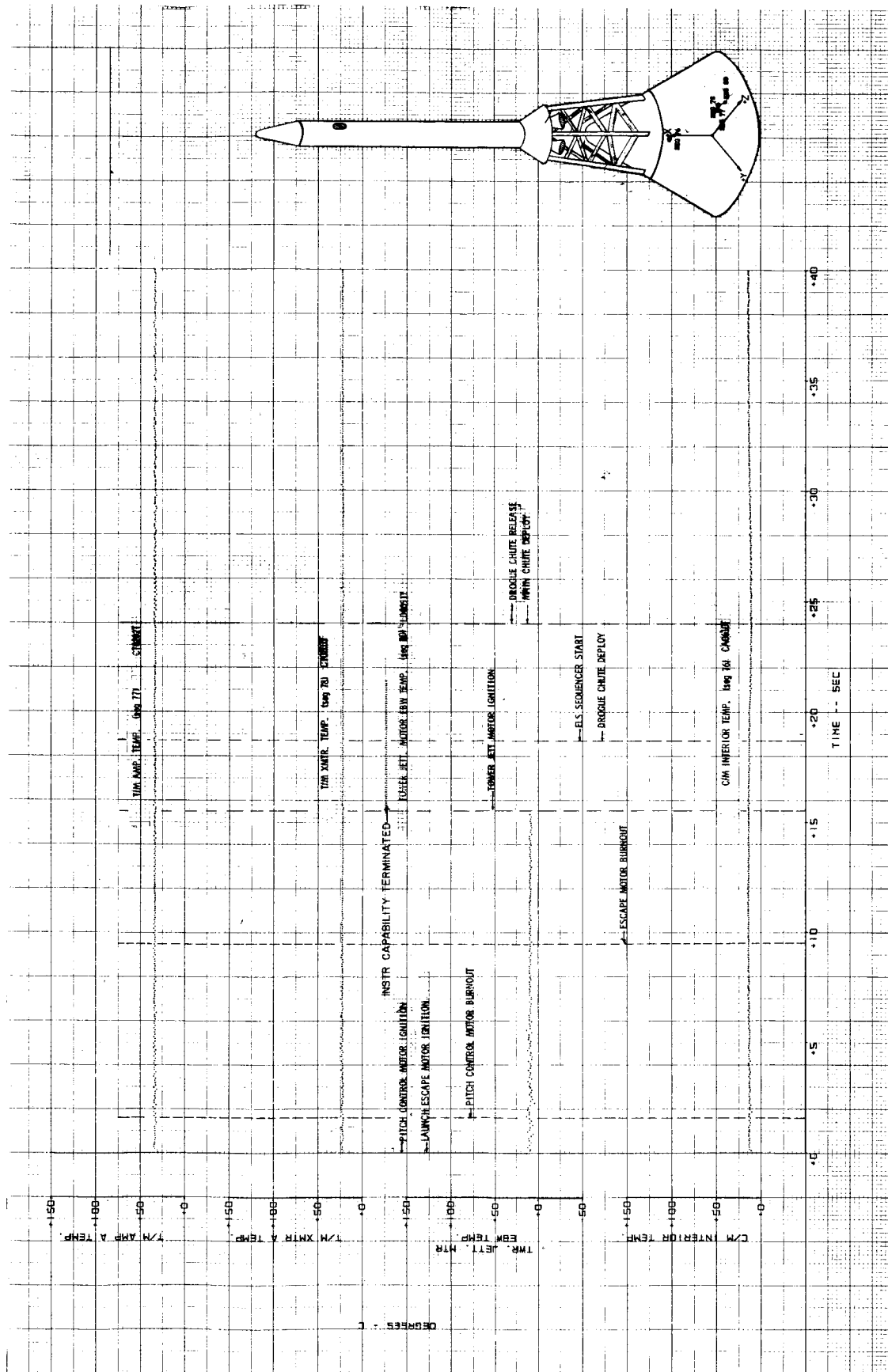
(a) 0 through 40 seconds.

Figure A4-8.- Command module interior and equipment temperatures.
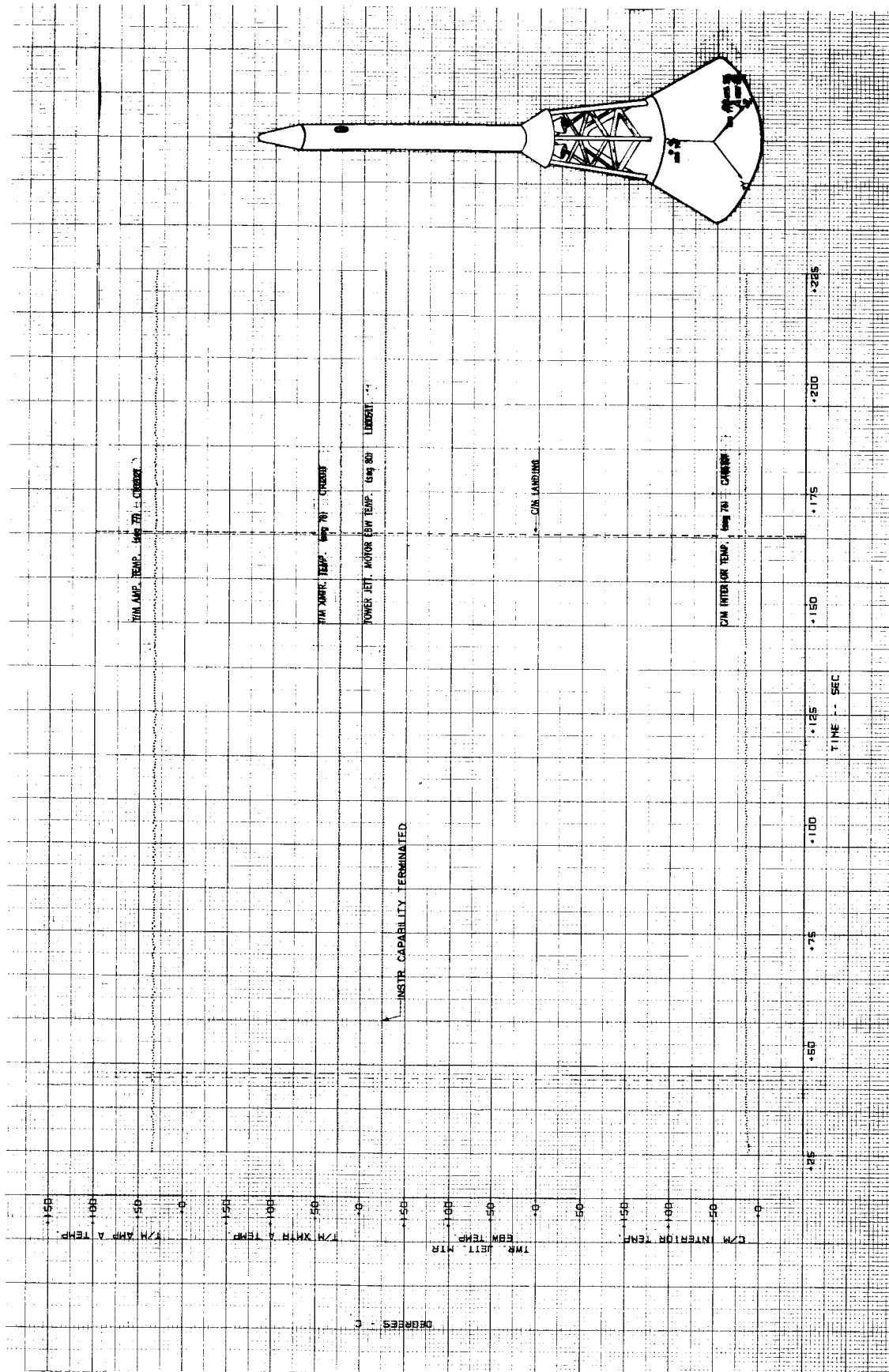
(b)  25 through 225 seconds.

Figure A4-8.- Concluded.

(a) 0 through 40 seconds.

Figure A4-9.- Command module electrical system data.
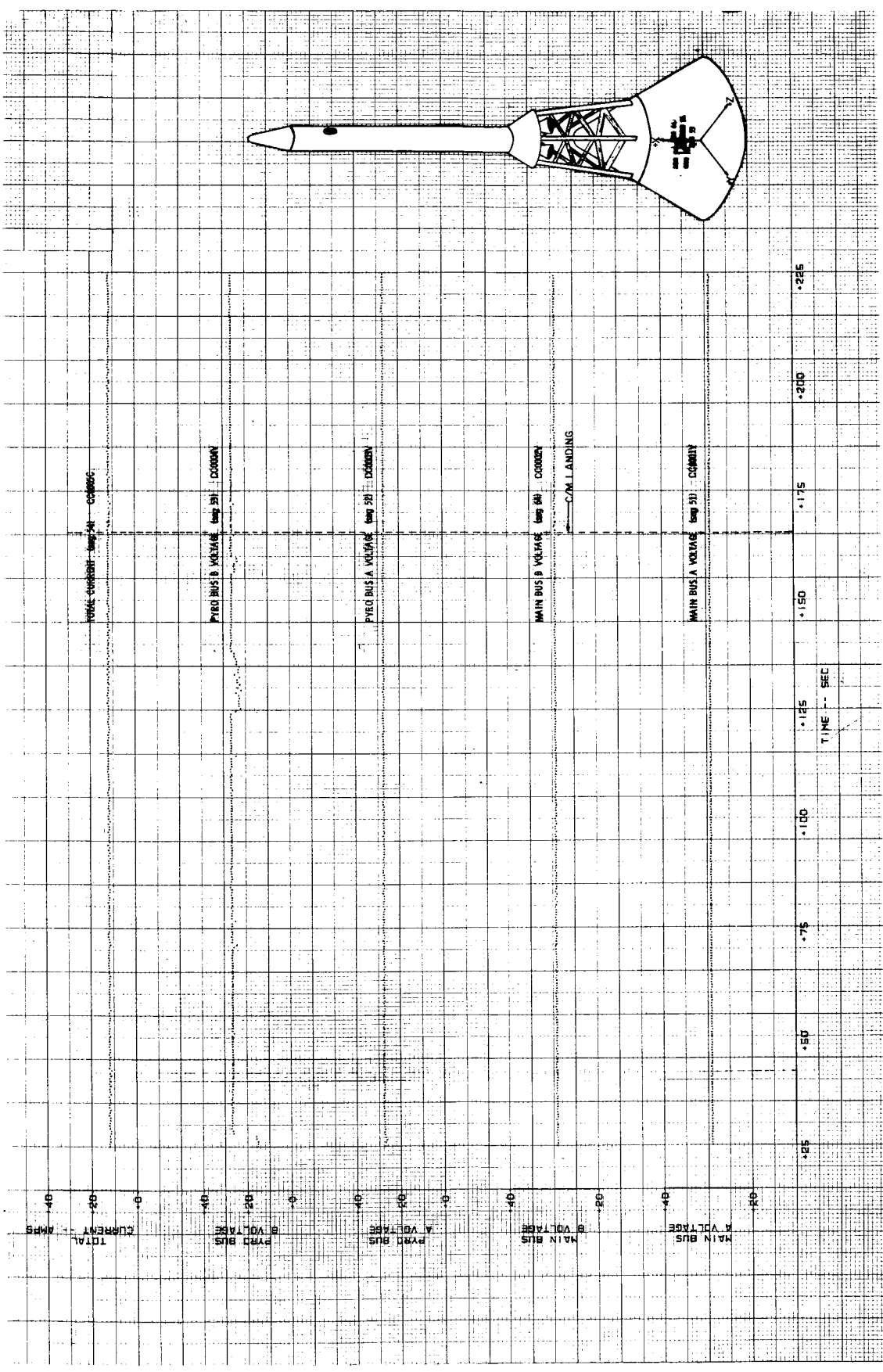
(b)  25 through 225 seconds.

Figure A4-9.- Concluded.
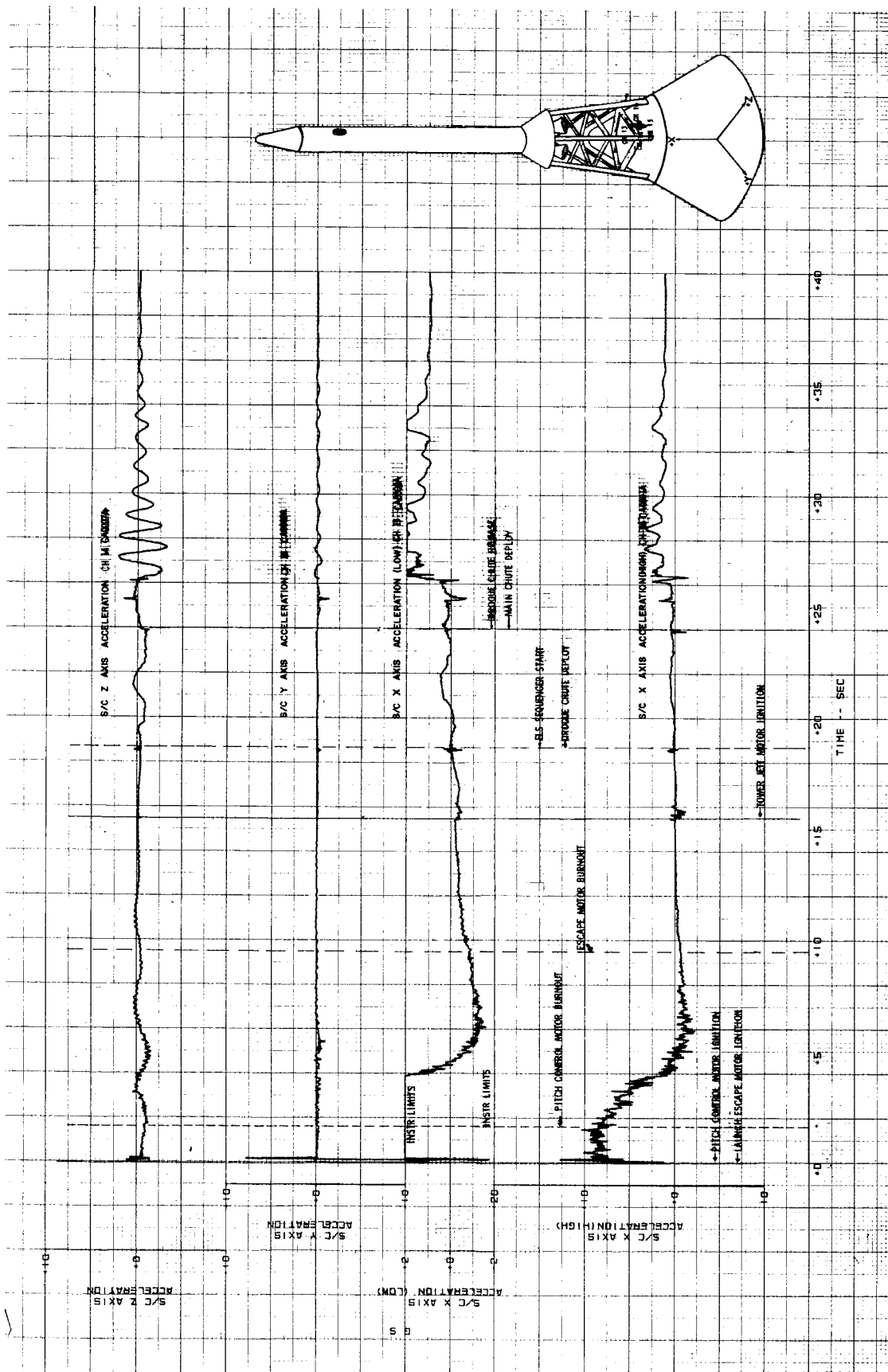
Figure A4-10.- Vehicle X, Y, and Z axes accelerations.

(a) 0 through 40 seconds.
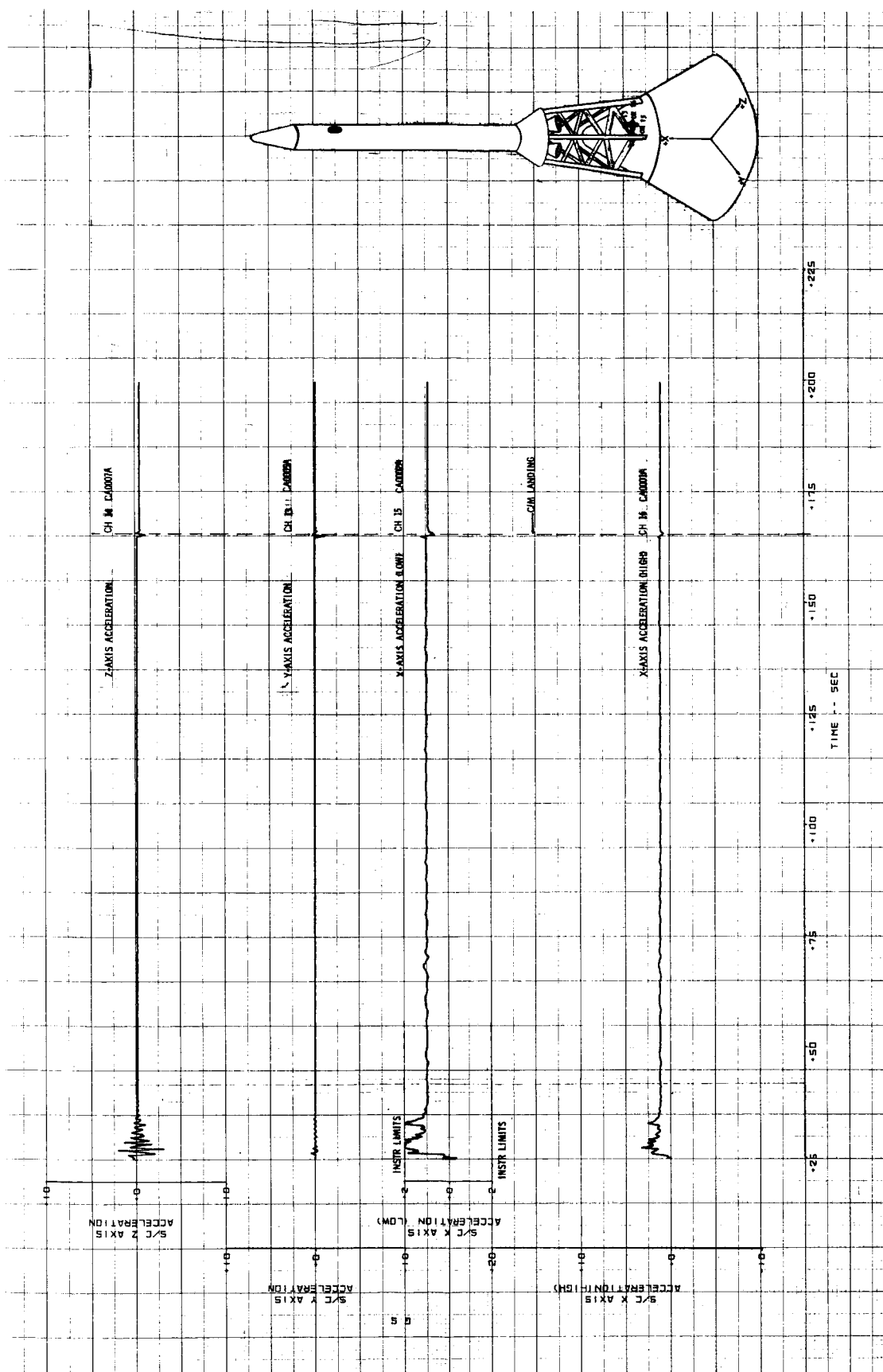
(b) 25 through 200 seconds.

Figure A4-10.- Concluded.
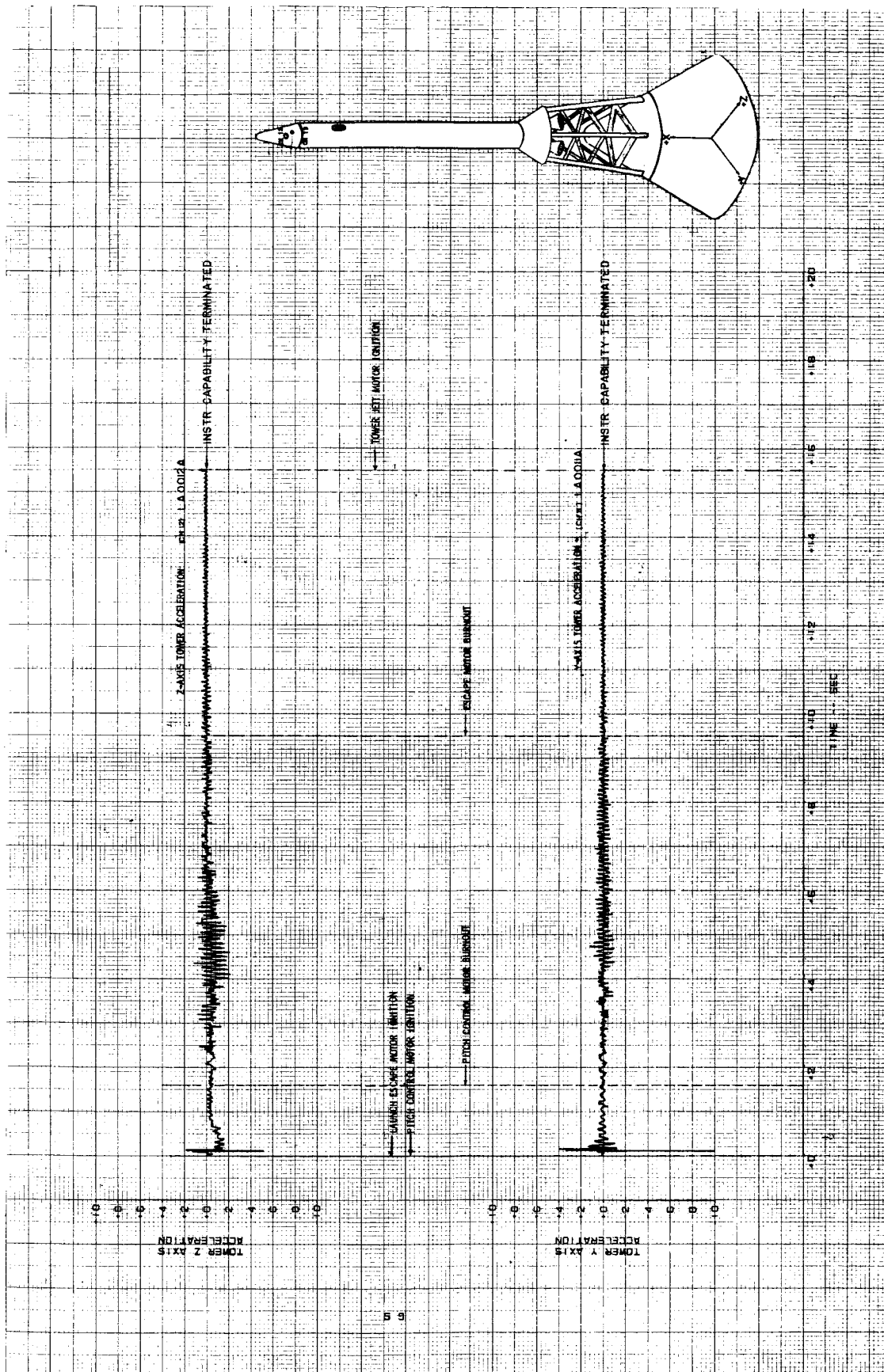
Figure A4-11.- Escape tower Y and Z axes accelerations.
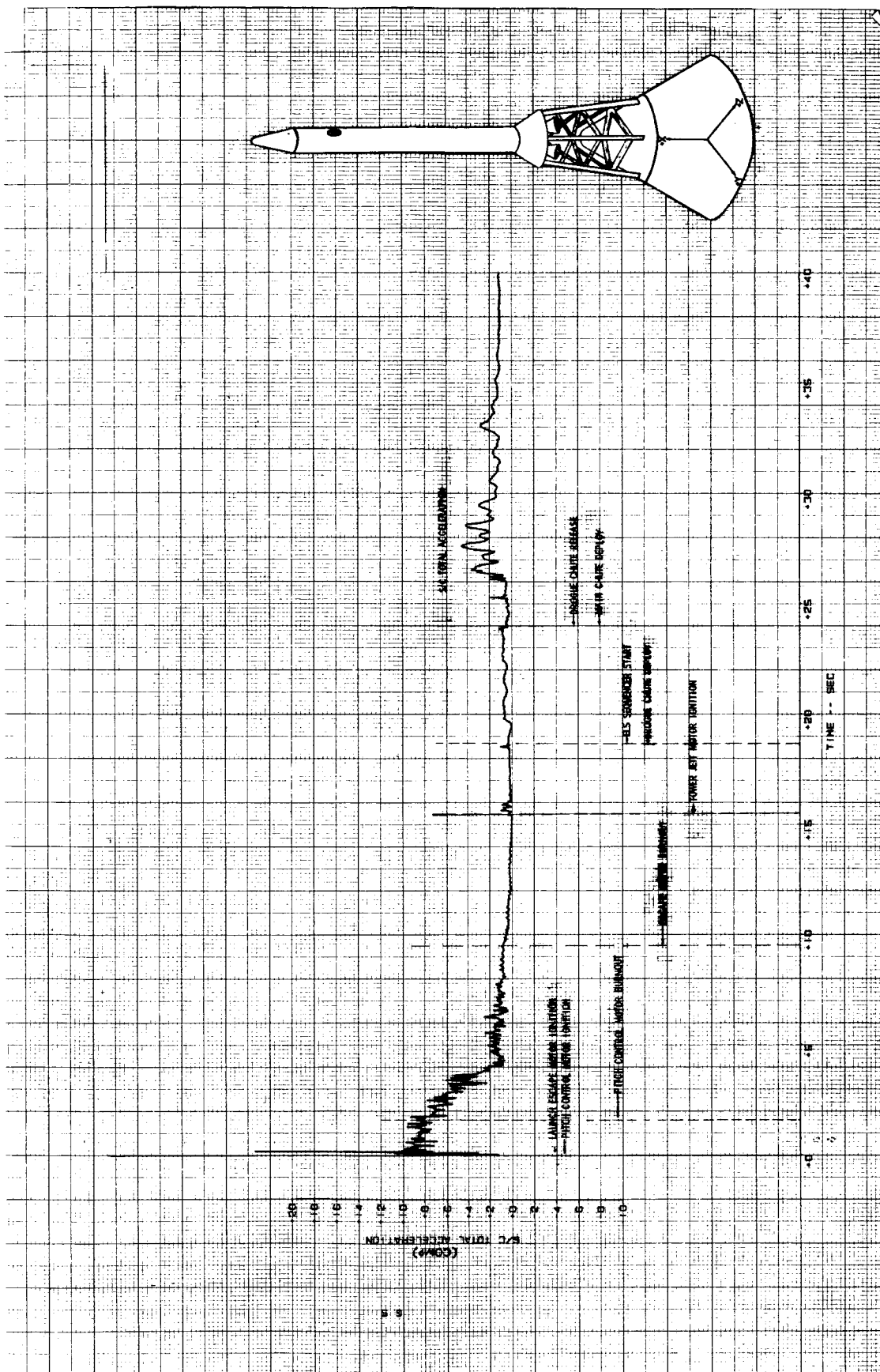
(a) 0 through 40 seconds.

Figure A4-12.- Vehicle computed total acceleration.
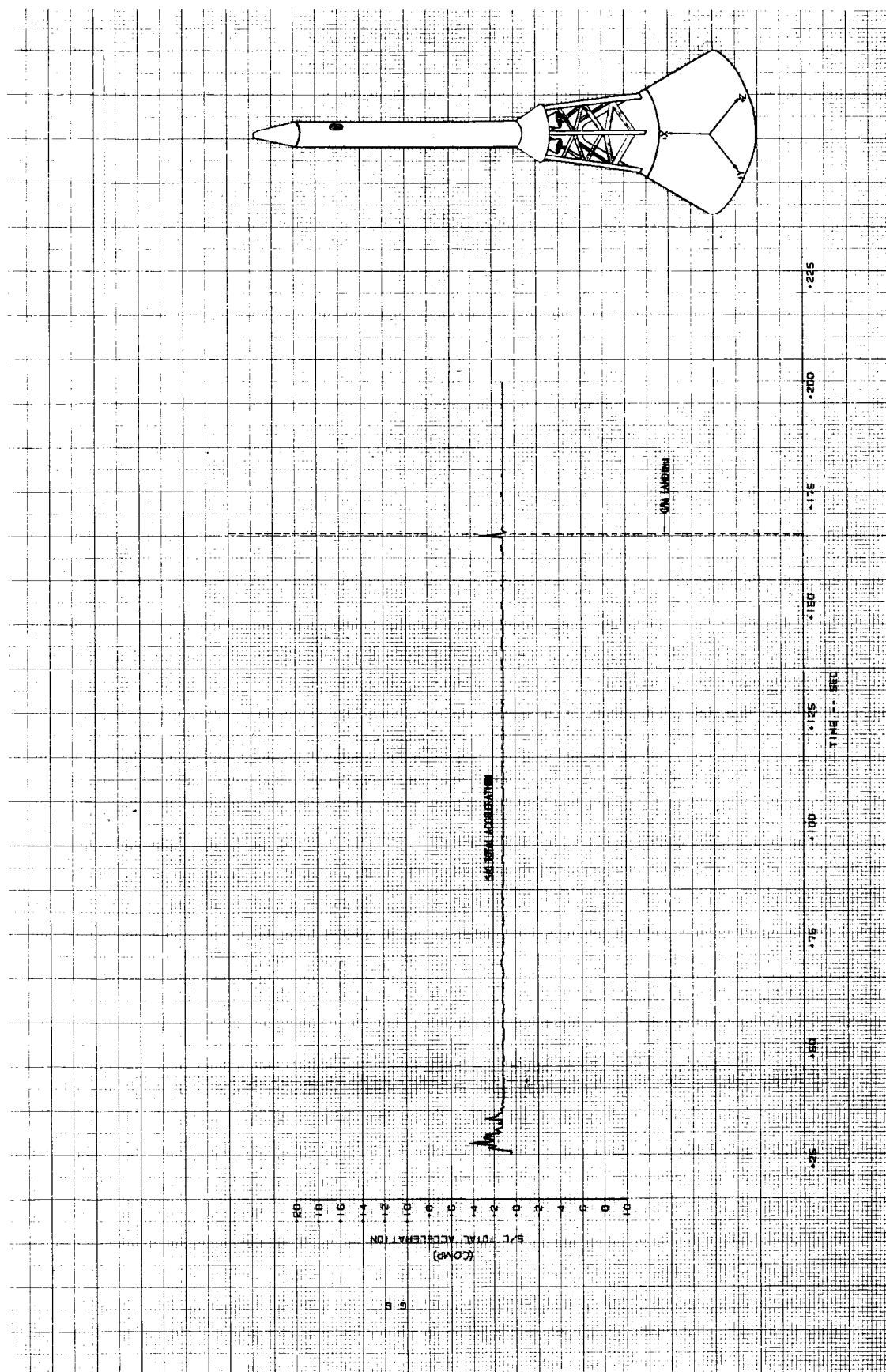
(b)  25 through 200 seconds.

Figure A4-12.- Concluded.
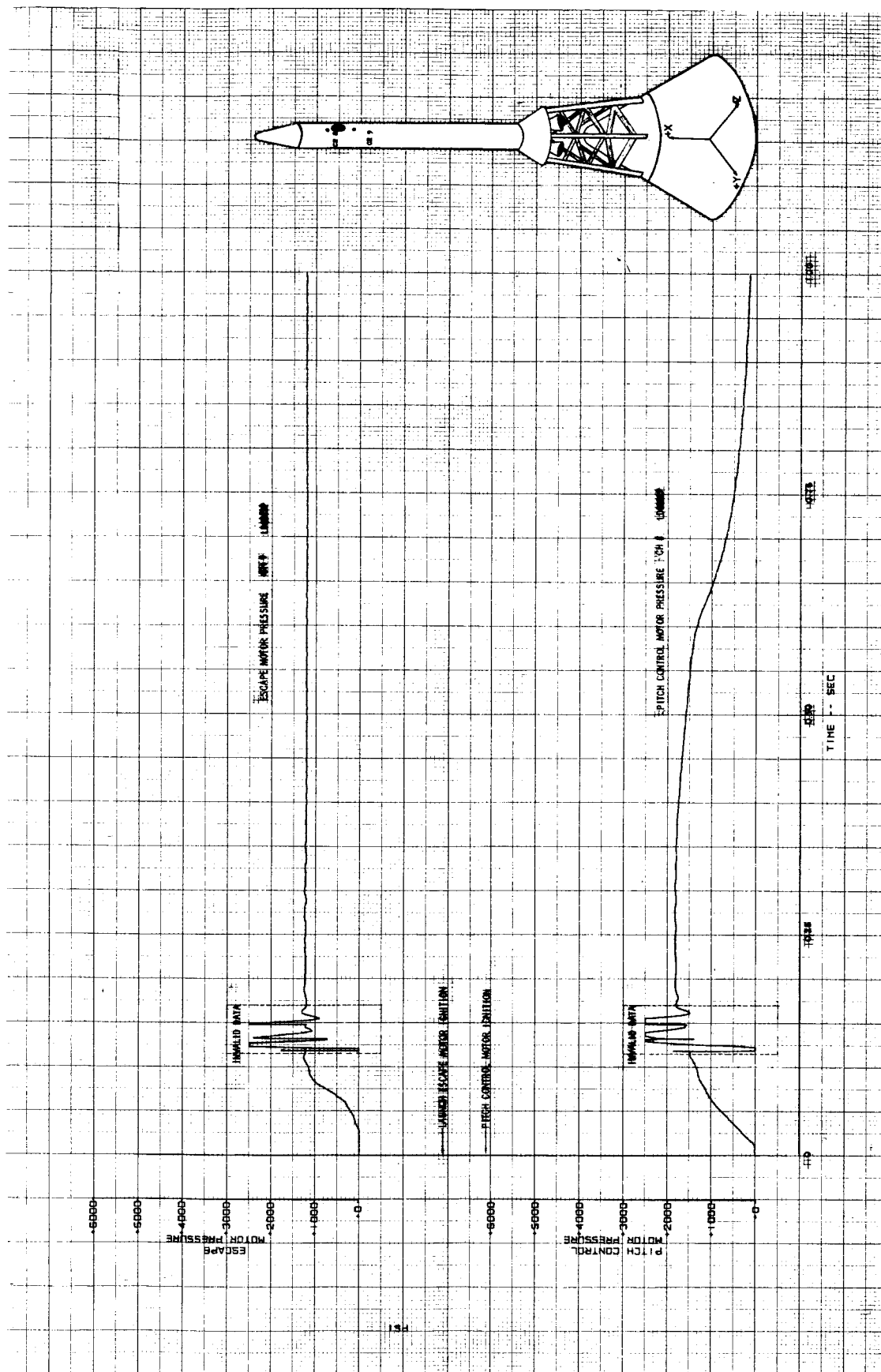
(a) 0 through 1 second.

Figure A4-13.- Pitch control and escape motor chamber pressure.
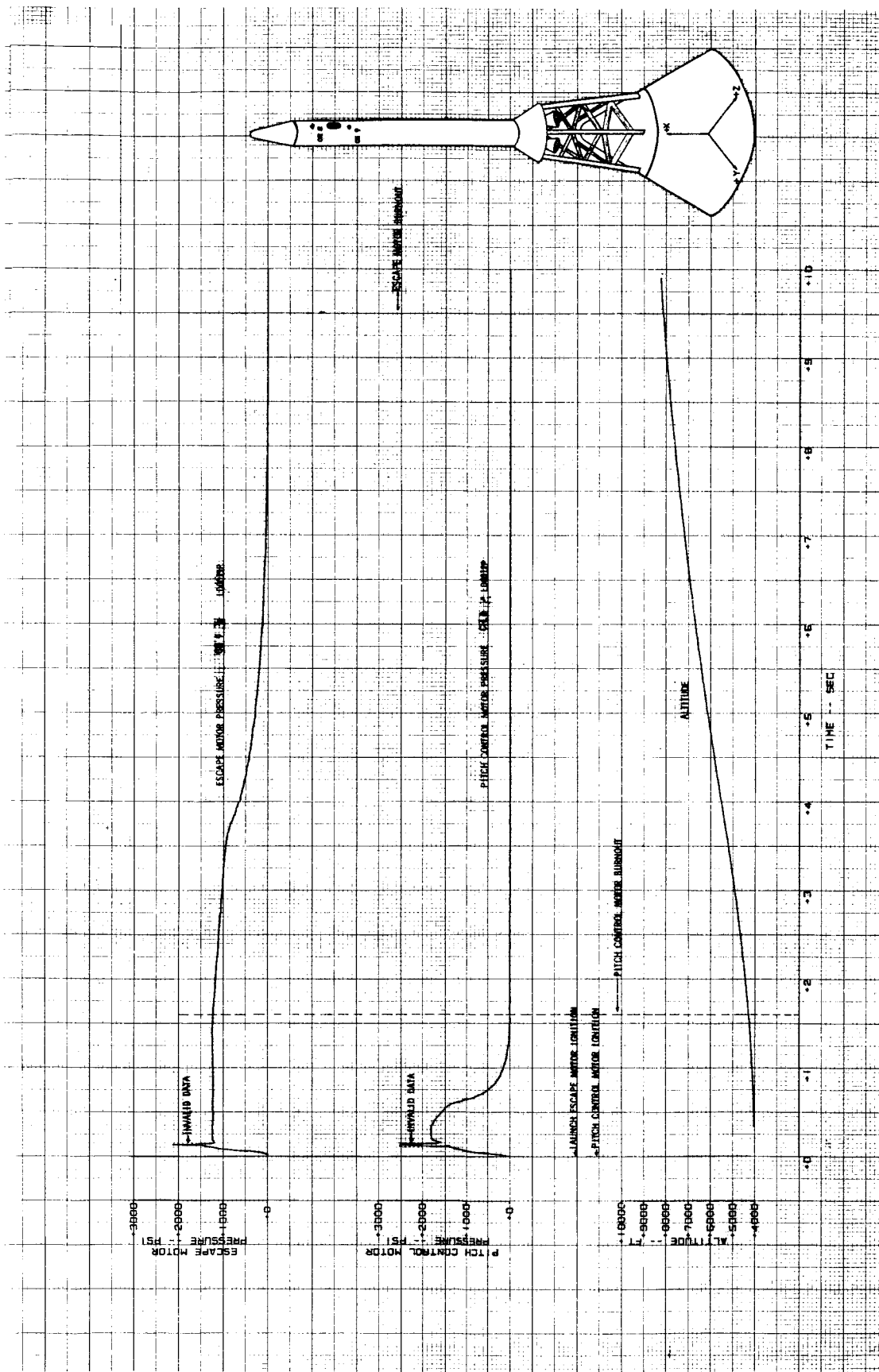
(b)  0 through 10 seconds.

Figure A4-13.- Concluded .

(a)  0 through 30 seconds.

Figure A4-14.- Vehicle gyroscope attitude data.
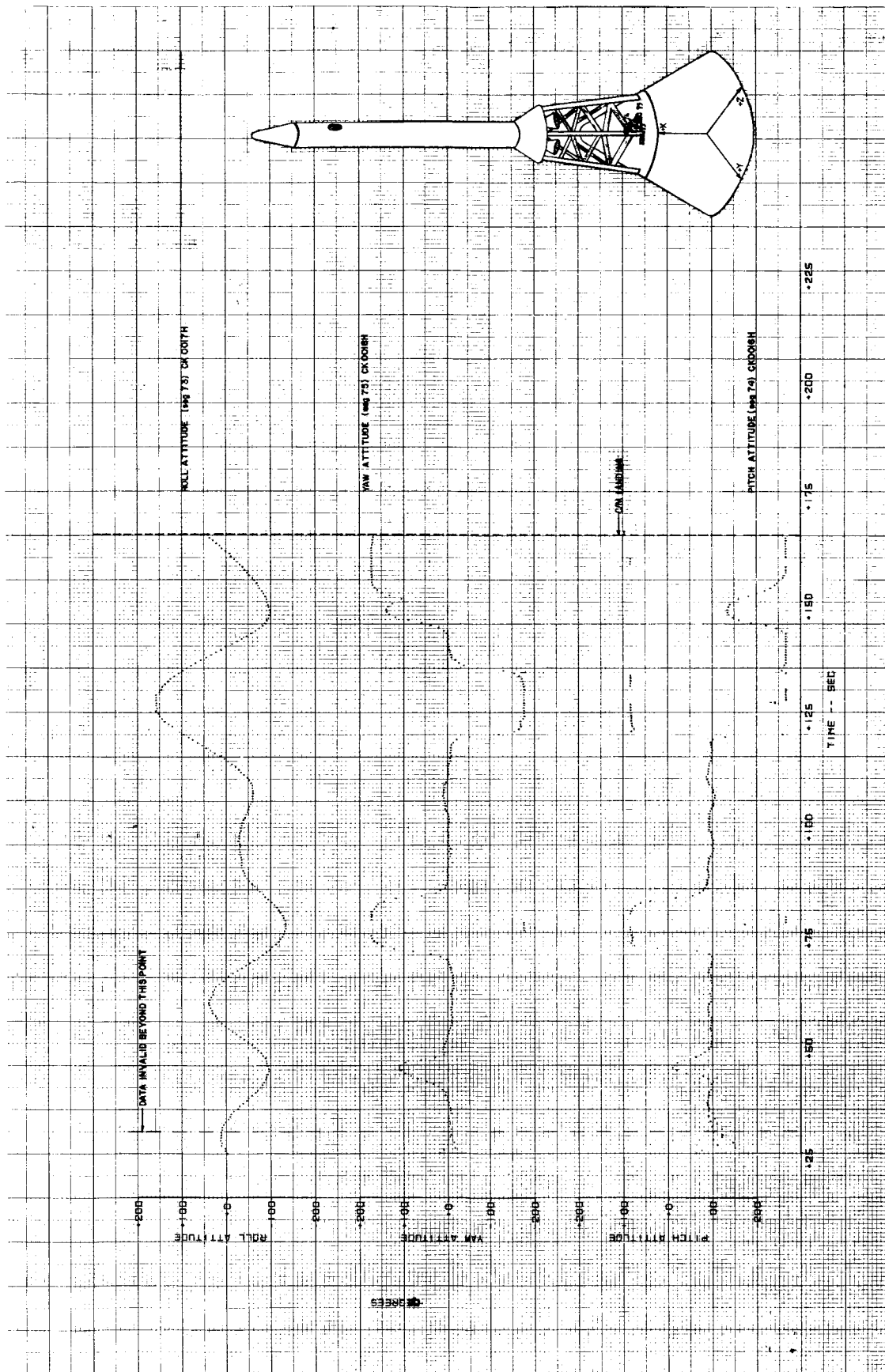
(b)  25 through 165 seconds.

Figure A4-14.- Concluded.
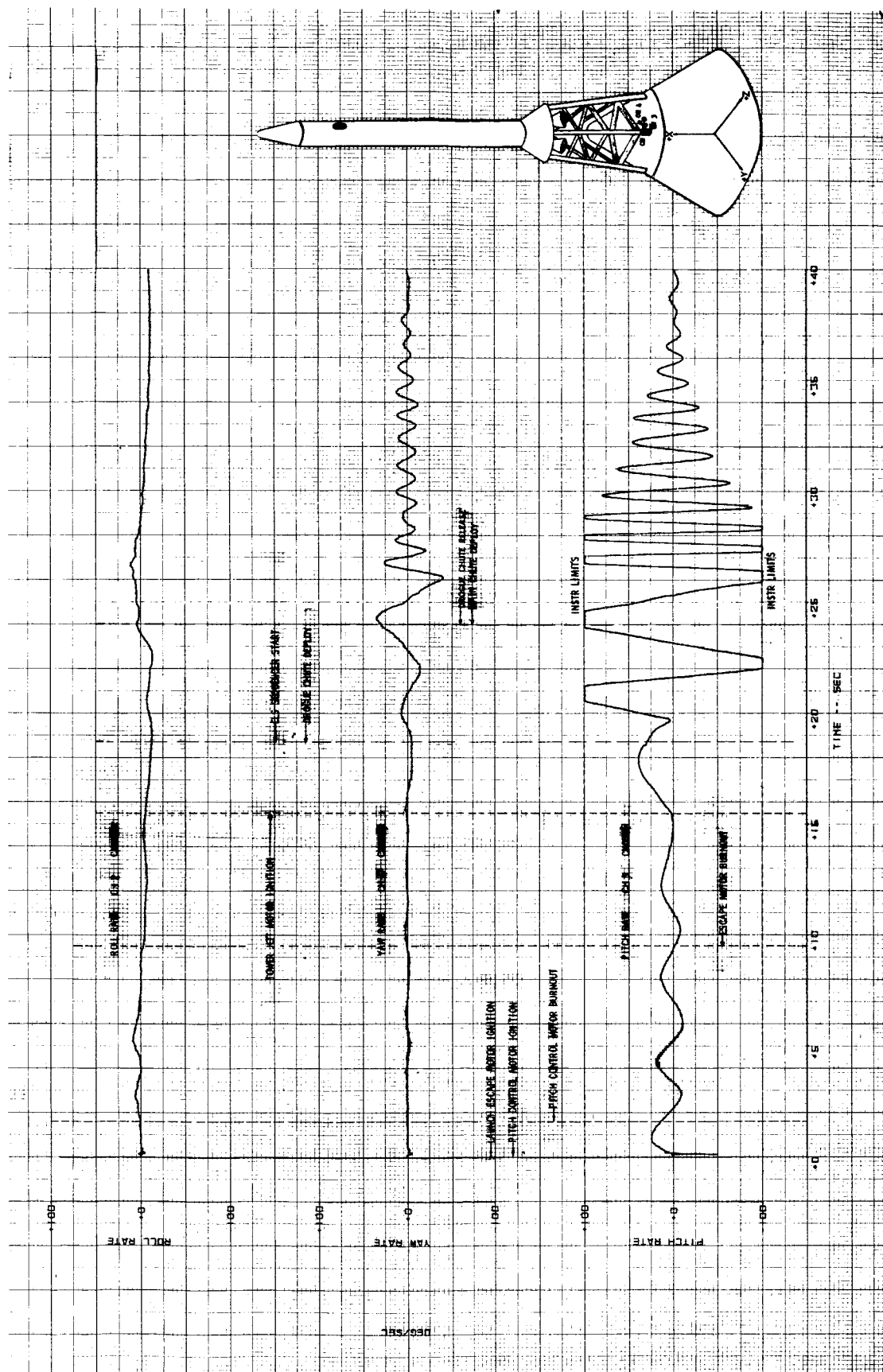
(a) 0 through 40 seconds.

Figure A4-15.- Vehicle gyroscope rate data.
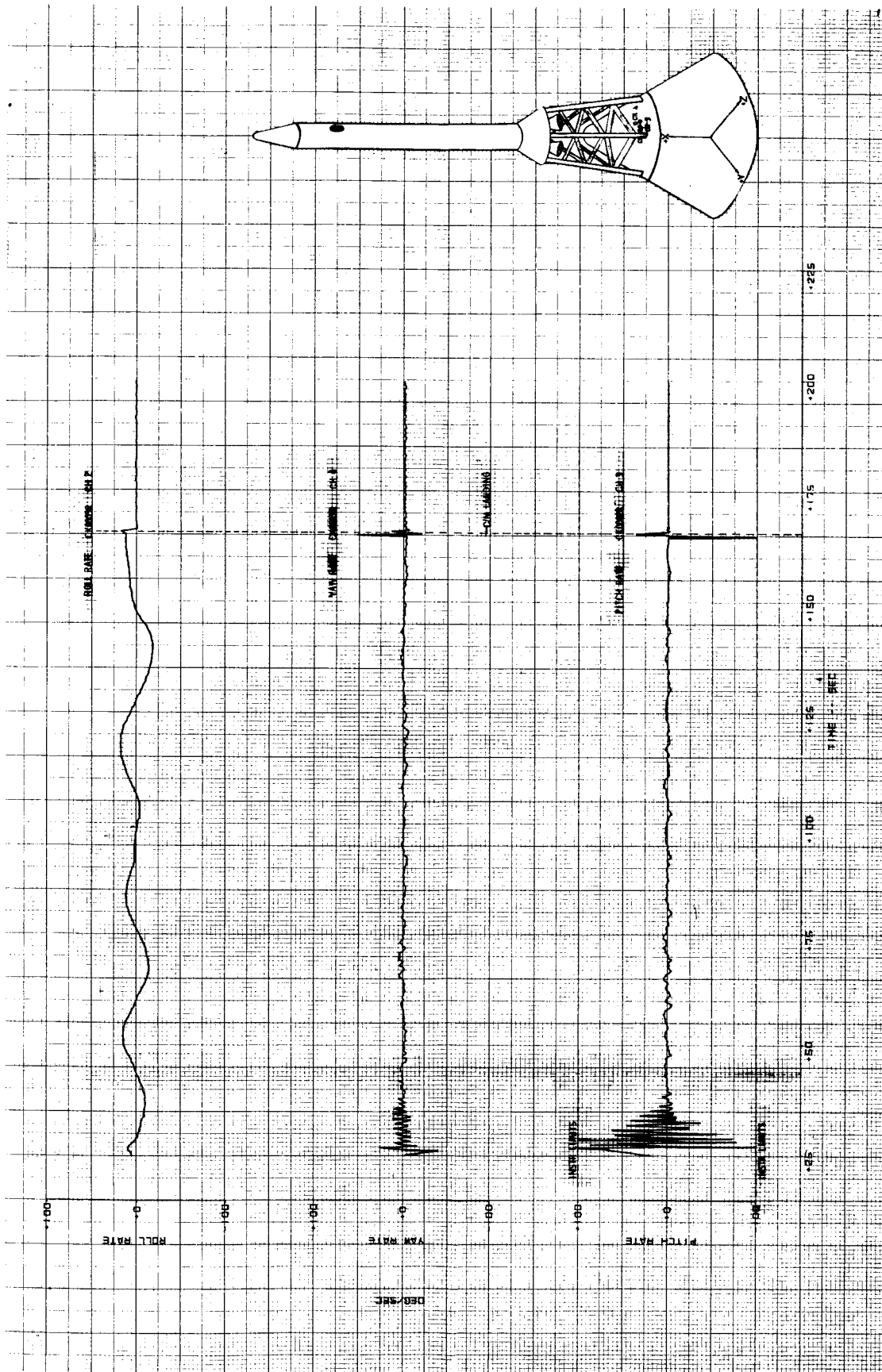
(b)  25 through 200 seconds.

Figure A4-15.- Concluded.
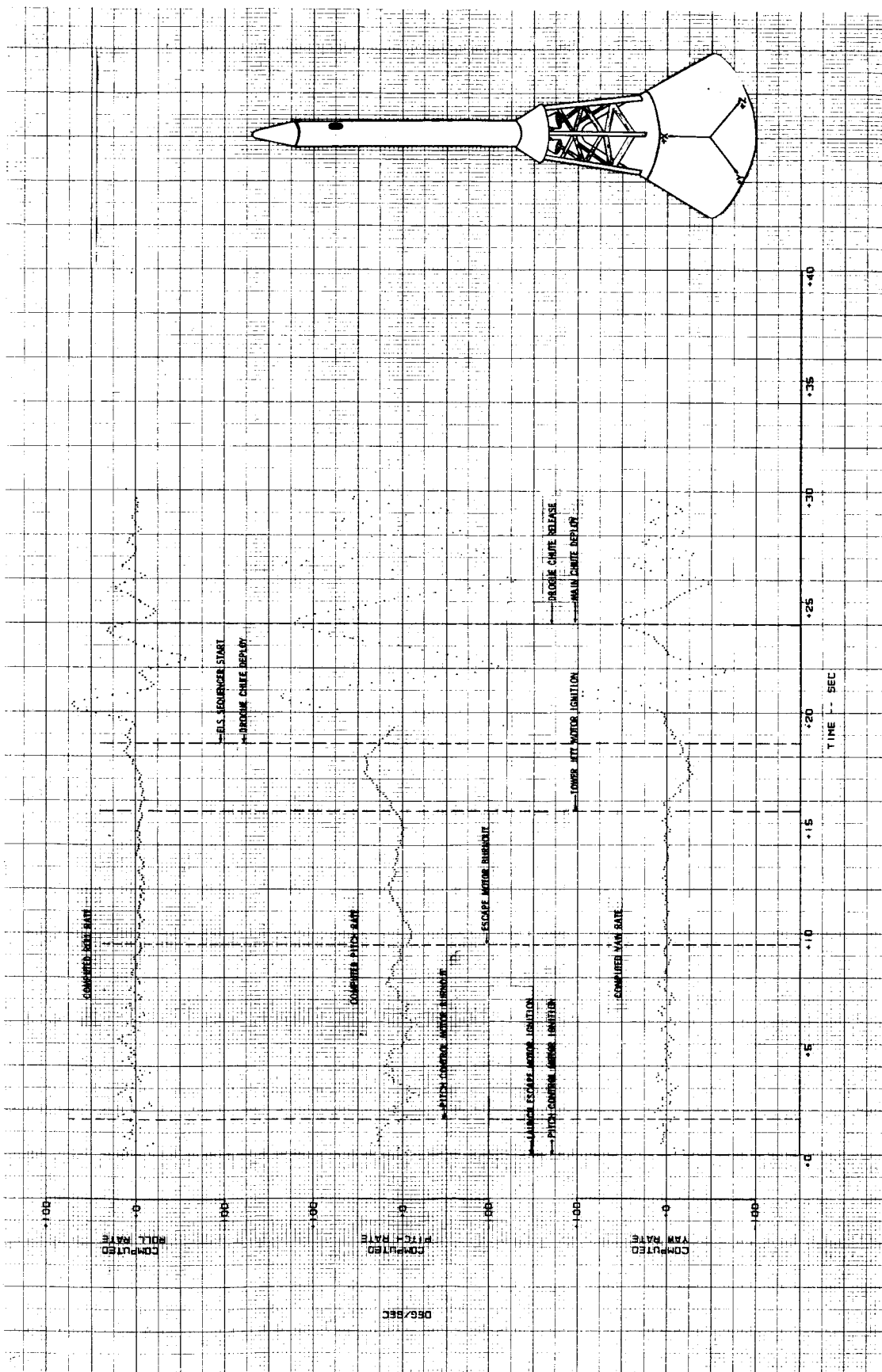
Figure A4-16.- Vehicle computed rate data.
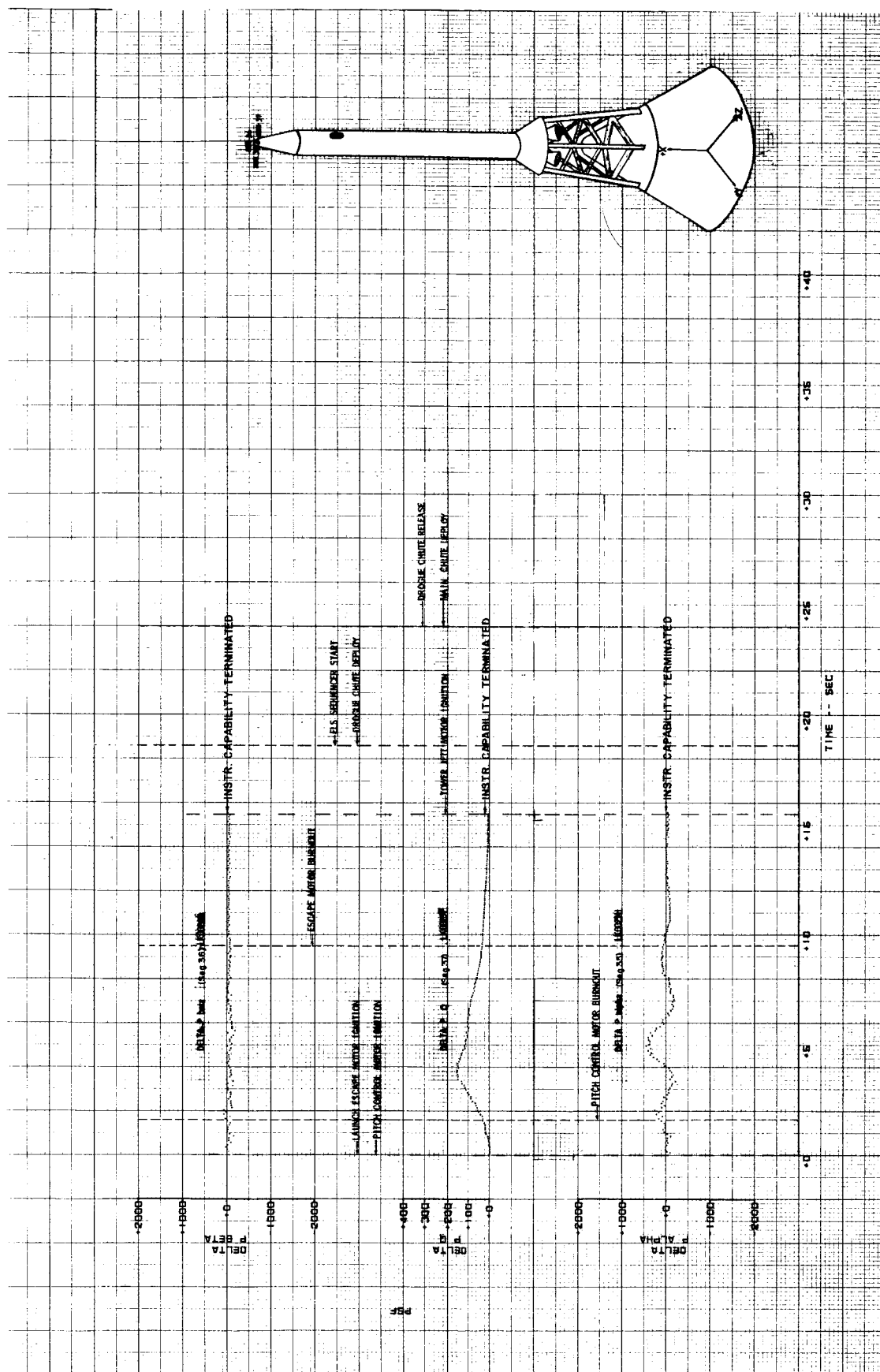
Figure A4-17.- Q-ball data.
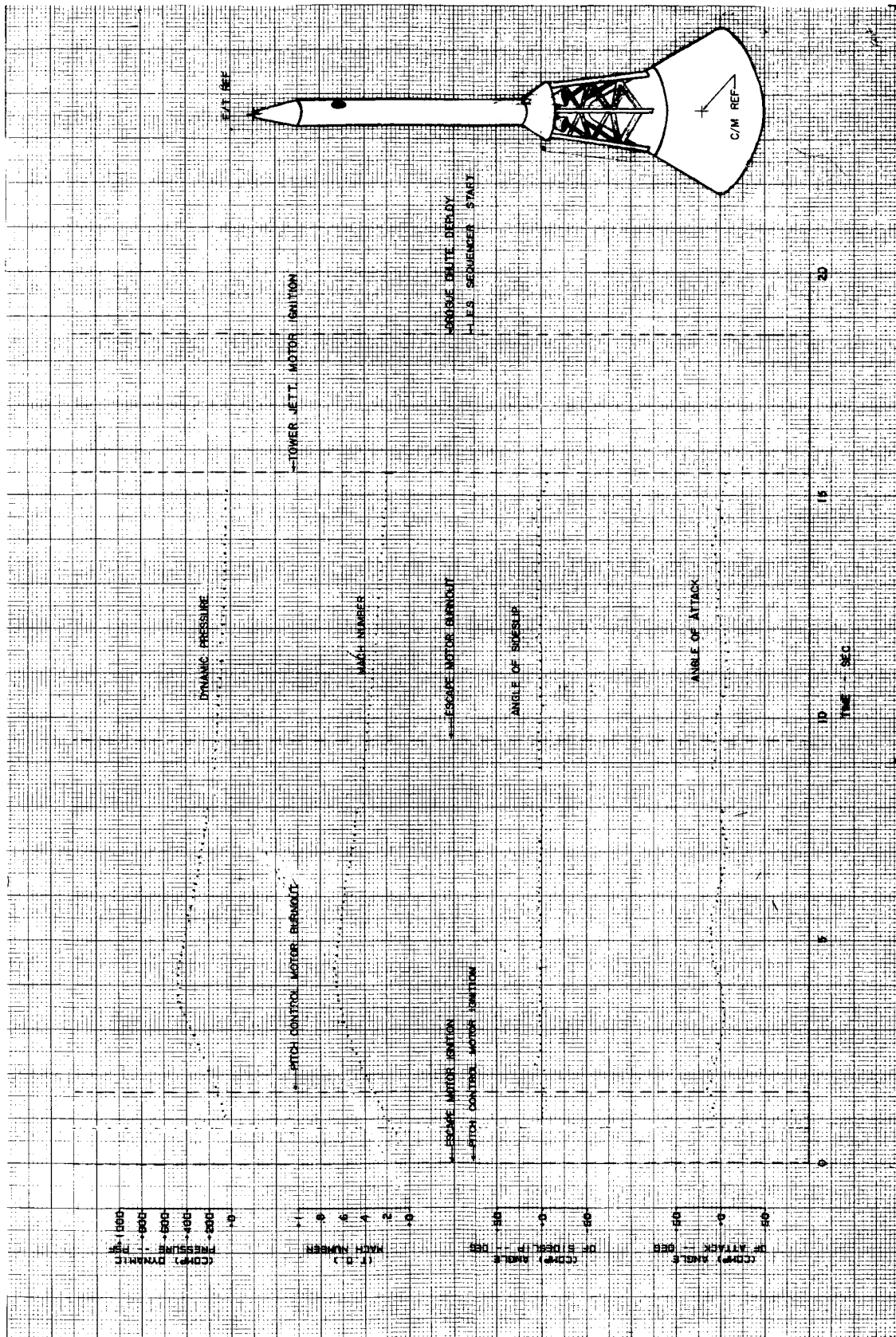
Figure A4-18.- Angle of attack, sideslip, mach number and dynamic pressure computed from Q-ball data.
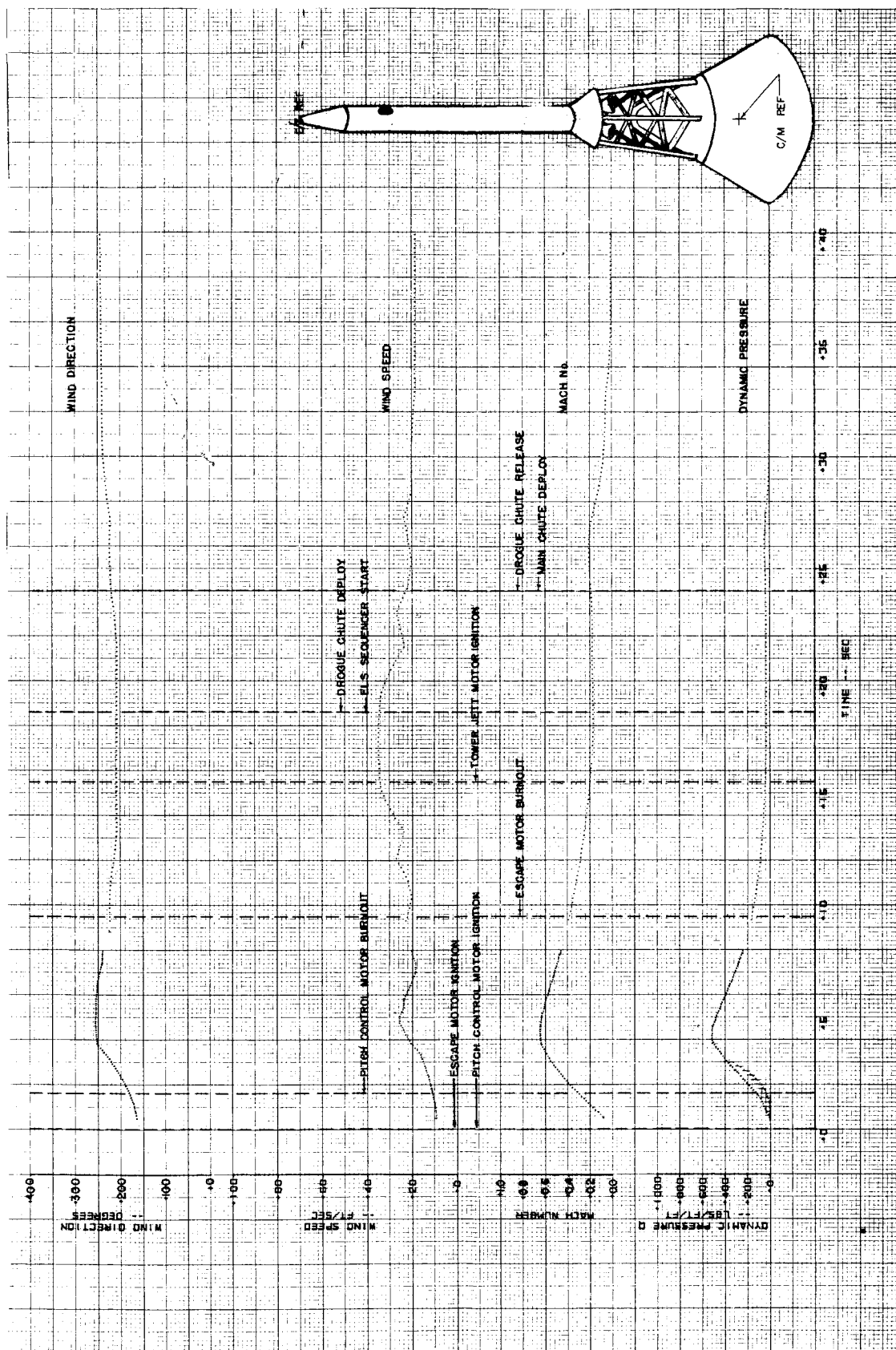
(a) 0 through 40 seconds.

Figure A4-19.- Dynamic pressure and mach number computed from phototheodolite data plus wind speed and wind direction.
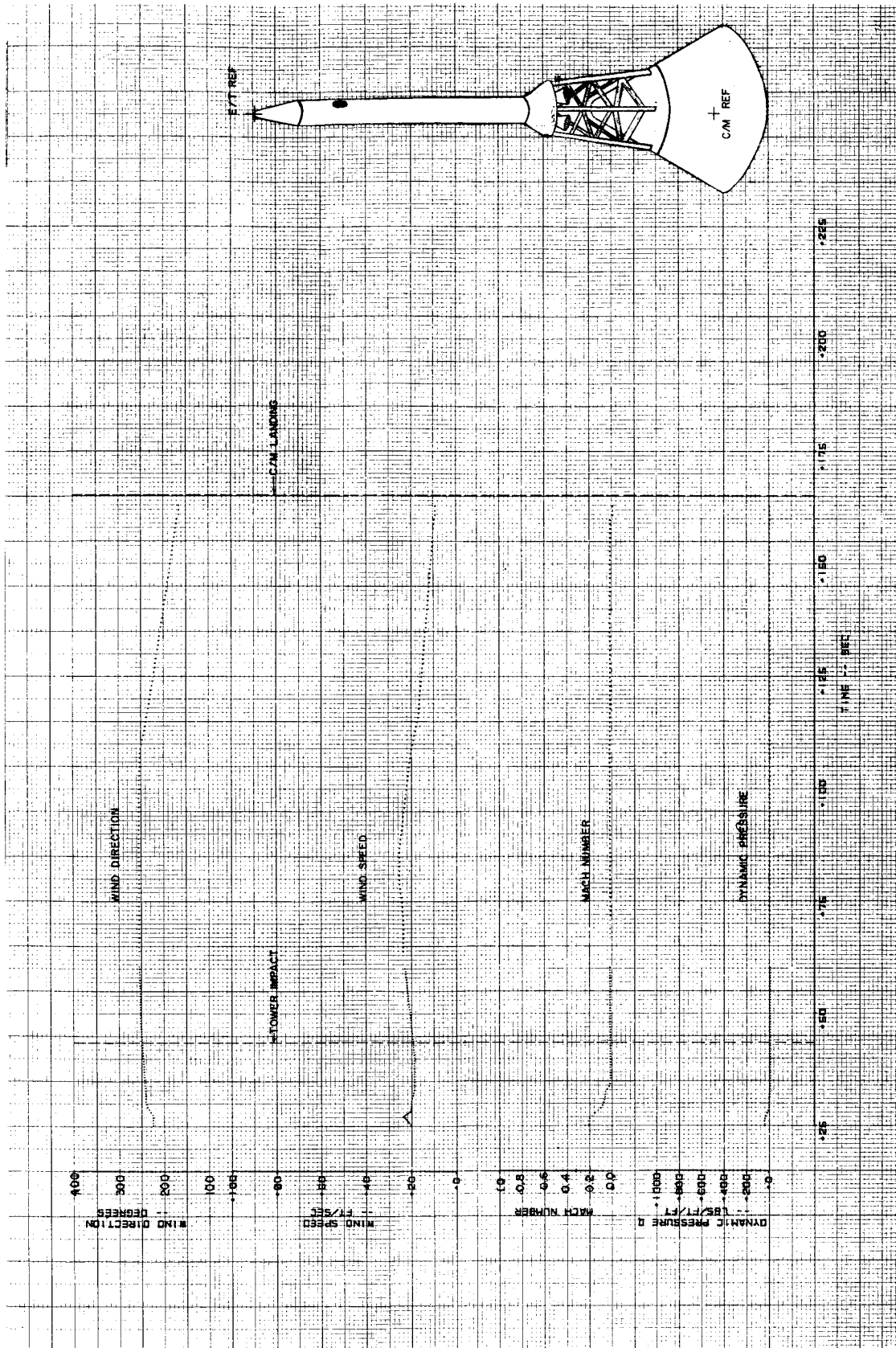
(b) 25 through 160 seconds.

Figure A4-19.- Concluded.
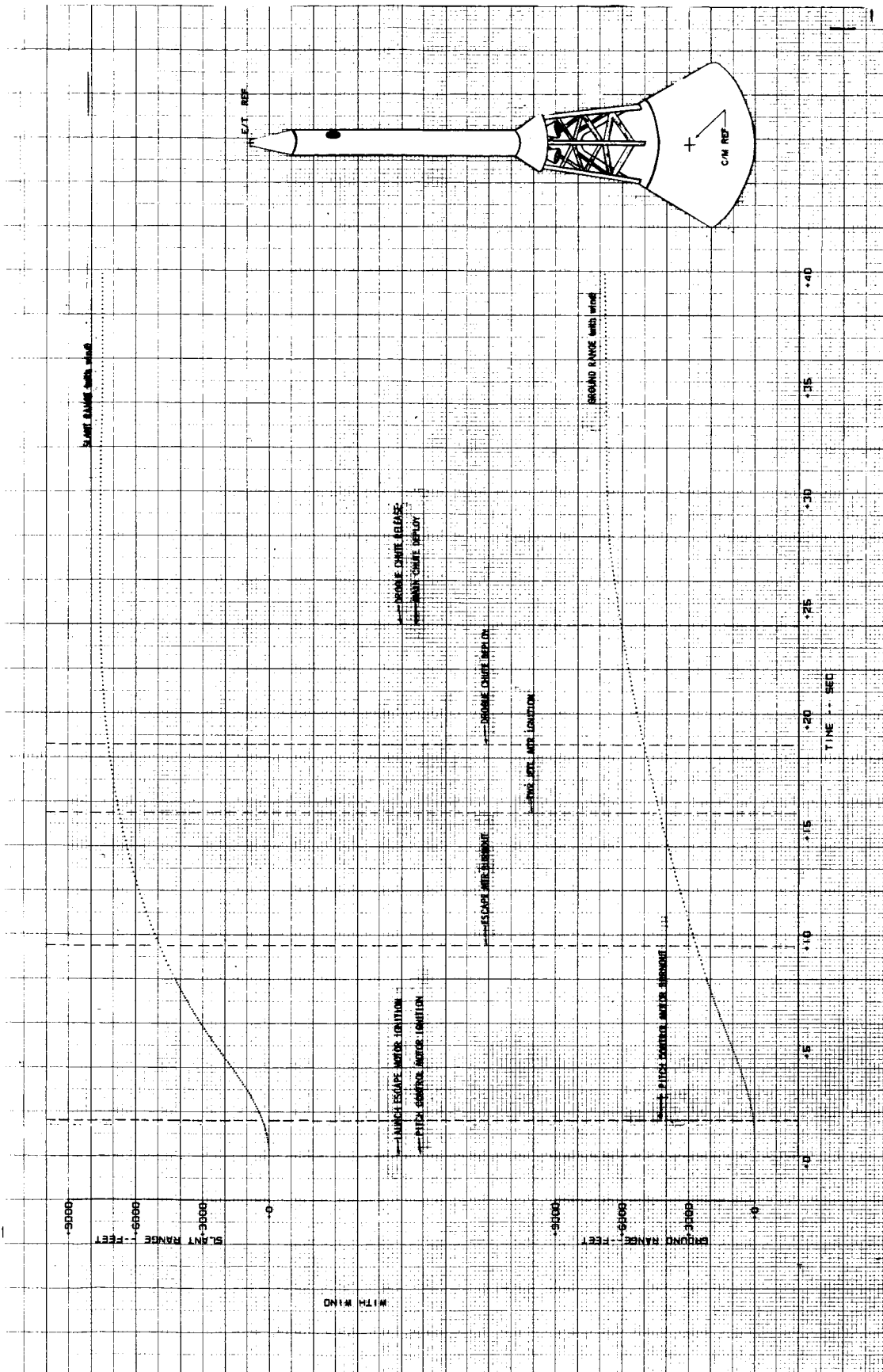
(a) 0 through 40 seconds,

Figure A4-20.- Ground and slant range, winds included.
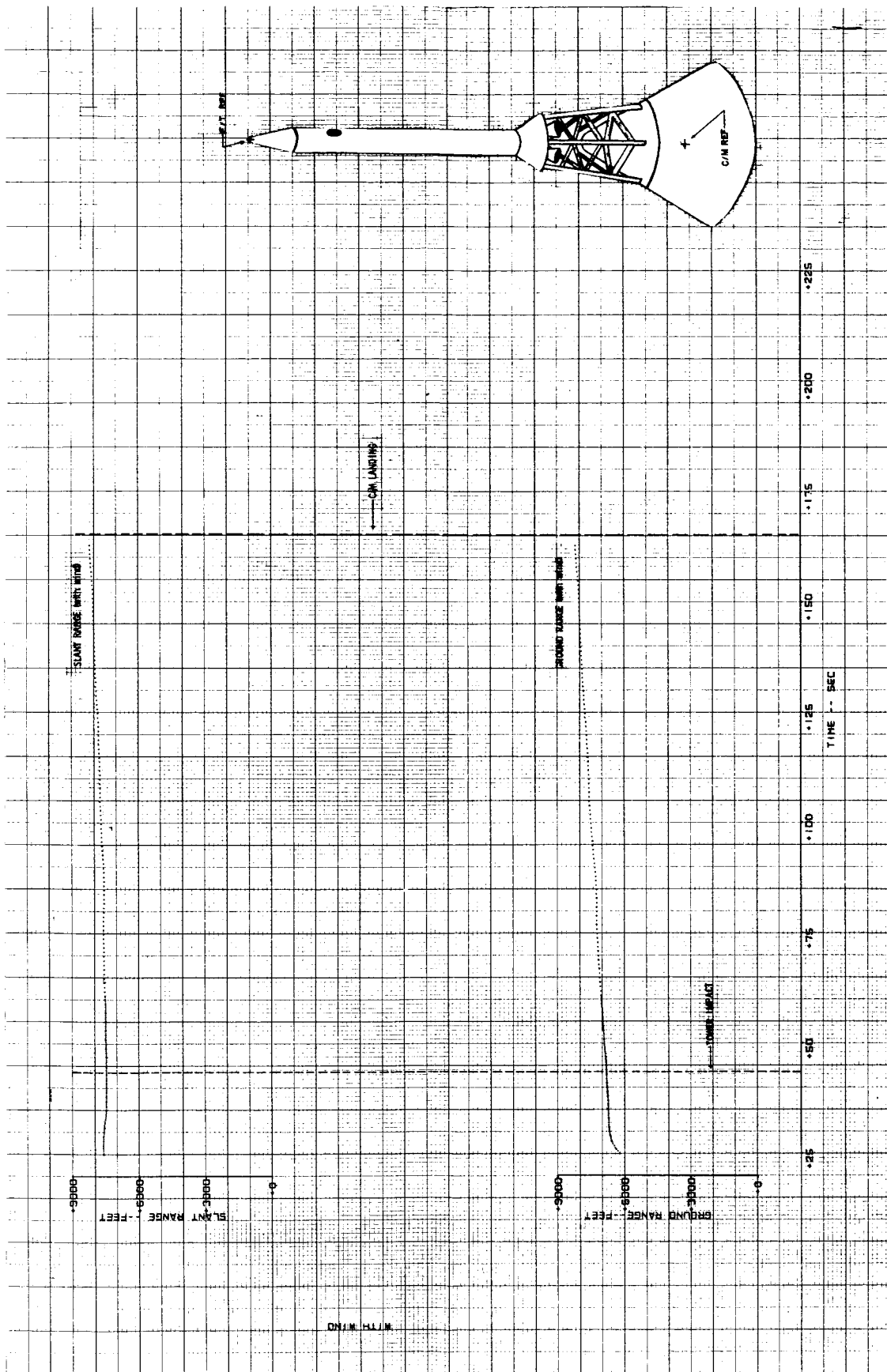
(b)  25 through 165 seconds.

Figure A4-20.- Concluded.
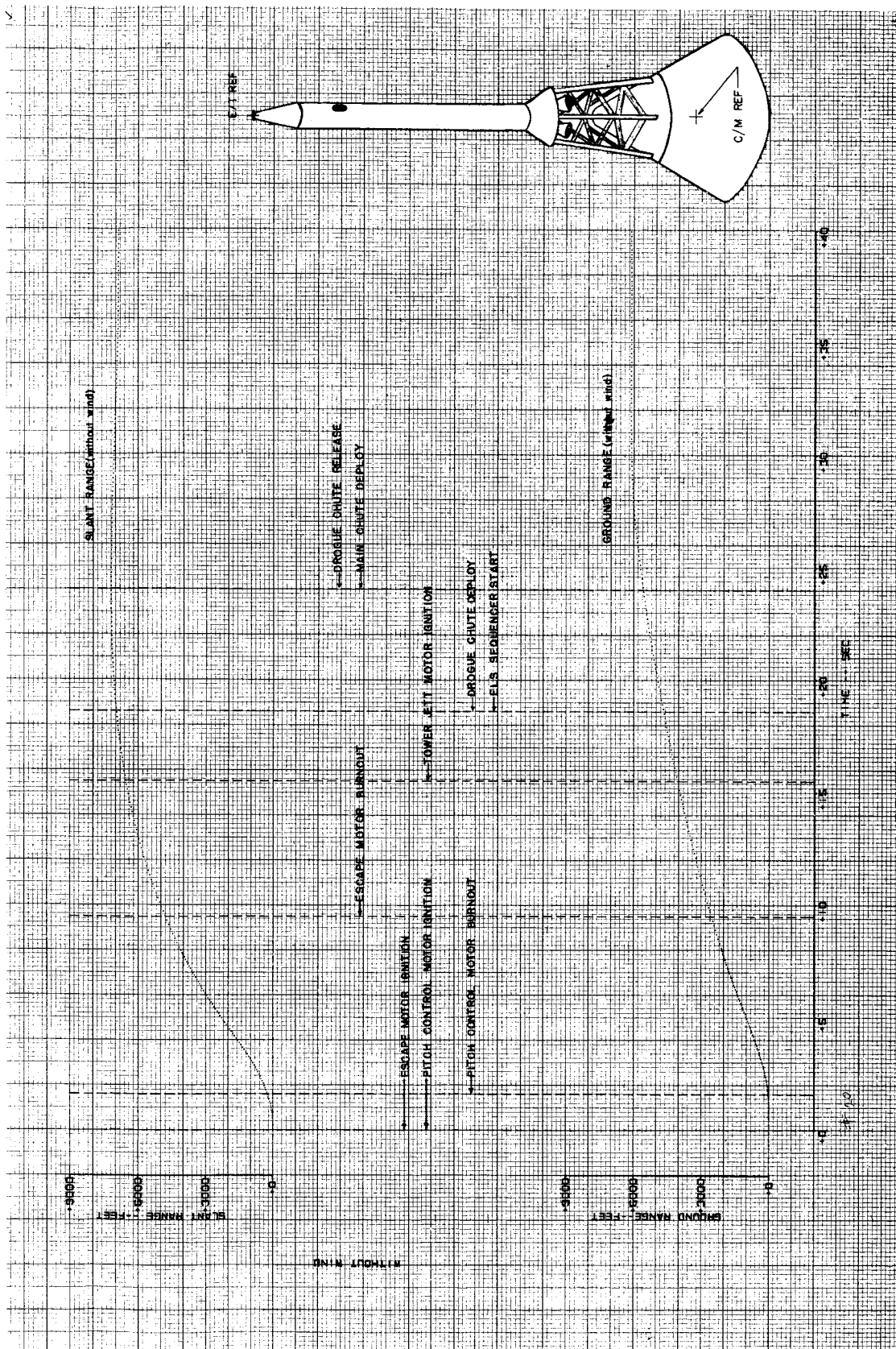
(a) 0 through 40 seconds,

Figure A4-21.- Ground and slant range, winds not included.
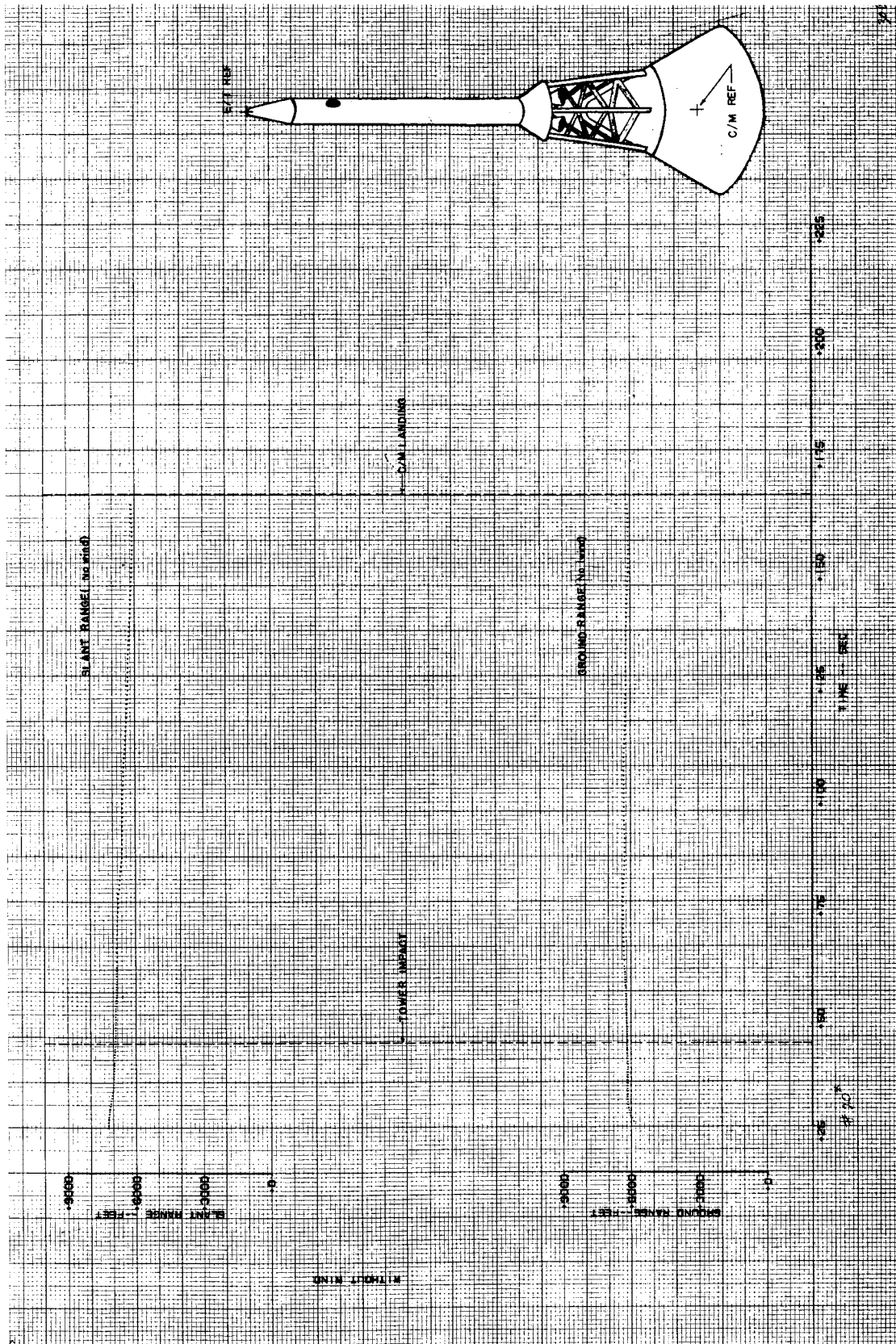
(b)  25 through 165 seconds.

Figure A4-21.- Concluded,
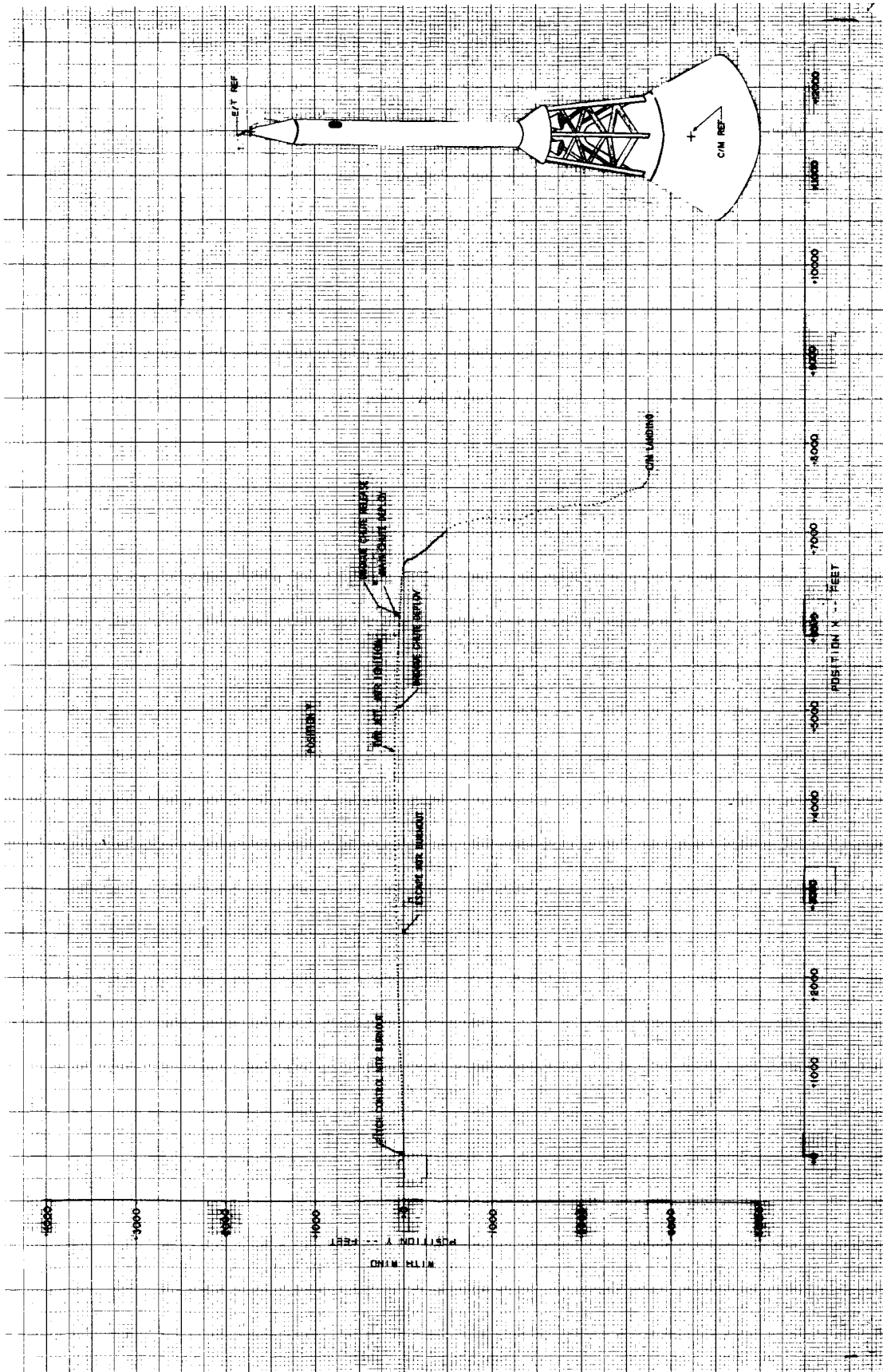
(a) Winds included.

Figure A4-22.- Position Y plotted against position X.
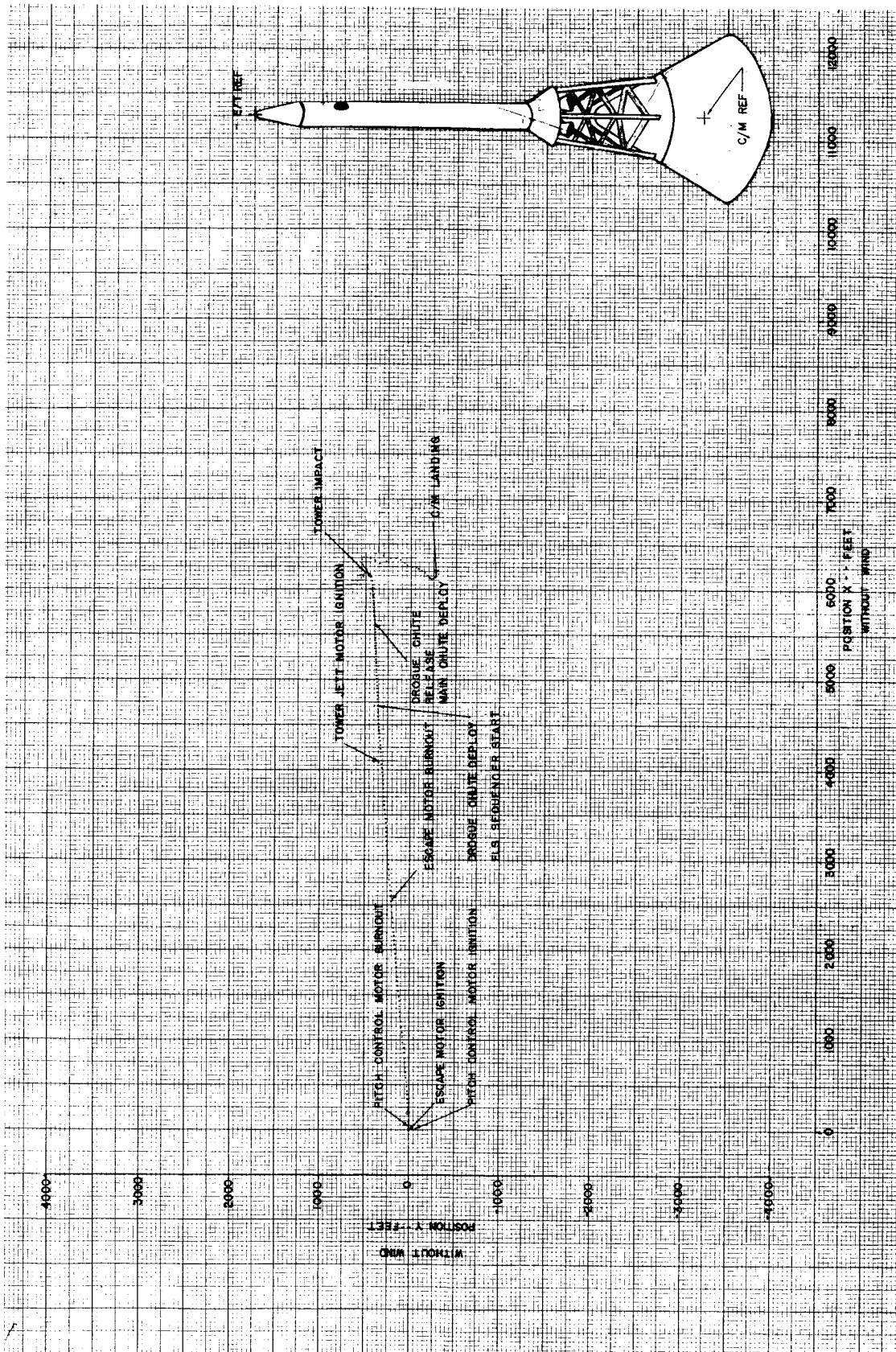
(b) Without wind.

Figure A4-22.- Position Y versus position X.
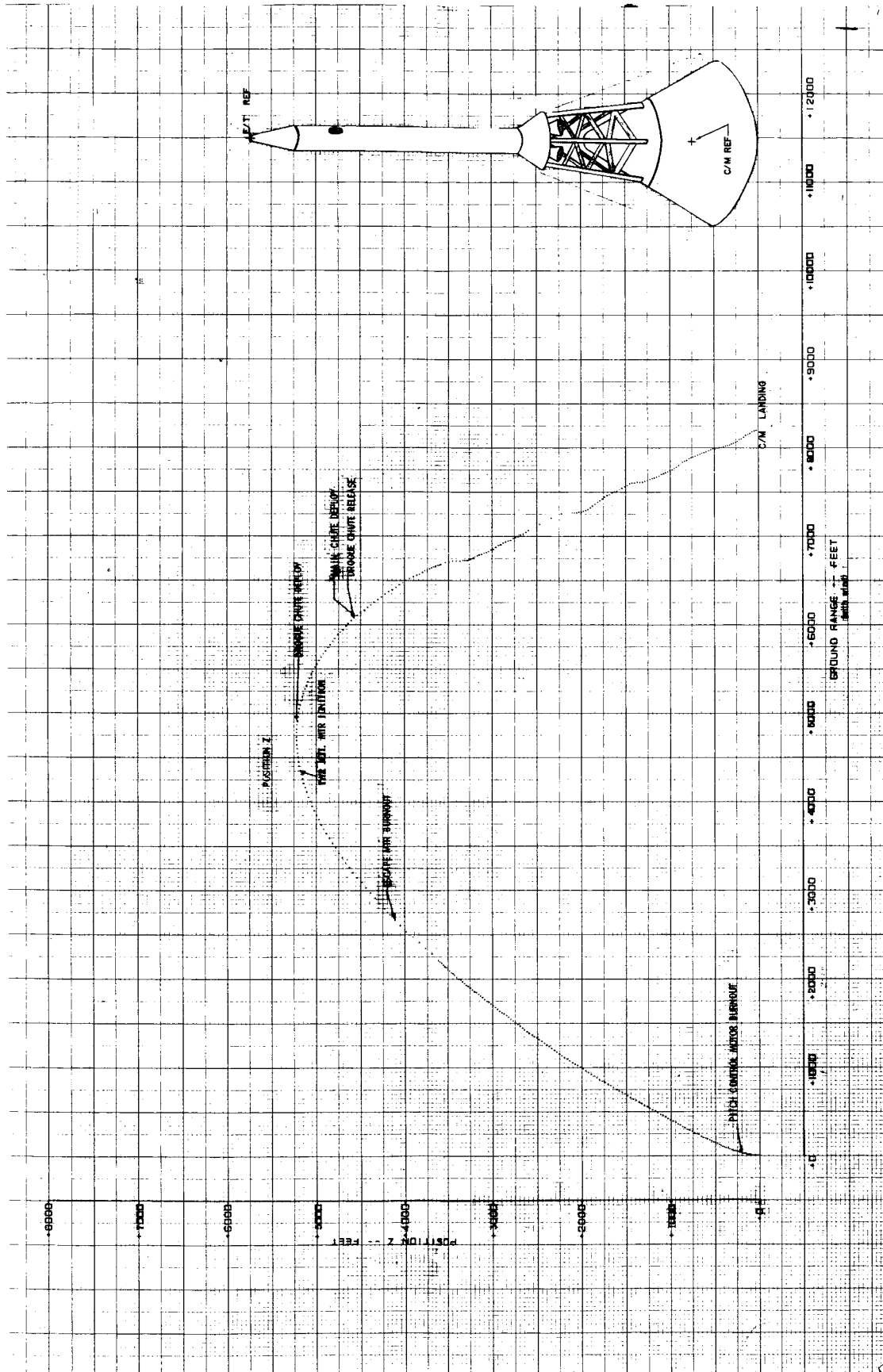
(a) With wind.

Figure A4-23.- Z position plotted against ground range.

CONFIDENTIAL
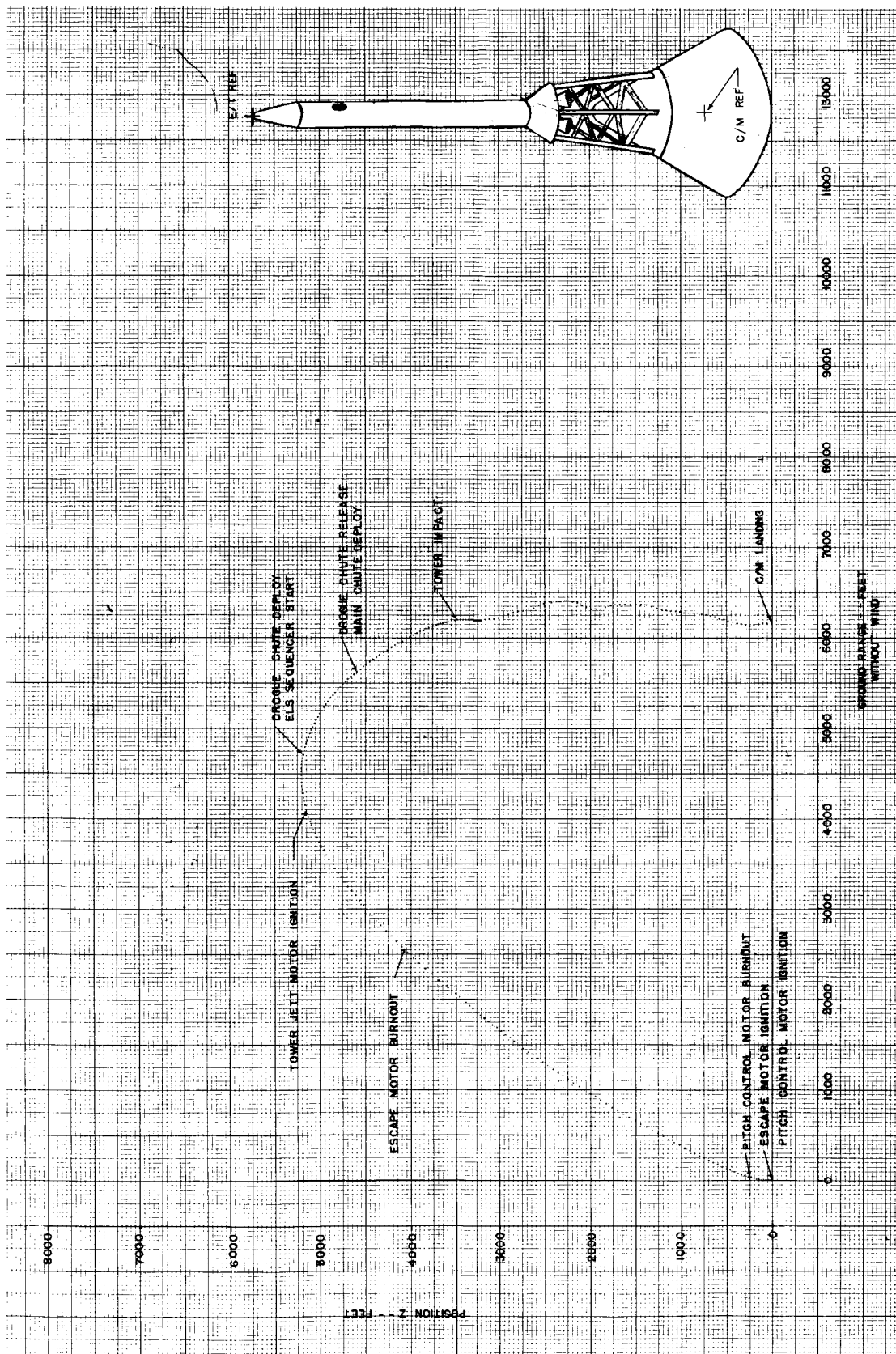


(b) Without wind.

Figure A4-23.- Concluded.

Figure A4-24.- Heading and flight path angle.

(a) 0 through 40 seconds.
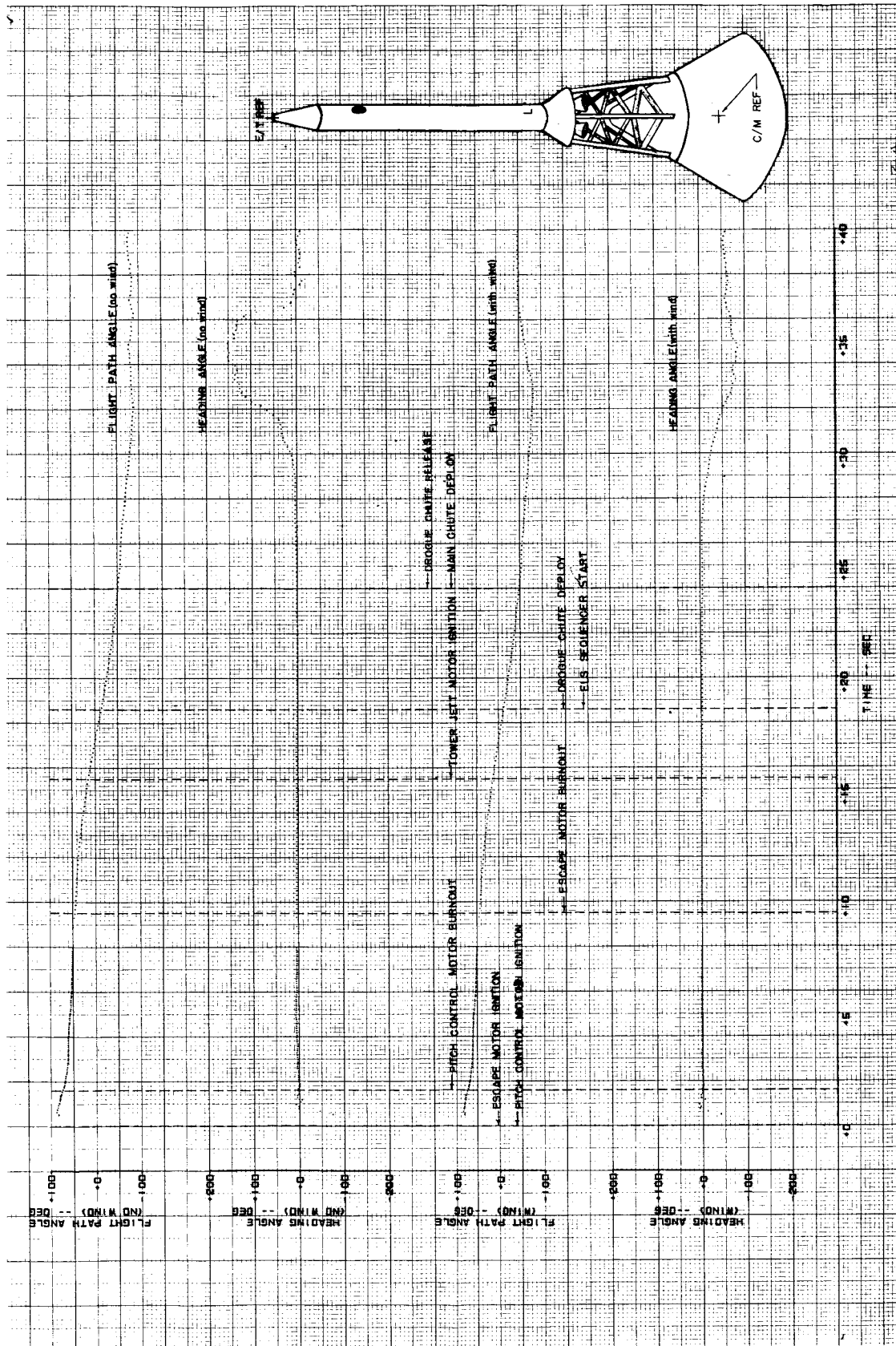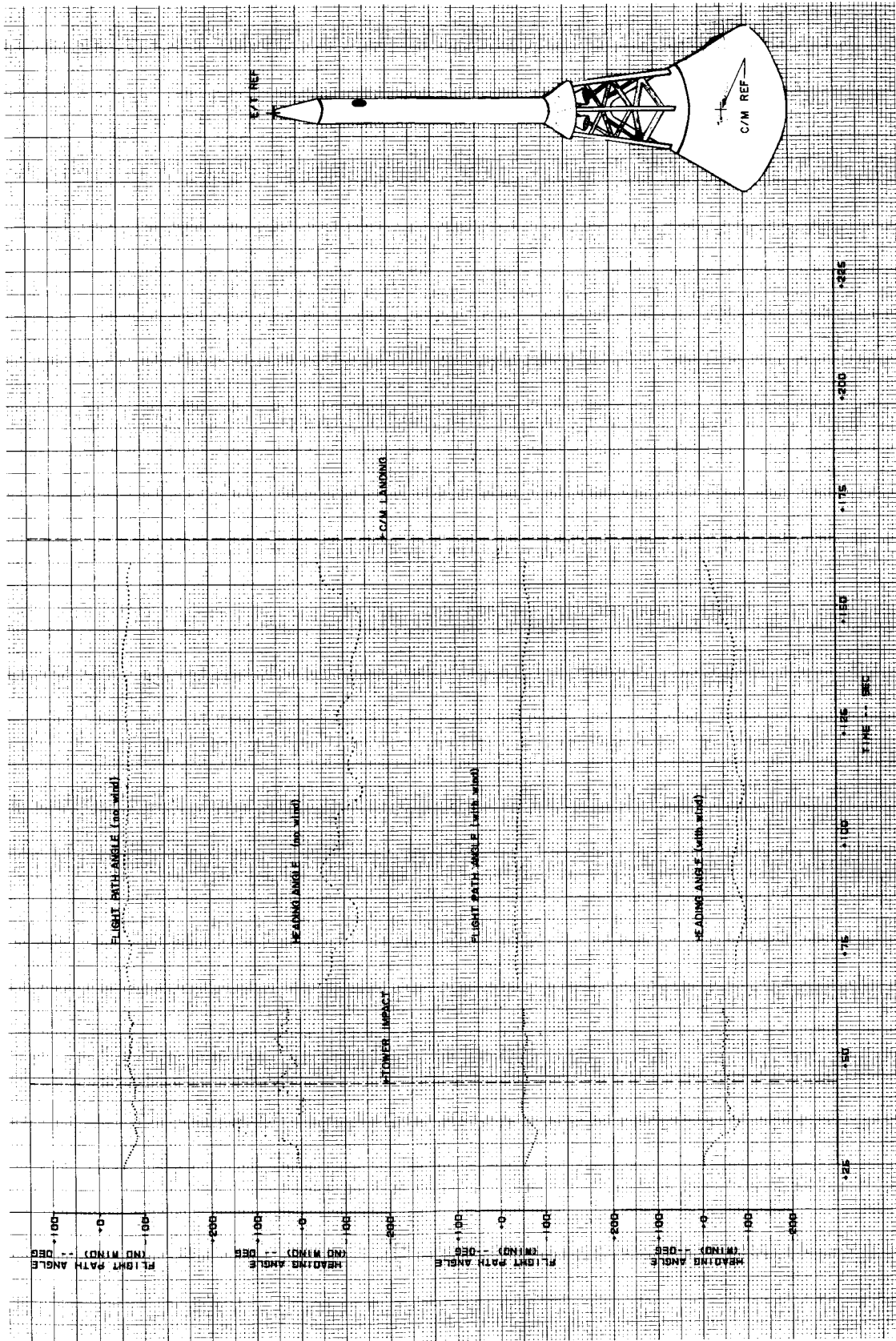
(b)  25 through 165 seconds

Figure A4-24.- Concluded.

(a)  0 through 40 seconds,

Figure A4-25.- Launch escape tower and command module altitude
and positions obtained from phototheodolite data, winds
included.
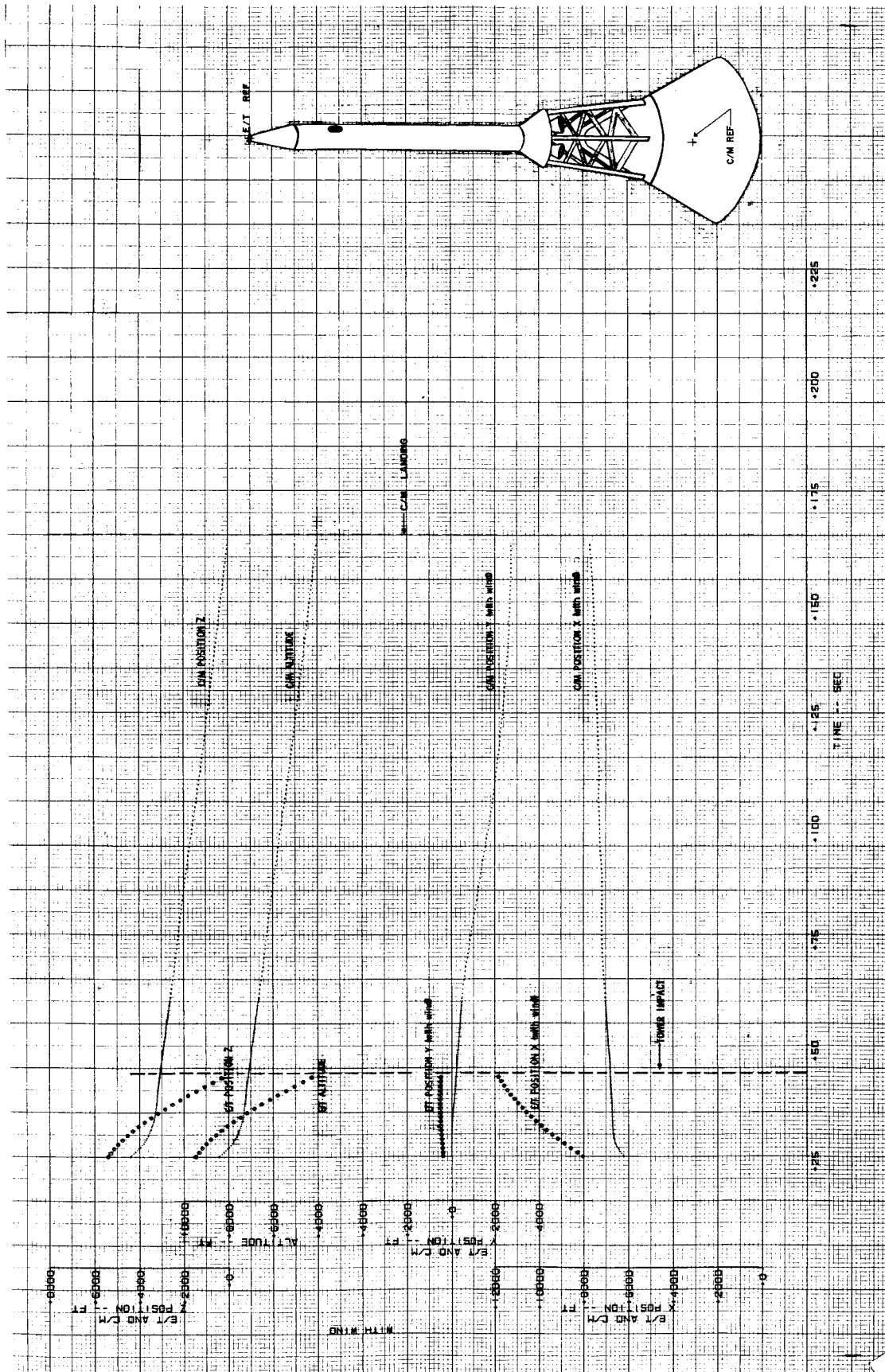
(b)  25 through 165 seconds.

Figure A4-25.- Concluded.

(a) 0 through 40 seconds.

Figure A4-26.- Launch escape tower and command module altitude and positions obtained from phototheodolite data, winds not included.
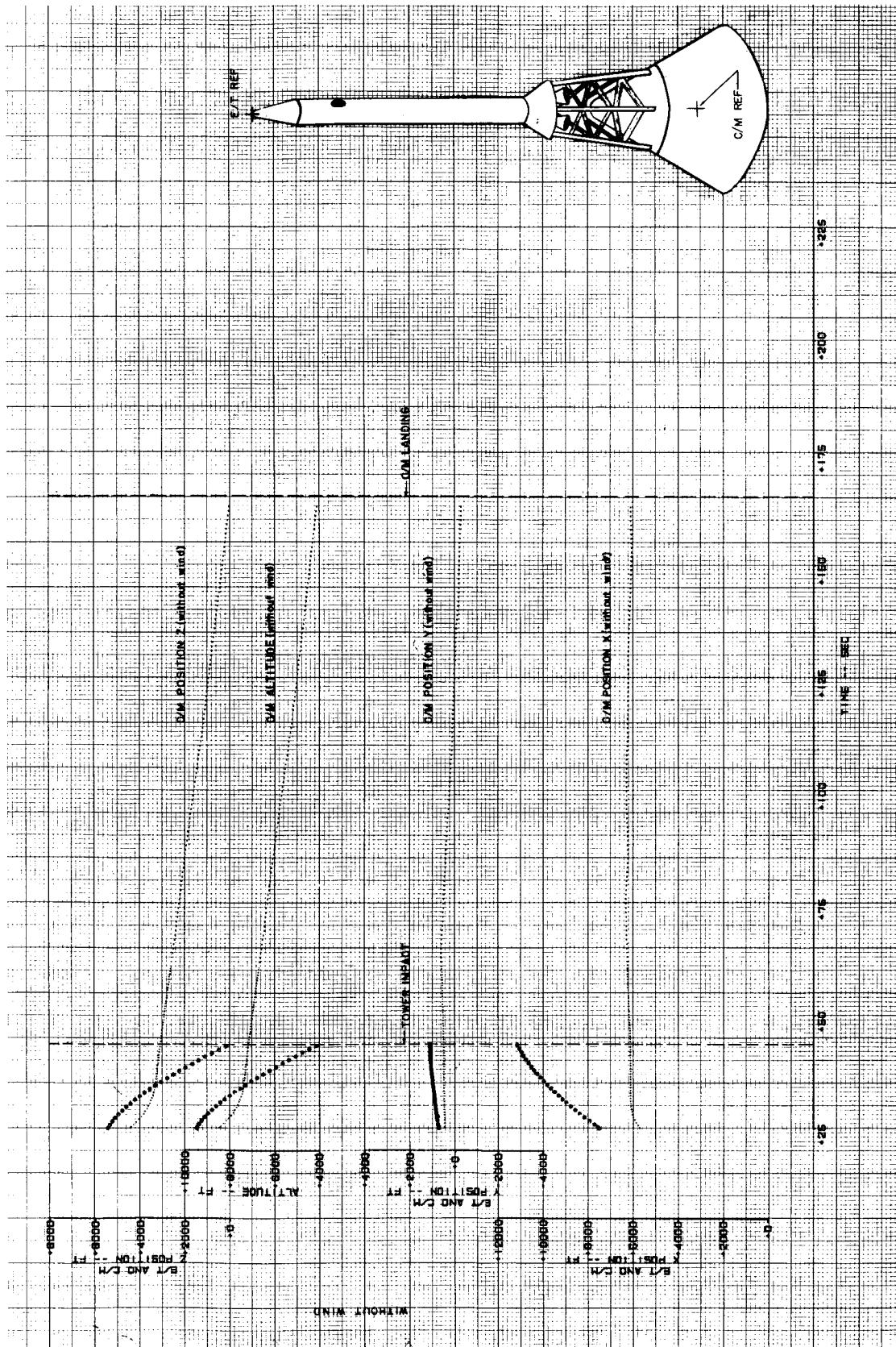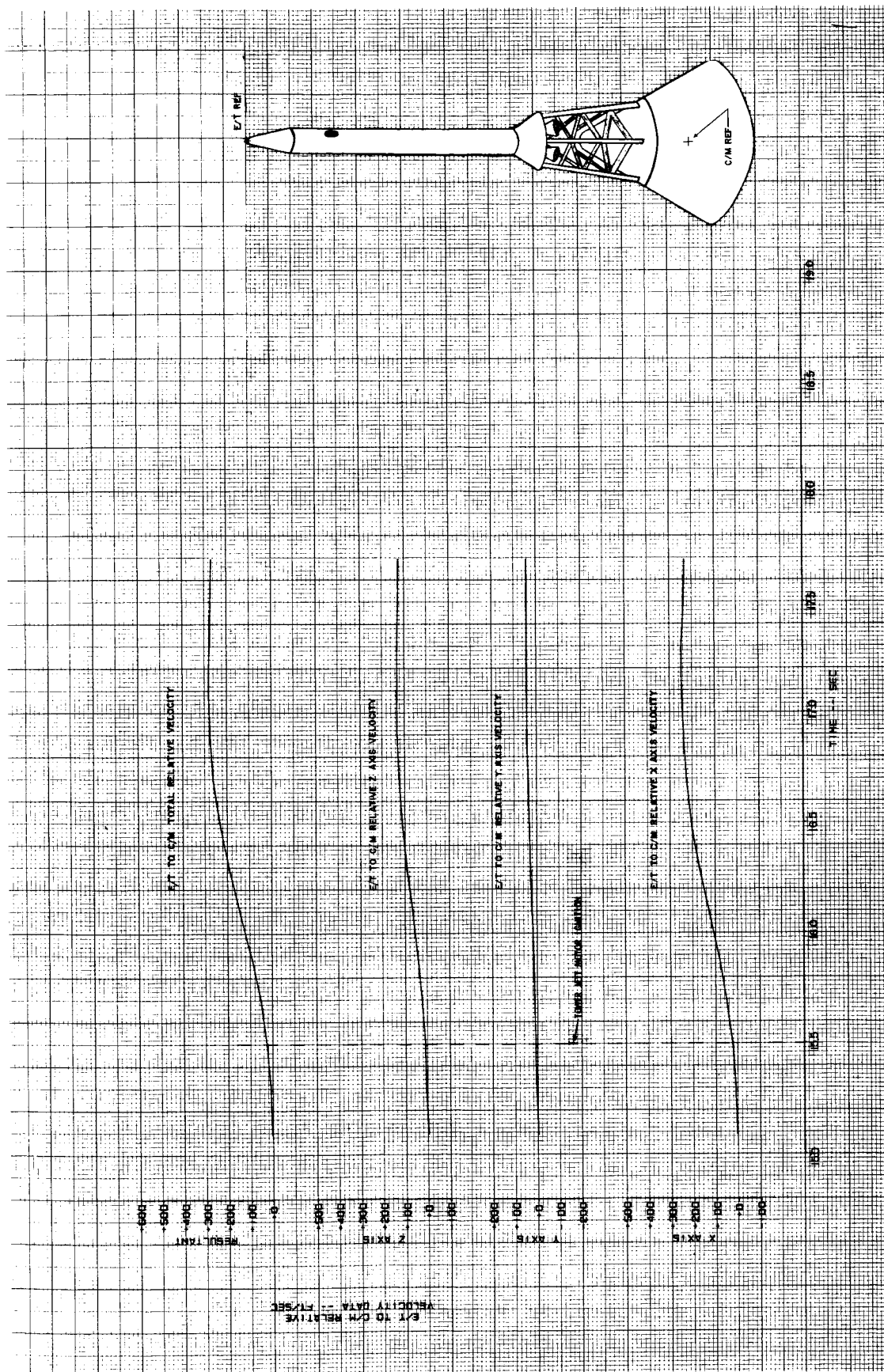
(b) 25 through 165 seconds.

Figure A4-26.- Concluded.
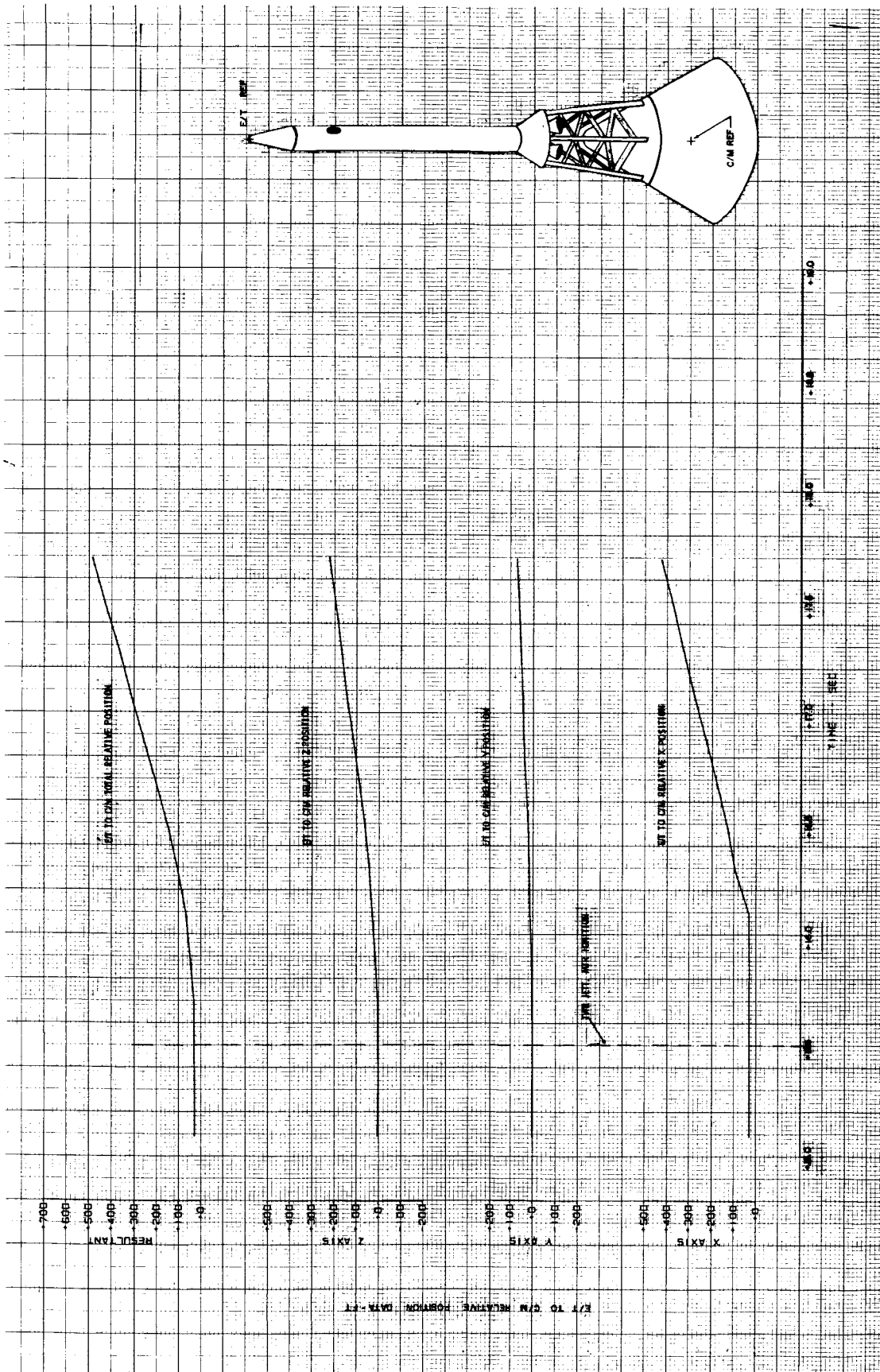
Figure A4-27.- Launch escape tower and command module relative positions.
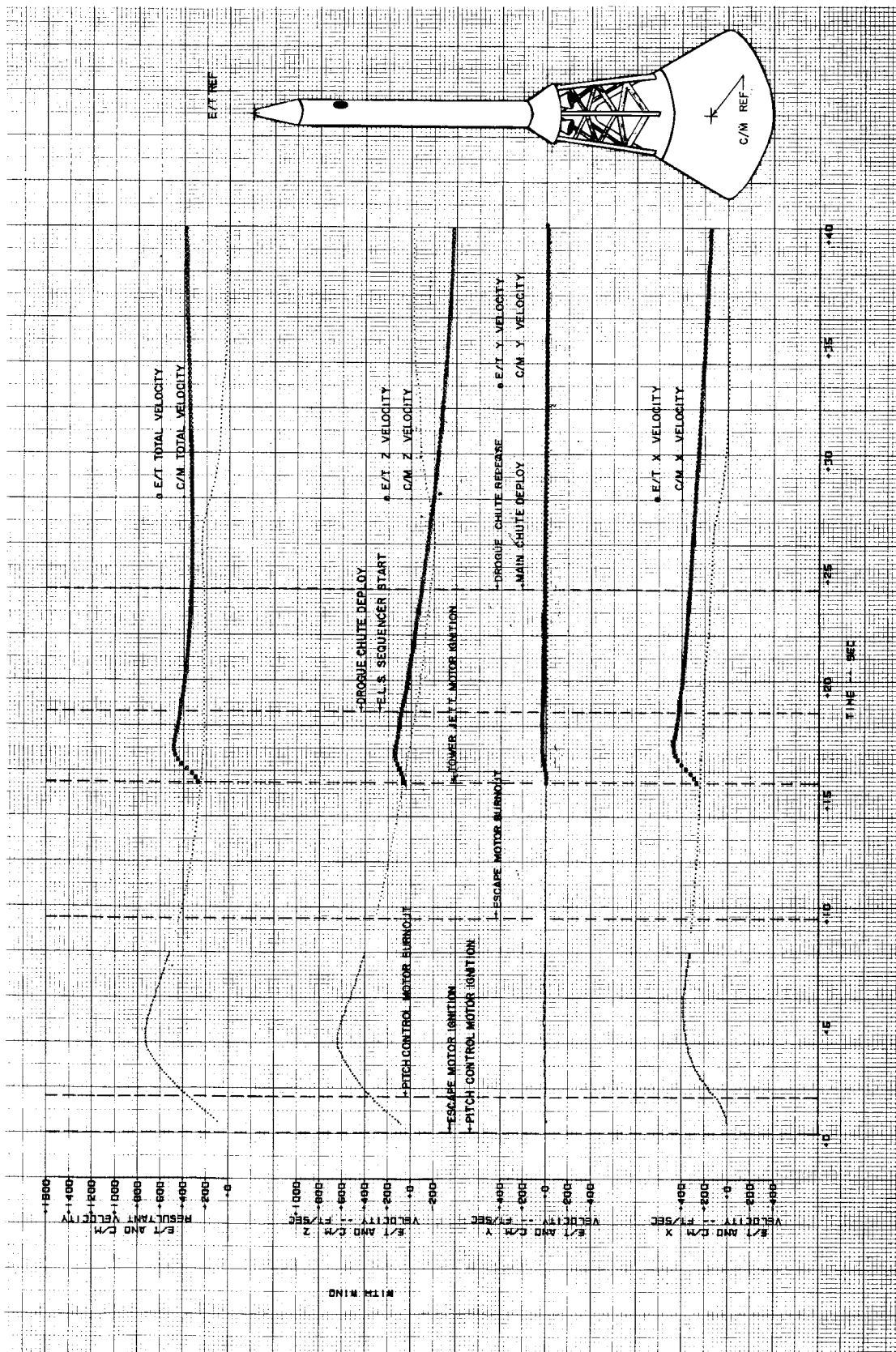
(a)  0 through 40 seconds.

Figure A4-28.- Launch escape tower and command module
velocities, winds included.
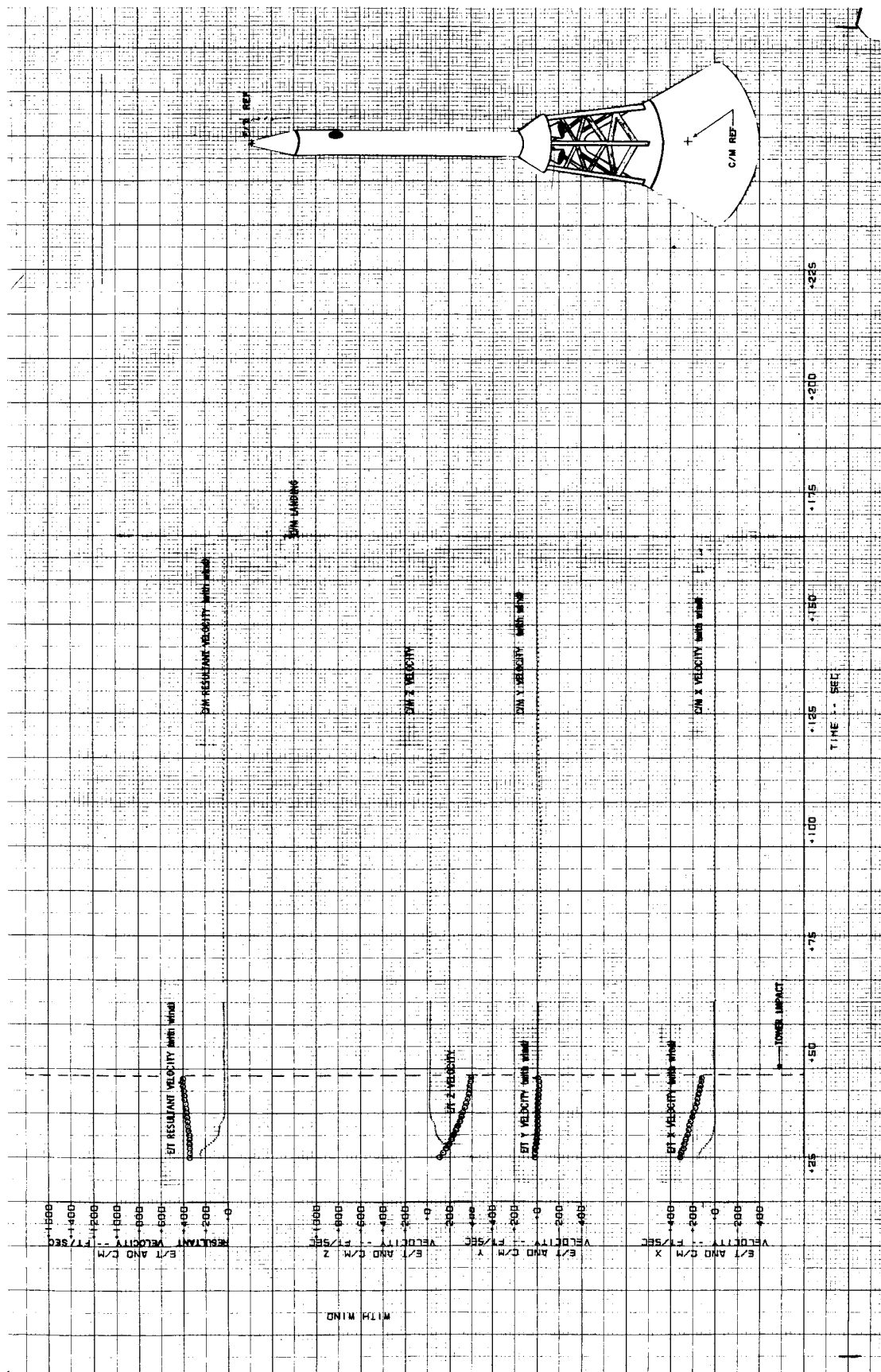
(b) 25 through 165 seconds.

Figure A4-28.- Concluded.
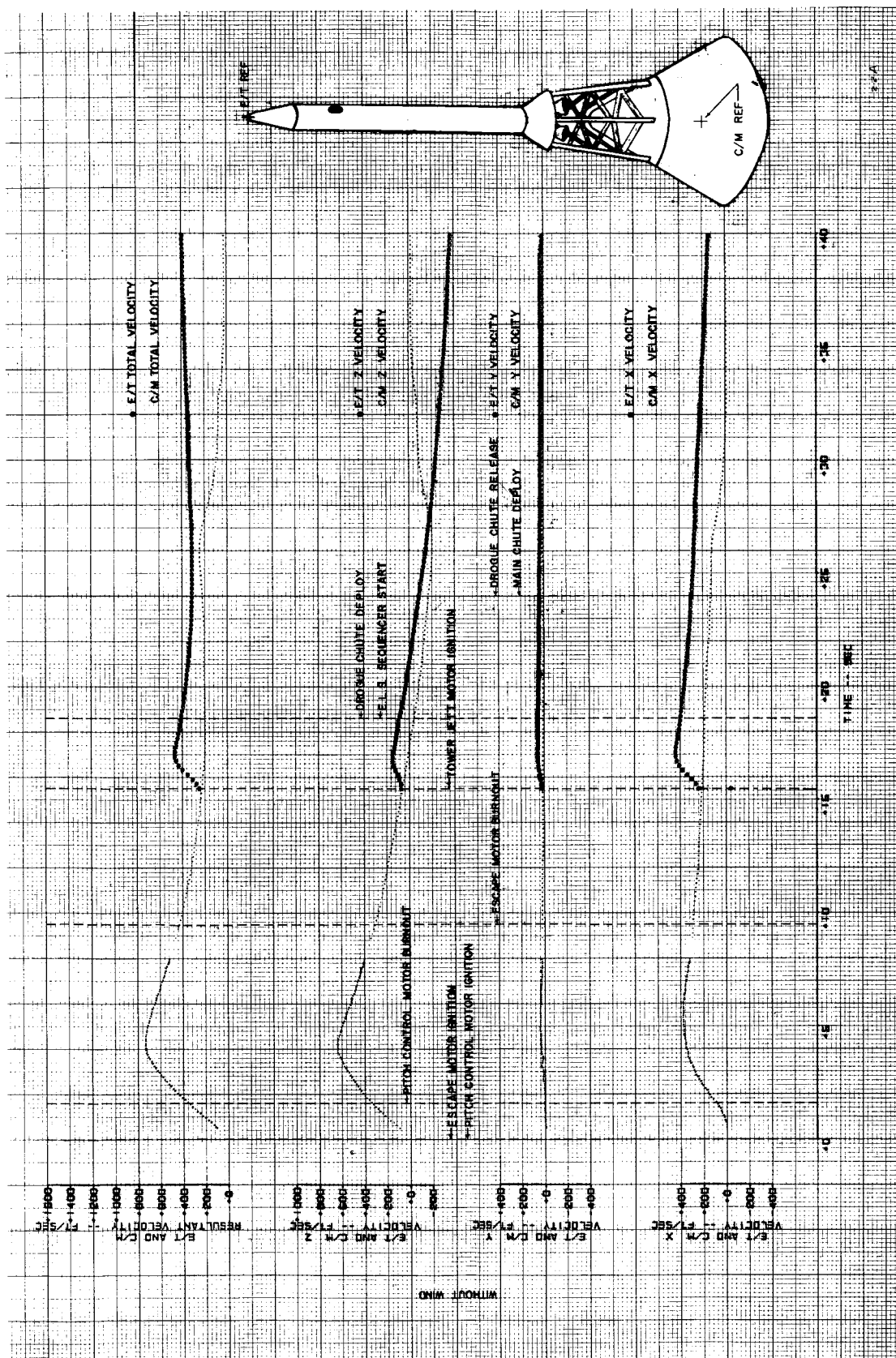
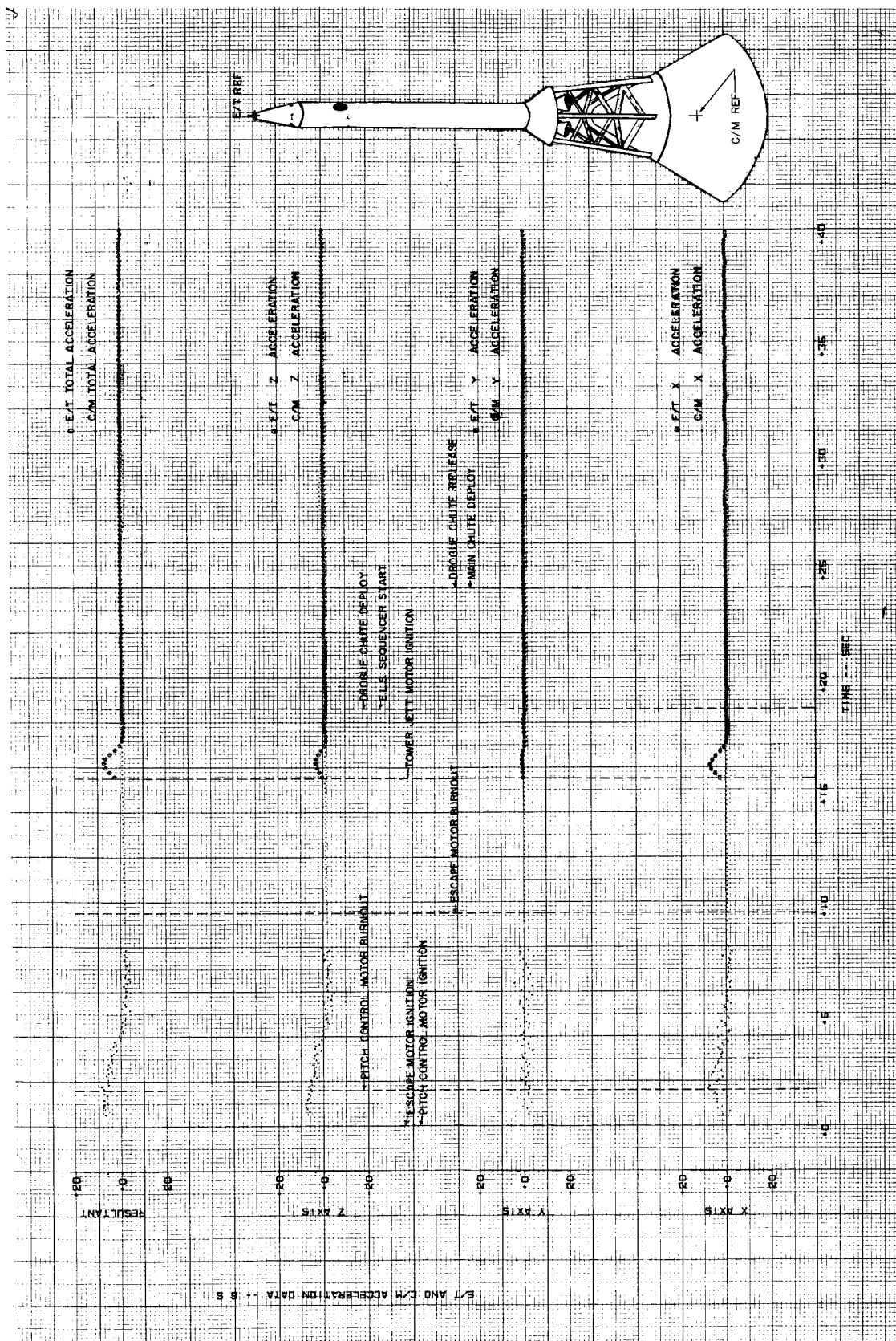Figure A4-29.- Launch escape tower and command module velocities, winds not included.

Figure A4-30.- Launch escape tower and command module relative velocities.

(a)  0 through 40 seconds.

Figure A4-31.- Launch escape tower and command module accelerations.
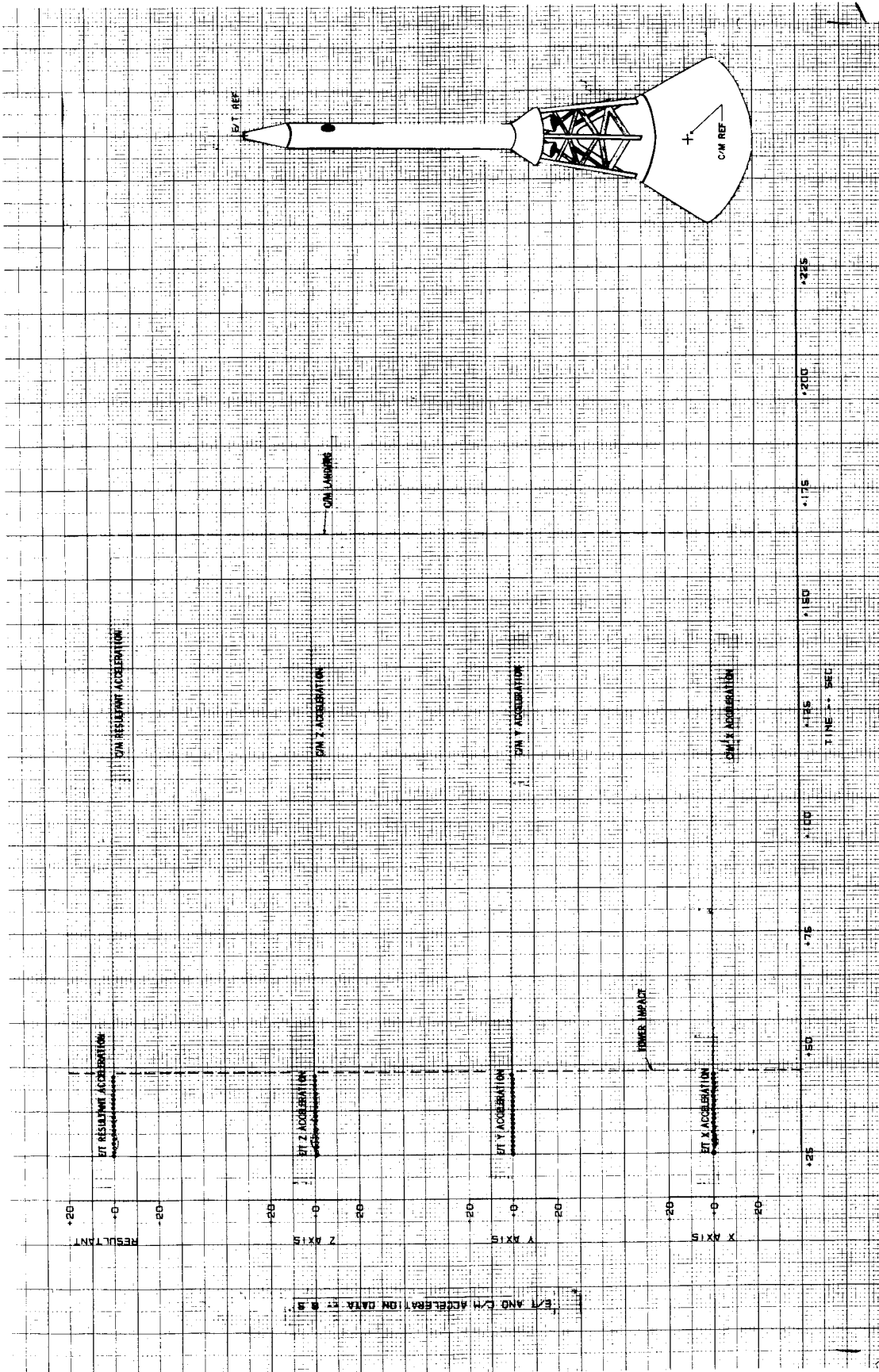
(b) 25 through 165 seconds.

Figure A4-31.- Concluded.
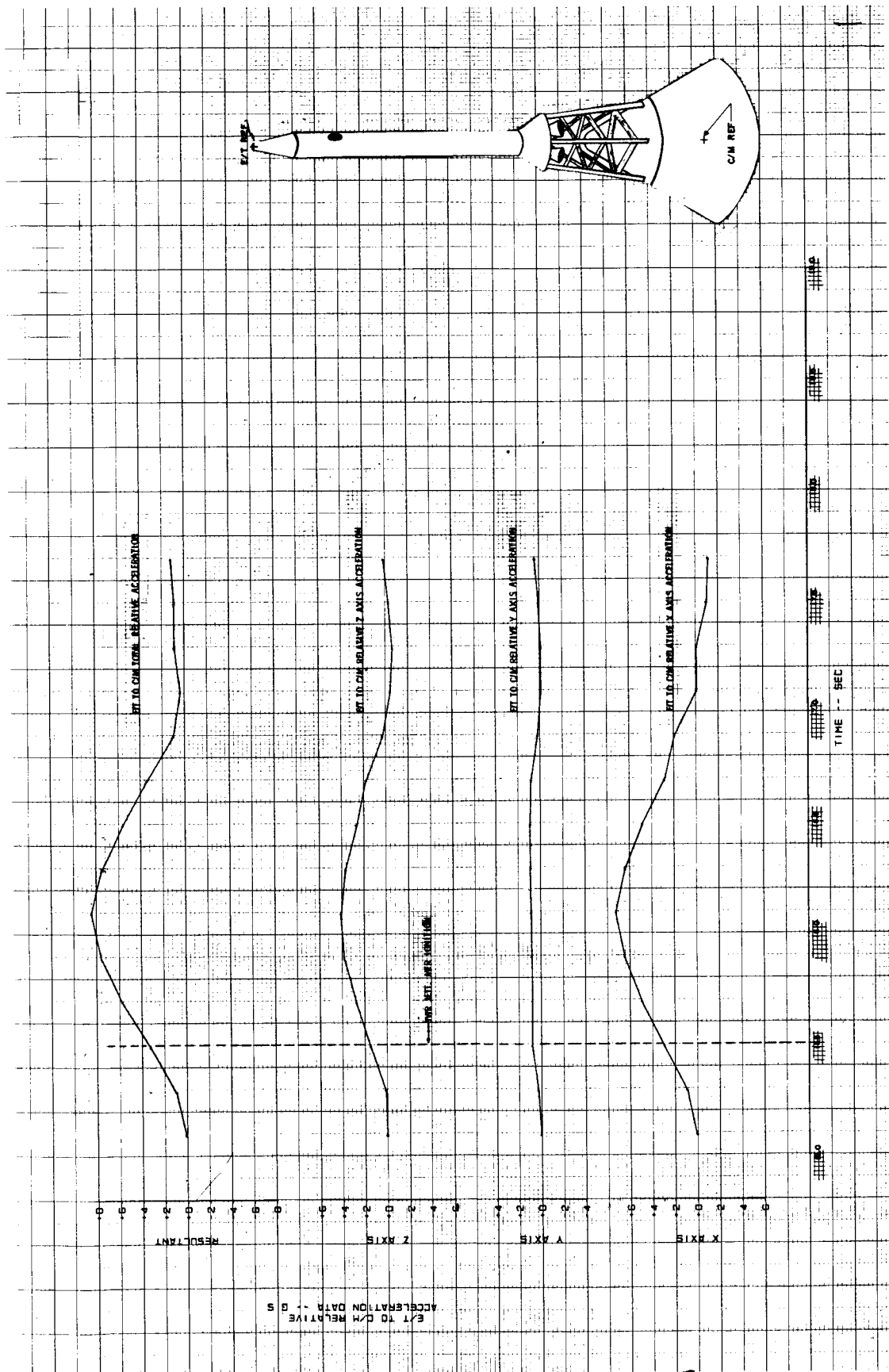
Figure A4-32.- Launch escape tower and command module relative accelerations.
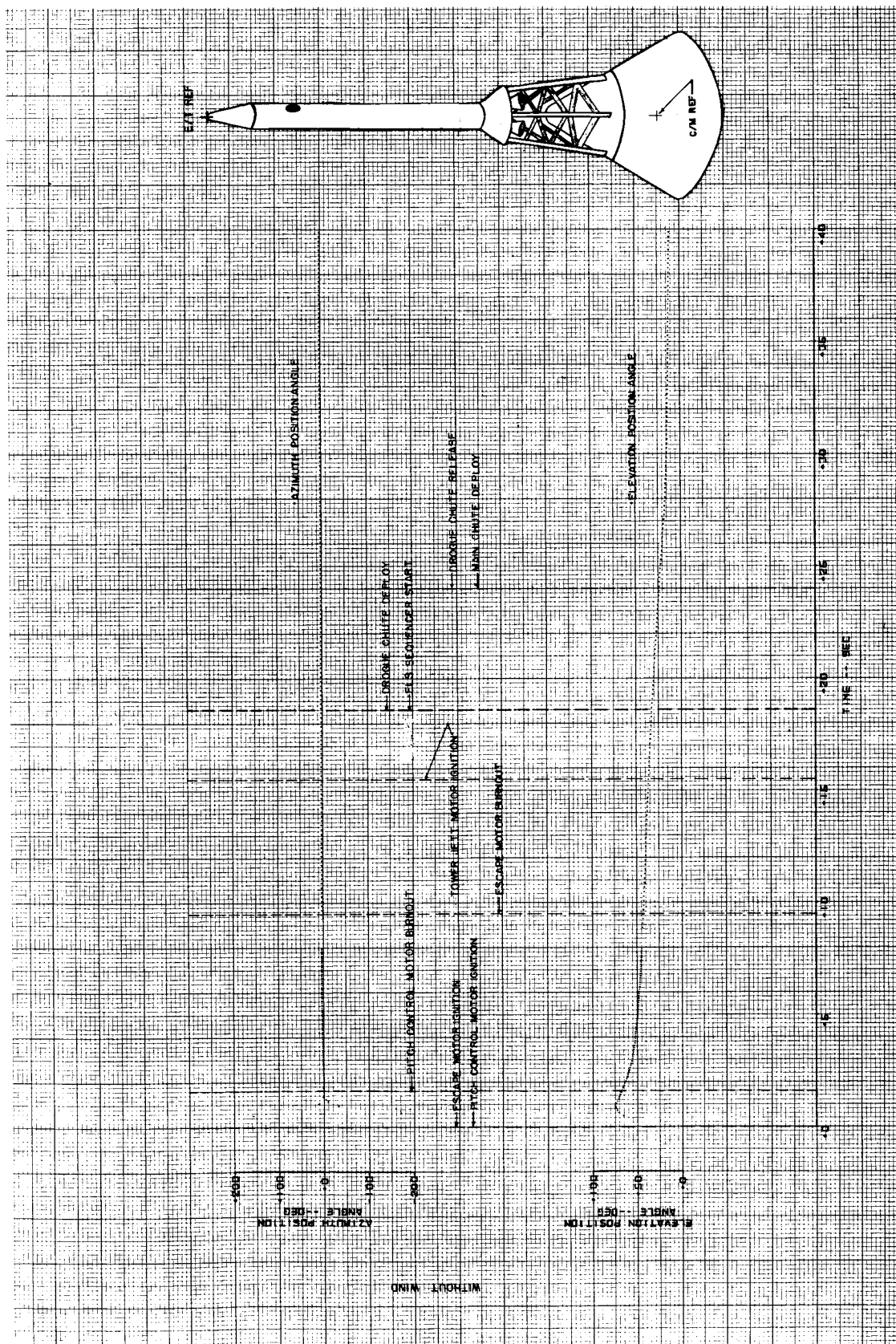
(a) 0 through 40 seconds.

Figure A4-33.- Azimuth and elevation position angles, winds not included.
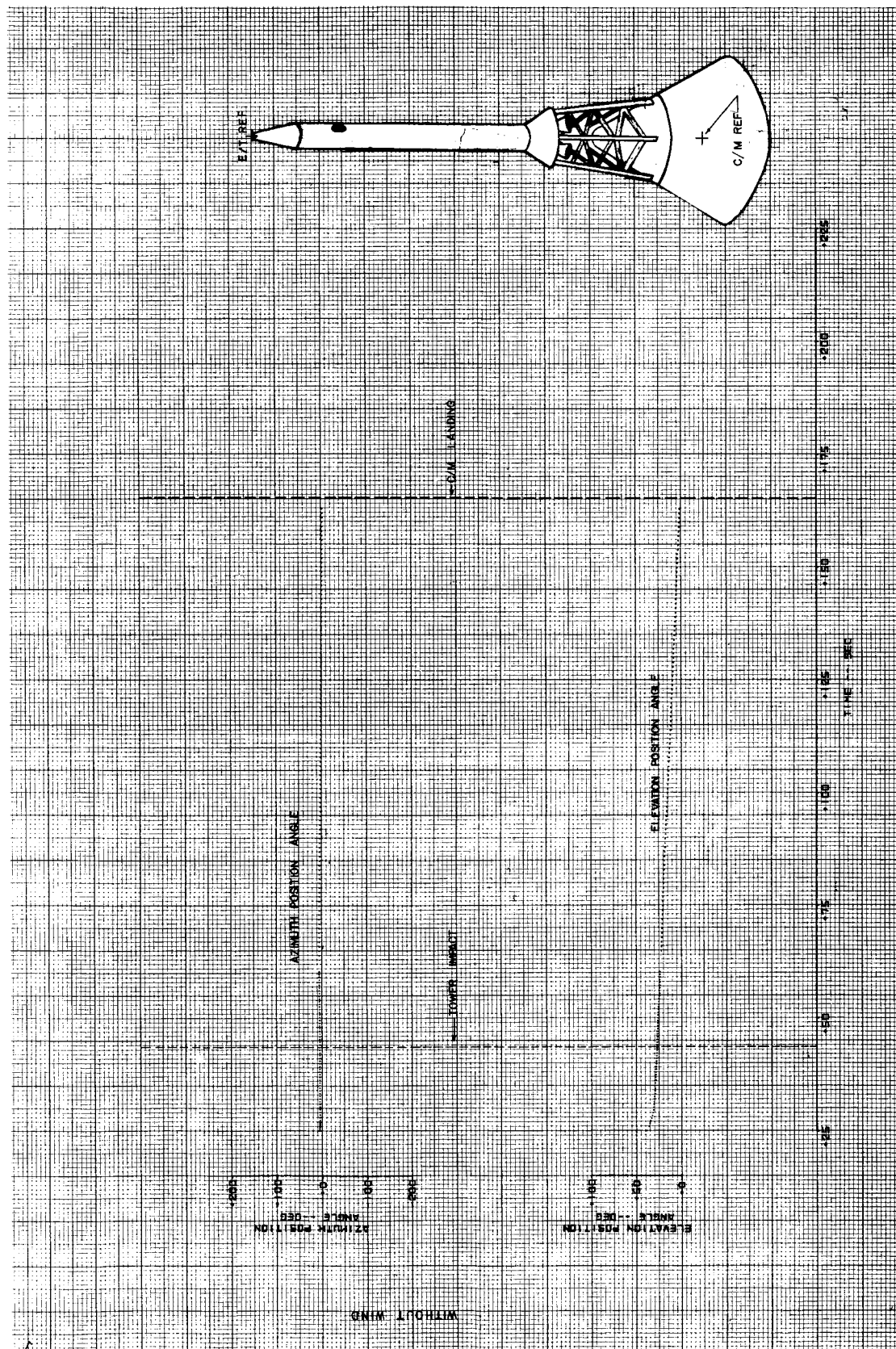
(b)  25 through 165 seconds.

Figure A4-33.- Concluded.

DISTRIBUTION


This Apollo Pad Abort I Postlaunch Memorandum Report has the
following distribution:


| | |
|---|---|
| D | Director (1) |
| DO | Deputy Director for Mission Requirements and Flight Operations (1) |
| DP | Deputy Director for Engineering and Development (1) |
| E | Assistant Director for Engineering and Development (2) |
| EST | Spacecraft Technology Division (6) |
| ECS | Crew Systems Division (6) |
| ESD | Systems Evaluation and Development Division (6) |
| ESE | Space Environment Division (6) |
| OFC | Flight Crew Operations Division (6) |
| OFO | Flight Operations Division (15) |
| M | Mercury Project Office (7) |
| G | Gemini Program Office (7) |
| S | Apollo Spacecraft Program Office (75) |
| PAO | Public Affairs Office (4) |
| Z | Astronaut Activities Office (17) |
| RFS | Reliability and Flight Safety Office (2) |
| PAE | Program Analysis and Evaluation Office (1) |
| AATC | Technical Information Division (2) |
| ACT | Technical Services Division (1) |
| RAA | Langley Research Center Representative, Mr. A. T. Mattson (1) |
| GSF-L | Goddard Space Flight Center Representative, Mr. W. B. Easter (1) |
| | Network Liaison Office, Port Canaveral, Fla. (5) |
| RFS | Reliability and Flight Safety Office, Port Canaveral, Fla. (2) |
| OPO | AMR Preflight Operations Division, NASA-MSC, Attn: Mr. G. M. Preston (20) |
| W | MSC/WSMR Operations, White Sands Missile Range, White Sands, New Mexico, Attn: Mr. W. E. Messing (30) |
| | NASA Hdqs., Wash., D.C., Attn: Mr. G. M. Low, MD(P) (8) |
| | Goddard Space Flight Center, Attn: Mr. H. J. Goett (1) |
| | Goddard Space Flight Center, Library (3) |
| | Langley Research Center, Attn: Director (1) |
| | Langley Research Center, Library (3) |
| | Ames Research Center, Attn: Director (1) |
| | Ames Research Center, Library (3) |

DISTRIBUTION - Concluded

Lewis Research Center, Attn: Director (1)
Lewis Research Center, Library (2)
NASA Flight Research Center, Attn: Director (1)
NASA Flight Research Center, Library (2)
NASA X-20 Dynosaur Office, Wright Patterson AFB,
   Ohio, Attn: Mr. P. F. Korycinski (2)
Marshall Space Flight Center, Attn: Director (1)
Marshall Space Flight Center, Library (2)
Launch Operations Center, Port Canaveral, Fla.,
   Attn: Director (5)

| | |
|---|---|
| SA | Mr. Jerry Valek (10) |
| SW | Mr. Harrison Rees (2) |
| SCR | Mr. G. Lemke (4) |
| NAA | S and ID, 12214 Lakewood Blve., Downey, Cal., Attn: Mr. E. E. Sack, Manager Contracts and Proposals (10) |
| AAOP | Publications and Distribution (Control Point) |